ABSTRACT

POORMAN, KELSEY ANNE. Comparative Cytogenomic Analysis of Canine Melanocytic Lesions. (Under the direction of Dr. Matthew Breen).

Melanoma arising from the mucosal surface is very rare; yet, is considered a highly malignant neoplasm. In people, malignant mucosal melanoma (MM) of the oral cavity accounts for only 0.2% to 2.0% of all reported melanomas, affecting approximately 1,500 individuals each year in the US. Due to the rarity of these tumors, extensive molecular and cytogenomic analysis has been limited. In contrast, each year over 50,000 dogs are affected by oral malignant melanoma in the US. Malignant MM in the domestic dog is the most common oral neoplasm, accounting for 40% of all canine oral tumors. These tumors arise spontaneously and present with similar histological features and biological outcomes to MM of the oral cavity in humans. However, compared to humans, little is known regarding the tumorigenesis of cutaneous or mucosal tumors in dogs.

Comparative aspects of canine melanocytic neoplasms were investigated using the first genome-wide cytogenomic study of canine mucosal melanoma, including genome-wide copy number analysis, gene expression profiling, targeted sequencing, and chemotherapeutic screening. Cytogenetic analysis of genome-wide copy number (CN) aberrations was completed on canine oral melanomas (n=44), benign melanocytomas (n=18), and cutaneous melanomas (n=5). Distinct sets of CN aberrations were detected between oral lesions and both benign and malignant cutaneous lesions. These CN aberrations were comparable between oral mucosal melanomas of human and dog, suggesting the validity of using the dog

as a model of human mucosal melanoma. Cytogenetic analysis also revealed structural chromosome aberrations, including varying translocations and fusions. As none of the canonical melanoma pathways fully explain this phenotype, transcriptome-wide gene expression analysis was performed on canine cell lines (n=6) and primary cases (n=7). Expression analysis identified 13 differentially expressed, biologically relevant genes, which were subsequently evaluated in a larger set of primary oral melanomas (n=17) and benign melanoctyoma (n=14). Numerous dysregulated genes were found to be part of the mitotic spindle and mitotic regulation pathways, previously unidentified in canine mucosal melanomas.

Finally, six cell lines of canine MM were evaluated for phenotypic variations in chemotherapeutic resistance; an important mechanism leading to poor survival. Resistance to doxorubicin and mitoxantrone was detected in n=4 and n=2 cell lines, respectively. While, the mechanism of resistance for these drugs has not been elucidated in canine melanoma; in humans, resistance to doxorubicin and mitoxantrone is mediated through overexpression of P-gp and BCRP, respectively. Expression of the genes that encode these proteins, *ABCB1* and *ABCG2*, as well as a non-related drug pump, *ABCC1,* were evaluated in six cells lines. Significant association between drug pump expression and resistance phenotype was found ($p=0.0029$ for *ABCG2*/mitoxantrone and $p=0.008$ for *ABCB1*/doxorubicin). These data indicate that cellular chemoresistance to doxorubicin and mitxantrone can be predicted through monitoring the expression of *ABCB1* and *ABCG2*, respectively. These findings suggest a direct clinical application in targeting effective treatments to individual patients

most likely to respond, avoiding unnecessary courses of chemotherapy in patients with predicted resistance.

In summary, this body of work established the use of the dog as a valid model for the investigation of human mucosal melanomas and that canine mucosal and cutaneous melanocytic lesions are different at the cytogenetic level. Similarities at the genetic level suggest an underlying mechanism of genetic instability present in both human and canine mucosal melanomas. Detailed karyotyping and gene expression analysis revealed the involvement of both the mitotic DNA damage and the spindle assemble checkpoint pathways. It also revealed the presence of minor clones, which presents a challenge in clinical therapeutic treatment. Investigation into therapeutic resistance also revealed a measureable pattern of chemoresistance. These pathways, previously unidentified in canine melanomas, present significant targets for more effective therapeutics.

Comparative Cytogenomic Analysis of Canine Melanocytic Lesions

by
Kelsey Anne Poorman

A dissertation submitted to the Graduate Faculty of
North Carolina State University
in partial fulfillment of the
requirements for the degree of
Doctor of Philosophy

Comparative Biomedical Sciences

Raleigh, North Carolina

2014

APPROVED BY:

_____	_____
Dr. Matthew Breen Committee Chair	Dr. Jeffrey Yoder
_____	_____
Dr. Marlene Hauck	Dr. Luke Borst

DEDICATION

This dissertation is dedicated to my family and friends who supported me throughout my studies. To my parents who gave me every opportunity to succeed, who were always there for me, supporting me, teaching me to love learning, and helping me to be the best person I can. To my friends who made me feel loved, made me laugh, and were always there to relax with at the end of the day. Finally, to all the teachers who inspired me to learn, without whom I would not be here today.

BIOGRAPHY

Kelsey Anne Poorman was born and raised in Raleigh, NC. After beginning her undergraduate studies at the University of North Carolina at Asheville in 2006, it was here that she was first introduced to scientific research. Kelsey found her love of scientific research blossom under the direction of Dr. Barbara Reynolds, with whom she completed a three-year undergraduate research project. However, it was not until her junior year that Kelsey found an interest in molecular sciences. After graduating in 2010 with a Bachelor's degree in Ecology and Evolutionary Biology, Kelsey began a graduate career at North Carolina State University's College of Veterinary Medicine in the Comparative Biomedical Sciences Graduate Program. Kelsey's dissertation work focused on the genomics of canine oral melanoma. She hopes to continue following her passion for scientific discovery in her career as a research scientist.

ACKNOWLEDGMENTS

I would like to thank the members of my committee for all the support you have given me during my time at NC State. To Dr. Yoder, thank you for the insightful discussions that were a constant guide and aid in my research. I would like to thank Dr. Hauck for taking the time to discuss the clinical aspects of my research, for which your expertise was invaluable. I would especially like to thank Dr. Borst for the time, resources, and effort you put into helping me develop the final part of this project. Not only did you take the time to sit with me one-on-one and go over my samples and data but were always willing to brainstorm and review both text and presentations. I would also like to thank the members of the Breen Lab, both past and present, especially Dr. Rachael Thomas, Christina Williams, Katie Kennedy, Susan Bowman, and Sarah Roode. I would not be here today without your constant help and support. I would like to thank the faculty who are a part of the CBS program, especially Dr. Barbara Sherry and Dr. Fred Fuller, and the other staff and graduate students at NCSU, particularly Rachael Stebbing, Efrain Rivera Serrano, and Mitsu Suyemoto. Finally, and most importantly, I would like to thank Dr. Breen, who has been an ever-supportive mentor. Not only did you go above and beyond to provide me with every opportunity I needed to learn, you were also a constant guide in my intellectual and personal development.

TABLE OF CONTENTS

LIST OF FIGURES

LIST OF TABLES

LIST OF ABBREVIATIONS

oaCGH – oligo-array Comparative Genomic Hybridization
FISH – Fluorescence *in situ* Hybridization
FFPE – Formalin Fixed Paraffin Embedded
H&E - Hematoxylin and Eosin
BAC - Bacterial Artificial Chromosome
SLP – Single Locus Probe
CNA – Copy Number Aberration
CFA – *Canis familiaris* (also used as a prefix to chromosome numbers)
HSA – *Homo sapiens* (also used as a prefix to human chromosome numbers)
C-KIT - V-kit Hardy-Zuckerman 4 feline sarcoma viral oncogene homolog
C-MYC - V-myc myelocytomatosis viral oncogene homolog (avian)
TP53 - cellular tumor antigen p53
BRAF - V-raf murine sarcoma viral oncogene homolog B1
RAS – Rat sarcoma gene
MAP-K - Mitogen-activated protein kinases
CCND1 - G1/S-specific cyclin-D1
RB-1 - Retinoblastoma 1
CDKN2A - Cyclin-dependent kinase inhibitor 2A
CDKN1A - Cyclin-dependent kinase inhibitor 1A
PTEN - Phosphatase and tensin homolog
CDK4 - Cyclin-dependent kinase 4
SPRED1 - Sprouty-related, EVH1 domain containing 1
TRPM7 - Transient receptor potential cation channel, subfamily M, member 7
TACC3 - Transforming, acidic coiled-coil containing protein 3
PLK - Polo-like Kinase
NEK - NIMA (never in mitosis gene a)-related kinase
Mps1/TTK - Monopolar spindle 1 kinase/Dual specificity protein kinase
ABCs - ATP-binding cassette
SAC - Spindle assembly checkpoints
GEP - Gene expression profiling
RT-qPCR - Real time quantitative polymerase chain reaction

CHAPTER I

Introduction and Literature Review

Melanoma is a malignant cancer of specialized cells called melanocytes. Melanoma is less common than other skin cancers; however, it is much more malignant causing the majority (75%) of skin cancer deaths. Melanoma is a highly complex disease partly due to various environmental exposures, which can induce tumor development, and also in part to the many different regions of the body that can be affected. Since its discovery in 1804 scientist have made great strides in understanding the cellular basis of melanoma development, facilitated by advances in molecular biology and comparative oncology. The following review will briefly introduce the fields of melanocyte biology, veterinary melanoma research, comparative oncology, and the basis of melanoma pathology and molecular development.

1.1 Melanocyte Biology

Melanocytes' primary cellular function is to produce a pigment called melanin. The melanin is distributed to neighboring cells and protects against the harmful damage of UV radiation. Melanin is produced and accumulates within melanocytes in cytoplasmic organelles called melanosomes. Within melanocytes, the production of melanin is reliant on the expression of tyrosinase, a copper-containing enzyme that is responsible for the hydroxylation of a monophenol and the conversion of an o-diphenol to the corresponding o-quinone (Bandarchi *et al.* 2013). The pigment is then transferred to neighboring keratinocytes by PAR-2 receptors on the surface of cells (Bandarchi *et al.* 2010). Transferred

melanin forms a cap on the nucleus of mitotically active basal cells to protect DNA from damage. Melanocytes are located most densely amongst the basal layers of the epidermis but can be found throughout the body in both epidermal and mucosal tissue layers.

Melanocyte precursors originate in the neural crest with cell fate specification occurring during embryonic development (Uong and Zon 2010). During early embryogenesis, neural crest stem cells are induced by BMP signaling and maintained in an immotile, undifferentiated state by E-cadherin. Migration away from the neural plate is induced by the snail/slug family of genes that transcriptionally represses E-cadherin expression and allow for epithelial-mesenchymal transition (EMT) to occur (Cano *et al.* 2000). Bipotent glial-melanocyte stem cells then undergo gradual lineage restriction toward the melanoblast fate by numerous signaling molecules including, *MITF*, *C-KIT*, *DCT*, and *Notch* (White and Zon 2008).

Notch family members maintain adult melanocyte stem cells, which differentiate into committed adult melanoblasts due to inhibition of Notch signaling and up-regulation of *C-KIT* expression (Uong and Zon 2010). *MITF*, a melanocyte linage-specific marker, is activated within melanoblast precursors through β-catenin and sox10 signaling pathways. Once active, *MITF* induces the expression of several pigment-producing genes including, *DCT* and tyrosinase (Uong and Zon 2010). After melanoblasts have reached their specific tissue location, melanocyte proliferation and differentiation are regulated by numerous factors within the tissue environment. Mature melanocytes rarely interact with other melanocytes or melanocytic precursors, as they are located in a bed of mature epithelial cells. Melanocytes remain attached to these surrounding cells through E-cadherin mediated

attachment (White and Zon 2008). Epithelial melanocytes are especially affected by keratinocytes. Each normal melanocyte within the basal layer of the epidermis is associated with a number of keratinocytes, which synthesize the following among others: endothelins, *SCF*, *HGF, LIF*, and *GM-CSF* (Hirobe 2011). Melanocyte proliferation within the mature epidermal layer is controlled by keratinocytes via excretion of extracellular paracrine growth factors, intracellular communication through secondary messengers, and cell-to-cell and cell-matrix adhesions.

1.2 Clinical perspectives of canine melanocytic lesions

In dogs, melanomas are the most common tumor of the oral cavity (Smith, Goldschmidt, and McManus 2002). Oral melanomas represent only 1% of all canine cancers (Ramos-Vara *et al.* 2000), yet 90% are malignant, readily invading into normal tissue and bone with a high metastatic propensity (Koenig *et al.* 2002; Spangler and Kass 2006; Bergman 2007). Malignant melanomas of the oral cavity are usually aggressive and respond poorly to standard chemotherapeutic treatments (Bergman 2007). These tumors vary widely in biologic behavior and histologic presentation. Oral melanomas are most common in Scottish terriers, golden retrievers, poodles, and dachshunds (Smith, Goldschmidt, and McManus 2002). Lesions usually present in older dogs with no gender predisposition (Overly, Goldschmidt, and Schofer 2001). Due to the limited number of studies performed, little is known about the molecular pathology of cutaneous melanomas and benign melanocytomas.

There are two main differential diagnoses of melanocytic lesions in veterinary medicine: malignant melanoma and benign melanocytomas. Most melanomas are diagnosed based on the presence of melanin granules within the tumor mass; however, roughly 25% of all canine melanomas are amelanotic, i.e. they present without melanin production. The main diagnostic criteria for amelanotic melanomas are the presence of junctional activity and nests of neoplastic cells within overlying epithelium (Smedley *et al.* 2011). Diagnosis of amelanotic melanomas can be further impeded due to the fact that they often do not stain with melanoma-specific immunohistochemical stains. Primary immunohistochemical markers of melanoma are Melan-A, PNL-2, and tyrosine reactive proteins (TRP-1 and TRP-2). One of the first immunohistologic markers to be identified for melanomas was Melan-A, also known as MART-1 (Busam *et al.* 1998; Jungbluth *et al.* 1998). In evaluation of Melan-A as a potential marker for canine oral melanomas, almost all (91.5-100%) lesions of melanocytic origin, regardless of percent pigmentation, were positive for Melan-A immunohistochemical staining, with positive staining in only 2.45% of neoplasia of non-melanocytic origin (Ramos-Vara *et al.* 2000; Koenig *et al.* 2001).

TRP-1 and TRP-2 are proteins related to the melanin production pathway. TRP-1 and TRP-2 are involved in maintenance of the melanosome structure, helping to regulate melanocyte proliferation and cell death (Shibata *et al.* 1992). These are only expressed in melanocytes, so act as a specific marker for melanocytic cell origin. PNL2 is a recently developed melanocyte reactive antibody used as a marker during immunohistochemical diagnosis (Rochaix *et al.* 2003). However, it has been reported as being highly specific, with 62% of canine melanocytic neoplasms tested staining positive with PNL2 as compared to

59% with Melan-A (Giudice *et al.* 2010). In a recent survey of the use of immunohistochemical markers for diagnosis of amelanotic melanomas, it was observed that Melan-A, PNL2, TRP-1, and TRP-2 were 93.9% sensitive and 100% specific for the diagnosis of canine oral amelanotic melanomas (Smedley *et al.* 2011).

For both melanotic and amelanotic melanomas, prognosis is primarily determined with clinical staging. Parameters evaluated in staging include size, site of primary disease, and histological characteristics (Spangler and Kass 2006). However, there is large debate among pathologists on the accuracy of diagnostic and prognostic criteria for canine malignant melanomas (Bergman 2007; Smedley *et al.* 2011; Withrow 2013). One of the most common prognostic factors is location of the primary tumor. Primary melanomas develop in four distinct locations in the dog: the oral mucosa, nail bed, cutaneous epithelium, and the eye (not discussed here).

Oral melanomas are the most common and most well-studied of the melanocytic lesions in the dog. The most common site for oral melanoma development was the labial mucosa or the mandibular gingiva (Ramos-Vara *et al.* 2000). Oral lesions tend to be the most aggressive of melanomas, with a high frequency of malignancy (Bergman 2007). Up to 48% percent of cases will develop a local recurrence of the primary tumor after radical surgical resection and 44-58% of primary tumors spread to distant organs (Proulx *et al*. 2003). Digital melanomas, arising from the nail bed, are also considered malignant, with 40% of cases metastasizing to distant organs (Bergman 2007). Reports vary on the mean survival time of these lesions, however two independent retrospective studies determined the two-year survival time of canine digital melanomas to be 11% and 13% respectively (Marino

et al. 1995; Henry *et al.* 2005). Melanomas of the cutaneous epithelium are the third most common malignant skin lesion in dogs (Villamil *et al.* 2011) representing 5-11% of all malignant melanomas (Smith, Goldschmidt, and McManus 2002). Cutaneous melanomas are most common in Vizslas, Miniature Schnauzers, and Chesapeake Bay Retrievers (Villamil *et al.* 2011). Lesions arising from the cutaneous epithelia are mostly considered benign (Smith, Goldschmidt, and McManus 2002); however, prognoses of cutaneous lesions are harder to define solely on histologic features (Smedley *et al.* 2011). One study reported that, after surgical treatment only, 45% of dogs diagnosed with malignant melanomas of the cutaneous epithelium died within one year, with 10% of dogs diagnosed with a benign lesion dying from disease after two years (Bostock 1979).

Melanocytomas are the most common melanocytic lesions of the skin, defined as any benign melanocytic tumor arising in the epidermis, dermis, or external root sheath of the hair follicles. They are most commonly found on the head or limbs, presenting as smooth, often highly pigmented masses, with infrequent ulceration (Goldschmidt and Shofer 2005). Melanoacanthomas are rare benign lesion, with only four reported cases in the literature (Sharif *et al*. 2014). Defined as tumors with features of a compound melanocytoma and a benign epithelial neoplasm. These lesions present with nodular masses containing polygonal melanocytes arranged into numerous nests within the neoplastic follicular epithelium. A rare subtype is the Balloon Cell melanocytoma, which is composed of large, round and epithelioid-like cells with finely granular-to-foamy cytoplasm and sparse pigment granules (Smith, Goldschmidt, and McManus 2002).

1.2.1 Prognostic histological characteristics

Independent of location, histological characteristics are the primary way in which prognosis is determined. Characteristics examined include: cell size, cell shape, nuclear size and shape, chromatin pattern, prominence of nucleoli, pigmentation, nuclear aptypia, hyperchromasia, mitotic figure density, junctional activity, and level of invasion into surrounding tissues. One study of 384 cases of melanocytic tumors found significant correlation of metastasis, increased mitotic index, nuclear atypia, WHO clinical stage, and increased volume with decreased patient survival (Spangler and Kass 2006). Recent evaluations into the accuracy of diagnostic and prognostic histology confirmed these characteristics in combination are about 90% accurate in determining patient outcome (Smedley *et al.* 2011).

One of the most frequent and most accurate prognostic characteristics, with an accuracy rate of about 93%, is mitotic index (MI), defined as the number of mitotic figures in 10 consecutive, non-overlapping, 40X fields (Smedley *et al.* 2011). MI has been shown to be prognostic in all three locations of primary tumor growth and is the most commonly evaluated characteristic, with the average MI for oral melanomas being 31.4. For proper MI evaluation, areas of ulceration must be avoided as they tend to have little proliferation. Higher MI is directly correlated to tumor aggression; oral lesions with an MI of greater than 40 have shown an increased risk of death within one year of diagnosis. For cutaneous lesions, an MI of greater than 30 is considered highly malignant (Smedley *et al.* 2011). Another study found that only 10% of dogs with cutaneous melanomas with MI of two or less died within two years, whereas 70% died if the tumor had an MI greater than three

(Bostock 1979). In most circumstances, an MI of three or less is considered diagnostic for benign lesions regardless of location. Other than MI, one of the most critical components for determining prognosis is the level of tumor invasion or radial growth. Characteristics that lead to worse prognosis include the radial component invading beyond the dermal mass (also known as poor circumscription), evidence of necrosis, and the absence of cellular differentiation (Smedley *et al.* 2011).

Another characteristic of malignancy is nuclear pleomorphism, defined as a variation in nuclear shape, size, and formation. Pleomorphism is found in 62.8% of all oral melanomas, with half of those being considered high pleomorphism (Ramos-Vara *et al.* 2000). Due to the subjective nature of such characteristics, evaluation requires highly specific and defined criteria. Most common criteria of nuclear atypia are large diffuse nuclei, many large nucleoli, and intensely clumped chromatin. This pattern is especially common in undifferentiated neoplastic cells; however, accurate assessment is based on evaluation of approximately 200 cells (Smedley *et al.* 2011). For a tumor to be considered malignant, atypia must be present in greater than 30% of nuclei. Determination of nuclear atypia can also be difficult in heavily pigmented lesions.

Degree of pigmentation itself is often considered prognostic, with cases of oral and lip melanomas showing pigmentation in greater than 50% of cells having longer survival times (Smedley *et al.* 2011). However, accurate diagnosis must first be confirmed for tumors lacking any pigmentation. Junctional activity, defined as the proliferation of nests of melanocytes along the dermo-epidermal junction (Smith, Goldschmidt, and McManus 2002), can be another diagnostic and prognostic characteristic, especially in amelanotic melanomas.

Junctional activity is found in 64.5% of all oral melanomas (Ramos-Vara *et al.* 2000). However, the presence of junctional activity differs with location of the primary tumor. In cutaneous lesions, junctional activity correlates with an increased survival rate, where in digital and oral lesions it correlates with decreased survival (Smedley *et al.* 2011). Other characteristics that are often evaluated have been shown to have no correlation to clinical prognosis, including cellular pleomorphism and tissue subtype (Smedley *et al.* 2011).

Many recent retrospective studies have discussed the subjectivity, and therefore inaccuracy, of prognostic histologic evaluation. In a study of 122 canine melanocytic tumors, mitotic index and location, classical markers of malignancy, were not significantly correlated with survival time (Ramos-Vara *et al.* 2000). Another seminal study on the accuracy of prognosis found that only 59% of cases determined to be histologically malignant exhibited biological malignancy (metastases or recurrence). The same study also determined that 74% of tumors of "ambiguous location" (feet or lips) were reported malignant via histology, but only 38% of these demonstrated malignant behavior (Spangler and Kass 2006). Finally, of the 227 melanocytic skin lesions, predominantly thought to be benign, 39% were reported as histologically malignant, with 12% exhibiting malignant behavior (Spangler and Kass 2006). Another review of 278 cases of melanocytic lesions arising from the oral cavity, lip, haired skin, and nail bed found that individual histologic features, when evaluated alone, could not predict the biological outcome (Schultheiss 2006).

The ambiguity of some histologic evaluation has brought on the evaluation of other marker of malignancy to aid in diagnosis and prognosis of ambiguous tumors (Smedley *et al.* 2011). One of the most common prognostic markers is Melan-A, which showed a direct

correlation between staining and biologically benign tumor behavior (Koenig *et al.* 2001). Other markers include s100, TRP-1, TRP-2, and PNL-2 (Smedley *et al.* 2011). Of these only PNL-2 has been shown to have significant differences in expression between benign and malignant lesions (Giudice *et al.* 2010; Ramos-Vara and Miller 2011).

1.2.2 Treatment options

Unfortunately, treatment options for aggressive oral melanomas are limited. Most cases of canine malignant melanoma will develop metastatic disease resulting in death within eight to 24 months after diagnosis (Modiano, Ritt, and Wojcieszyn 1999). The most common treatment option is surgical excision of the mass. The extent of surgical margins is determined by the location of the tumor and size of the mass. Oral melanomas often require partial mandibulectomy or maxillectomy (Bergman 2007). Surgical excision encompassing wide margins of a primary tumor with no detectable metastatic disease results in a median survival time of three to 12 months (Modiano, Ritt, and Wojcieszyn 1999). More recent studies support this survival rate, reporting a stage I oral melanoma treated with surgery and radiation as having a mean survival time of 12 to 14 months (Bergman 2007). However, most survival rates are based on the level of primary tumor involvement. A primary stage I oral melanoma rostrally located, without bone involvement or microscopic disease, treated with radiation and some form of pre-irradiation surgical procedure carries an average survival time of 22 months (Proulx *et al.* 2003). For all stage III tumors that time drops to only three months.

Radiation therapy also plays a role in treatment when full surgical excision cannot be achieved or when metastasis has occurred or is likely. Most radiation therapy courses consist of fractions of three to four gray (Gy) given daily or every other day; however, melanomas have been observed to be resistant to smaller fractionations (Smith, Goldschmidt, and McManus 2002). To account for such resistance, larger doses of radiation of four to six Gy given weekly for a total dose of 24 to 35 Gy have been used. This schematic has shown complete remission rates of 53 to 69% (Proulx *et al.* 2003) and partial remission of 25 to 30% (Bergman and Wolchok 2008). However, even with initial remission, recurrence of the primary tumor or metastasis to distant organs was observed in all studies. Chemotherapy treatments are also often used, although numerous studies have shown significant resistance to chemotherapeutic agents. The most common agents used are carboplatin, which showed an overall response rate of 28% (Rassnick, Ruslander, and Cotter 2001), and cisplatin in conjunction with piroxicam, which showed an 18% response rate and a median survival time of five months (Boria, Murry, and Bennett 2004). Other traditional chemotherapeutics including doxorubicin, dacarbazine (DITC), and melphalan show limited response rates (Bergman 2007).

The fact that traditional chemotherapies and radiation therapies have been shown to be ineffective with more advanced disease suggests that the canonical pathways leading to regulated apoptosis within melanoma cells is altered in a way to avoid cell death due to these agents (Modiano, Ritt, and Wojcieszyn 1999). This is further supported by investigation into the functionality of these pathways in canine oral melanomas (described below). Additional types of therapies including immunogene therapy and xenogenic vaccines have been

developed to treat canine oral melanoma, but will not be discussed here (Bergman *et al.* 2006; Bergman and Wolchok 2008; von Euler *et al.* 2008; Bergman 2010; Finocchiaro and Glikin 2012; Westberg *et al.* 2013).

1.3 Molecular pathology of canine melanocytic lesions

There is limited knowledge on the initiation, development, or potential adjuvant targets of canine oral melanoma given that the molecular mechanisms related to pathogenesis have not been fully elucidated. There is also very limited molecular knowledge of the other canine melanocytic lesions, in particular malignant cutaneous melanoma, which is poorly understood and rarely studied. However, some molecular markers have been identified, which play a role in the pathogenesis of canine oral melanoma. Such markers not only act as prognostic makers for aggressive behavior, but also help elucidate the underlying mechanism of tumor development. Some of these proteins include: TP53, PTEN, RB-1, CDKN1A, CDKN2A, and VEGF (Modiano, Ritt, and Wojcieszyn 1999; Koenig *et al.* 2001; Koenig *et al.* 2002). An extensive study to evaluate the role of canonical tumor suppressors (discussed in detail in section 1.10.4) in the development of canine malignant melanoma, found that although *TP53* mRNA expression was unaltered, TP53 protein expression was decreased in 30% (n=9/30) of primary cases. When subcellular location could be determined, it was seen that in 78% (n=25/32) of cases TP53 was located in the cytoplasm and not the nucleus (Koenig *et al.* 2002). This suggests TP53 protein is non-functional and unable to monitor and inhibit cell cycle progression when DNA is damaged, causing proliferation of cells with aberrant DNA.

Similarly *CDKN1A*, which encodes the tumor suppressor p21/waf1, showed no decrease in mRNA expression but protein loss and improper subcellular localization in a third of cases (n=9/27). RB-1 protein showed normal expression and accumulation in the nucleus, suggesting it is not key in the pathogenesis of canine oral melanoma (Koenig *et al.* 2002). What was also interesting was that there was no difference between the benign and malignant lesions in terms of expression of these tumor suppressors. Of the tumor suppressors surveyed, those with the highest level of dysregulation were *PTEN* and *CDKN2A*. *CDKN2A*, mutated in 50% of all human melanomas, encodes the tumor suppressor p16/ink4A. Loss of expression of p16 product was seen in 72% (n=24/33) of cases and when present it was not localized to the nucleus. PTEN, which inhibits cellular proliferation, was decreased in 58% (n=20/34) of samples (Koenig *et al.* 2002).

Cell growth and dysregulation are also regulated through master transcription factors, especially c-MYC. Overexpression of c-MYC was seen in highly aggressive canine melanoma cells that readily metastasized to the lungs; however, the overepxression was not detected in non-metastatic cell lines (Ahern *et al.* 1993). However, other key cellular proliferation pathways such as the MAPK pathway (discussed in detail in section 1.10.3) have shown limited involvement. One such study assessed levels of c-KIT protein, a receptor tyrosine kinase which initiates the MAPK signaling cascade, in canine mucosal melanomas and showed decreased expression correlated with decreased survival time (Newman *et al.* 2011). This suggests that c-KIT production is decreased with malignancy; however, neither the molecular circumstances of this process, nor how it is directly involved in pathogenesis were assessed. A more recent assessment of c-KIT and its role in canine oral

melanoma showed that although 51% (n=20/39) of cases were positive for c-KIT protein, there was no significant difference between c-KIT expression and overall survival. Moreover, none of the samples surveyed showed any mutations of c-KIT exon 11, the most commonly mutated exon in human melanomas (Murakami *et al.* 2011). Other frequently mutated genes in the MAPK signally cascade are the three members of the RAS gene family. A study to assess the mutational frequency of the RAS family of kinases in canine oral melanoma found only 2 of 16 cases were positive for mutation in NRAS exon 1 (Mayr *et al.* 2003). An independent follow up study showed none of 11 tumors screened showed the characteristic mutations in any of the three RAS hotspot codons (Richter 2005). These data support the lack of molecular involvement in canine oral melanoma development.

One of the most common mutations affecting growth pattern in human cutaneous melanoma is in BRAF, a key member of the MAPK pathway. One mutational investigation assessed for presence of the BRAF V600E mutation in canine oral melanomas and found none of 17 cases evaluated showed the mutation. However, after growth factor starvation, the ERK signaling protein, found downstream of BRAF, was still over-phosphorylated. This suggests activation of the MAPK pathway, even in the absence of the BRAF V600E mutation, possibly by another activation mutation in BRAF (Shelly *et al.* 2005). One study assessed the expression of the melanin production enzyme tyrosinase (*TRY*), which is one downstream effector of the MAPK signaling cascade, confirmed that both canine oral melanomas and canine non-oral melanocytomas had a higher expression of the *TYR* gene (Phillips 2012). These results, partnered with the phosphorylative activation of ERK in canine oral melanomas, described above, suggest the MAPK pathway is being activated and

that the downstream effectors are contributing to the development of the disease; yet previous studies have not yet elucidated the mechanism by which activation is occurring. A main reason for this is that none have evaluated a significantly large population or the presence of mutations for the entire pathway within one individual. These studies were also limited in that they only assessed the most common activating mutations identified in human common cutaneous melanomas, which may not be directly biologically comparable to those mechanisms in canine melanoma.

1.4 Previous cytogenetic studies of canine oral melanoma

Little is known about the cytogenetic aberrations of canine melanomas as few studies have been performed specifically investigating the chromosome aberrations. In a review of chromosome aberrations in three canine oral melanomas, all were show to have different abnormal karyotypes. Hyperdiploidy was seen in two of the three cases, along with centric fusions, and many bi-armed chromosomes. The last case showed only one chromosomal abnormality, a fusion between chromosome 1 and 25 (Hörsting *et al.* 1999). Another study of chromosome aberration in a canine cutaneous melanoma showed hyperdiploidy in 50% of the cells, one isochromosome i(12), and again many bi-armed chromosomes (Mayr *et al.* 1992).

1.5 Canine as a model of human disease

There is a great deal of information being acquired on canine melanoma in many aspects; however, very few are considered comparative. The majority of veterinary

melanoma research is based purely on clinical perspective and only addresses limited comparative aspects. Similarly, a great deal of research goes into comparative oncology in general, but a limited amount is specifically aimed at melanoma.

Comparative medicine is defined as the parallel studies of human and animal populations, for the benefit of both (Baba and Câtoi 2007). It arose from the identification that diseases found in many animal species were similar in terms of development and symptoms. These diseases, including cancer, were then compared according to their causative factors between the different animal species and humans. Comparative studies of cancer, or comparative oncology, derived from the acknowledgment that there was much to gain in bringing together research efforts from both the basic and veterinary aspects of medicine. Comparative oncology has developed to include two branches of activity: spontaneous oncology and experimental oncology. For the purposes of this document, I will only focus on the principles of spontaneous comparative oncology.

Spontaneous comparative oncology studies aspects of carcinogenesis, epidemiology, diagnosis, and treatment of cancer in two or more species (Baba and Câtoi 2007). In-depth scientific research of spontaneous tumors has uncovered numerous conditions in which cancer development is common to both humans and animals including: nutrition, age, environmental factors, genetic predisposition, and tissue specific factors. Other common properties of the tumors themselves include cellular morphology and molecular and genetic characteristics. The most promising aspect of using canine disease as a model for humans is that, unlike mice or other laboratory models, dogs spontaneously develop cancer (Simpson *et al.* 2014). The problem with most mouse models is that to study cancer, one must first either

alter the natural genetic state of the animal to induce the disease or inject cultured cells into a new host environment. This can lead to inapplicable molecular changes and inappropriate cellular responses to treatments. Such studies in rodent models can miss underlying interactions of complex gene networks that can be responsible for or contribute to the development of cancers.

Another significant advantage canine models have over rodents is the shared genetics of dogs and humans. Dogs and humans share approximately 650Mb of ancestral DNA (Lindblad-Toh *et al.* 2005), which are not shared with mice (Rowell, McCarthy, and Alvarez 2011). Protein sequences within canine coding DNA are also more similar to human sequences, suggesting many aspects of human biology, disease processes, and the underlying genetic changes are more similar between dogs and humans than mice (Lindblad-Toh *et al.* 2005) (Lindblad-Toh *et al.* 2005; Khanna *et al.* 2006). Some of these same underlying genetics may also explain why dogs and humans share similar amounts of phenotypic diversity. It has been observed that in humans, certain ethic groups are much more likely to develop specific kinds of cancer (Network 2009). Similarly, specific canine breeds are much more predisposed to develop certain cancers (Dobson 2013). It is possible that the genetics responsible for such drastic phenotypic plasticity also enable specific disease processes, including cancer development, in a certain cell type. Dogs also share the same environment with humans and are therefore exposed to the same chemicals and elements as humans who develop cancer. This shared environment can be exploited for the benefit of epidemiological and toxicological investigations into the causation of tumorigenesis.

With specific reference to cancers of the skin; in dogs the incidence of tumor types as is follows, with highest incidence first: basal cell carcinomas, squamous cell carcinomas, perianal gland tumors, and melanomas (Hauck 2013). This incidence pattern is similar to what has been reported in human skin cancers. For both species, melanoma is not the most frequent of skin neoplasms, but is by far the most malignant. It has also been observed that there is significant overlap in the clinical and histopathological features of mucosal melanomas between canines and humans (Simpson *et al.* 2014). Both species also have both malignant and benign subtypes of melanocytic lesions. However, unlike canine melanomas human benign lesions often evolve into malignant lesions. Both canine and human mucosal melanomas (discussed in detail in section 1.10.3) show infrequent *BRAF*, *NRAS*, and *c-KIT* mutations (Simpson *et al.* 2014). Yet, both species present with molecular activation of the MAPK and AKT signaling pathways.

1.6 Melanocytic lesions in humans

More than one million cases of skin cancer will be diagnosed in the United States each year (WHO 2013). Approximately 80% of new skin cancers are acanthokaryocytomas, previously known as basal cell carcinoma, and 16% are squamous cell carcinomas. Malignant melanomas only account for approximately 5% of all human skin tumors, but are responsible for 60%-77% of skin cancer-related deaths (Abdulla *et al.* 2005). Currently, between two and three million non-melanoma skin cancers and 132,000 melanomas are diagnosed globally each year (WHO 2014). According to the American Cancer Society, roughly 76,690 new melanomas are diagnosed in the United States each year with over 9,480

melanoma related deaths (ACS 2013). Rates of melanomas vary greatly between ethnic groups, with an overall lifetime risk of developing melanoma of ~2% (1 in 50) for Caucasians, 0.1% (1 in1,000) for African Americans, and 0.5% (1 in 200) for Hispanics (SEER 2010). The trunk (chest and back) is the most common site for melanomas to occur in men, with legs being the most common site in women. There are two main categories of melanoma; familial melanomas that account for 8-12% of malignant melanomas (Hansson 2010), and spontaneous melanomas that develop in individuals with no family history of malignant melanoma. Spontaneous melanomas have numerous risk factors, including UV-radiation, presence of dysplastic nevi, and fair skin (Slingluff *et al.* 2011).

Spontaneous melanomas are further classified into subtypes based on visual growth patterns and environmental conditions. Growth pattern classifications are spitzoid malignant melanomas, lentigo maligna melanoma, nodular melanoma, acral lentiginous melanoma, and common cutaneous melanomas also called superficial spreading melanoma, which is further divided into chronic sun-exposed and non-chronic sun-exposed (Lange JR, Fecher LA, and WH 2008). The most frequent of these subtypes are common cutaneous melanomas (CCM) with an incidence of 20.8 per 100,000 (SEER 2010), which can develop on any epithelial surface. These lesions often present with variable pigmentation and histological presentation. Approximately 75% of primary lesions occur *de novo* (Bastian *et al.* 2003); however they can arise from a preexisting melanocytic nevus. Molecular markers have been identified that distinguish nevi from melanomas and a timeline of molecular mutations has been established for the progression of these lesions (discussed in detail in section 1.7). The second most common subtype of melanoma is nodular melanoma, which account for 15% of all

melanomas (Langley, Sober, and Fitzpatrick 1998). These tumors grow rapidly, but often do not proceed into the radial growth phase making them less likely to metastasize. Due to this tendency, nodular melanomas can be controlled easily with surgical excision (Clark, Elder, and Horn 1986).

Acral melanomas are much less frequent with an incidence of 0.18 per 100,000 (SEER 2010), representing about 2% to 10% of all melanomas, and are considerably more aggressive than CCM (Bradford *et al.* 2009). Acral melanomas are most common melanoma among Japanese, African Americans, Latin Americans, and Native Americans, accounting for ~50% of all melanomas in African Americans and fewer than 10% melanomas in Caucasians (Bastian *et al.* 2003). The most common location of melanoma in African Americans is the acral surfaces of the feet, with 60% of patients having plantar or subungual lesions of the toenail, generally arising from the nail matrix (Langley, Sober, and Fitzpatrick 1998). Desmoplastic melanomas are a rare subtype of melanoma that is locally aggressive and invades quickly into the surrounding dermal tissues. Due to the depth of invasion, a high rate of local recurrence is common. Approximately 50% of desmoplastic melanomas develop in association with a lentigo maligna melanoma, but no causal link has been found between the two subtypes (Langley, Sober, and Fitzpatrick 1998). Lentigo maligna melanomas, also known as melanoma *in situ*, are considered to be the least common subtype of melanoma. Lesions normally occur on chronically sun-damaged atrophic skin in the elderly and grow slowly for 5 to 15 years with less than 50% advancing to an invasive malignant stage (Albert, Fewkes, and Sober 1990). The lesions are usually quite large (3-

6cm or greater), but do not invade into the dermis and are rarely amelanotic (Smalberger, Siegel, and Khachemoune 2008).

Another uncommon and the least understood variant of melanoma in humans is mucosal melanoma. Lesions can occur on any mucosal surface, but usually develop on the mucosal surfaces of the head and neck (sinonasal and oral cavities), genital, or anorectal mucosa. Mucosal melanomas usually show highly aggressive behavior with poor prognosis (Hicks and Flaitz 2000), occuring to a greater extent in Asians and less frequently in Caucasians (Guo *et al.* 2011). Due to the location of these tumors they are often not diagnosed until they have progressed to an advanced stage. A definitive precursor lesion for mucosal melanoma has not yet been identified and there is no unified malignancy classification scheme currently in place specifically for mucosal melanomas (Pfister *et al.* 2012). Local recurrence occurs in 43.3% of cases, with an overall survival rate of only 17%. In a retrospective study of mucosal melanomas, the 1, 2, 3, and 5-year survival rates were 53.3%, 40%, 15% and 10%, respectively (McLean, Tighiouart, and Muller 2008).

About 70% of mucosal melanomas of the head and neck occur in the nasal cavity or paranasal sinus region, and about 25% develop in the oral cavity (Bachar *et al.* 2008). Mucosal melanomas of the oral cavity (OMM) represent 0.5% of all oral malignancies and 0.2-8.0% of all melanomas (Meleti *et al.* 2007). Most OMMs arise *de novo*; however, approximately 30% arise from areas of pigmentation within the oral cavity, which can persist for several months or even years prior to primary tumor development (Rapini *et al.* 1985). Patients often present with oral bleeding, a smooth or ulcerated pigmented mass, pain, and increased mobility of teeth (Tanaka *et al.* 2004). There are several histological subtypes of

benign melanocytic lesions of the oral mucosa, including mucosal melanosis, which results in macular hyperpigmentation. Nevi usually consist of junctional proliferation of melanocytes with or without cytological atypia (Rapini *et al.* 1985).

Five subtypes of OMM have been identified based on clinical appearance: pigmented nodular type, nonpigmented nodular type, pigmented macular type, pigmented mixed type, and nonpigmented mixed type (Tanaka *et al.* 2004). Like all mucosal melanomas, OMMs are usually discovered, and subsequently biopsied, at an advanced stage, which may contribute to the level of heterogeneity in microscopic patterns (Meleti *et al.* 2008). Histologic heterogeneity may also suggest differences in the molecular biology of tumor cells. Prognosis is poor, with a 5-year survival rate of approximately 15% (Meleti *et al.* 2007). In a review of clinical outcome with or without surgical excision, the 5-year survival rate was 35.3% in the surgery group, 15.4% in the non-surgery group. Distant metastasis was present in 64.7% (11/17) of the non-surgery group and 76.9% (10/13) of the surgery group (Tanaka *et al.* 2004). This suggests that while surgical excision of the primary lesion doubles the probability of a 5-year survival, it does little to inhibit the spread of the disease.

As with malignant melanomas, benign melanocytic lesions, or melanocytic nevi, have various subtypes: acquired melanocytic nevi, congenital melanocytic nevi, blue nevi, dysplastic nevi (or Clark's nevi), and Spitz nevi. Each of these subtypes has its own diagnostic criteria and carry their own prognosis. Although reports vary on the percentage of melanomas that directly develop from preexisting nevi, it is well established that presence of a benign nevi of any type is a risk factor for developing melanoma.

Acquired melanocytic nevi are benign proliferations of melanocytes that usually appear in early childhood or adolescence (Takata and Saida 2006). These lesions present with even pigmentation and smooth borders and are commonly found on sun-exposed sites. They are usually small, typically less than 1cm in circumference (often < 6mm) (LeLeux 2013). Congenital melanocyti nevi are lesions present at birth and are classified by their size. Small congenital nevi are less than 1.5cm in diameter, medium-sized nevi are between 1.5 and 20cm, and giant nevi are larger than 20cm in diameter (Tannous *et al.* 2005). Giant nevi are often surrounded by several smaller satellite nevi (Schwartz 2013). Occasionally, nevi called congenital nevus tardive will develop during the first two years of life that are histologically identical to congenital nevi (Clemmensen and Kroon 1988). Four different histological patterns of secondary proliferations found within congenital nevi have been described: masses resembling superficial spreading melanomas; masses resembling nodular melanomas; masses described as "proliferative neurocristic hamartoma," in which various neural or mesenchymal differentiate cells have invaded deep in the dermis or subcutaneous epithelium; and true melanomas (Clark, Elder, and Guerry 1990).

Dysplastic nevi, also known as Clark's nevi, are benign lesions with clinically atypical features (Takata and Saida 2006) that account for up to 30% of all pigmented lesions (Torres-Cabala *et al.* 2010). These lesions are acquired and can develop at any location and at any time during a person's lifetime; however, they are most prevalent in patients younger than 40 years (Naeyaert and Brochez 2003). Dysplastic melanocytic nevi present with a slightly elevated or papular section surrounded by a smooth or macular region with irregular, ill-defined borders, variable tan to dark brown pigmentation, and an erythematous base

(Friedman *et al.* 2009). The final subtype of benign melanocytic lesions is the Spitz nevi. Spitz nevi are small lesions usually seen in children or young adults. Histologically, they can resemble their malignant counterpart, Spitzoid melanomas, which can make diagnosis and prognosis difficult (Takata and Saida 2006).

Gene mutations are also found in benign melanocytic lesions. *BRAF* point mutations were found to be common in acquired nevi, congenital nevi, and dysplastic nevi (Pollock *et al.* 2002). This is suggestive that the *BRAF*-activating SNP is in fact a driving mutation that is required for melanoma development in these subtypes. However, melanomas cannot develop from these benign *BRAF*-mutated lesions until a second mutation arises that allows for melanocytes to proliferate without undergoing cellular contact inhibition and consequent cellular senescence (Takata and Saida 2006). *NRAS* mutations have also been seen in acquired nevi, congenital nevi, and dysplastic nevi, though at a lower frequency. Few chromosome aberrations are present in benign lesions. The only two subtypes with reported chromosome abnormalities are Spitz nevi, with a copy number gain of HSA 11p, and giant congenital nevus, which have been observed with various aberrations (Takata and Saida 2006). A more in-depth review of cytogenetic changes in both melanoma and melanocytic nevi is discussed in section 1.8.

1.7 Histological diagnostic and prognostic characteristics of human melanomas

Clinical staging of melanomas is critical to determining treatment and estimating biological outcome. The primary means of diagnosis and prognosis of human melanomas is based on the American Joint Committee on Cancers (AJCC) standardized criteria (AJCC

2010). Extensive texts have been assembled on the histopathology associated with diagnosis and prognosis of melanomas in humans; reviewed in (Massi and LeBoit 2014). In summary, initial melanoma staging was based on size and thickness of the primary tumor and metastases to either the lymph nodes or distant organs, also known as the TMN model. With the advancement of melanoma research and clinical technologies, a revised system of staging was developed by the AJCC to include not only size and presence of metastases, but also histologic and biological markers; reviewed in (Balch *et al.* 2009).

Prognostic markers of malignant melanoma now include: Breslow thickness, ulceration, mitotic rate, micro- and macro-metastases, blood serum LDH levels, angiotropism, and epithelial tropism (Balch *et al.* 2009; Bandarchi *et al.* 2010). Histologic factors associated with an improved prognosis include lesions located on the extremities and histologically negative lymph nodes. Histologic factors associated with a worsened prognosis include: increased tumor thickness, deeper level of dermal invasion, increased mitotic rate, ulceration, diminished lymphoid response in primary tumor, vascular invasion, and polygonal tissue morphology (Bandarchi *et al.* 2010). A review of the effectiveness of these criteria found substantial reproducibility between pathologists suggesting the validity of using a histopathology based classification system. They found the highest reproducibility in Breslow thickness (intraclass correlation coefficient (ICC) $p=0.984$), mitotic rate (ICC $p=0.833$), and ulceration (kappa statistic=0.823) (Niebling *et al.* 2013).

Immunohistochemistry is widely utilized during diagnosis of human melanomas. The three most common antibodies in standard use for melanoma diagnosis are s100, Melan-A, and HMB-45 (Kucher *et al.* 2006). A study on the specificity and sensitivity of these

antigens revealed Melan-A to be the most effective for clinical settings (Jing, Michael, and Theoharis 2013). Although numerous histologic criteria are used in diagnosis, no one single characteristic is sufficient to establish a differential diagnosis, much like canine malignant melanomas. Therefore, differentiating between benign pigmented lesions and melanoma may be difficult and lead to ambiguity in both diagnosis and prognosis (Shoo, Sagebiel, and Kashani-Sabet 2010).

1.8 Molecular cytogenetics in diagnostics and prognostics in human melanomas

Diagnosis by histopathology alone can lead to misdiagnosis in ambiguous cases, such as amelanotic melanomas or differentiating between malignant and benign lesions. As such, the use of unique cytogenetic aberrations as diagnostic markers has been developed to increase the accuracy and effectiveness of diagnosis of melanomas in human medicine. One of the very first cytogenetics papers to investigate the role of chromosome aberrations in melanomas found that tumors bearing structural abnormalities had significantly shorter survival times (Trent *et al.* 1990). This began the investigation into what role chromosome aberrations may play in the pathogenesis of melanomas, but also into use as a diagnostic tool. The use of molecular cytogenetics in melanoma has been thoroughly reviewed (Gerami and Busam 2012). One of the primary uses of cytogenetics is in determination of benign from malignant melanocytic lesions. Comparative genomic hybridization (CGH) analysis revealed that 96% of all melanomas have on average seven copy number aberrations, which are absent the majority of benign nevi (Bastian *et al.* 2003). Congenital nevi have been observed with few chromosomal aberrations, when present typically appear as an aneuploidy of an entire

chromosome (Bastian *et al.* 2002). This is unlike most malignant melanomas, which contain aberrations of chromosome fragments or targeted loci. Exclusion of malignancy based on unique aberrations found in benign lesions has also been demonstrated. For example, copy number gain of HSA 11p is only seen in Spitz nevi and is not seen in any other melanoma or melanocytic subtype (Bauer and Bastian 2006). This suggests that identification of cytogenetic patterns may be useful as a tool in distinguishing benign from malignant melanocytic lesions.

Cytogenetics has also revealed the genetic heterogeneity within different subtypes of melanoma. A seminal paper investigating whole chromosome aberrations in all histological subtypes of melanomas observed that melanomas from different locations and environmental factors have distinguishing patterns of chromosome aberrations (Curtin *et al.* 2005). This was true not only for spontaneous melanomas, but also those that developed from preexisting benign lesions. When melanomas did arise from such benign lesions, such as congenital nevi, they showed aberrations found in no other subtype (Bastian *et al.* 2002). The diversity in chromosomal aberrations within subtypes of melanomas indicates that the underlying genetic causation of each subtype may differ and therefore therapeutic targets may differ as well (Bauer and Bastian 2006).

Such differences have allowed for diagnostic tests to be developed to distinguish melanocytic lesions for clinical benefit. The first study to do so used an identified set of regions on HSA 6p25 (RREB1), 6q23 (MYB), 11q13 (CCDN1), and the centromeric region of HSA6. Using fluorescent *in situ* hybridization (FISH), they found a high level of sensitivity (87%) and specificity (95%) in diagnosis of malignant melanoma (Gerami, Jewell,

and Morrison 2009). A later study of 22 melanocytic lesions, including 12 histologically ambiguous cases, used a set of four fluorescent probes at HSA 6p25, 6q23, 11q13, and centromeric region of HSA6 to distinguish malignant from benign lesions. They found only 60% sensitivity and 50% specificity in correlating FISH results to clinical behavior (Gaiser *et al.* 2010). A review of studies using the same set of FISH probes showed varying levels of sensitivity and specificity, suggesting the need for identification of appropriate tumor candidates to be evaluated and rigid standards on marking FISH results (Song *et al.* 2011).

Cytogenetics can also help determine amelanotic melanomas from other non-melanocytic skin cancers, such as clear cell sarcomas (Blokx, van Dijk, and Ruiter 2010). This is especially true in cases where an unequivocal diagnosis could not be determined by either traditional histology or immunohistochemistry. Melanocytic lesions in which such diagnostic difficulties are common include: Spitz nevi; recurrent melanocytic nevi; lesions of acral, genital, or mammary origin; lesions located on highly irritated surfaces of the skin; and proliferative nodules of congenital nevi (Bauer and Bastian 2006). Inappropriate diagnosis can impede proper patient care in terms of prognosis and treatment regimes. A review of two cases where CGH was able to provide additional clinically relevant diagnostic information to histologically ambiguous cases prove that cytogenetics has a place beyond basic epidemiological research (Bauer and Bastian 2006).

The classic uses of cytogenetic studies are for the identification of target loci for understanding the development of tumors and identify novel targetable genes (Bauer and Bastian 2006). Numerous regions and loci of interest have been identified using whole genome and targeted copy number studies (Matsuta *et al.* 1997; Curtin *et al.* 2005; Bauer and

Bastian 2006; Moore *et al.* 2008). This can help determine activated oncogenes within particular cancer or cancer subtype, which can then be targeted for therapeutic drug development. Finally, cytogenetics can reveal what is different about various subtypes of melanocytic lesions, but also what they have in common. Such similarities may be suggestive of an underlying mechanism of tumor development that is essential for melanocyte transformation. One such aberration that has been found in all melanocytic lesions is a copy number gain of 11q13 (*CCND1*) (Bastian *et al.* 2003). Such amplifications can lead to increased expression of the functional protein (Sauter *et al.* 2002; Spivey *et al.* 2012). Gene dysregulations, caused by gene amplification, can have important biological effects on tumorigenesis and, when inhibited, can lead to tumor reduction or even ablation.

1.9 Molecular and genetic dysregulation in human mucosal melanomas

Much of what is known about mucosal melanomas was discovered as part of large comparative studies to other more common subtypes of melanomas. As such, little is known about the underlying genetic and cytogenomic changes that occur in human mucosal melanomas. One of the first papers to investigate the genetics changes that accompany different subtypes of melanoma found that mucosal melanomas shared few genetic aberrations with the most common UV-induced cutaneous melanomas (Curtin *et al.* 2005). Other studies have shown that many of the underlying mutations found in cutaneous melanomas, often single point mutations in cellular growth-related genes, such as *BRAF* and *NRAS*, are not or rarely present in the mucosal subtype (Wong *et al.* 2005; Buery *et al.* 2011; Furney *et al.* 2013). A study investigating protein expression of oncogenes in oral mucosal

melanomas found CCND1 expression in greater than 30% of cells in 60% of cases, and no overexpression of CDK4 in any oral mucosal melanoma cases (Hsieh *et al.* 2013). The same study also found a complete loss of p16 protein in 50% of cases and a loss of phosphorylated RB-1 in 70% of cases. However, these alterations within the CDKN2A and MAPK pathway were found in disparate points within the tumor population, suggesting no one essential mutation within the cohort.

Alterations to other canonical pathways have also been studied in mucosal melanomas. An early study into the role of tumor suppressors in mucosal melanomas found a correlation of loss of protein expression of p53, RB-1, and p16 with tumor aggression (Tanaka *et al.* 2001). A later investigation into the expression cell cycle regulators, p16, p27, p21, and CCND1 via immunohistochemistry found mucosal nevi had high expression of p16 and p27, with little to no expression of p21 or CCND1. Expression in oral melanomas was inverse to that of nevi, with moderate expression of p21 and CCND1 and low to no expression of p16 and p27 (de Andrade *et al.* 2012). Another study further investigated the role of tumor suppressors p16, p53, and bcl-2, in mucosal melanomas of the head and neck. Expression of p16, p53, and bcl-2 proteins was observed in 25%, 21%, and 74% of tumors, respectively. Expression levels were then correlated with biological aggression; expression of bcl-2 was associated with better survival, loss of p16 was seen with tumor progression, and aberrant p53 expression was frequent in undifferentiated tumor cells. However, expression of these markers did not correlate with necrosis, vascular, or deep tissue invasion (Prasad *et al.* 2012). Together, these studies suggest a likely role of loss of expression of

tumor suppressors, such as p16, RB-1, and p53, in the initial tumorigenesis of mucosal melanomas.

One of the most well-characterized set of mutations in mucosal melanomas are point mutations found in the *c-KIT* gene sequence; reviewed by Blokx and colleauges. They found that out of nine studies, *c-KIT* was mutated in 15-22% of mucosal melanomas. This percentage was higher than in both UV damaged and non-UV damaged cutaneous melanomas. They also found that the *c-KIT* containing region of HSA chromosomes 4, 4q12-13, had a copy number amplification in mucosal melanomas (Blokx, van Dijk, and Ruiter 2010). A more recent study found *c-KIT* mutations in 7-35% of mucosal melanomas based on location (Omholt *et al.* 2011). They also showed *c-KIT* transcript amplification in 19% of cases, which correlated with *c-KIT* mutation status ($p < 0.001$). They also found overexpression of p-ERK and p-AKT, markers of activation of the MAPK and PI3K/AKT pathways, respectively. However, pathway activation was not correlated with *c-KIT*, *RAS*, or *BRAF* mutation, suggesting an alternate mechanism of activation (Omholt *et al.* 2011). An investigation into c-KIT protein expression with mutation status found high levels of c-KIT expression in most cases and missense mutations in 22% of cases; however, mutations status was associated with increased protein expression in only two cases (Rivera *et al.* 2008).

A study of how c-KIT activation in mucosal melanomas compares to those of other subtypes found that mucosal melanomas were the second most common subtype to carry a *c-KIT* mutation, with the most common being acral melanomas. Almost all the *c-KIT* mutations observed were predicted to be sensitive to c-KIT kinase inhibitory drugs. The same study also reviewed *NRAS* and *BRA*F mutations and found mutations present in 25%

and 0% of mucosal melanomas respectively, and saw there was no overlap with the presence of a *c-KIT* mutation. Targeted copy number aberrations for the *c-KIT* loci were investigated and saw increased *c-KIT* copy number in 26.3% of mucosal melanomas. Interestingly it was also found that CD117 expression, the protein encoded by *c-KIT*, did not correlate with either *c-KIT* mutation status or *c-KIT* copy number (Beadling *et al*. 2008).

Unique patterns of chromosome aberrations, as well as targeted gene mutations, have been observed in different tumor types. CGH analysis of 14 nasopharyngeal mucosal melanomas showed copy number gains of HSA 1q, 6p, and 8q (van Dijk *et al.* 2003). A later study recapitulated the finding from the earlier study, but also identified other regions of recurrent copy number aberrations in mucosal melanomas including amplification of HSA 11q13, 4q12, and 12q14, which contain *CCND1*, *C-KIT*, and *CDK4* respectively (Curtin *et al.* 2005). Such targeted loci amplifications are suggestive that these genes may be involved in the pathogenesis of mucosal melanomas.

1.10 Molecular pathways in cancer and melanoma development

Like the histological classifications, the molecular pathways that are involved in the development of melanomas are complex and differ greatly with location and cellular phenotype. The most common form of melanoma, common cutaneous melanoma (CCM), has the most well-understood molecular pathway involvement. Numerous mutations within several cellular pathways have been linked to the initiation and progression of melanocytic lesions, leading to the development of targeted therapeutics. Numerous extensive reviews have been compiled on the molecular changes during melanoma development (Curtin *et al.*

2005; Curtin *et al.* 2006; Bandarchi *et al.* 2010; Blokx, van Dijk, and Ruiter 2010; Bandarchi *et al.* 2013). A brief summary of the involvement of particular cellular pathways is presented below.

1.10.1 Cell cycle regulation

Cell cycle progression is carefully regulated by a group of proteins called cyclin-dependent kinases (CDK) and their regulatory-binding partners, known as cell cyclins. Not only are these proteins responsible for initiating cell division, but also halting cell cycle in response to DNA damage and to allow time for repair of DNA damage or defects in the mitotic structure. There are two groups of catalytic subunits, which are phylogenetically distinct from each other (Matsushime *et al.* 1992). CDK1 and CDK2, which are responsible for the G_1 to S phase and S to M phase transitions of the cell cycle, are members of the canonical CDK family. CDK4 and CDK6, which are key in the G_0 to G_1 transition are considered atypical CDKs. Each group has its own specificity for binding partners, which helps tightly regulate activation and cell progression. In normal cell proliferation, extracellular cues, such as growth factors, stimulate expression of cyclins that initiate cellular division. However, when the regulation of cyclin expression or CDK activation is altered, cells can spontaneously proliferate or divide with insufficient genomic integrity or stability (Musgrove *et al.* 2011).

One of the first discovered and most well-studied of the cyclins is Cyclin-D1 (CCND1). The primary function of CCND1, as well as all of the D-type cyclins, is to promote cell proliferation (Malumbres and Barbacid 2009). This function is mediated

through the binding of CCND1 to its catalytic partners CDK4 and CDK6 that activates the catalytic subunit of CDK4 and CDK6, which in turn phosphorylates cell cycle inhibitor RB-1 (Weinberg 1995). RB-1 phosphorylation promotes E2F transcription factor to begin the DNA replication process of cell division (Chen, Tsai, and Leone 2009). CCND1-CDK4 binding has other catalytic cellular functions including proliferation and differentiation of specific cell types via transcription factors like SMAD3, GATA4, and members of the RUNX and MEF2 gene families (Musgrove *et al.* 2011). CCND1-CDK4 activation has also been shown to regulate BRCA-1, which helps in DNA damage repair to maintain genomic stability (Kehn *et al.* 2007). CDK4 and CDK6 have also been shown to have catalytic function in cell mobility, cell adhesion, and cytoskeletal remodeling (Zhong *et al.* 2010). Cells with decreased or no expression of CCND1 have shown reduced migration ability; however, this is dependent on the ability of CCDN1 to activate CDK4 and CDK6 (Musgrove *et al.* 2011). Therefore, an overexpression or inappropriate activation of the CCDN1-CDK4/6 complex can not only lead to increased cell proliferation, replication of cells with aberrant DNA, but also increase cellular motility allowing for metastasis of tumor cells (Vizkeleti *et al.* 2012).

CDK4 and its regulatory substrate, CCND1, have been shown to be dysregulated in melanoma cells (Wolfel *et al.* 1995; Vizkeleti *et al.* 2012). One common way in which this complex is activated is through targeted gene amplification of the gene regions or gene products. This is most commonly seen in acral melanomas (Curtin *et al.* 2005). Such amplification are found not only in malignant acral melanomas (Bastian *et al.* 2000), but also in very early lesions (Ishihara *et al.* 2006). This, like BRAF mutations found in benign

lesions, is suggestive that amplifications might be an initiating mutation in the development of this melanoma subtype.

1.10.2 Mitotic regulation

After the cell cycle has been initiated and DNA has been replicated, chromosomes must be paired and separated. This task is highly complex and is regulated through a series of kinase proteins. The function of these proteins has been thoroughly; reviewed by both Bayliss and colleagues (Bayliss *et al.* 2012) and Hoi Tang and Poon (Hoi Tang and Poon 2011). In summary, the main regulatory event is phosphorylation that peaks at specific times and locations during mitosis. Phosphorylation then alters the cell's shape, intracellular structure, protein interaction, and biochemistry. These changes allow for duplicated chromosomes to be segregated, a function carried out by mitotic spindles regulated through microtubules and protein attachments (Bayliss *et al.* 2012). The fidelity of chromosome segregation is ensured by spindle assembly checkpoints (SACs). Mitotic events require precise coordination, which involves large numbers of proteins and accurate activation of each protein through phosphorylation. Phosphorylation events are regulated through several families of protein kinases each with their own unique function including Auroras, cyclin-dependent kinases (CDKs), polo-like kinases (PLKs), NEKs, and Mps1/TTK as seen in Figure 1.1. Each of these kinases is briefly reviewed below.

The cyclin-dependent kinases have been described above for their role in cell cycle initiation and DNA replication. However, a different set of CDKs and their regulators, cell cyclins, are involved in mitotic division. The main CDK involved in mitotic regulation is

CDK1, which is at its highest level of activation during mitosis by the binding of CCNB1. Levels and location of CCNB1 fluctuate during the cell cycle, with levels of CDK1 remaining relatively stable within the nucleus (Hoi Tang and Poon 2011). CCNB1 is primarily located within the cytoplasm during interphase and then translocates to the nucleus during mitotic entry.

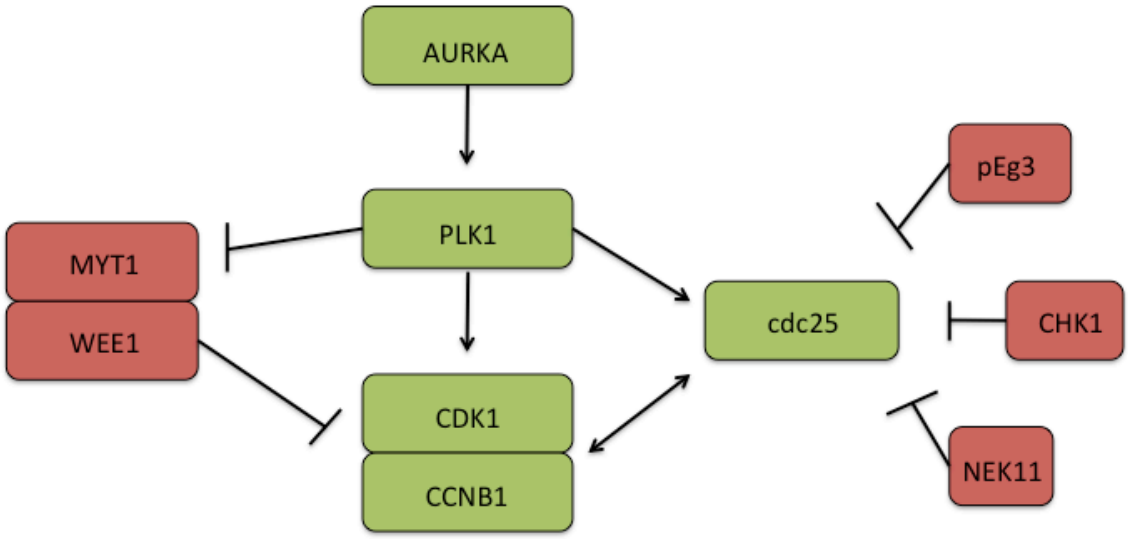

Figure 1.1 Kinase pathway involved in mitotic initiation. Schematic of protein interactions involved in mitotic initiation. Adapted from Tang and Poon, 2011.

CDK1/CCNB1 complex activation initiates cellular mitosis through regulating chromosome condensation, nuclear envelope breakdown, and spindle formation and assembly (Enserink and Kolodner 2010). CDK1 is activated though the dephosporylation of Thr14 and Tyr15 by phosphatase Cdc25 (Takizawa and Morgan 2000). CDK1 also activated another of the mitotic kinases, PLK1, which will be discussed in more detail later. PLK1 and CKD1 are part of an activation feedback loop involving MYT1 and WEE1, inhibitors of

mitosis (Hoi Tang and Poon 2011). CDK1 is inhibited by the presence of MYT1 and WEE1; however, both of these can too be inhibited by expression of PLK1 allowing for the activation of CKD1. During anaphase, CCNB1 is ubiquitinated by the anaphase-promoting complex/cyclosome (APC/C) and marked for destruction allowing for mitotic exit (Bayliss *et al.* 2012).

PLK1 is a kinase that functions primarily to control centromere maturation, spindle attachment, chromosome segregation, and cytokinesis (Hoi Tang and Poon 2011). Like cyclins, PLK1 levels vary during the cell cycle. Expression of PLK1 is highest in late G2, where it functions in the regulation of CDK1/CCNB1 activity (Bayliss *et al.* 2012) as mentioned above. The localization of PLK1 is also a key regulator of its function. As it phosphorylates its targets directly, PLK1 must be co-localized with both structural and protein targets. During mitosis, PLK1 is located at the centrosome during prophase and metaphase and then dissociates during cell separation; however, a fraction does remain at the spindle-binding site during anaphase. Phosphorylation of PLK1, and subsequent activity, is highest between metaphase and anaphase. PLK1 is activated through phosphorylation by upstream kinase Aurora-A (Archambault and Carmena 2012).

The Aurora kinases (AURKA and AURKB) each have their own distinct function during mitosis. AURKA associates with the centrosome and function to help regulate entry into mitosis, centrosome maturation, mitotic spindle assembly, and activation of microtubule-associated proteins such as TACC3 (Bayliss *et al.* 2012). Activation of AURKA requires the binding of several cofactors, which causes autophosphorylation of the proteins (Hoi Tang and Poon 2011). AURKB is part of the chromosome passenger complex and functions in the

chromosome-microtubule interaction, sister chromatid cohesion, and cytokinesis (Hoi Tang and Poon 2011). AURKB is also a key member of the spindle assembly checkpoint, which helps control irregular chromosome division into daughter cells (Bayliss *et al.* 2012).

TTK kinase (also known as monopolar spindle 1, MPS1) is an essential component of the spindle assembly checkpoint and is required for normal segregation of chromosomes during mitosis (Hoi Tang and Poon 2011). TTK regulates the duplication of the spindle pole body, which is a functional equivalent of the centrosome (Liu and Winey 2012). TTK is required for proper chromosome alignment and segregation (Bayliss *et al.* 2012). Due to its function in chromosome segregation, it has been shown that high levels of TTK contribute to the ability of cells to tolerate aneuploidy and chromosomal structural aberrations (Daniel *et al.* 2011). This may be due to the fact that TTK also functions to recruit other members of the spindle assembly checkpoint complex including MAD1, MAD2, BUB1, BUBR1, and BUB3 (Bayliss *et al.* 2012).

The dysregulation of each member of the mitotic kinase pathway can lead to irregular cell divisions, as mentioned in the case of TTK. PLK1 activity can act toward the bypass of the DNA damage checkpoint, as it has been shown to regulate p53 protein stability thorough its phosphorylation of the TOPORS region, leading to p53 degradation (Hoi Tang and Poon 2011). Therefore, an overexpression of PLK1 could lead to a decreased in p53 activity. Aurora kinases have been shown to be overexpressed in numerous cancer types (Li and Li 2006) and correlated with chromosomal instability and clinically aggressive disease (Katayama, Brinkley, and Sen 2003). Aurora B has been shown to be highly expressed in metastatic melanoma cells, independent of BRAF mutation (Bonet *et al.* 2012). As each of

these has been shown to be dysregulated in different types of cancer, targeted drugs have been developed to be used as therapeutic treatments in the clinic, which is reviewed by Schmidt and Bastian (Schmidt and Bastians 2007).

1.10.3 Cellular growth and differentiation

The mitogen-activated protein kinase (MAPK) signaling pathways have been shown to play a key role in the transduction of extracellular signals to cellular responses including proliferation, differentiation, and transformation. There are three main MAPK pathways; extracellular signal-regulated kinase (ERK), Jun kinase (JNK/SAPK) and p38 MAPK (Kim and Choi 2010). Each pathway contains at least three enzymes a MAPK kinase kinase, a MAPK kinase, and a MAP kinase. Here I will focus on the ERK pathway as seen in Figure 1.2.

The Raf-MEK-ERK kinase pathway represents one of the most well-characterized MAPK signaling pathways. The pathway starts with the signaling activation of a tyrosine kinase receptor (RTK), including EGFR, FGFR, PDGFR, and SCFGR. The V-kit Hardy-Zuckerman 4 feline sarcoma viral oncogene homolog (*c-KIT),* which codes for the RTK mast/stem cell growth factor receptor (SCGFR), also known as CD117, has been established as essential for proper normal melanocyte development and migration (Giebel and Spritz 1990; Uong and Zon 2010; Sommer 2011; O'Reilly-Pol and Johnson 2013). However, the role of *c-KIT* in malignant transformation and melanogenesis is not as clearly understood. Early studies in human cutaneous melanoma cell lines expressing *c-KIT* mRNA showed *c-KIT* was not constitutively activated and *c-KIT* ligand did not induce a cellular response or

proliferation (Funasaka *et al.* 1992). However, many more recent studies have shown that over-activation of *c-KIT* is essential to development of acral and mucosal melanomas, but is less common in UV-induced cutaneous melanomas (Curtin *et al.* 2005; Curtin *et al.* 2006) (Beadling *et al.* 2008; Uong and Zon 2010), suggesting the involvement of this gene is dependent on the location of the primary tumor development.

Regardless of which RTK is involved at the initiation of the MAPK pathway, phosphorylation of the tyrosine residues leads to binding of an intermediary docking protein, such as GRB2, at an SH2 domain. This docking then binds to a guanine nucleotide exchange factor (GEF), such as SOS, by way of the two SH3 domains located on the docking protein (Schulze et al, 2005). Activation of the GEF catalyzes the removal of a GDP from a member of the RAS subfamily (most notably N-RAS or K-RAS), allowing the Ras member to bind GTP and become activated (Zarich *et al.* 2006). An activated RAS protein begins the start of kinase phosphorylation cascade. RAS phosphorylates a serine/threonine-selective protein kinase from the Raf kinase family (most notably BRAF) (Avruch J 2001). The Raf kinase will then phosphorylate either MEK1 or MEK2, MAPK kinases. These then phosphorylate the final member of the cascade – a MAP kinase, either ERK1 or ERK2. Finally, phosphorylated ERK will translocate to the nucleus and activate different transcription factors, including *ELK-1*, *Sap-1a*, *Ets1*, *c-MYC*, *Tal,* and *FOXO3A* (Seger and Krebs 1995; Satzger *et al.* 2008; Kim and Choi 2010; Cargnello and Roux 2011). By altering the levels and activities of transcription factors, MAPK leads to altered transcription of genes that are important for proliferation, differentiation, migration, and cell cycle progression (McCubrey *et al.* 2007).

Within common cutaneous melanomas (CCM), the most critical mutation is an activating mutation to the tyrosine kinase v-Raf murine sarcoma viral oncogene homolog B1 (*BRAF*), which affects cellular growth. This mutation is found in 65% of all CCM and the most frequent mutation is a single nucleotide polymorphism (SNP) that causes an amino acid shift from a valine to a glutamate at codon 600. This V600E mutation accounts for 95% of all *BRAF* mutations (Davies *et al.* 2002). The shift from valine to glutamate transforms the conformation of the *BRAF* protein into one that mimics the phosphorylated active state. This in turn causes constitutive activation of the *BRAF* kinase and the ERK-MAPK signaling cascade. The *BRAF* activation has been shown to be an essential early mutation during tumorigenesis, often found in benign precursor melanocytic lesions.

Other members of this cascade can also be mutated to have constitutive activation of their kinase activity, including *N-RAS*, which is activated in 20% of both CMM and mucosal melanomas (Curtin *et al.* 2005; Wong *et al.* 2005). The majority of mutations within the *N-RAS* gene are missense mutations that introduce an amino acid substitution at positions 12, 13, or 61 (Ball et al, 1994). Activating mutations of both *N-RAS* and *BRAF* have been found in both precursor melanocytic nevi and malignant melanomas (Bandarchi *et al.* 2010), suggesting their role and initiating mutations. Upstream mutations within this pathway can also occur. Mutations to *c-KIT* have been seen in both acral and mucosal subtypes of melanoma, 20% and 15% respectively (Beadling *et al.* 2008), tumor types that usually possess wild type sequence for both *NRAS* and *BRAF*. An activating mutation within exon 11 of the juxtamembrane domain of *c-KIT* results in an amino acid substitution at position 559 in *c-KIT*, from a valine (V) to an alanine (A). This results in the increased kinase

activity of *c-KIT* via autophosphorylation without ligand binding (Growney *et al.* 2005). The tumorigenic cellular response caused by such activations have long latency periods due to their ability to cause cellular senescence in vivo, which is why alone such mutations are not sufficient to cause malignant transformation (Swick and Maize 2012). The tumors must accumulate additional genetic mutations that can overcome cellular senescence for tumor progression to occur.

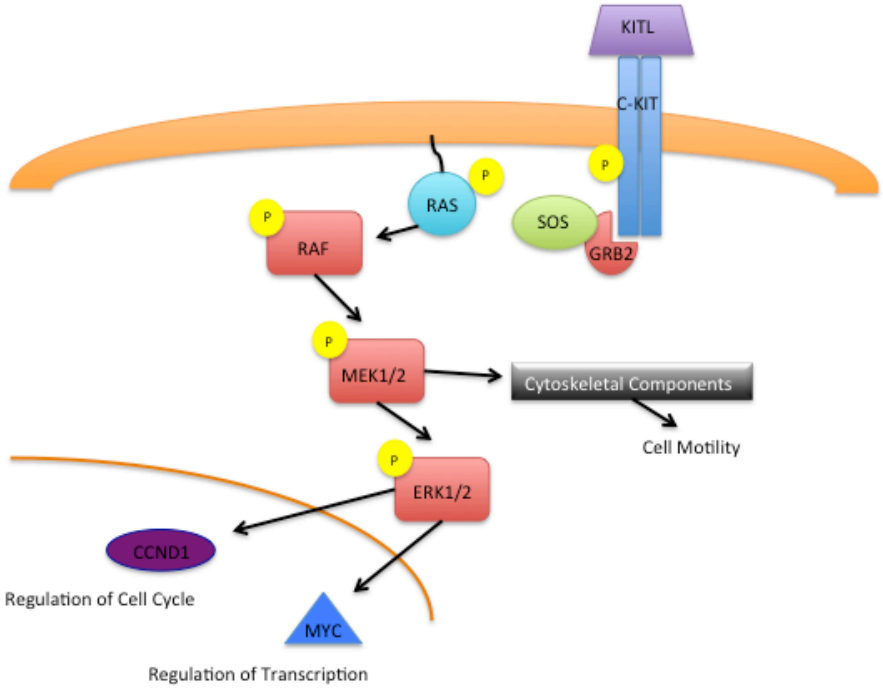

Figure 1.2 Schematic of the MAP-Kinase pathway. Schematic of the MAP-Kinase pathway involved in tumorigenesis and melanoma development, adapted from (Inamdar, Madhunapantula, and Robertson 2010).

Another way tumors can activate the MAPK pathway is through copy number aberrations, leading to increased gene dosage. CMM have been shown to have increased copy number of the 7q region, the chromosome region containing the BRAF gene sequence (Bastian *et al.* 2003). Increased copy number of *c-KIT* is seen in 30% of acral and 25% of mucosal melanomas, but was less common (5%) among cutaneous melanomas. However, this did not correlate with CD117 expression (Beadling *et al.* 2008).

An additional mechanism that is dysregulated during melanogenesis is the interaction between mature melanocytes and the surrounding keratinocytes. As mentioned previously, normal melanocytes interact with keratinocytes through E-cadherin, normally expressed in epithelial cells (Uong and Zon 2010). Melanoma development is marked by the loss of proper E-cadherin function and by the appearance of melanoma cell adhesion molecules. Loss of function of E-cadherin is thought to contribute to progression in cancer by increasing proliferation, invasion, and/or metastasis (Han *et al.* 2013). The loss of the E-cadherin attachments in normal melanocytes are then replaced by N-cadherin bridges, expressed in neuronally derived cells, between melanoma cells (Uong and Zon 2010). This marks a regression of the melanocyte from a mature differentiated epithelia cell to a state in which it regains dedifferentiated neuronal like characteristics of melanocytic precursors.

1.10.4 Tumor suppressors

The most common secondary mutations in CMM are a functional loss of *TP53*, *PTEN*, or *CDKN2A,* which encodes the tumor suppressor proteins (Swick and Maize 2012).

Tumor suppressors are proteins that inhibit or prevent cell cycle progression, proliferation, and lead to apoptosis. TP53 is a small DNA binding protein that helps maintain DNA integrity and promotes apoptosis in cells with DNA damage. TP53 functions by modulating cell cycle arrest, apoptosis, senescence, DNA repair, or changes in metabolism by regulating the expression of target genes. TP53 targets include *RB-1*, *BAX*, *FAS*, *CCNG1*, and *CDKN1A* (Menendez, Inga, and Resnick 2009; Freeman and Espinosa 2012). Point mutations caused by UV-damage often inactivates TP53 activity, leading to unchecked replication of mutated DNA. In cases of human melanoma with mutated DNA, TP53 will accumulate in the cytoplasm, unable to enter the nucleus (Stretch *et al.* 1991; Lassam, From, and Kahn 1993; Kanoko *et al.* 1996).

One molecular target of TP53 is *CDKN1A*, which encodes p21/waf1 protein (Li *et al.* 1994). The protein p21/waf1 is a member of proteins called the cyclin-dependent kinase inhibitors (CDKI), and is considered a universal CDKI, as it can inhibit any of the cyclin-dependent kinases responsible for progression through any stage of the cell cycle (Xiong *et al.* 1993). Expression of p21/waf1 inhibitor is regulated by TP53 activity. In cells with damaged DNA, TP53 becomes activated, which leads to the expression of p21/waf1 to halt the cell cycle until the DNA can be repaired (Macleod *et al.* 1995). Another member of this family of proteins is p16/ink4a, which is encoded by the gene *CDKN2A*. The protein p16/ink4a is more specific in that it only inhibits CDK4 and CDK6, proteins essential to the G1/S phase transition (Wolfel *et al.* 1995; Serrano 1997). Loss of either p21/waf1 or p16/ink4a can lead to uncontrolled cellular proliferation due to unchecked cell cycle progression. Germline mutations of *CDKN2A* are seen in 25% of familial melanomas

(Satyamoorthy and Herlyn 2003), but are infrequent in sporadic melanomas (Fujimoto *et al.* 1999). Mutations of this locus are most common in highly aggressive tumors or melanoma metastases (Maelandsmo *et al.* 1996).

Another key tumor suppressor that is often mutated in melanoma and other cancers is phosphatase and tensin homologue deleted in from chromosome ten, PTEN. PTEN has two major biological abilities as a lipid and protein phosphatase. The lipid phosphatase ability of PTEN functions in the cell to inhibit AKT activation via PI3K and stimulating apoptotic signals (Wu, Goel, and Haluska 2003). PI3K is a downstream effector of RAS, independent of the canonical MAPK signaling cascade, and triggers a second pathway that also ends in cyclin-D activation and cell proliferation (Swick and Maize 2012). PTEN also functions as a protein phosphatase to inhibit focal adhesion, cell spreading and migration, and MAPK pathway signaling. A recent study investigated alternate functions of PTEN and found that disruption of normal PTEN function leads to extensive centromere breakage and chromosomal translocations (Shen *et al.* 2007). They observed that PTEN localized at centromeres and co-localized with CENP-C, an integral component of the kinetochore. PTEN with mutations of the C-terminal were seen to no longer associate with centromeres and cause centromeric instability. Furthermore, cells lacking any PTEN expression exhibited spontaneous DNA double-strand breaks (Shen *et al.* 2007).

Mutations of PTEN are observed in 40-50% (Mishra *et al.* 2010) of melanomas often with increased levels of invasion (Takata and Saida 2006), which links to the inhibition of the protein phosphatase function leading to increased cell spreading. PTEN has been shown to be mutated via loss of heterozygosity of the PTEN locus in 30-50% of melanomas

(Robertson *et al.* 1999; Stahl *et al.* 2003), by somatic mutation in 10% of melanomas (Guldberg *et al.* 1997; Birck *et al.* 2000), and loss of protein expression in 20% of melanomas (Goel *et al.* 2006). Wu and colleauges (Wu, Goel, and Haluska 2003) review a full list of reported mutation of PTEN in melanomas.

1.10.5 Drug resistance

The ATP-binding cassette (ABC) family of proteins transport numerous molecules across the cell membrane. ABC pumps are located within the plasma membrane on either the apical or basolateral surface of polarized cells and transport of molecules occurs in an ATP-dependent manner (Schinkel and Jonker 2003). There are three major sub-families of ABC proteins based on their biochemical structures. Members of the ABC protein family have been indicated in many disease processes as well as being identified as a major mechanism of resistance to chemotoxic agents (Bandarchi *et al.* 2013). ABC proteins have also been indicated in the progression and aggressive nature of human melanoma (Heimerl *et al.* 2007). While these proteins have been shown to be integral to the chemoresistance pathway of many human cancers, their role in canine cancers has yet to be fully elucidated.

ABCB1 gene encodes one of the most studied of these proteins, p-glycoprotein (P-gp), also known as multi-drug resistance gene 1 (MDR1). P-gp is located on the apical surface of the plasma membrane, with an intracellular ATP binding site and a heavily glycosylated extracellular loop (Hipfner, Deeley, and Cole 1999). P-gp can export a diverse range of substrates including numerous chemotherapeutic agents such as doxorubicin and mitoxantrone. However, all of P-gp's substrates tend to be organic, uncharged, hydrophobic,

and amphipathic. For transport to occur, substrates must first insert into the inner "hemi-leaflet" structure of the cell membrane. Only substrates that are amphipathic can insert in this fashion, explaining why this property is common to most P-gp substrates.

P-gp is mainly present in epithelial cells; however, high levels of P-gp expression are also found in luminal membranes of endothelial cells (Schinkel 1997). Studies have shown high levels of expression on the apical membranes of the lungs and intestines (Thiebaut *et al.* 1987). This can cause faster clearance of drugs, limit the bioavailability of orally administered drugs, and obstruct delivery of drugs to important sites of metastasis (Sparreboom *et al.* 1997). Oral bioavailability is an important parameter for the practical use of many drugs, and directed inhibition of P-gp might improve oral bioavailability of P-gp substrate drugs (Wacher, Wu, and Benet 1995). Targeted inhibition of P-gp function may also improve effectiveness of chemotherapeutic agents in treating cells that have metastasized to distant organs. Inhibition of P-gp has been extensively investigated with promising results (Mayer *et al.* 1997; Hendrikse *et al.* 1998; Polli *et al.* 2001). The main focus of most inhibition is the use of competitive inhibitors that allow highly diffusible drugs to enter the cells, and slow the rate of export of the desired drug by P-gp.

The *ABCC1* gene encodes the first member of the multi-drug resistance protein family, multi-resistance protein one (MRP1). MRP1 acts as a transporter or cotransporter with P-gp for numerous drugs (Cole *et al.* 1992). Located on the basolateral side of epithelial cells, MRP1 exports molecules toward the basolateral membrane boundary (Evers *et al.* 1996). It has both hydrophobic and hydrophilic regions and can effectively export organic anions, non-anions, and hydrophobic drugs (Cole *et al.* 1994; Hooijberg *et al.* 1999).

However, the export of non-anions and hydrophobic drugs is dependent on the supply of glucuronic acid (GSH), which binds to these drugs and acts as a conjugated export partner (Leier *et al.* 1994). Although it is located on the basolateral side, MRP1 has been shown to have important pharmacological function. Knockout mice with a complete loss of function of MRP1 were more sensitive to the toxicity of intravenously administered etoposide, a chemotherapeutic drug used to treat various cancers (Wijnholds *et al.* 1997). Importantly for oral melanoma, sensitivity was localized to the oropharyngeal mucosal layer of cells (Wijnholds *et al.* 1998). This can be partially explained by the natural expression of MRP1 in these cells, which acts to protect the cells from blood-borne toxins by epithelia that have the basolateral membrane facing the blood circulation.

The last of the major ABC pumps to be discovered was breast cancer resistance protein (BCRP), which is encoded by the gene *ABCG2*. It was first discovered in a breast cancer cell line (Doyle *et al.* 1998), from which it gets its name, but has been shown to be overexpressed in numerous other cancer types. BCRP is a smaller export protein and has been shown to act as a homodimer (Schinkel and Jonker 2003). When murine Bcrp1, a homologue of BCRP, was expressed in polarized canine epithelial cell lines, drug export was mediated through the apical surface, indicating that Bcrp1 localizes to the apical membrane in polarized cells (Jonker *et al.* 2000). BCRP can cause resistance to various types of chemotherapeutic agents via ATP-hydrolysis (Honjo *et al.* 2001), such as mitoxantrone. Cisplatin, a common chemotherapeutic drug used in canine oral melanoma treatment, is not a substrate of BCRP. Another drug that was first thought to be a substrate of BCRP was doxorubicin (Doyle *et al.* 1998). However, the first description of doxorubicin as being a

substrate of BCRP was done using an *ABCG2* clone isolated from a cancer cell line. When sequencing of the gene was done it was shown that the clone had an activating point mutation, R482T to R482G, which allowed for both mitoxantrone and doxorubicin to be exported (Honjo *et al.* 2001). Subsequent studies using a wild-type (WT) clone of *ABCG2*, showed that doxorubicin is not a substrate for WT BCRP (Honjo *et al.* 2001). Another mechanism of over-activation of this gene product in cancers is through targeted amplification of the gene loci (Allen *et al.* 1999).

1.11 Thesis outline

Canine oral melanoma (COM) represents a significant clinical problem in the veterinary medical community due to its aggressive nature and the inefficiency of current treatments. Similarly, mucosal melanoma in human patients, although rare, is highly aggressive and carries a high mortality rate. Currently, there is limited understanding into the mechanism of development of mucosal melanomas. Previous lines of research have established that various subtypes of melanomas, based on either location or environmental exposure, are different at both the cytogenetic and gene expression levels. There are also limited treatment options, as only the traditional cancer managements are applicable in the treatment of mucosal melanomas. There is also a benefit to using the dog as a model organism, in the direct benefits to veterinary patients, but also in translation of research finding to human patients as well.

The first goal of this project was to identify if mucosal melanoma was the same at the genetic level in humans and canines, and to identify regions of aberration that may play a

role in the development of mucosal melanoma. Investigation into whole genome cytogenetic aberrations present in COM had not been performed previously. With this data, a profile of COM could be established for the purpose of identification of diagnostic loci and molecular targets for deeper understanding into the mechanism of disease development. It would also establish the basis of further investigation into mechanisms of dysregulation during mucosal melanoma tumorigenesis. Furthermore, no direct comparison of whole-genome aberrations in canine and human mucosal melanomas has been previously performed. This comparison would establish the validity of using the dog as a cytogenetic model for human mucosal melanomas.

The next goal was to investigate functional aspects of mucosal melanoma tumor progression. Previous studies into gene dysregulation in mucosal melanomas have focused on genes identified in human cutaneous melanomas. While many of these genes fall within important cancer pathways, there is limited comparative value between mucosal and cutaneous melanoma subtypes. Whole transcriptome analysis of canine oral melanomas, which has not been previously performed, was carried out to identify gene expression changes that may be involved in tumor development. Using this approach, we aim to identify previously overlooked pathways of tumorigenesis and by better understanding mechanism of tumor development, lay the foundation for development of targeted therapies.

Finally, we wanted to investigate why current therapies are not effective in the treatment of canine oral melanoma. Canine oral melanomas are known to be resistant to most chemotherapies. However, the mechanism of this resistance has yet to be identified. If a particular mechanism of resistance is identified, there is potential for developing protocols

to identify patients who will respond to additional therapies. Identification of specific targets also allows for the investigation of directed inhibition therapies to increase the effectiveness of treatments in patients. The aim of this research will be to benefit clinical care of both veterinary and human patients from diagnosis to therapeutics.

REFERENCES

Abdulla, F. R., Feldman, S. R., Williford, P. M.*, et al.* (2005). "Tanning and skin cancer." Pediatric Dermatology **22**(6): 501-512.

ACS. (2013). "Melanoma Skin Cancer." from http://www.cancer.org/acs/groups/cid/documents/webcontent/003120-pdf.pdf.

Ahern, T., Bird, R., Bird, A.*, et al.* (1993). "Overexpression of c-erbB-2 and c-myc but not c-ras, in canine melanoma cell lines, is associated with metastatic potential in nude mice." Anticancer Res **13**(5A): 1365-1371.

AJCC (2010). Melanoma of the skin. AJCC Cancer Staging Manual. New York**:** 325-344.
Albert, L., Fewkes, J. and Sober, A. (1990). "Metastatic lentigo maligna melanoma." J Dermatol Surg Oncol **16**: 56-58.

Allen, J. D., Brinkhuis, R. F., Wijnholds, J.*, et al.* (1999). "The mouse Bcrp/Mxr/Abcp gene: amplification and over- expression in cell lines selected for resistance to topotecan, mitoxantrone, or doxorubicin." Cancer Res **59**: 4237– 4241.

Archambault, V. and Carmena, M. (2012). "Polo-like kinase-activating kinases: Aurora A, Aurora B and what else?" Cell Cycle **11**(8): 1490-1495.

Avruch J, K. A., Kyriakis JM, Luo Z, Tzivion G, Vavvas D, Zhang XF. (2001). "Ras activation of the Raf kinase: tyrosine kinase recruitment of the MAP kinase cascade." Recent Prog Horm Res **56**: 127-155.

Baba, A. and Câtoi, C. (2007). Comparative Oncology., The Publishing House of the Romanian Academy.

Bachar, G., Loh, K. S., O'Sullivan, B.*, et al.* (2008). "Mucosal melanomas of the head and neck: The Princess Margaret Hospital experience." Head and Neak **30**(10): 1325-1331.

Balch, C. M., Gershenwald, J. E., Soong, S. J.*, et al.* (2009). "Final version of 2009 AJCC melanoma staging and classification." J Clin Oncol **27**(36): 6199-6206.

Bandarchi, B., Ma, L., Navab, R.*, et al.* (2010). "From Melanocyte to Metastatic Malignant Melanoma." Dermatology Research and Practice **2010**: 1-8.

Bandarchi, B., Jabbari, C. A., Vedadi, A.*, et al.* (2013). "Molecular biology of normal melanocytes and melanoma cells." J Clin Pathol **66**(8): 644-648.

Bastian, B. C., Kashani-Sabet, M., Hamm, H.*, et al.* (2000). "Gene amplifications characterize acral melanoma and permit the detection of occult tumor cells in the surrounding skin." Cancer research **60**(7): 1968-1973.

Bastian, B. C., Xiong, J., Frieden, I. J.*, et al.* (2002). "Genetic changes in neoplasms arising in congenital melanocytic nevi: differences between nodular proliferations and melanomas." The American journal of pathology **161**(4): 1163-1169.

Bastian, B. C., Olshen, A. B., LeBoit, P. E.*, et al.* (2003). "Classifying Melanocytic Tumors Based on DNA Copy Number Changes." The American Journal of Pathology **163**(5): 1765-1770.

Bauer, J. and Bastian, B. C. (2006). "Distinguishing melanocytic nevi from melanoma by DNA copy number changes: comparative genomic hybridization as a research and diagnostic tool." Dermatologic Therapy **19**: 40-49.

Bayliss, R., Fry, A., Haq, T.*, et al.* (2012). "On the molecular mechanisms of mitotic kinase activation." Open Biol **2**(11): 120136.

Beadling, C., Jacobson-Dunlop, E., Hodi, F. S.*, et al.* (2008). "KIT gene mutations and copy number in melanoma subtypes." Clin Cancer Res **14**(21): 6821-6828.

Bergman, P. (2007). "Canine Oral Melanoma." Clinical Techniques in Small Animal Practice **22**(2): 55-60.

Bergman, P. J., Camps-Palau, M. A., McKnight, J. A.*, et al.* (2006). "Development of a xenogeneic DNA vaccine program for canine malignant melanoma at the Animal Medical Center." Vaccine **24**(21): 4582-4585.

Bergman, P. J. and Wolchok, J. D. (2008). "Of Mice and Men (and Dogs): development of a xenogeneic DNA vaccine for canine oral malignant melanoma." Cancer Therapy **6**: 817-826.
Bergman, P. J. (2010). "Cancer Immunotherapy." Veterinary Clinics of North America: Small Animal Practice **40**(3): 507-518.

Birck, A., Ahrenkiel, V., Zeuthen, J.*, et al.* (2000). "Mutation and allelic loss of the PTEN/MMAC1 gene in primary and metastatic melanoma biopsies." Journal of investigative dermatology **114**(2): 277-280.

Blokx, W. A., van Dijk, M. C. and Ruiter, D. J. (2010). "Molecular cytogenetics of cutaneous melanocytic lesions - diagnostic, prognostic and therapeutic aspects." Histopathology **56**(1): 121-132.

Bonet, C., Giuliano, S., Ohanna, M.*, et al.* (2012). "Aurora B is regulated by the mitogen-activated protein kinase/extracellular signal-regulated kinase (MAPK/ERK) signaling pathway and is a valuable potential target in melanoma cells." J Biol Chem **287**(35): 29887-29898.

Boria, P., Murry, D. and Bennett, P. (2004). "Evaluation of cisplatin combined with piroxicam for the treatment of oral malignant melanoma and oral squamous cell carcinoma in dogs." J Am Vet Med Assoc **224**(3): 288-294.

Bostock, D. (1979). "Prognosis after surgical excision of canine melanomas." Vet Pathol **16**(1): 32-40.

Bradford, P., Goldstein, A., McMaster, M.*, et al.* (2009). "Acral lentiginous melanoma: incidence and survival patterns in the United States, 1986-2005." Arch Dermatol **145**(4): 427-434.

Buery, R. R., Siar, C. H., Katase, N.*, et al.* (2011). "NRAS and BRAF mutation frequency in primary oral mucosal melanoma." Oncol Rep **26**(4): 783-787.

Busam, K., Chen, Y., Old, L.*, et al.* (1998). "Expression of melan-A (MART1) in benign melanocytic nevi and primary cutaneous malignant melanoma." Am J Surg Pathol **22**(8): 976-982.

Cano, A., Pérez-Moreno, M., Rodrigo, I.*, et al.* (2000). "The transcription factor snail controls epithelial-mesenchymal transitions by repressing E-cadherin expression." Nat Cell Biol **2**(2): 76-83.

Cargnello, M. and Roux, P. P. (2011). "Activation and function of the MAPKs and their substrates, the MAPK-activated protein kinases." Microbiol Mol Biol Rev **75**(1): 50-83.

Chen, H.-Z., Tsai, S.-Y. and Leone, G. (2009). "Emerging roles of E2Fs in cancer: an exit from cell cycle control." Nature Reviews Cancer **9**(11): 785-797.

Clark, W. H., Elder, D. E. and Horn, M. V. (1986). "The biologic forms of malignant melanoma." Human Pathology **17**(5): 443-450.

Clark, W. H., Elder, D. E. and Guerry, D. (1990). Dysplastic nevi and malignant melanoma. Pathology of the Skin. E. R. Farmer and A. F. Hood. New York, McGraw-Hill**:** 729-735.

Clemmensen, O. J. and Kroon, S. (1988). "The histology of "congenital features" in early acquired melanocytic nevi." Journal of the American Academy of Dermatology **19**(4): 742-746.

Cole, S. P. C., Bhardway, G., Gerlach, J. H.*, et al.* (1992). "Overexpression of a transporter gene in a multidrug-resistant human lung cancer cell line." Science **258**: 1650-1654.

Cole, S. P. C., Sparks, K. E., Fraser, K.*, et al.* (1994). "Pharmacological characterization of multidrug resistant MRP-transfected human tumor cells." Cancer Res **54**: 5902-5910.

Curtin, J. A., Fridlyand, J., Kageshita, T.*, et al.* (2005). "Distinct Sets of Genetic Alterations in Melanoma " New England Journal of Medicine **353**(20): 2135-2147.

Curtin, J. A., Busam, K., Pinkel, D.*, et al.* (2006). "Somatic Activation of KIT in Distinct Subtypes of Melanoma." Journal of Clinical Oncology **24**(26): 4340-4346.

Daniel, J., Coulter, J., Woo, J. H.*, et al.* (2011). "High levels of the Mps1 checkpoint protein are protective of aneuploidy in breast cancer cells." Proc Natl Acad Sci U S A **108**(13): 5384-5389.

Davies, H., Bignell, G. R., Cox, C.*, et al.* (2002). "Mutations of the BRAF gene in human cancer." Nature **417**(6892): 949-954.

de Andrade, B. A., Leon, J. E., Carlos, R.*, et al.* (2012). "Immunohistochemical expression of p16, p21, p27 and cyclin D1 in oral nevi and melanoma." Head Neck Pathol **6**(3): 297-304.

Dobson, J. M. (2013). "Breed-predispositions to cancer in pedigree dogs." ISRN Vet Sci **2013**: 941275.

Doyle, L. A., Yang, W., Abruzzo, L. V.*, et al.* (1998). "A multidrug resistance transporter from human MCF-7 breast cancer cells." Proc Natl Acad Sci U S A **95**: 15665–15670.
Enserink, J. M. and Kolodner, R. D. (2010). "An overview of Cdk1-controlled targets and processes." Cell Div **5**: 11.

Evers, R., Zaman, G. J. R., Deemter, L. v.*, et al.* (1996). "Basolateral localization and export activity of the human multidrug resistance-associated protein (MRP) in polarized pig kidney cells." J. Clin. Invest. **97**: 1211-1218.

Finocchiaro, L. and Glikin, G. (2012). "Cytokine-enhanced vaccine and suicide gene therapy as surgery adjuvant treatments for spontaneous canine melanoma: 9 years of follow-up." Cancer gene therapy **19**(12): 852-861.

Freeman, J. A. and Espinosa, J. M. (2012). "The impact of post-transcriptional regulation in the p53 network." Briefings in functional genomics: els058.

Friedman, R. J., Farber, M. J., Warycha, M. A.*, et al.* (2009). "The "dysplastic" nevus." Clin Dermatol **27**(1): 103-115.

Fujimoto, A., Morita, R., Hatta, N.*, et al.* (1999). "p16INK4a inactivation is not frequent in uncultured sporadic primary cutaneous melanoma." Oncogene **18**(15): 2527-2532.

Funasaka, Y., Boulton, T., Cobb, M.*, et al.* (1992). "c-Kit-kinase induces a cascade of protein tyrosine phosphorylation in normal human melanocytes in response to mast cell growth factor and stimulates mitogen-activated protein kinase but is down-regulated in melanomas." Molecular biology of the cell **3**(2): 197-209.

Furney, S. J., Turajlic, S., Stamp, G.*, et al.* (2013). "Genome sequencing of mucosal melanomas reveals that they are driven by distinct mechanisms from cutaneous melanoma." J Pathol **230**(3): 261-269.

Gaiser, T., Kutzner, H., Palmedo, G.*, et al.* (2010). "Classifying ambiguous melanocytic lesions with FISH and correlation with clinical long-term follow up." Modern Pathology **23**(3): 413-419.

Gerami, P., Jewell, S. S. and Morrison, L. E. (2009). "Fluorescene *in situ* hybridization (FISH) as an ancillary diagnostic tool in the diagnosis of melanoma." American Journal of Surgical Pathology **33**: 1146-1156.

Gerami, P. and Busam, K. (2012). "Cytogenetic and mutational analyses of melanocytic tumors." Dermatol Clin **30**(4): 555-566.

Giebel, L. B. and Spritz, R. A. (1990). "The Molecular Basis of Type I (Tyrosinase−Deficient) Human Oculocutaneous Albinism." Pigment Cell Research **3**(S2): 101-106.

Giudice, C., Ceciliani, F., Rondena, M.*, et al.* (2010). "Immunohistochemical investigation of PNL2 reactivity of canine melanocytic neoplasms and comparison with Melan A." J Vet Diagn Invest **22**(3): 389-394.

Goel, V. K., Lazar, A. J., Warneke, C. L.*, et al.* (2006). "Examination of mutations in BRAF, NRAS, and PTEN in primary cutaneous melanoma." J Invest Dermatol **126**(1): 154-160.

Goldschmidt, M. H. and Shofer, F. S. (2005). "Benign Melanocytic Tumors." OncoLink, from http://www.oncolink.org/types/article.cfm?c=623&id=9518.

Growney, J. D., Clark, J. J., Adelsperger, J.*, et al.* (2005). "Activation mutations of human c-KIT resistant to imatinib mesylate are sensitive to the tyrosine kinase inhibitor PKC412." Blood **106**(2): 721-724.

Guldberg, P., thor Straten, P., Birck, A.*, et al.* (1997). "Disruption of the MMAC1/PTEN gene by deletion or mutation is a frequent event in malignant melanoma." Cancer research **57**(17): 3660-3663.

Guo, J., Si, L., Kong, Y.*, et al.* (2011). "Phase II, Open-Label, Single-Arm Trial of Imatinib Mesylate in Patients With Metastatic Melanoma Harboring c-Kit Mutation or Amplification." Journal of Clinical Oncology **29**(21): 2904-2909.

Han, J. I., Kim, Y., Kim, D. Y.*, et al.* (2013). "Alteration in E-cadherin/beta-catenin expression in canine melanotic tumors." Vet Pathol **50**(2): 274-280.

Hansson, J. (2010). "Familial cutaneous melanoma." Adv Exp Med Biol **685**: 134-145.
Hauck, M. (2013). Tumors of the Skin and Subcutaneous Tissues. Small Animal Clinical Oncology. S. J. Withrow, Elsevier**:** 305-320.

Heimerl, S., Bosserhoff, A. K., Langmann, T.*, et al.* (2007). "Mapping ATP-binding cassette transporter gene expression profiles in melanocytes and melanoma cells." Melanoma Research **17**(5): 265-273.

Hendrikse, N. H., Schinkel, A. H., Vries, E. G. E. D.*, et al.* (1998). "Complete in vivo reversal of P-glycoprotein pump function in the blood-brain barrier visualized with positron emission tomography." British Journal of Pharmacology **124**: 1413-1418.

Henry, C., Brewer, W., Whitley, E.*, et al.* (2005). "Canine digital tumors: a veterinary cooperative oncology group retrospective study of 64 dogs." J Vet Intern Med **19**(5): 720-724.

Hicks, M. J. and Flaitz, C. M. (2000). "Oral mucosal melanomas: epidemiology and patholobiology." Oral Oncol **36**(2): 152-162.

Hipfner, D., Deeley, R. and Cole, S. (1999). "Structural, mechanistic and clinical aspects of MRP1." Biochem Biophys Acta **1461**: 359-376.

Hirobe, T. (2011). "How are proliferation and differentiation of melanocytes regulated." Pigment Cell Melanoma Res **24**(3): 462-478.

Hoi Tang, M. and Poon, R. (2011). "How protein kinases co-ordinate mitosis in animal cells." Biochem J **435**: 17-31.

Honjo, Y., Hrycyna, C. A., Robey, R. W.*, et al.* (2001). "Acquired mutations in the MXR/BCRP/ABCP gene alter substrate specificity in MXR/BCRP/ABCP-overexpressing cells." Cancer Res **61**: 6635–6639

Hooijberg, J. H., Broxterman, H. J., Kool, M.*, et al.* (1999). "Antifolate resistance mediated by the multidrug resistance proteins MRP1 and MRP2." Cancer Res **59**: 2532-2535.

Hörsting, N., Wohlsein, P., Reimann, N.*, et al.* (1999). "Cytogenetic analysis of three oropharyngeal malignant melanomas in dogs." Research in Veterinary Science **67**(2): 149-151.

Hsieh, R., Nico, M., Coutinho-Camillo, C.*, et al.* (2013). "The CDKN2A and MAP Kinase Pathways: Molecular Roads to Primary Oral Mucosal Melanoma." Am J Dermatopathol **35**(2): 167-175.

Inamdar, G. S., Madhunapantula, S. V. and Robertson, G. P. (2010). "Targeting the MAPK pathway in melanoma: Why some approaches succeed and other fail." Biochemical Pharmacology **80**(5): 624-637.

Ishihara, Y., Saida, T., Miyazaki, A.*, et al.* (2006). "Early acral melanoma *in situ*: correlation between the parallel ridge pattern on dermoscopy and microscopic features." The American journal of dermatopathology **28**(1): 21-27.

Jing, X., Michael, C. W. and Theoharis, C. G. (2013). "The use of immunocytochemical study in the cytologic diagnosis of melanoma: evaluation of three antibodies." Diagn Cytopathol **41**(2): 126-130.

Jonker, J. W., Smit, J. W., Brinkhuis, R. F.*, et al.* (2000). "Role of breast cancer resistance protein in the bioavailability and fetal penetration of topotecan." J. Natl. Cancer Inst. **92**: 1651 – 1656.

Jungbluth, A., Busam, K., Gerald, W.*, et al.* (1998). "A103: An anti-melan-a monoclonal antibody for the detection of malignant melanoma in paraffin-embedded tissues." Am J Surg Pathol **22**(5): 595-602.

Kanoko, M., Ueda, M., Nagano, T.*, et al.* (1996). "Expression of p53 protein in melanoma progression." Journal of dermatological science **12**(2): 97-103.

Katayama, H., Brinkley, W. R. and Sen, S. (2003). "The Aurora kinases: role in cell transformation and tumorigenesis." Cancer Metastasis Review **22**(4): 451-464.

Kehn, K., Berro, R., Alhaj, A.*, et al.* (2007). "Functional consequences of cyclin D1/BRCA1 interaction in breast cancer cells." Oncogene **26**(35): 5060-5069.

Khanna, C., Lindblad-Toh, K., Vail, D.*, et al.* (2006). "The dog as a cancer model." Nat Biotechnol **24**(9): 1065-1066.

Kim, E. K. and Choi, E. J. (2010). "Pathological roles of MAPK signaling pathways in human diseases." Biochim Biophys Acta **1802**(4): 396-405.

Koenig, A., Wojcieszyn, J., Weeks, B. R.*, et al.* (2001). "Expression of S100a, Vimentin, NSE, and Melan A/MART-1 in Seven Canine Melanoma Cell Lines and Twenty-nine Retrospective Cases of Canine Melanoma." Veterinary Pathology **38**(4): 427-435.

Koenig, A., Bianco, S. R., Fosmire, S.*, et al.* (2002). "Expression and Significance of p53, Rb, p21/waf-1, p16/ink-4a, and PTEN Tumor Suppressors in Canine Melanoma." Veterinary Pathology **39**(4): 458-472.

Kucher, C., Zhang, P. J., Acs, G.*, et al.* (2006). "Can Melan-A replace S-100 and HMB-45 in the evaluation of sentinel lymph nodes from patients with malignant melanoma?" Applied Immunohistochemistry & Molecular Morphology **14**(3): 324-327.

Lange JR, Fecher LA and WH, S. (2008). Melanoma. Abeloff's Clinical Oncology. Abeloff MD, Armitage JO, Niederhuber JE, Kastan MB and M. WG. Philadelphia, Pa, Elsevier**:** 1229-1252.

Langley, R., Sober, A. and Fitzpatrick, T. (1998). Clinical Characteristics. Cutaneous Melanoma. C. M. Balch, H. AN and A. J. Sober. St. Louis, MO, Quality Medical Publishing**:** 82-101.

Lassam, N., From, L. and Kahn, H. (1993). "Overexpression of p53 is a late event in the development of malignant melanoma." Cancer research **53**(10): 2235-2238.

Leier, I., Jedlitschky, G., Buchholz, U.*, et al.* (1994). "The MRP gene encodes an ATP-depen- dent export pump for leukotriene C4 and structurally related conjugates." J. Biol. Chem. **269**: 27807-27810.

LeLeux, L. (2013). "Pathology of Benign Melanocytic Nevi " MedScape, 2014, from http://emedicine.medscape.com/article/1962932-overview - aw2aab6b5.

Li, J. J. and Li, S. A. (2006). "Mitotic kinases: the key to duplication, segregation, and cytokinesis errors, chromosomal instability, and oncogenesis." Pharmacology & therapeutics **111**(3): 974-984.

Li, Y., Jenkins, C. W., Nichols, M. A.*, et al.* (1994). "Cell cycle expression and p53 regulation of the cyclin-dependent kinase inhibitor p21." Oncogene **9**(8): 2261-2268.

Lindblad-Toh, K., Wade, C. M., Mikkelsen, T. S.*, et al.* (2005). "Genome sequence, comparative analysis and haplotype structure of the domestic dog." Nature **438**(7069): 803-819.

Liu, X. and Winey, M. (2012). "The MPS1 family of protein kinases." Annu Rev Biochem **81**: 561-585.

Macleod, K. F., Sherry, N., Hannon, G.*, et al.* (1995). "p53-dependent and independent expression of p21 during cell growth, differentiation, and DNA damage." Genes & Development **9**(8): 935-944.

Maelandsmo, G., Flørenes, V., Hovig, E.*, et al.* (1996). "Involvement of the pRb/p16/cdk4/cyclin D1 pathway in the tumorigenesis of sporadic malignant melanomas." British journal of cancer **73**(8): 909.

Malumbres, M. and Barbacid, M. (2009). "Cell cycle, CDKs and cancer: a changing paradigm." Nature Reviews Cancer **9**(3): 153-166.

Marino, D., Matthiesen, D., Stefanacci, J.*, et al.* (1995). "Evaluation of dogs with digit masses: 117 cases (1981-1991)." J Am Vet Med Assoc **207**(6): 726-728.

Massi, G. and LeBoit, P. E. (2014). Histological Diagnosis of Nevi and Melanoma, Springer-Verlag.

Matsushime, H., Ewen, M. E., Strom, D. K.*, et al.* (1992). "Identification and properties of an atypical catalytic subunit (p34< sup> PSK-J3</sup>/cdk4) for mammalian D type G1 cyclins." Cell **71**(2): 323-334.

Matsuta, M., Imamura, Y., Matsuta, M.*, et al.* (1997). "Detection of numerical chromosomal aberrations in malignant melanomas using fluorescence *in situ* hybridization." Journal of cutaneous pathology **24**(4): 201-205.

Mayer, U., Wagenaar, E., Dorobek, B.*, et al.* (1997). "Full blockade of intestinal P-glycoprotein and extensive inhibition of blood-brain barrier P-glycoprotein by oral treatment of mice with PSC833." J Clin Invest **100**(10): 2430-2436.

Mayr, B., Eschborn, U., Schleger, W.*, et al.* (1992). "Cytogenetic studies in a canine malignant melanoma." J Comp Pathol **106**(3): 319-322.

Mayr, B., Schaffner, G., Reifinger, M.*, et al.* (2003). "N-ras mutations in canine malignant melanomas." Vet Journal **165**(2): 169-171.

McCubrey, J. A., Steelman, L. S., Chappell, W. H.*, et al.* (2007). "Roles of the Raf/MEK/ERK pathway in cell growth, malignant transformation and drug resistance." Biochim Biophys Acta **1773**(8): 1263-1284.

McLean, N., Tighiouart, M. and Muller, S. (2008). "Primary mucosal melanoma of the head and neck. Comparison of clinical presentation and histopathologic features of oral and sinonasal melanoma." Oral Oncol **44**(11): 1039-1046.

Meleti, M., Leemans, C. R., Mooi, W. J.*, et al.* (2007). "Oral malignant melanoma: A review of the literature." Oral Oncology **43**(2): 116-121.

Meleti, M., Vescovi, P., Mooi, W. J.*, et al.* (2008). "Pigmented lesions of the oral mucosa and perioral tissues: a flow-chart for the diagnosis and some recommendations for the management." Oral Surgery, Oral Medicine, Oral Pathology, Oral Radiology, and Endodontology **105**(5): 606-616.

Menendez, D., Inga, A. and Resnick, M. A. (2009). "The expanding universe of p53 targets." Nature reviews Cancer **9**(10): 724-737.

Mishra, P., Ha, L., Rieker, J.*, et al.* (2010). "Dissection of RAS downstream pathways in melanomagenesis: a role for Ral in transformation." Oncogene **29**(16): 2449-2456.

Modiano, J. F., Ritt, M. G. and Wojcieszyn, J. (1999). "The Molecular Basis of Canine Melanoma: Pathogenesis and Trends in Diagnosis and Therapy." Journal of Veterinary Internal Medicine **13**: 163-174.

Moore, S. R., Persons, D. L., Sosman, J. A.*, et al.* (2008). "Detection of copy number alterations in metastatic melanoma by a DNA fluorescence *in situ* hybridization probe panel and array comparative genomic hybridization: a southwest oncology group study (S9431)." Clin Cancer Res **14**(10): 2927-2935.

Murakami, A., Mori, T., Sakai, H.*, et al.* (2011). "Analysis of KIT expression and KIT exon 11 mutations in canine oral malignant melanomas." Veterinary and Comparative Oncology **9**(3): 219-224.

Musgrove, E. A., Caldon, C. E., Barraclough, J.*, et al.* (2011). "Cyclin D as a therapeutic target in cancer." Nature Reviews Cancer **11**(8): 558-572.

Naeyaert, J. M. and Brochez, L. (2003). "Dysplastic nevi." New England Journal of Medicine **349**(23): 2233-2240.

Network, N. C. I. (2009). Cancer Incidence and Survival By Major Ethnic Group, England, 2002-2006. London, National Cancer Intelligence Network.

Newman, S. J., Jankovsky, J. M., Rohrbach, B. W.*, et al.* (2011). "C-kit Expression in Canine Mucosal Melanomas." Veterinary Pathology **49**(5): 760-765.

Niebling, M. G., Haydu, L. E., Karim, R. Z.*, et al.* (2013). "Reproducibility of AJCC Staging Parameters in Primary Cutaneous Melanoma: An Analysis of 4,924 Cases." Annals of Surgical Oncology **20**(12): 3969-3975.

O'Reilly-Pol, T. and Johnson, S. L. (2013). "Kit signaling is involved in melanocyte stem cell fate decisions in zebrafish embryos." Development **140**(5): 996-1002.

Omholt, K., Grafstrom, E., Kanter-Lewensohn, L.*, et al.* (2011). "KIT pathway alterations in mucosal melanomas of the vulva and other sites." Clin Cancer Res **17**(12): 3933-3942.

Overly, B., Goldschmidt, M. H. and Schofer, F. (2001). "Canine Oral Melanoma: A Retrospective Study." Veterinary Cancer Society Proceedings **21**(43).

Pfister, D. G., Ang, K.-K., Brizel, D. M.*, et al.* (2012). "Mucosal melanoma of the head and neck." Journal of the National Comprehensive Cancer Network **10**(3): 320-338.

Phillips, J. C. (2012). "Evaluation of tyrosinase expression in canine and equine melanocytic tumors " American Journal of Veternairy Research **73**(2): 272-278.

Polli, O. W., Wring, S. A., Humphreys, J. E.*, et al.* (2001). "Rational Use of in Vitro P-glycoprotein Assays in Drug Discovery." The Journal of Pharmacology and Experimental Therapeutics **299**(2): 620-628.

Pollock, P. M., Harper, U. L., Hansen, K. S.*, et al.* (2002). "High frequency of BRAF mutations in nevi." Nature genetics **33**(1): 19-20.

Prasad, M. L., Patel, S. G., Shah, J. P.*, et al.* (2012). "Prognostic significance of regulators of cell cycle and apoptosis, p16(INK4a), p53, and bcl-2 in primary mucosal melanomas of the head and neck." Head Neck Pathol **6**(2): 184-190.

Proulx, D., Ruslander, D., Dodge, R.*, et al.* (2003). "A retrospective analysis of 140 dogs with oral melanoma treated with external beam radiation." Vet Radiol Ultrasound **44**: 352-359.

Ramos-Vara, J. A., Beissenherz, M. E., Miller, M. A.*, et al.* (2000). "Retrospective Study of 338 Canine Oral Melanomas with Clinical, Histologic, and Immunohistochemical Review of 129 Cases." Veterinary Pathology **37**(6): 597-608.

Ramos-Vara, J. A. and Miller, M. A. (2011). "Immunohistochemical identification of canine melanocytic neoplasms with antibodies to melanocytic antigen PNL2 and tyrosinase: comparison with Melan A." Vet Pathol **48**(2): 443-450.

Rapini, R. P., Golitz, L. E., Jr, R. O. G.*, et al.* (1985). "Primary malignant melanoma of the oral cavity. A review of 177 cases." Cancer **55**(7): 1543-1551.

Rassnick, K., Ruslander, D. and Cotter, S. (2001). "Use of carboplatin for treatment of dogs with malignant melanoma: 27 cases (1989-2000)." J Am Vet Med Assoc **218**(9): 1444-1448.

Richter, A. (2005). "RAS Gene Hot-Spot Mutations in Canine Neoplasias." Journal of Heredity **96**(7): 764-765.

Rivera, R. S., Nagatsuka, H., Gunduz, M.*, et al.* (2008). "C-kit protein expression correlated with activating mutations in KIT gene in oral mucosal melanoma." Virchows Arch **452**(1): 27-32.

Robertson, G. P., Herbst, R. A., Nagane, M.*, et al.* (1999). "The chromosome 10 monosomy common in human melanomas results from the loss of two separate tumor suppressor loci." Cancer research **59**(15): 3596-3601.

Rochaix, P., Lacroix-Triki, M., Lamant, L.*, et al.* (2003). "PNL2, a new monoclonal antibody directed against a fixative-resistant melanocyte antigen." Mod Pathol **16**(5): 481-490.

Rowell, J., McCarthy, D. and Alvarez, C. (2011). "Dog models of naturally occurring cancer." Trends Mol Med **17**(7): 380-388.

Satyamoorthy, K. and Herlyn, M. (2003). "p16INK4A and familial melanoma." Methods in Molecular Biology **222**: 185-195.

Satzger, I., Schaefer, T., Kuettler, U.*, et al.* (2008). "Analysis of c-KIT expression and KIT gene mutation in human mucosal melanomas." Br J Cancer **99**(12): 2065-2069.

Sauter, E. R., Yeo, U.-C., von Stemm, A.*, et al.* (2002). "Cyclin D1 is a candidate oncogene in cutaneous melanoma." Cancer research **62**(11): 3200-3206.

Schinkel, A. (1997). "The physiological function of drug-transporting P-glycoproteins." Semin Cancer Biol. **8**(3): 161-170.

Schinkel, A. H. and Jonker, J. W. (2003). "Mammalian drug efflux transporters of the ATP binding cassette (ABC) family: an overview." Advanced Drug Delivery Reviews **55**: 3-29.

Schmidt, M. and Bastians, H. (2007). "Mitotic drug targets and the development of novel anti-mitotic anticancer drugs." Drug Resist Updat **10**(4-5): 162-181.

Schultheiss, P. (2006). "Histologic features and clinical outcomes of melanomas of lip, haired skin, and nail bed locations of dogs." J Vet Diagn Invest **18**(4): 422-425.

Schwartz, R. A. (2013). "Congenital Nevi." MedScape, 2014, from http://emedicine.medscape.com/article/1118659-overview - a0104.

SEER. (2010). "SEER Stat Fact Sheets: Melanoma of the Skin." Surveillance, Epidemiology, and End Results Program.

Seger, R. and Krebs, E. G. (1995). "The MAPK signaling cascade." The FASEB journal **9**(9): 726-735.

Serrano, M. (1997). "The Tumor Suppressor Protein p16< sup> INK4a</sup>." Experimental cell research **237**(1): 7-13.

Sharif, M., Eldaghayes, I., Kammon, A., et al. (2014). "Melanoacanthoma in a Dog: A Case Report." J Veterinar Sci Technol 5(167).

Shelly, S., Chien, M. B., Yip, B.*, et al.* (2005). "Exon 15 BRAF mutations are uncommon in canine oral malignant melanomas." Mammalian Genome **16**(3): 211-217.

Shen, W. H., Balajee, A. S., Wang, J.*, et al.* (2007). "Essential role for nuclear PTEN in maintaining chromosomal integrity." Cell **128**(1): 157-170.

Shibata, K., Takeda, K., Tomita, Y.*, et al.* (1992). "Downstream region of the human tyrosinase-related protein gene enhances its promoter activity." Biochem Biophys Res Commun **184**(2): 568-575.

Shoo, B. A., Sagebiel, R. W. and Kashani-Sabet, M. (2010). "Discordance in the histopathologic diagnosis of melanoma at a melanoma referral center." J Am Acad Dermatol **62**(5): 751-756.

Simpson, R. M., Bastian, B. C., Michael, H. T.*, et al.* (2014). "Sporadic naturally occurring melanoma in dogs as a preclinical model for human melanoma." Pigment Cell & Melanoma Research **27**(1): 37-47.

Slingluff, C., Flaherty, K., Rosenberg, S.*, et al.* (2011). Cutaneous melanoma. DeVita, Hellman, and Rosenberg's Cancer: Principles and Practice of Oncology. DeVita VT, Lawrence TS and R. SA. Philadelphia, Pa, Lippincott Williams & Wilkins**:** 1643-1691.

Smalberger, G., Siegel, D. and Khachemoune, A. (2008). "Lentigo maligna." Dermatol Ther **21**(6): 439-446.

Smedley, R. C., Lamoureux, J., Sledge, D. G.*, et al.* (2011). "Immunohistochemical diagnosis of canine oral amelanotic melanocytic neoplasms." Vet Pathol **48**(1): 32-40.

Smedley, R. C., Spangler, W. L., Esplin, D. G.*, et al.* (2011). "Prognostic Markers for Canine Melanocytic Neoplasms: A Comparative Review of the Literature and Goals for Future Investigation." Veterinary Pathology **48**(1): 54-72.

Smith, S. H., Goldschmidt, M. H. and McManus, P. M. (2002). "A Comparative Review of Melanocytic Neoplasms." Veterinary Pathology **39**(6): 651-678.

Sommer, L. (2011). "Generation of melanocytes from neural crest cells." Pigment cell & melanoma research **24**(3): 411-421.

Song, J., Mooi, W. J., Petronic-Rosic, V.*, et al.* (2011). "Nevus versus melanoma: to FISH, or not to FISH." Advances in anatomic pathology **18**(3): 229-234.

Spangler, W. L. and Kass, P. H. (2006). "The Histologic and Epidemiologic Bases for Prognostic Considerations in Canine Melanocytic Neoplasia." Veterinary Pathology **43**(2): 136-149.

Sparreboom, A., van Asperen, J., Mayer, U.*, et al.* (1997). "Limited oral bioavailability and active epithelial excretion of paclitaxel (Taxol) caused by P-glycoprotein in the intestine." Proc Natl Acad Sci U S A **94**(5): 2031-2035.

Spivey, T. L., De Giorgi, V., Zhao, Y., *et al.* (2012). "The stable traits of melanoma genetics: an alternate approach to target discovery." BMC Genomics **13**(1): 156.

Stahl, J. M., Cheung, M., Sharma, A., *et al.* (2003). "Loss of PTEN promotes tumor development in malignant melanoma." Cancer research **63**(11): 2881-2890.

Stretch, J. R., Gatter, K. C., Ralfkiaer, E., *et al.* (1991). "Expression of mutant p53 in melanoma." Cancer research **51**(21): 5976-5979.

Swick, J. M. and Maize, J. C. (2012). "Molecular biology of melanoma." Journal of the American Academy of Dermatology **67**(5): 1049-1054.

Takata, M. and Saida, T. (2006). "Genetic alterations in melanocytic tumors." J Dermatol Sci **43**(1): 1-10.

Takizawa, C. G. and Morgan, D. O. (2000). "Control of mitosis by changes in the subcellular location of cyclin-B1–Cdk1 and Cdc25C." Current opinion in cell biology **12**(6): 658-665.

Tanaka, N., Odajima, T., Mimura, M., *et al.* (2001). "Expression of Rb, pRb2/p130, p53, and p16 proteins in malignant melanoma of oral mucosa." Oral oncology **37**(3): 308-314.

Tanaka, N., Mimura, M., Kimijima, Y., *et al.* (2004). "Clinical investigation of amelanotic malignant melanoma in the oral region." Journal of Oral and Maxillofacial Surgery **62**(8): 933-937.

Tanaka, N., Mimura, M., Ogi, K., *et al.* (2004). "Primary malignant melanoma of the oral cavity: assessment of outcome from the clinical records of 35 patients." International Journal of Oral and Maxillofacial Surgery **33**(8): 761-765.

Tannous, Z. S., Mihm, M. C., Jr., Sober, A. J., *et al.* (2005). "Congenital melanocytic nevi: clinical and histopathologic features, risk of melanoma, and clinical management." J Am Acad Dermatol **52**(2): 197-203.

Thiebaut, F., Tsuruo, T., Hamada, H.*, et al.* (1987). "Cellular localization of the multidrug-resistance gene product P-glycoprotein in normal human tissues." Proc Natl Acad Sci U S A **84**(21): 7735-7738.

Torres-Cabala, C. A., Plaza, J. A., Diwan, A. H.*, et al.* (2010). "Severe architectural disorder is a potential pitfall in the diagnosis of small melanocytic lesions." Journal of Cutaneous Pathology **37**(8): 860-865.

Trent, J. M., Meyeskens, F., Salmon, S.*, et al.* (1990). "Relation of Cytogenetic Abnormalities and Clinical Outcome in metastatic Melanoma." The New England Journal of Medicine **322**(21): 1508-1511.

Uong, A. and Zon, L. I. (2010). "Melanocytes in development and cancer." J Cell Physiol **222**(1): 38-41.

van Dijk, M., Sprenger, S., Rombout, P.*, et al.* (2003). "Distinct chromosomal aberrations in sinonasal mucosal melanoma as detected by comparative genomic hybridization." Genes, Chromosomes and Cancer **36**(2): 151-158.

Villamil, J. A., Henry, C. J., Bryan, J. N.*, et al.* (2011). "Identification of the most common cutaneous neoplasms in dogs and evaluation of breed and age distributions for selected neoplams." JAVMA **239**(7): 960-965.

Vizkeleti, L., Ecsedi, S., Rakosy, Z.*, et al.* (2012). "The role of CCND1 alterations during the progression of cutaneous malignant melanoma." Tumour Biol **33**(6): 2189-2199.

von Euler, H., Sadeghi, A., Carlsson, B.*, et al.* (2008). "Efficient adenovector CD40 ligand immunotherapy of canine malignant melanoma." Journal of Immunotherapy **31**(4): 377-384.

Wacher, V., Wu, C. and Benet, L. (1995). "Overlapping substrate specificities and tissue distribution of cytochrome P450 3A and P-glycoprotein: implications for drug delivery and activity in cancer chemotherapy." Mol Carcinog **13**(3): 129-134.

Weinberg, R. A. (1995). "The retinoblastoma protein and cell cycle control." Cell **81**(3): 323-330.

Westberg, S., Sadeghi, A., Svensson, E.*, et al.* (2013). "Treatment efficacy and immune stimulation by AdCD40L gene therapy of spontaneous canine malignant melanoma." Journal of Immunotherapy **36**(6): 350-358.

White, R. and Zon, L. (2008). "Melanocytes in development, regeneration, and cancer." Cell Stem Cell **3**(3): 242-252.

WHO. (2014). "Skin cancers." from http://www.who.int/uv/faq/skincancer/en/index1.html.

Wijnholds, J., Evers, R., Leusden, M. R. v.*, et al.* (1997). "Increased sensitivity to anticancer drugs and decreased inflammatory response in mice lacking MRP." Nature Med **3**: 1275–1279.

Wijnholds, J., Scheffer, G. L., Valk, M. v. d.*, et al.* (1998). "Multidrug resistance protein 1 protects the oropharyngeal mucosal layer and the testicular tubules against drug-induced damage." J. Exp. Med **188**: 797–808.

Withrow, S. J., D. M. Vail, and R. Page (2013). Small Animal Clinial Oncology, Elsevier.

Wolfel, T., Hauer, M., Schneider, J.*, et al.* (1995). "A p16INK4a-insensitive CDK4 mutant targeted by cytolytic T lymphocytes in a human melanoma." Science **269**(5228): 1281-1284.

Wong, C. W., Fan, Y. S., Chan, T. L.*, et al.* (2005). "BRAF and NRAS mutations are uncommon in melanomas arising in diverse internal organs." J Clin Pathol **58**(6): 640-644.

Wu, H., Goel, V. and Haluska, F. G. (2003). "PTEN signaling pathways in melanoma." Oncogene **22**(20): 3113-3122.

Xiong, Y., Hannon, G. J., Zhang, H.*, et al.* (1993). "p21 is a universal inhibitor of cyclin kinases." nature **366**(6456): 701-704.

Zarich, N., Oliva, J. L., Martinez, N.*, et al.* (2006). "Grb2 is a negative modulator of the intrinsic Ras-GEF activity of hSos1." Mol Biol Cell **17**(8): 3591-3597.

Zhong, Z., Yeow, W.-S., Zou, C.*, et al.* (2010). "Cyclin D1/cyclin-dependent kinase 4 interacts with filamin A and affects the migration and invasion potential of breast cancer cells." Cancer research **70**(5): 2105-2114.

CHAPTER II

Cytogenetic Characterization of Primary Canine Melanocytic Lesions

This chapter was completed in collaboration with Siddarth Roy under the direction of Dr. Alison Motsiger-Reif. Sections 2.3.6, 2.3.7, 2.4.5, and Figure 2.3 were written and completed by Siddarth Roy with permission to include here.

2.1 Abstract

Malignant and benign melanocytic lesions, originating from either the oral mucosa or cutaneous epithelium, are common in the general dog population, with approximately 100,000 diagnoses each year in the US. Oral melanoma is the most common canine neoplasm of the oral cavity and is highly aggressive, while cutaneous melanocytomas occur frequently, but rarely develop into a malignant form. Despite the differential prognosis, it has been assumed that melanoma subtypes represent the same disease. Since little is known about the genomic status of these lesions, we used molecular cytogenetic methods to assess three subtypes of canine melanocytic lesions. Results of comparative genomic hybridization (CGH) analysis indicated highly aberrant copy number status across the tumor genome for both of the malignant melanoma subtypes, but with distinct differences between them. The most common aberrations included gain of dog chromosome (CFA) 13 and 17 and loss of CFA 22. Melanocytomas presented with fewer genome wide aberrations and showed a recurrent gain of the region CFA 20q15.3-17. A distinguishing copy number profile, evident only in oral melanomas, was a sigmoidal pattern of copy number loss followed immediately by a gain around CFA 30q14. Our results also revealed copy number aberrations of targeted

genes when assessed by fluorescence *in situ* hybridization (FISH). We propose that canine melanomas of the oral mucosa and cutaneous epithelium are discrete, and initiated by different molecular pathways. This finding concurs with the results of studies of human melanomas, in which unique CGH profiles associate with environmental factors and pathways of tumorigenesis.

2.2 Introduction

Melanocytes are highly motile melanin-producing cells, usually found in the basal layer of the epidermis. The primary function of these cells is to protect the nuclei of neighboring epithelial cells from UV damage, yet they can also give rise to both benign melanocytomas and malignant melanomas. In dogs, melanomas are the most common tumor of the oral cavity, 90% of which are malignant, readily invading into normal tissue and bone, with a high metastatic propensity (Ramos-Vara *et al.* 2000; Koenig *et al.* 2002; Spangler and Kass 2006; Bergman 2007). Malignant melanomas of the oral cavity are usually aggressive and respond poorly to standard chemotherapeutic treatments (Bergman 2007). Melanomas of the cutaneous epithelium are the third most common malignant skin lesion in dogs (Villamil *et al.* 2011) representing 5-11% of all malignant melanomas (Smith, Goldschmidt, and McManus 2002). There is also large debate among veterinary pathologists on the accuracy of prognostic criteria for canine malignant melanomas (Withrow 2013).

Numerous retrospective studies have revealed varying results correlating survival with physical characteristics of the tumor including anatomical site, sex, volume of tumor, and histological parameters such as pigmentation and mitotic index (Ramos-Vara *et al.* 2000; Avruch J 2001; Kudnig, Ehrhart, and Withrow 2003; Spangler and Kass 2006). In a study of 122 canine melanocytic tumors, mitotic index and location, classical markers of malignancy, were not significantly correlated with survival time (Ramos-Vara *et al.* 2000). A later study of 384 cases of melanocytic tumors found significant correlation of metastasis, mitotic index, nuclear atypia, WHO clinical stage, and volume with decreased patient survival (Spangler and Kass 2006). However, the same study also found that only 59% of cases determined to

be histologically malignant exhibited biological malignancy (metastases or recurrence). It was also determined that 74% of tumors of "ambiguous location" (feet or lips) were reported malignant via histology, but only 38% of these demonstrated malignant behavior. Finally, of the 227 melanocytic skin lesions, predominantly thought to be benign, 39% were reported as histologically malignant, with 12% exhibiting malignant behavior (Spangler and Kass 2006). This demonstrates the need for more accurate diagnostic and prognostic markers.

Cytogenetic studies of human melanomas have revealed that the underlying genetic mutations associated with these lesions differ significantly depending on the location of the primary tumor (Curtin *et al.* 2005; Blokx, van Dijk, and Ruiter 2010; Furney *et al.* 2012). It is now believed these lesions are initiated from and subsequently develop through molecularly different pathways, reflecting the variation in therapeutic response (Bastian *et al.* 2003; Bauer and Bastian 2006). Cytogenetic studies also identified specific DNA copy number aberrations correlating with tumor malignancy, which have allowed for sensitive diagnostic and prognostic assays to be developed (Bauer and Bastian 2006). Such cytogenetic studies have also allowed for the discovery of novel genes and pathways leading to targeted therapeutics (Sevastre *et al.* 2007).

Recent developments in the field of molecular veterinary biotechnology have made it possible to characterize tumors through genome-wide cytogenetics (Breen 2009). Genome-wide studies expedite the discovery of novel mutations and facilitate the development of both molecular markers and targeted therapies to obtain better clinical outcome. Previous investigations have identified important cancer-related proteins in the pathogenesis of canine oral melanoma (Ritt, Wojcieszyn, and Modiano 1998; Koenig *et al.* 2002; Bianco *et al.* 2003;

Newman *et al.* 2011). In parallel to observations in human studies, it has been hypothesized that dysregulation of comparable genes in dogs may be a function of aberrant gene dosage and/or functional translocation (Sevastre *et al.* 2007). However, no study has investigated the role of copy number aberrations in canine melanocytic lesions.

We hypothesize canine oral melanomas will show genome-wide cytogenetic changes comparable to those of human mucosal melanomas and different from those found in UV-induced cutaneous melanomas. We also hypothesize that benign canine cutaneous melanocytic lesions will show different cytogenetic changes to those of malignant oral melanomas. Therefore, the goal of this study was to characterize cytogenetic changes evident in canine melanocytic lesions, using oligonucleotide array comparative genomic hybridization array (oaCGH) and multicolor fluorescence *in situ* hybridization (FISH), and to assess the comparative value of these data by consideration of features shared with subtypes of human melanomas.

2.3 Materials and Methods

2.3.1 Clinical Specimens

Canine oral melanomas and benign melanocytomas were obtained as biopsy specimens from patients as part of their routine diagnostic procedure, with informed owner consent. All cases were diagnosed by pathology evaluation of formalin fixed paraffin embedded (FFPE) specimens and any histologic evaluation was recorded from initial diagnosis report. Where the diagnostic Hematoxylin and Eosin (H&E) slide was made available (56/67 cases), the initial diagnosis was independently confirmed by three board-

certified veterinary pathologists (SM, PL, and LB) and evaluated for percent pigmentation, mitotic index, presence of junctional activity, and tissue morphology as previously described (Smedley *et al.* 2011). Differences in histologic characteristics between melanomas and benign melanocytomas were analyzed for statistical significance with a one-tailed Mann-Whitney U Test.

The cohort for DNA isolation comprised specimens from 67 individuals. Of these 53 were available to the study only as the fixed tissue specimen, 11 were available only as a snap frozen tumor punch biopsies, and three were available as both FFPE and snap frozen tumor tissue. The cases used for DNA isolation were as follows: 44 biopsies of primary oral melanomas (FFPE (n=32) or fresh frozen (n=12)), five biopsies of cutaneous melanomas (FFPE (n=3) and fresh frozen (n=2)) and 18 biopsies of primary cutaneous melanocytoma (all FFPE). All unfixed tumor specimens (punch biopsies) were snap frozen in liquid nitrogen at the time of removal and subsequently stored at -80°C. It was demonstrated that punch biopsies were not infiltrated with normal non-neoplastic tissues as a direct comparison of copy number profiles from fresh tissue, and the corresponding tumor-enriched FFPE sample showed no difference in aberrations (Fig. 2.6). Detailed descriptions of the specimens used in the study are provided in Table 2.1.

2.3.2 Genomic DNA Extraction

Genomic DNA was extracted from tumor punch biopsies using a DNeasy© Kit (according to manufacturer's recommendations, Qiagen, Germantown, MD, USA) and

assessed for quality and quantity by spectrophotometry. Genomic DNA integrity, assessed by agarose gel electrophoresis, indicated little to no degradation.

Within the cohort of FFPE samples, several contained margins with bordering non-neoplastic tissues that would 'contaminate' the DNA of the tumor cell population. Areas of tissue enriched for tumor and areas of non-neoplastic margin were thus identified and indicated on a representative H&E-stained 5μm slide by three veterinary pathologists (SM, PL, and LB). Three adjacent 25μm sections were then obtained from each FFPE specimen and the normal/margin tissue was macro-dissected away. Genomic DNA was extracted from the remaining neoplastic regions using a QIAamp DNA FFPE Tissue Kit (according to manufacturer's recommendations, Qiagen, Germantown, MD, USA), and subsequently assessed for quality and quantity by spectrophotometry. Genomic DNA integrity was assessed by agarose gel electrophoresis, indicating that while all exhibited some degree of degradation, the majority of the DNA was >10kb.

2.3.3 Fluorescence in situ Hybridization (FISH) of archival specimens.

In this study, FISH was performed using 5μm FFPE sections of the cases in the cohort to detect and quantify hybridization sites of target genomic regions. Each 5μm FFPE section was mounted onto a charged glass slide and incubated at 56°C for 18 hours in a moisture-free slide chamber. Slides were then de-waxed by soaking in fresh xylene for 15 minutes, dehydrated through an ethanol series, and air-dried. Slides were incubated for 1 hour at 37°C in 60mg/mL collagenase II (Sigma, Saint Louis, MO) in Hank's Balanced Salt Solution (HBSS) (Mediatech, Corning, NY) and then for 45 minutes at 37°C in Tris-Buffer

Saline (Boston BioProducts, Boston, MA) containing 15000unit/mL of Bovine Testicular Hyaluronidase (Sigma, Saint Louis, MO). Slides were rinsed with ultra pure water for 3 minutes between treatments. Sections were then treated with an Abbott Paraffin Pretreatment Kit II (according to the manufacturer's recommendation, Abbott Laboratories, Abbott Park, IL, USA).

Tissue slices were assessed by FISH to evaluate the copy number of canine bacterial artificial chromosome (BAC) probes designed to represent ten genes, selected to correspond to those identified by previous human studies of melanoma: *CDKN2A*, *CDKN1A*, *PTEN*, *B-RAF*, *TP53*, *CCND1*, *c-MYC*, *c-KIT*, *CDK4*, and *RB-1*. The BACs were selected from the CHORI-82 (https://bacpac.chori.org/library.php?id=253) library based on their genome position indicated for the canine genome build CanFam2 in the UCSC canine genome browser (http://genome.ucsc.edu). To increase the size of the FISH signal for assessment of archival specimens, a probe pool was developed for each locus, comprising three overlapping BAC clones: a primary clone containing the gene of interest and at least one overlapping BAC clone selected on either side. This approach resulted in probe contigs for each locus with DNA sequence extending the final probe size to approximately 500Kb. A summary of the BAC clones used is shown in Table 2.8. To verify that each BAC pool had a unique cytogenetic location cytogenetic location, all were first hybridized to metaphase preparations from six clinically healthy dogs, generated by conventional mitogen stimulation of peripheral lymphocytes (Breen, Bullerdiek, and Langford 1999), using multicolor single locus probe (SLP) FISH analysis as described previously (Breen *et al.* 2004).

To establish a baseline of expected mean copy number of each probe when hybridized to non-neoplastic FFPE samples, each of the ten probes was first enumerated in the nuclei of a series of 5μm sections of FFPE specimens of healthy tissue matched controls. A minimum of 50 cells was imaged using a BioView Legato system (BioView, Israel) set to acquire multiplane images of 19 adjacent focal planes at 0.5μm increments. The mean copy number of each probe in >50 nuclei of 5μm sections of FFPE biopsy specimens was then obtained using the same process, and normalized to the mean of the corresponding controls. Classification of FISH signals as gains or losses was performed as described previously for human diagnostics (Gaiser *et al.* 2010) where the mean must be based on no fewer than 50 separate cells. Additionally, aberrant signals must be found in at least 50% of the cell population analyzed.

2.3.4 Comparative Genomic Hybridization (CGH)

Oligo array-CGH (oa-CGH) was performed by co-hybridization of tumor (test) DNA and a common reference DNA sample, where the latter comprised an equimolar pool of genomic DNA samples from multiple healthy individuals of various breeds. DNA extracted from FFPE samples was slightly degraded, as expected, but this was shown not to have an adverse effect on data quality. DNA was labeled using a SureTag Labeling Kit (Agilent Technologies, Santa Clara, CA) with all test samples labeled with Cyanine-3-dCTP and the common reference sample labeled with Cyanine-5-dCTP. Fluorchrome incorporation and final probe concentrations were determined using routine spectrophotometric parameters with readings taken from a Nanodrop1000. Fluorescently labeled test and reference samples

were co-hybridized to Canine SurePrint G3 180,000 feature CGH arrays (Agilent, AMADID 025522) for 40 hours at 65°C and 20 rpm, as described previously (Angstadt *et al.* 2011). Arrays were scanned at 3µm using a high-resolution microarray scanner (Agilent, Model G2505C) and data extracted using Feature Extraction (v10.9) software. Scan data were assessed for quality by the Quality Metrics report in Agilent's Feature extraction software (v10.5) (Agilent Technologies, Santa Clara, CA, USA) and aligned to the genome position indicated for the canine genome build CanFam2 (http://genome.ucsc.edu/cgi-bin/hgGateway?db=canFam2).

Copy number data were analyzed with NEXUS Copy Number v7.0 software (Biodiscovery Inc., CA, USA). The Log_2 data for each probe provided from Feature Extraction were centered using diploid regions. NEXUS generated copy number aberrations using a FASST2 Segmentation algorithm with a significance threshold of 5.05^{-6}. Aberrations were defined as a minimum of three consecutive probes with log2 tumor: reference value of 0.2 to 1.13 (gain), >1.14 (high gain), -0.23 to -1.1 (loss), < -1.1 (homozygous loss). Recurrent copy number aberrations within each subtype were determined within NEXUS using a stringent involvement threshold of 50%. Significance of these regions was then determined in NEXUS using the GISTIC algorithm with a G-score cut off of G >1.0 and a significance of Q <0.05. Copy number aberration (CNA) frequency comparisons among sample groups were performed in NEXUS using Fisher's exact test with differential threshold of >50% and significance p <0.05. Significance of each probe between the two groups was calculated in NEXUS using a Mann-Whitney Test for median comparison.

2.3.5 Humanization of canine CGH data

Canine oaCGH data were recoded into "virtual" human genome format to facilitate direct visual comparison of cytogenetic profiles of human and canine melanoma, as described previously (Thomas *et al.* 2011). Briefly, the genome coordinates of each of the 180,000 60-mer canine oligonucleotides were imported into the Liftover Batch Coordinate Conversion Tool (http://genome.ucsc.edu/cgi-bin/hgLiftOver), using default settings to establish the orthologous nucleotide sequence coordinates within the human genome sequence assembly (February 2009, GRCh37/hg19). Using these recoded coordinates, the tumor:reference signal intensity data for each array were reprocessed to output the oaCGH profile according to these "virtual" human chromosome locations.

2.3.6 Clustering of oaCGH Profiles

Hierarchical clustering was performed to evaluate how genome-wide CGH profiles differentiate between the two groups. Hierarchical clustering using Ward's method for linkage was performed on the genome-wide log2 ratio data for each sample. Analysis was performed using the R statistical software, version 2.13.0 (R Development Core Team, Vienna, Austria), using the gplots package.

2.3.7 Statistical Analysis of oaCGH and Histology Profiles

Correlation analysis was performed between oaCGH clusters and the corresponding histological characteristics to determine if DNA copy number aberrations were significantly associated with pathological cellular morphologies. Initial analysis was based on

pathological diagnosis alone. To test molecular association, two clusters were established based on oaCGH copy number profiles as performed above. These two groups were then assessed for statistical differences between histological characteristics. A Wilcoxon rank-sum test was performed for pigmentation and log mitotic values and a Fisher's exact test was performed for association analysis with group status and nuclear atypia.

2.4 Results

2.4.1 Clinical Assessment

A total of 49 canine melanomas and 18 benign melanocytomas were profiled by oaCGH during this study. Melanomas presented from two locations: the oral cavity (n=44) and unspecified haired skin (n=5). Benign melanocytomas presented primarily from haired skin (n=13) with rare presentation from the oral cavity (n=5). Breed was not a consideration in case selection and so there were 29 breeds of dog included in this study, with the most frequent (21%) being of mixed breed (n=14). Overall, melanomas presented with a more aggressive histologic presentation, including a significantly higher mitotic index (p= 3.810E-06), lower percent pigmentation (p= 0.000116), and higher percent nuclear atypia (p= 1.833E-10). A detailed summary of the histopathologic findings of each case is presented in Table 2.1.

2.4.2 Detection of CNA by oaCGH

Individuals represented within the oral (mucosal) melanoma cohort presented with highly complex genome-wide oaCGH profiles (Figure 2.1). In most cases, the oaCGH

profiles showed regions of the genome where the $\log_2$ ratios of test:reference signal indicated either a unidirectional gain or loss of one copy of a locus within the majority of cells of the tumor, or a high level of cellular heterogeneity within the tumor cell population. This was clarified by FISH analysis of copy number within individual cells, which corroborated single copy aberrations (described below). Highly recurrent CNAs (>50% penetrance across the cohort) were assessed in detail (Table 2.2) with significance of each region determined as a GISIC q-value (Table 2.3). For the cohort of oral melanomas the most frequent DNA copy number gain was a 600Kb region of dog chromosome (CFA) 30 located at CFA 30: 19,102,383-19,660,901 (q= 4.25E-10), along with whole chromosome gains of CFA 13, 17, 20, 29, and 36. The most frequent DNA copy number losses involved the full lengths of CFA 22 and 27, as well as 15Kb and 122.5Kb segments located at CFA 10: 20,583,579-20,598,892 (q= 6.26E-05), and CFA 26: 30,241,704-30,306,343 (q= 1.34E-08), respectively.

Several regions of the genome had oaCGH profiles suggestive of structural changes, denoted by a copy number gain followed immediately by a loss, most notably on CFA10 and CFA30, both of which were found to be statistically significant using the GISTIC algorithm (Table 2.3). The chromosome break point region on CFA 30, evident in 60% of the oral melanomas analyzed, spans 5Mb of sequence located between 14Mb and 19Mb (Figure 2.2). The log2 values within this region of CFA 30 were suggestive of a heterozygous loss followed by an immediate gain, with 97% of affected cases suggestive of a copy number of ≥ 4.

Cutaneous melanomas, although small in number (n=5), also presented with highly aberrant oaCGH profiles (Figure 2.1). The largest and most common aberration was a gain of

CFA 20 that spanned 46.2Mb of the chromosome CFA 20: 10,929,869-57,175,686, present in four of the five cases. The most frequent copy number losses were a 131kb region of CFA 6: 48,260,040-49,569,575, a 385Kb region of CFA 18: 21,439,849-21,824,376, and the full length of chromosome 22. Due to the small number of cases none of these aberrations were statistically significant using the GISTIC algorithm (Table 2.3).

While individuals represented within the cutaneous melanocytoma cohort (n=18) presented with relatively stable oaCGH profiles, some recurrent aberrations were evident (Figure 2.1). The most common aberration was gain of a 233Kb region of CFA 20, CFA 20: 60,767,150-61,000,000 (q= 4.22E-07). Other common aberrations were gains on CFA 9: 20,973,038-21,556,711 (q= 4.89E-09), CFA 10: 48,818,794-48,878,597 (q= 3.95E-05), and CFA 11: 55,214,228-55,245,594 (q= 4.99E-08). Melanocytomas had only one significant recurrent copy number loss, involving a 200Kb region at CFA 8: 76,368,492-76,582,392 (q= 7.78E-04).

2.4.3 Comparison of Melanomas to Melanocytomas

A number of CNAs were either detected in only one subtype, or were shared between two of the three subtypes (Table 2.4). Cutaneous melanomas and melanocytomas shared several common recurrent aberrations that were rare or absent in oral melanomas, most significantly a 17.5Mb region of gain at CFA 20: 39,655,694- 57,175,686, found in approximately 45% of melanocytomas and 80% of cutaneous melanomas (in CM $q<0.01$). Another notable similarity between these two groups was the presence of a 9Mb copy number gain between 35Mb and 44Mb on chromosome 30 (Figure 2.2(a) and 2.2(c)). There

were no aberrations shared between cutaneous and oral melanomas at the 50% differential level. However, when the stringency was dropped to 40%, several regions were found in common, including a 140Kb loss of CFA 3: 65,280,294-65,432,693 and a 260Kb gain of CFA 13: 8,127,632-8,394,801 (data not shown). Aberrations unique to one subtype were also evident. Deletion of a 385Kb segment of CFA18 at CFA 18: 21,439,849- 21,824,376 was highly recurrent only in cutaneous melanomas and a complex copy number profile along a 13Mb region of CFA 30, CFA 30: 8,290,472- 21,411,530, was observed only in oral melanomas.

2.4.5 Hierarchical Clustering of All Melanocytic Lesions

Hierarchical clustering of segmented oaCGH profiles separated samples into three well-defined groups (Figure 2.3). The first and third group contained only malignant samples while the second group contained an equal mix of benign (n=17) and malignant samples (n=21). The clustering of 21 malignant samples with the benign samples is partially explained by the reduced level of aberrations within those particular malignant lesions. Within this larger group, the malignant samples and benign samples also appear to cluster separately.

Clusters were further evaluated by consideration of their histological characteristics, to identify correlation of cellular morphology with genome-wide CGH profiles. The malignant samples that clustered with benign samples (n=21) showed significantly higher pigmentation ($p= 0.018$), lower mitotic index ($p= 0.023$), and a lower, but not statistically significant, nuclear atypia ($p= 0.222$) than the group of malignant melanomas that clustered

together (n=28). These data demonstrate that molecular aberrations in canine malignant melanomas correlate with the cellular phenotype and histology.

2.4.6 Detection of CNA by FISH analysis of FFPE sections

All targeted loci (n=10) evaluated by FISH analysis showed aberrant copy number in oral melanomas. The most frequent unidirectional changes were a gain of c-*MYC (*80% of cases) and loss of *CDKN2A (*68% of cases) and *RB-1* (35% of cases). The other seven loci evaluated showed bidirectional changes (Figure 2.4(a)). As expected, based on the whole genome oaCGH data, benign lesions showed lower percentages of targeted locus aberrations (Figure 4b). The most common of the targeted CNAs evident in the benign lesions were loss of *TP53* and *CDKN2A*. It is important to note that these aberrations were observed only as a heterozygous loss, indicating the retention of one allele for production of downstream product (if unmutated). Neither tumor types showed significant copy number amplification of regions encompassing *BRAF* or *CCND1,* both highly aberrant in human UV-induced cutaneous melanomas. The population of canine oral melanomas showed a combination of both copy number gain and loss for these gene regions, suggesting overall chromosome instability, but not targeted gene amplification.

2.4.7 Comparison of Canine to Human Melanocytic Lesions

Humanization of the canine oaCGH data allowed for direct comparison of the canine data collected in this study (Table 2.6) to the CNA status of human melanomas accessible from previous studies. When aligned with genome-wide oaCGH profiles of different

subtypes of human melanoma, striking similarities were present between canine oral melanoma, and both human mucosal melanoma and human acral melanoma (Figure 2.5). Human mucosal and acral melanomas have been shown to present with more complex genome-wide oaCGH profiles than cutaneous melanomas (Curtin *et al.* 2005; Furney *et al.* 2012), paralleling the data for canine melanomas in the current study. Many CNAs were shared between human and dog, including a characteristically complex oaCGH profile in mucosal melanomas of both species, involving the evolutionarily conserved chromosome segments represented by human chromosome chr15:38,701,609- 49,824,200 and canine chromosome CFA 30: 8,290,472- 21,411,530. Notably, this distinct aberration was not detected in canine cutaneous melanomas, or in human common cutaneous melanomas. Human mucosal and acral melanomas showed additional smaller shared aberrations (Table 2.7).

2.5 Discussion

2.5.1 Aberrations within Melanomas and Melanocytomas: Tumorigenesis Implications

The oaCGH analysis of human melanomas established that subgroups of melanocytic lesions, based on anatomic location, environmental factors, and malignancy, present with distinct copy number aberrations (Curtin *et al.* 2005). Aberrations such as amplification of *CCND1* and *BRAF* and loss of *CDKN2A* have been linked to driving factors of tumor development and progression (Berger *et al.* 2012). Such aberrations are also distinct to particular subgroups of melanoma, suggesting the underlying mechanism in malignant progression may differ. This has caused a shift in targeted therapeutics specific to each

subtype and the molecular profile of each tumor. As in humans, it has been suggested that subtypes of canine melanoma might also initiate tumorigenesis through different molecular pathways (Bergman 2007), which are marked by recurrent CNAs. Currently, all canine malignant melanomas are treated with the same therapeutic regime regardless of anatomic location, based on the lack of information separating subtypes at the molecular level and specific targeted therapies.

Our data suggest that, as with human melanomas, canine melanomas present with cytogenetically distinct profiles based on malignancy and the anatomic location in which they arise. The most striking evidence of this is the presence of a characteristic aberration of CFA 30 in oral melanomas, which is absent in cutaneous lesions. Melanocytomas, which are primarily cutaneous, had noticeably fewer aberrations than both subtypes of melanoma. However, approximately 40% of these were shared with cutaneous melanoma, including the recurrent copy number gain of CFA 20: 39,655,694-57,175,686, evident in cutaneous but not oral lesions (Table 2.3). These features may represent hallmarks of an epithelial growth pattern and targeted investigation into this region may elucidate tumor initiation specific to this tissue location. There are also significant clinical implications of the molecular differentiation of the two locations. The separation of these two diseases provides insight into the initiation and development of the different subtypes of melanomas and could lead to the development of specific treatment regimes based on the site of primary tumor growth.

The most recurrent aberration specific to the oral melanoma cohort was the distinctive complex copy number profile on CFA 30, present in 60% of cases and indicative of a structural rearrangement. Due to the high incidence of this particular complex CNA, it is

probable the rearrangement on CFA 30 is also key to the development of canine oral melanoma, or progression toward a malignant phenotype. This aberration has potential for use as a signature to differentiate between lesions that are likely to progress, requiring additional treatments, and those that are likely to remain benign. Further study into the cause and biological effect of the breakage may also provide further insight into why oral melanomas are behaviorally more aggressive than other melanocytic subtypes. The 5Mb region of genome sequence surrounding the breakage (CFA 30: 15Mb-20Mb) is within a gene desert, surrounded by gene rich areas. This is reminiscent of unstable chromosome regions in the human genome, such as the breakpoint cluster region (*BCR)* at 22q11.23.

Within the complex region of CNA on CFA 30 are nine annotated genes, six of which were subject to increase in copy number and three to decrease in copy number (Table 4). One gene with a copy number loss was *SPRED1*, a suppressor of Ras/MAPK activation. Since deletion of *SPRED1* can positively regulate the activation of the RAS/MAPK pathway, this aberration in canine melanoma suggests a possible mechanism of tumorigenesis. The involvement of the MAPK pathway is also supported by the presence of the gene *TRPM7,* located within the region of copy number gain on CFA30. Increase in gene dosage may be associated with increased expression, and overexpression of *TRPM7* has been shown to be involved in both melanoma development (Guo, Carlson, and Slominski 2012) and the regulation of the MAPK pathway (Meng *et al.* 2013). Additionally, targeted FISH analysis of canine oral melanomas indicated copy number gain of both *C-KIT*, which initiates the RAS/MAPK pathway, and *C-MYC,* which is downstream of the MAP-K phosphorylation cascade. Both *C-MYC* and *C-KIT* showed copy number gain in canine oral melanomas (80%

and 65% of cases respectively). This further supports the involvement of the MAP-kinase signaling pathway in the development of canine oral melanomas.

Aberrations detected in both malignant forms of canine melanoma, but not in melanocytomas, suggest that these specific mutations are essential for the development of malignant and aggressive neoplasms. This was further confirmed by the high degree of correlation between patterns of genome-wide CNAs and cellular histology. Malignant melanomas presenting with less complex oaCGH profiles (similar to those of benign lesions) had significantly different cellular morphologies to those with complex copy number profiles. This confirms the molecular basis of cellular phenotype and suggests that specific CNAs present within these particular malignant lesions give rise to a more malignant phenotype. Regions of shared CNA within the malignant populations contain numerous genes (Table 2.5). Based on the cellular function of each protein, the dysregulation of these genes may offer molecular insight into the development of malignant characteristics, including complex genome-wide CNAs, dedifferentiated cell morphologies, and presentation of histologically ambiguous features. For example, the most frequent aberration observed in both cutaneous and oral melanomas was a copy number loss of the segment CFA 3: 62,368,641-62,381,281. Within this region is the coding sequence for *TACC3*, which acts as a stabilizer of mitotic spindles during mitosis and has been proposed to play a role in cell differentiation. The deletion of this gene may help explain the propagation and continued growth of cells with large regions of CNA and whole chromosome aberrations due to inappropriate spindle formation and a breakdown of proper chromosome segregation

checkpoints. It may also give molecular insight to the frequency of these tumors to dedifferentiate and present with histologically ambiguous features.

All ten loci evaluated by FISH analysis showed aberrant copy number in canine oral melanomas. Seven of the loci evaluated showed a combination of gains and losses, suggesting more random genomic instability at these regions than targeted functional pathway alterations. This suggestion is supported by the fact that no homozygous losses and few high amplification events were detected involving any of these seven loci. Three genes showed only unidirectional CNA among the cohort, *C-MYC*, *RB-1*, and *CDKN2A,* suggesting these are not merely random CNAs due to end stage mitotic instability, but targeted alterations advantageous to tumor development. The dysreguation of mRNA expression in these genes has been previously established (Ritt, Wojcieszyn, and Modiano 1998; Koenig *et al.* 2002; Bianco *et al.* 2003). Presence of these specific CNAs offers a molecular mechanism with which tumor cells regulate gene expression leading to tumorigenesis of canine oral melanoma.

2.5.2 Comparison of Canine to Human Melanocytic Lesions

Oral mucosal melanomas in humans are rare and poorly understood, representing only 2% of all melanomas (Chu *et al.* 2013). Due to the small number of cases, limited large-scale genomic research has been performed and so details of the genetics of development of mucosal melanomas and the majority of genetic drivers remain unknown. Through clinical observations of similar anatomical location and behavior, it has been proposed that the mucosal subtype of human melanoma would be analogous to oral canine

melanomas, which would support the use of the dog as a model system to study the development of these rare tumors. Curtain and colleagues first assembled cytogenetic hallmarks of human acral and mucosal melanoma through BAC-array CGH in 2005 (Curtin *et al.* 2005). Using those published data as a reference, we were able to directly compare CNAs reported in these forms of human melanoma with those identified in canine cases in the present study. The comparison revealed mucosal melanomas in both species to have a much more complex genome-wide copy number profile. This is suggestive of decreased genome stability and increased susceptibility to karyotype rearrangements, corroborated by recent whole-genome sequence data (Furney *et al.* 2012). In general, the CNAs most common to canine melanoma were shared with those detected in human mucosal melanomas. Further, the canine CNAs were different from those evident in UV-induced human cutaneous melanomas, which also differ from human mucosal melanomas. The most remarkable similarity between canine melanomas and their human counterparts was a conserved and complex copy number profile along the length of CFA 30/HSA 15. The characteristic copy number signature on HSA 15 has been reported only in mucosal and acral melanomas. We propose that this characteristic feature is associated with a key evolutionarily conserved mechanism of pathogenesis in the development and/or progression of mucosal melanomas. It was also noted that no individual within the canine data set showed the characteristic *BRAF* amplification or associated *CCND1* amplification commonly detected in UV-induced cutaneous melanomas in humans. Other notable conserved mutations are seen as a gain on CFA 13 (cf HSA 4: 70,508,745-70,808,489), loss of CFA 4 and 11 (cf HSA 5: 50,515,301-76,556,132), and gain of CFA 10 and 26 (cf HSA 12: 48,133,151- 52,785,962). These data

indicate the underlying pathway of development in all mucosal melanomas, regardless of species, may be different to that of cutaneous UV-induced melanomas. They also encourage more detailed and statistically powerful studies of the etiology and treatment of mucosal melanomas.

In agreement with other recent proposals (Gillard *et al.* 2014; Simpson *et al.* 2014), our data further supports the role of the dog model as a valuable aide in the study of disease pathogenesis of non-UV-induced mucosal melanomas. Previous comparative studies of melanoma have relied solely on histology and targeted sequencing, highlighting the dissimilarity of canine melanoma and human common cutaneous melanoma, and limited homology with mucosal melanomas. The genome-wide molecular cytogenetic analysis in this study revealed remarkable similarities shared between human and dog mucosal melanomas. These data suggest that pathways specific to melanogenesis of mucosal surfaces may be elucidated by a comparative oncology approach, with integrated consideration of genomics data from both species.

Acknowledgements

I would like to thank Dr. Scott Moroff (SM), Dr. Philippe Labelle (PL), and Dr. Luke Borst (LB) for assistance in pathological diagnostics and Dr. Rachael Thomas for assistance in recoding of canine aoCGH data to human output.

REFERENCES

Angstadt, A. Y., Motsinger-Reif, A., Thomas, R.*, et al.* (2011). "Characterization of canine osteosarcoma by array comparative genomic hybridization and RT-qPCR: Signatures of genomic imbalance in canine osteosarcoma parallel the human counterpart." Genes, Chromosomes and Cancer **50**(11): 859-874.

Avruch J, K. A., Kyriakis JM, Luo Z, Tzivion G, Vavvas D, Zhang XF. (2001). "Ras activation of the Raf kinase: tyrosine kinase recruitment of the MAP kinase cascade." Recent Prog Horm Res **56**: 127-155.

Bastian, B. C., Olshen, A. B., LeBoit, P. E.*, et al.* (2003). "Classifying Melanocytic Tumors Based on DNA Copy Number Changes." The American Journal of Pathology **163**(5): 1765-1770.

Bauer, J. and Bastian, B. C. (2006). "Distinguishing melanocytic nevi from melanoma by DNA copy number changes: comparative genomic hybridization as a research and diagnostic tool." Dermatologic Therapy **19**: 40-49.

Berger, M. F., Hodis, E., Heffernan, T. P.*, et al.* (2012). "Melanoma genome sequencing reveals frequent PREX2 mutations." Nature.

Bergman, P. (2007). "Canine Oral Melanoma." Clinical Techniques in Small Animal Practice **22**(2): 55-60.

Bianco, S. R., Sun, J., Fosmire, S. P.*, et al.* (2003). "Enhancing antimelanoma immune responses through apoptosis." Cancer Gene Therapy **10**(9): 726-736.

Blokx, W. A. M., van Dijk, M. C. R. F. and Ruiter, D. J. (2010). "Molecular cytogenetics of cutaneous melanocytic lesions: diagnostic, prognostic and therapeutic aspects." Histopathology **56**(1): 121-132.

Breen, M., Bullerdiek, J. and Langford, C. F. (1999). "The DAPI banded karyotype of the domestic dog (Canis familiaris) generated using chromosome-specific paint probes." Chromosome Research **7**(7): 575.

Breen, M., Hitte, C., Lorentzen, T. D.*, et al.* (2004). "An intergrated 4249 marker FISH/RH map of the canine genome." BMC Genomics **5**(1): 65.

Breen, M. (2009). "Update on Genomics in Veterinary Oncology." Topics in Companion Animal Medicine **24**(3): 113-121.

Chu, P. Y., Pan, S. L., Liu, C. H.*, et al.* (2013). "KIT gene exon 11 mutations in canine malignant melanoma." Vet J **196**(2): 226-230.

Curtin, J. A., Fridlyand, J., Kageshita, T.*, et al.* (2005). "Distinct Sets of Genetic Alterations in Melanoma " New England Journal of Medicine **353**(20): 2135-2147.

Furney, S. J., Turajlic, S., Fenwick, K.*, et al.* (2012). "Genomic Characterisation of Acral Melanoma Cell Lines." Pigment Cell & Melanoma Research.

Gaiser, T., Kutzner, H., Palmedo, G.*, et al.* (2010). "Classifying ambiguous melanocytic lesions with FISH and correlation with clinical long-term follow up." Modern Pathology **23**(3): 413-419.

Gillard, M., Cadieu, E., De Brito, C.*, et al.* (2014). "Naturally occurring melanomas in dogs as models for non-UV pathways of human melanomas." Pigment Cell & Melanoma Research **27**(1): 90.

Guo, H., Carlson, J. A. and Slominski, A. (2012). "Role of TRPM in melanocytes and melanoma." Experimental Dermatology **21**(9): 650-654.

Koenig, A., Bianco, S. R., Fosmire, S.*, et al.* (2002). "Expression and Significance of p53, Rb, p21/waf-1, p16/ink-4a, and PTEN Tumor Suppressors in Canine Melanoma." Veterinary Pathology **39**(4): 458-472.

Kudnig, S. T., Ehrhart, N. and Withrow, S. J. (2003). "Survival Analysis of Oral Melanomas in Dogs." Veterinary Cancer Society Proceedings **23**(39).

Meng, X., Cai, C., Wu, J.*, et al.* (2013). "TRPM7 mediates breast cancer cell migration and invasion through the MAPK pathway." Cancer Letters **333**(1): 96-102.

Newman, S. J., Jankovsky, J. M., Rohrbach, B. W.*, et al.* (2011). "C-kit Expression in Canine Mucosal Melanomas." Veterinary Pathology **49**(5): 760-765.

Ramos-Vara, J. A., Beissenherz, M. E., Miller, M. A.*, et al.* (2000). "Retrospective Study of 338 Canine Oral Melanomas with Clinical, Histologic, and Immunohistochemical Review of 129 Cases." Veterinary Pathology **37**(6): 597-608.

Ritt, M. G., Wojcieszyn, J. and Modiano, J. F. (1998). "Functional Loss of p21/Waf-1 in a Case of Benign Canine Multicentric Melanoma." Veterinary Pathology **35**(2): 94-101.

Sevastre, B., van Ederen, A. M., Terlou, M.*, et al.* (2007). "Immunohistochemical expression of tenascin in melanocytic tumours of dogs." J Comp Pathol **136**(1): 49-56.

Simpson, R. M., Bastian, B. C., Michael, H. T.*, et al.* (2014). "Sporadic naturally occurring melanoma in dogs as a preclinical model for human melanoma." Pigment Cell & Melanoma Research **27**(1): 37-47.

Smedley, R. C., Spangler, W. L., Esplin, D. G.*, et al.* (2011). "Prognostic Markers for Canine Melanocytic Neoplasms: A Comparative Review of the Literature and Goals for Future Investigation." Veterinary Pathology **48**(1): 54-72.

Smith, S. H., Goldschmidt, M. H. and McManus, P. M. (2002). "A Comparative Review of Melanocytic Neoplasms." Veterinary Pathology **39**(6): 651-678.

Spangler, W. L. and Kass, P. H. (2006). "The Histologic and Epidemiologic Bases for Prognostic Considerations in Canine Melanocytic Neoplasia." Veterinary Pathology **43**(2): 136-149.

Thomas, R., Seiser, E. L., Motsinger-Reif, A.*, et al.* (2011). "Refining tumor-associated aneuploidy through 'genomic recoding' of recurrent DNA copy number aberrations in 150 canine non-Hodgkin lymphomas. ." Leukemia and Lymphoma **52**(7): 1321-1335.

Villamil, J. A., Henry, C. J., Bryan, J. N.*, et al.* (2011). "Identification of the most common cutaneous neoplasms in dogs and evaluation of breed and age distributions for selected neoplams." JAVMA **239**(7): 960-965.

Withrow, S. J., D. M. Vail, and R. Page (2013). Small Animal Clinial Oncology, Elsevier.

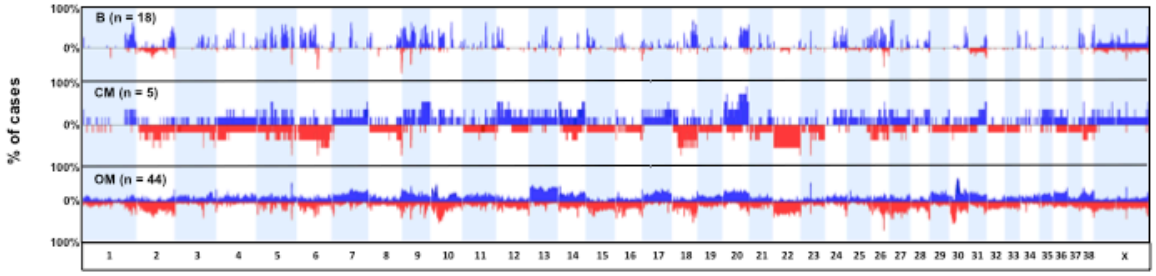

Figure 2.1. Oligo-aCGH analysis of primary canine oral melanoma (OM), primary canine cutaneous melanoma (CM), and canine cutaneous melanocytoma (B). Penetrance plots of recurrent CNAs, at 26kb intervals, identified within 67 canine melanocytic lesions. Genomic locations are plotted along the x-axis, and the y-axis indicates the percentage of the three subtypes with copy number gain (shown in blue above the midline) or loss (shown in red below the midline) of the corresponding intervals along each chromosome. In oral melanomas (OM, n=44) the most frequent gain was located on CFA 30: 18,527,413-18,592,465, along with whole chromosome gains of CFA 13, 17, 20, 29, and 36. The most frequent losses were found on CFA 10: 20,583,579-20,598, 892, chr26: 30,241,704-30,306,343, CFA 30: 10,620,776-10,658,526 and all of CFA 2, 22, and 27. In cutaneous melanomas (CM, n=5) the largest and most common aberration was a gain of CFA 20: 10,929,869-57,175,686. In melanocytomas (B, n=18), the most frequent aberration was a gain of a small region of CFA 27: 9,965,501-10,052,495, as well as less frequent gains on CFA 9: 20,973,038-21,556,711, CFA 10: 48,818,794-48,878,597, and CFA 11: 55,214,228-55,245,594.

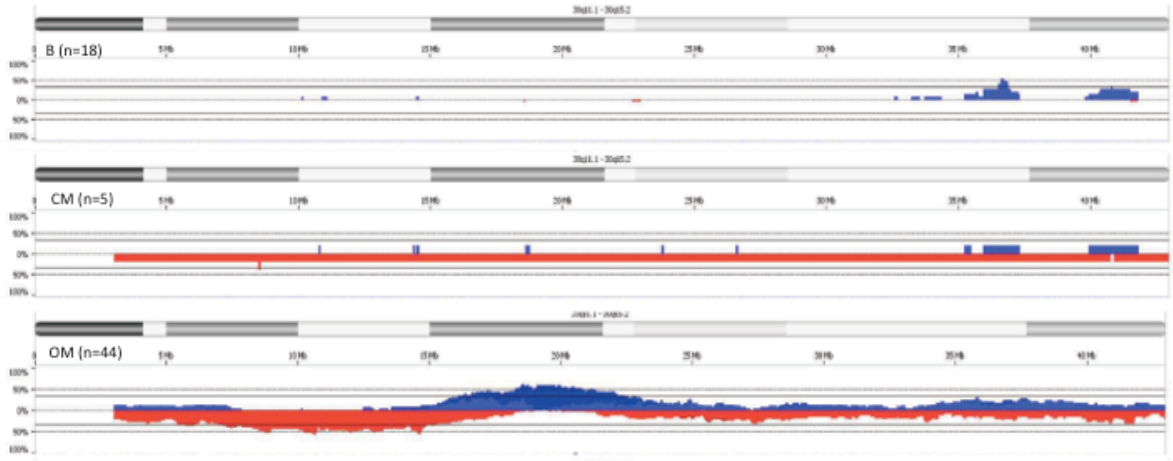

Figure 2.2. Penetrance plots of DNA copy number aberrations along the length of CFA 30 in oral melanoma (OM), cutaneous melanoma (CM), and melanocytoma (B). Oral melanomas showed a distinct pattern of copy number loss (spanning 3-18Mb) partially overlapping a region of copy number gain (spanning 12-25Mb), indicative of a variable chromosome breakage event. This breakage region, centered at 15Mb-18Mb was not present in either cutaneous melanomas or benign melanocytomas. Evaluation revealed 50% (n=9) of melanocytomas showed a gain of two small regions at the distal end of chromosome 30 (35-37Mb and 40-42Mb), also seen in 20% (n=1) of cutaneous melanomas.

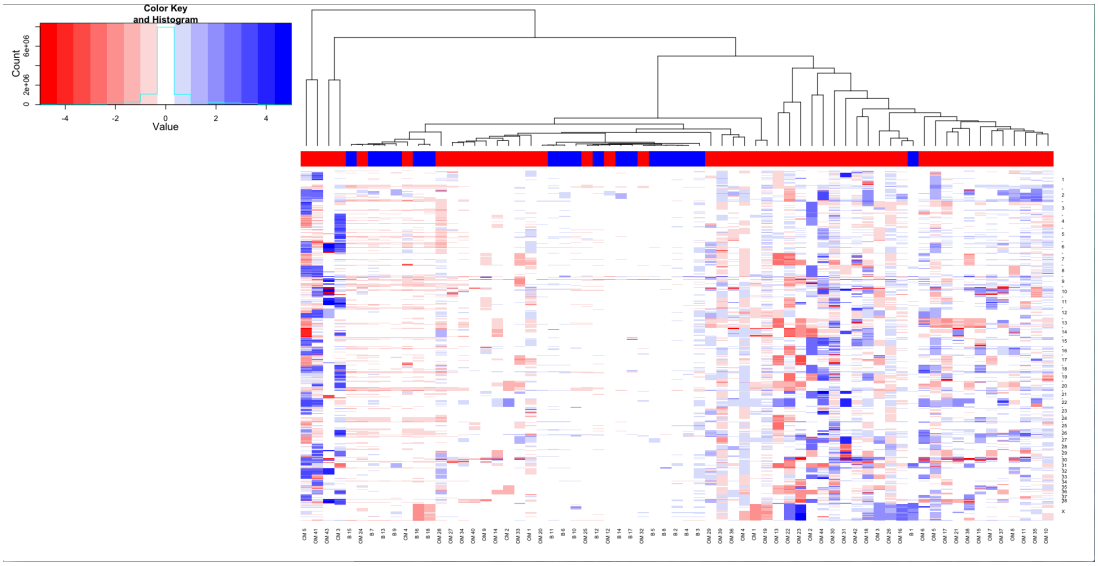

Figure 2.3. Clustering analysis of 44 cases of primary canine oral melanoma (OM), five cases of primary canine cutaneous melanoma (CM), and 18 cases of primary canine melanocytoma (B) based on genome-wide oaCGH profiles. Segmented oaCGH profiles were subjected to hierarchical clustering. Individual cases are plotted along the x-axis, with chromosomes plotted along the y-axis. Cases were grouped and a schematic depicting a lineage tree of relatedness is drawn above. Blue, red and white represent CN gain, loss, and neutrality. The CN log2 ratio is represented in the intensity of the coloration gradient as per the inset. Colored bars above each sample indicate malignant (red) or benign (blue) cases. In general, cases with more complex copy number profiles clustered together. Twenty-one malignant melanomas, each with few copy number aberrations, clustered into the same bin as all but one of the benign lesions. Further analysis showed these 21 cases showed histological characteristics significantly different from melanomas that clustered together. The one benign lesion that clustered with a group of malignant lesions had two whole chromosome gains, CFA 31 and CFA X.

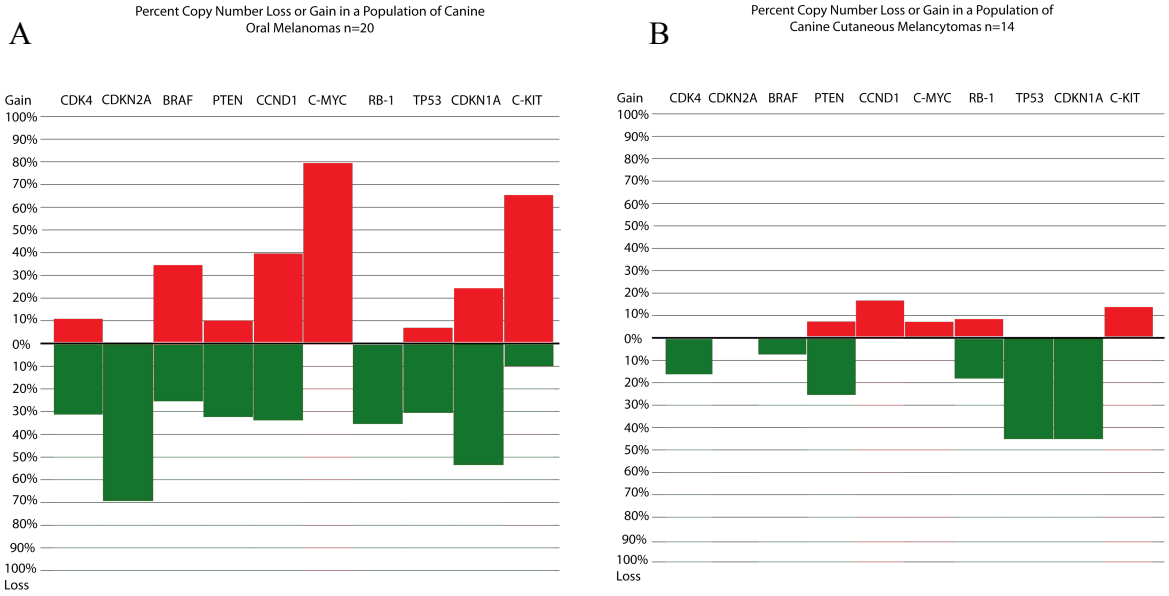

Figure 2.4. Penetrance of aberration of 10 specific genomic regions in (A) primary canine oral melanoma and (B) canine melanocytoma. Gains and losses are plotted above or below the x-axis respectively. The length of the bar represents the percentage of the sampled population that showed a particular aberration (y-axis). Full locus identity and location are provided in Table 2.8. Canine oral melanomas showed higher percentage of cases with targeted genomic aberrations than benign melanocytomas, validating the oaCGH data. It also revealed targeted regions with unidirectional changes, suggesting their involvement in downstream pathway dysregulation and tumorigenesis.

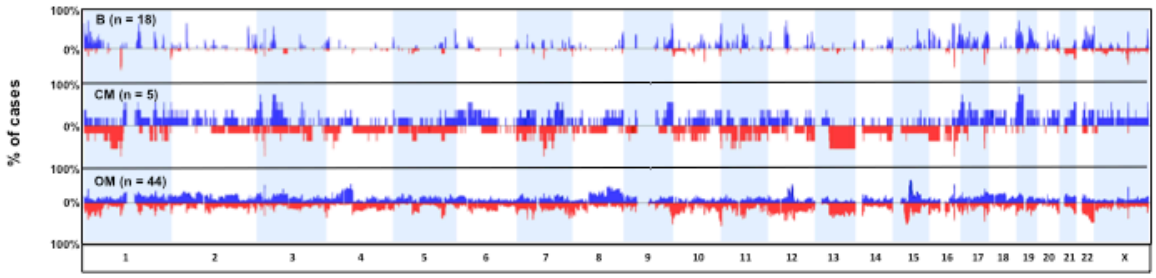

Figure 2.5. Canine oral melanoma (OM), cutaneous melanoma (CM), and benign melanocytoma (B) oaCGH profile data recoded as human. Canine oral melanomas (n=44), cutaneous melanomas (n=5), and cutaneous melanoctyomas (n=18) were recoded and output with human genome coordinates. This allowed for comparison to known aCGH profiles compiled for human melanoma subtypes. Hallmarks of human mucosal melanoma are copy number amplification of 1q31, 4q12, 12q14, 11q13, 8q, and 6p as well as copy number loss of 3q, 4q, 8p, 10, 11p, and 21q (Curtain et al, 2005). Similar aberrations were found within the canine oral melanoma population. Most notably, the breakage area on CFA 30 matches a similar pattern of loss followed by gain seen on HSA chromosome 15, the orthologous region on the human genome.

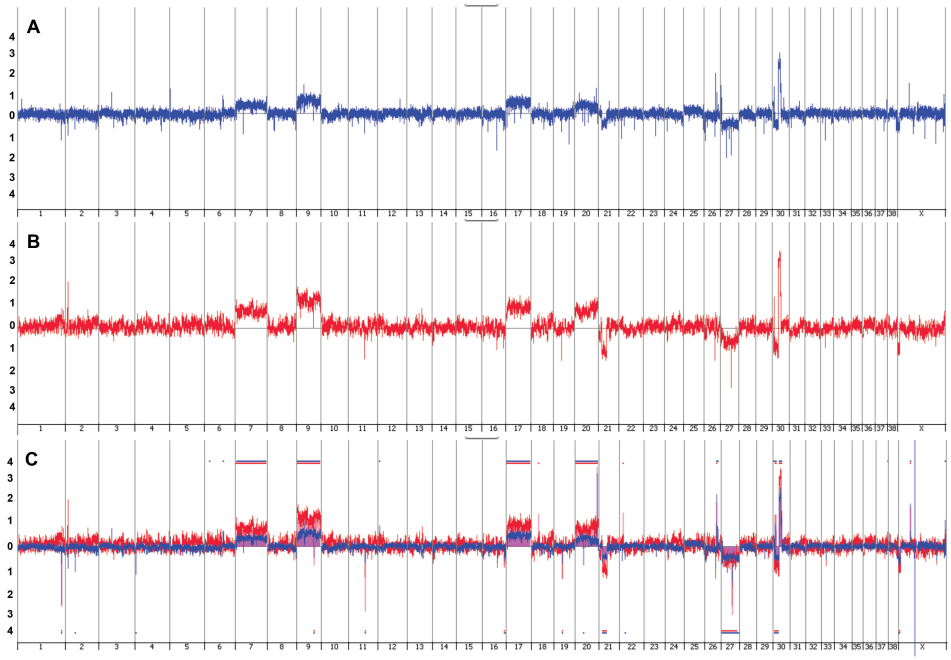

Figure 2.6. Comparison of oaCGH analysis of fresh frozen tissue (A) and formalin fixed paraffin embedded tissue (B) from the same tumor. DNA from both the fresh frozen tissue and the FFPE section (after microdisection for tumor enrichment) were available for the same case and analyzed with oaCGH. Visualization of individual cases and overlay was completed in Agilent Genomic Workbench with CNAs called using the ADM2 algorithm. Chromosomes are presented along the x-axis with log2 ratio of copy number changes presented along the y-axis centered at y=0. **(C)** Shows a direct overlay of the two cases with the fresh tissue in blue and the FFPE tissue in red. Bars (fresh tissue in blue and FFPE tissue in red) above and below the CNAs delineate the length of aberration across each chromosome. Length of the bar indicates the length of the bar along the chromosome.

Table 2.1. Histological description of primary tumors from formalin fixed paraffin embedded (FFPE) and fresh frozen samples.

FFPE Oral Melanomas									
Cases	**Primary Site**	**Breed**	**Age**	**Sex**	**Mitotic Index**	**Pigmentation**	**Nuc. Atypia**	**Junctional Activity**	**Tissue Subtype**
OM 1	Oral - Mandible w/ g&t	Golden Retriever	11Y	F	41	< 5%	high	yes	mixed
OM 2	Oral - Caudal oral cavity	English Shepard Dog	9Y	M	13	< 5%	high	yes	polygonal
OM 3	Oral - Gum	Airedale Terrier	11Y	F	8	40%	low	no	mixed
OM 4	Oral - Maxilla	Scottish Terrier	10Y	F	39	0%	high	no	spindeloid
OM 5	Oral	Golden Retriever	9Y	F	48	10%	high	no junction available	spindeloid
OM 6	Oral	Mixed	10Y	M	50	5%	high	no	polygonal
OM 7	Oral	Schipperke	14Y	M	44	0%	med	no junction available	spindeloid
OM 8	Oral	Rottweiler	6Y	M	34	50%	high	no junction available	polygonal
OM 9	Oral	Beagle	12Y	F	4	50%	high	yes	polygonal
OM 10	Oral	Cocker Spaniel	n/a	M	140	0%	high	yes	polygonal
OM 11	Oral	not identified	16Y	M	8	0%	high	no	spindeloid
OM 12	Oral	Australian Shepherd	8Y	M	2	50%	low	yes	mixed
OM 13	Oral	Labrador Retriever	10Y	M	42	5%	high	yes	polygonal
OM 14	Oral	Yorkshire Terrier	11Y	F	26	50%	med	yes	polygonal
OM 15	Oral	Labrador Retriever	9Y	M	48	0%	med	yes	polygonal
OM 16	Oral	Golden Retriever	9Y	F	too pigmented	100%	low	no junction available	spindeloid
OM 17	Oral	Mixed	13Y	M	170	0%	high	no	mixed
OM 18	Oral	Mixed	n/a	F	85	5%	low	mixed	spindeloid
OM 19	Oral	Labrador Retriever	13Y	M	3	10%	high	mixed	ulcerated mix
OM 20	Oral - Lip	Jack Russel Terrier	10Y	F	11	5%	low	no junction available	polygonal
OM 21	Oral	Not Identified	15Y	F	34	0%	low	no junction available	mixed
OM 22	Oral	Lhasa Apso	15Y	F	9	< 5%	low	yes	ulcerated polygonal
OM 23	Oral	Mixed	14Y	M	14	0%	high	yes	mixed
OM 24	Oral	Labrador Retriever	8Y	M	too pigmented	95%	low	yes	mixed
OM 25	Oral	Cocker Spaniel	13Y	M	12	50%	low	no	polygonal
OM 26	Oral	Mixed	10Y	F	5	20%	high	yes	necrotic spindeloid
OM 27	Oral	English Springer Spaniel	n/a	F	6	0%	high	no	spindeloid
OM 28	Oral	Not Identified	13Y	F	33	< 5%	mid	no	polygonal
OM 29	Oral	Pekinese	14Y	M	12	0%	high	yes	polygonal
OM 30	Oral	Flat Coated Retreiver	10Y	M	50	0%	high	no junction available	mixed
OM 31	Oral	Gordon Setter	11Y	M	18	5%	high	no	mixed
OM 32	Oral	Yorkshire Terrier	9Y	M	7	10%	low	no	spindeloid
Fresh Oral Melanomas									
Cases	**Primary Site**	**Breed**	**Age**	**Sex**	**Mitotic Index**	**Pigmentation**	**Nuc. Atypia**	**Junctional Activity**	**Tissue Subtype**
OM 33	Oral	Mixed	n/a	M	67	> 50%	high	yes	mixed
OM 34	Oral	Mini Schnauzer	n/a	F	0	> 50%	low	no	polygonal
OM 35	Oral	Belgian Malamute	n/a	F	3	< 5%	high	no junction available	spindeloid
OM 36	Oral	Mixed	n/a	M	15	> 50%	high	yes	mixed
OM 37	Oral	Poodle	n/a	M	19	< 5%	high	no junction available	polygonal
OM 38	Oral	Mini Schnauzer	10Y	F	26	70%	med	yes	spindeloid
OM 39	Oral	Labrador Retriever	14Y	F	n/a	0%	n/a	n/a	n/a
OM 40	Oral	Mixed	14Y	F	0	50%	no	no junction available	polygonal
OM 41	Oral	German Shorthaired Pointer	10Y	F	5	50%	high	no junction available	polygonal
OM 42	Oral	Cocker Spaniel	10Y	M	n/a	0%	high	no junction available	polygonal
OM 43	Oral	Poodle	12Y	F	40	0%	med	no junction available	mixed
OM 44	Oral	English Setter	11Y	F	15	0%	high	yes	polygonal
FFPE Melanocytomas									
Cases	**Primary Site**	**Breed**	**Age**	**Sex**	**Mitotic Index**	**Pigmentation**	**Nuc. Atypia**	**Junctional Activity**	**Tissue Subtype**
B 1	Oral	Miniature Schnauzer	7Y	M	too pigmented	80%	no	no junction available	too pigmented
B 2	Skin	Goldern Retriever	5Y	M	0	80%	no	no junction available	spindeloid
B 3	Skin	not identified	8Y	F	0	25%	no	no	mixed
B 4	Skin	Poodle	10Y	F	2	50%	low	no	polygonal
B 5	Skin	Boxer	13Y	M	2	20%	low	mix	mixed
B 6	Skin	Jack Russel Terrier	12Y	M	2	20%	low	no junction available	spindeloid
B 7	Skin	Mixed	13Y	M	2	80%	no	yes	polygonal
B 8	Skin	Miniature Schnauzer	8Y	M	2	20%	low	no junction available	spindeloid
B 9	Skin	Not Identified	7Y	F	4	60%	no	yes	spindeloid
B 10	Oral	Mixed	7Y	M	3	80%	low	yes	spindeloid
B 11	Skin	Lhasa Apso	14Y	F	5	20%	no	no	spindeloid
B 12	Skin	Mixed	6Y	M	too pigmented	80%	no	yes	spindeloid
B 13	Skin	Portuguese Water Dog	6Y	F	too pigmented	100%	no	no junction available	spindeloid
B 14	Skin	Pug	5Y	M	too pigmented	100%	low	no junction available	spindeloid
B 15	Skin	Miniature Schnauzer	8Y	M	too pigmented	90%	no	yes	too pigmented
B 16	Oral	Mixed	10Y	M	too pigmented	90%	low	yes	too pigmented
B 17	Oral	Mixed	6Y	M	3	0%	low	no	mixed
B 18	Oral	Gordon Setter	11Y	M	5	50%	high	no	ulcerated
Cutaneous Melanomas Fresh and FFPE									
Cases	**Primary Site**	**Breed**	**Age**	**Sex**	**Mitotic Index**	**Pigmentation**	**Nuc. Atypia**	**Junctional Activity**	**Tissue Subtype**
CM 1	Skin - ear tip	Doberman Pincher	11Y	M	4	50%	low	yes	spindeloid
CM 2	Skin - Foot pad	German Shepherd	9Y	F	5	70%	high	no junction available	spindeloid
CM 3	Skin	Golden Retiever	14Y	M	8	0%	high	no junction available	spindeloid
CM 4	Skin	Mixed	12Y	F	50	0%	high	yes	spindeloid
CM 5	Skin	Basset Hound	8Y	F	7	0%	low	yes	mixed

Table 2.2. Genome-wide DNA copy number aberrations with at least 50% penetrance for three subtypes of canine melanocytic lesions, oral melanoma (OM), benign melanocytoma (B), and cutaneous melanoma (CM).

OM n=44					
Region chr:bp start-bp end	**Length in bp**	**Cytoband**	**Event**	**Genes**	**Frequency %**
chr10:20,583,579-20,598,892	15313	q21	CN Loss	0	56.82
chr26:30,261,091-30,306,343	45252	q24	CN Loss	2	75.00
chr30:19,102,383-19,660,901	558518	q14.1	CN Gain	7	61.36
chr30:19,876,904-19,996,814	119910	q14.1	CN Gain	1	61.36
chr30:20,116,984-20,240,659	123675	q14.1	CN Gain	2	59.09
chr30:20,387,339-20,525,268	137929	q14.1	CN Gain	3	59.09
CM n=5					
Region chr:bp start-bp end	**Length in bp**	**Cytoband**	**Event**	**Genes**	**Frequency %**
chr5:81,157,085-81,422,820	265735	q35	CN Loss	0	80.00
chr6:48,260,040-49,569,575	1309535	q23.1	CN Loss	0	80.00
chr18:21,439,849-21,824,376	384527	q21	CN Loss	1	80.00
chr20:10,929,869-57,175,686	46245817	q11-17	CN Gain	359	80.00
chr22:63,472,754-63,531,977	59223	q24	CN Loss	2	80.00
chr23:23,552,949-23,718,671	165722	q21.1	CN Loss	0	80.00
BM n=18					
Region chr:bp start-bp end	**Length in bp**	**Cytoband**	**Event**	**Genes**	**Frequency %**
chr1:117,087,221-117,377,134	289913	q37	CN Gain	13	60.00
chr5:59,367,552-59,417,133	49581	q32	CN Gain	4	60.00
chr5:67,518,696-67,532,344	13648	q33	CN Gain	3	60.00
chr5:81,157,085-81,374,416	217331	q35	CN Gain	0	60.00
chr6:41,862,591-42,008,647	146056	q22	CN Gain	13	60.00
chr6:48,348,336-48,987,554	639218	q23.1	CN Loss	0	60.00
chr7:44,579,697-44,813,300	233603	q17	CN Gain	12	60.00
chr8:76,368,492-76,582,392	213900	q33.3	CN Loss	9	60.00
chr9:20,973,038-21,556,711	583673	q14	CN Gain	9	66.67
chr9:53,793,547-53,944,034	150487	q25	CN Gain	1	60.00
chr10:48,818,794-48,878,597	59803	q21	CN Gain	1	66.67
chr11:55,214,228-55,245,594	31366	q21	CN Gain	7	66.67
chr18:49,035,472-49,406,866	371394	q25.1	CN Gain	10	60.00
chr18:55,807,318-55,861,598	54280	q25.3	CN Gain	10	60.00
chr18:55,899,795-55,986,610	86815	q25.3	CN Gain	2	60.00
chr20:60,767,150-61,000,000	232850	q17	CN Gain	18	60.00
chr27:5,862,415-6,022,827	160412	q11	CN Gain	15	60.00
chr27:9,965,501-10,052,495	86994	q12	CN Gain	5	73.33
chrX:1-143,538	143538	p22.3	CN Gain	12	60.00

Table 2.3.1 Significant genome-wide DNA copy number aberrations using GISTIC for canine oral melanoma (OM).

OM Regions with GISTIC Significance					
Region	**Extended Region**	**Type**	**Q-Bound**	**G-Score**	**% of CNV Overlap**
chr2:86,827,776-86,968,017	chr2:86,827,776-86,968,017	CN Gain	0.01624276	10.16	0
chr5:81,189,945-81,349,070	chr5:81,189,945-81,406,580	CN Gain	3.70E-06	16.37	0
chr9:21,086,878-21,202,655	chr9:21,029,083-21,202,655	CN Gain	0.01106026	10.52	0
chr10:13,879,089-14,012,498	chr10:13,831,766-14,545,158	CN Gain	4.25E-10	41.10	0
chr10:4,760,299-4,831,368	chr10:4,646,739-4,831,368	CN Gain	9.56E-09	20.29	0
chr10:53,156,724-53,472,065	chr10:52,387,783-53,749,886	CN Gain	0.00107783	12.49	0
chr13:65,919,719-66,047,830	chr13:65,730,802-66,047,830	CN Gain	0.01503172	10.22	0
chr14:10,075,226-10,292,604	chr14:8,574,711-10,686,666	CN Gain	0.00203921	11.99	0
chr16:62,203,097-62,515,898	chr16:62,203,097-62,515,898	CN Gain	0.02525589	9.65	0
chr20:56,256,652-56,280,086	chr20:56,256,652-56,286,566	CN Gain	0.01691585	10.10	0
chr23:23,587,149-23,718,671	chr23:23,552,949-23,759,722	CN Gain	2.04E-06	16.76	0
chr26:30,241,704-30,261,091	chr26:30,235,074-30,306,343	CN Gain	2.28E-04	13.61	0
chr30:19,396,688-19,516,412	chr30:19,085,315-19,660,901	CN Gain	4.25E-10	58.15	0
chr30:36,243,187-36,304,668	chr30:34,265,324-37,004,574	CN Gain	0.00558962	11.17	0
chr31:7,929,632-8,198,080	chr31:5,859,849-13,293,969	CN Gain	0.01663631	10.13	0
chr38:3,405,422-3,538,896	chr38:3,189,443-4,217,229	CN Gain	0.03959025	9.17	0
chrX:74,854,890-74,974,869	chrX:74,807,177-75,285,514	CN Gain	0.00293874	11.67	0
chr1:114,637,937-114,656,865	chr1:114,637,937-114,665,364	CN Loss	1.34E-08	22.13	0
chr2:86,827,776-86,968,017	chr2:86,827,776-86,968,017	CN Loss	0.00213317	10.15	0
chr3:65,296,031-65,396,261	chr3:65,232,960-65,432,693	CN Loss	0.01628326	7.89	0
chr4:3,015,106-3,070,165	chr4:3,015,106-3,113,601	CN Loss	3.90E-04	11.72	0
chr5:81,406,580-81,422,820	chr5:81,406,580-81,422,820	CN Loss	4.95E-08	18.26	0
chr6:41,862,591-41,926,348	chr6:41,862,591-43,080,399	CN Loss	0.00476427	9.47	0
chr7:4,481,626-4,583,154	chr7:4,144,974-4,583,154	CN Loss	0.02337253	7.43	0
chr8:76,376,971-76,418,529	chr8:76,376,971-76,418,529	CN Loss	9.40E-07	16.42	0
chr9:42,294,685-42,320,234	chr9:42,294,685-42,320,234	CN Loss	2.77E-08	18.74	0
chr9:20,488,956-20,590,682	chr9:20,474,456-20,633,826	CN Loss	0.00126535	10.62	0
chr10:19,910,771-19,977,267	chr10:19,689,248-21,835,975	CN Loss	6.26E-05	13.87	0
chr11:44,252,111-44,285,901	chr11:44,211,059-44,467,159	CN Loss	1.07E-04	13.50	0
chr12:75,148,337-75,267,772	chr12:75,130,246-75,302,377	CN Loss	0.01794901	7.76	0
chr13:5,458,646-5,505,233	chr13:5,458,646-5,505,233	CN Loss	0.02156167	7.52	0
chr14:46,598,461-46,678,089	chr14:46,584,383-46,678,089	CN Loss	0.01063497	8.48	0
chr15:23,472,577-23,517,219	chr15:23,472,577-27,817,003	CN Loss	3.49E-04	11.96	0
chr16:62,203,097-62,515,898	chr16:62,203,097-62,515,898	CN Loss	3.72E-04	11.76	0
chr16:4,213,825-4,239,959	chr16:4,213,825-4,258,636	CN Loss	0.01680828	7.84	0
chr18:49,213,222-49,233,985	chr18:49,035,472-52,294,642	CN Loss	4.63E-04	11.56	0
chr20:56,256,652-56,280,086	chr20:56,256,652-56,280,086	CN Loss	1.34E-08	30.47	0
chr21:33,751,639-33,837,189	chr21:33,703,628-33,837,189	CN Loss	0.02392112	7.39	0
chr22:23,845,574-24,002,337	chr22:14,537,344-38,654,160	CN Loss	0.00177263	10.30	0
chr23:23,563,470-23,718,671	chr23:23,563,470-23,759,722	CN Loss	0.00190609	10.24	0
chr23:23,787,810-23,842,143	chr23:23,759,722-23,856,187	CN Loss	0.04076074	6.84	0
chr24:49,984,397-50,090,042	chr24:49,900,755-50,241,858	CN Loss	0.01730606	7.80	0
chr26:30,261,091-30,306,343	chr26:30,241,704-30,306,343	CN Loss	1.34E-08	66.80	0
chr26:4,131,462-4,206,619	chr26:3,473,009-7,813,608	CN Loss	0.01065659	8.46	0
chr26:40,924,095-40,968,469	chr26:40,904,816-40,994,620	CN Loss	0.0138418	8.07	0
chr27:28,729,469-28,883,372	chr27:28,729,469-28,934,553	CN Loss	1.34E-08	20.46	0
chr27:40,740,881-40,754,138	chr27:40,740,881-40,754,138	CN Loss	0.01007504	8.55	0
chr27:5,828,184-6,011,259	chr27:5,029,882-6,022,827	CN Loss	0.04019147	6.85	0
chr28:43,262,646-43,385,184	chr28:42,633,500-44,164,395	CN Loss	0.00419263	9.59	0
chr30:10,620,776-10,640,884	chr30:10,245,871-10,747,987	CN Loss	2.07E-04	12.88	0
chr30:26,188,574-26,199,784	chr30:25,874,552-26,560,890	CN Loss	0.01130433	8.35	0
chr31:38,197,745-38,214,020	chr31:38,197,745-38,952,636	CN Loss	2.94E-04	12.51	0
chrX:74,807,177-74,854,890	chrX:74,807,177-75,308,693	CN Loss	1.34E-08	41.91	0
chrX:32,220,251-32,247,960	chrX:32,220,251-32,279,028	CN Loss	1.34E-08	27.09	0
chrX:85,524,761-85,581,869	chrX:85,524,761-85,581,869	CN Loss	0.00425608	9.56	0

Table 2.3.2 Significant genome-wide DNA copy number aberrations using GISTIC for canine cutaneous melanoma (CM).

CM Regions with GISTIC Significance					
Region	**Extended Region**	**Type**	**Q-Bound**	**G-Score**	**% of CNV Overlap**
chr14:58,094,987-58,849,668	chr14:46,802,954-63,000,000	CN Gain	0.01270454	4.78	0

Table 2.3.3 Significant genome-wide DNA copy number aberrations using GISTIC for canine benign melanocytoma (B).

B Regions with GISTIC Significance					
Region	**Extended Region**	**Type**	**Q-Bound**	**G-Score**	**% of CNV Overlap**
chr1:117,087,221-117,212,244	chr1:108,245,814-117,540,015	CN Gain	1.79E-05	4.68	0
chr1:119,496,512-120,447,489	chr1:119,459,266-125,000,000	CN Gain	0.01648036	2.48	0
chr1:3,839,223-4,167,983	chr1:3,662,504-4,182,287	CN Gain	0.01184963	2.60	0
chr2:82,590,966-82,665,656	chr2:81,151,300-84,212,283	CN Gain	2.54E-05	4.59	0
chr2:82,590,966-82,665,656	chr2:81,151,300-84,212,283	CN Gain	2.54E-05	4.59	0
chr3:63,363,880-63,750,539	chr3:59,402,935-65,504,828	CN Gain	0.04345763	2.14	0
chr3:76,831,901-76,967,393	chr3:76,831,901-76,994,058	CN Gain	0.00435091	2.94	0
chr3:94,000,000-94,171,927	chr3:94,000,000-94,171,927	CN Gain	0.04345763	2.13	0
chr4:31,908,866-32,379,618	chr4:30,373,234-32,851,368	CN Gain	0.04605908	2.11	0
chr4:39,053,116-39,170,521	chr4:39,042,223-39,194,034	CN Gain	7.85E-10	6.76	0
chr4:62,114,752-62,159,956	chr4:61,830,636-62,168,311	CN Gain	0.01473081	2.52	0
chr4:91,000,000-91,398,109	chr4:91,000,000-91,398,109	CN Gain	0.01262203	2.57	0
chr5:22,776,305-22,816,038	chr5:11,096,260-22,923,069	CN Gain	3.94E-05	4.49	0
chr5:34,619,831-34,709,337	chr5:33,442,777-36,845,062	CN Gain	5.57E-04	3.62	0
chr5:59,113,319-59,488,835	chr5:59,082,995-67,699,985	CN Gain	0.00659926	2.81	0
chr5:81,157,085-81,349,070	chr5:81,126,189-81,406,580	CN Gain	4.89E-09	6.39	0
chr5:81,406,580-81,422,820	chr5:81,406,580-81,452,184	CN Loss	0.00188539	7.21	0
chr6:19,774,410-19,798,691	chr6:19,774,410-19,798,691	CN Gain	8.64E-05	4.22	0
chr6:34,178,794-34,314,993	chr6:34,178,794-34,449,912	CN Gain	0.02869225	2.28	0
chr6:42,849,001-43,096,405	chr6:40,051,056-43,209,457	CN Gain	8.36E-08	5.83	0
chr7:3,723,393-3,918,808	chr7:3,006,080-5,095,917	CN Gain	0.00184027	3.22	0
chr7:44,698,054-44,807,027	chr7:44,414,914-44,822,142	CN Gain	1.03E-06	5.33	0
chr7:82,799,910-83,000,000	chr7:82,744,812-83,000,000	CN Gain	0.04605908	2.12	0
chr8:6,607,735-6,694,814	chr8:4,558,537-6,694,814	CN Gain	0.00769219	2.75	0
chr8:75,373,210-75,898,491	chr8:75,020,904-76,011,252	CN Gain	6.76E-05	4.29	0
chr8:76,368,492-76,418,529	chr8:76,365,171-76,582,392	CN Loss	7.77E-04	8.56	0
chr9:21,408,895-21,530,272	chr9:21,408,895-21,903,081	CN Gain	4.89E-09	6.37	0
chr9:25,565,335-25,623,323	chr9:25,565,335-27,688,929	CN Gain	1.10E-04	4.15	0
chr9:45,217,496-45,500,017	chr9:45,054,425-60,003,763	CN Gain	9.92E-04	3.44	0
chr9:5,390,342-5,538,635	chr9:3,092,279-7,244,778	CN Gain	2.41E-04	3.88	0
chr10:23,187,573-23,306,445	chr10:20,598,892-23,334,650	CN Gain	0.00113505	3.40	0
chr10:31,563,018-31,893,061	chr10:31,563,018-32,036,160	CN Gain	0.04461882	2.13	0
chr10:4,510,998-4,831,368	chr10:3,004,950-4,923,812	CN Gain	0.00705634	2.78	0
chr10:48,818,794-48,878,597	chr10:48,629,439-48,878,597	CN Gain	3.94E-05	4.48	0
chr11:55,214,228-55,245,594	chr11:55,204,045-55,321,496	CN Gain	4.99E-08	5.93	0
chr12:4,554,654-4,607,625	chr12:3,031,642-4,607,625	CN Gain	0.02115983	2.39	0
chr12:5,623,620-5,667,555	chr12:5,608,152-6,861,836	CN Gain	6.91E-10	6.82	0
chr13:40,394,483-40,777,502	chr13:40,373,884-40,967,200	CN Gain	8.97E-06	4.85	0
chr14:46,506,654-46,584,383	chr14:46,499,831-46,584,383	CN Gain	1.99E-08	6.10	0
chr14:7,937,663-8,121,364	chr14:7,434,627-8,553,791	CN Gain	0.0184279	2.44	0
chr15:23,192,685-23,592,383	chr15:20,997,597-23,592,383	CN Loss	4.25E-05	10.51	0
chr15:4,348,577-4,531,244	chr15:4,325,685-4,531,244	CN Gain	1.88E-04	3.95	0
chr16:12,113,382-12,144,999	chr16:12,113,382-12,204,649	CN Gain	0.0032828	3.03	0
chr16:17,971,591-18,121,626	chr16:17,347,364-18,227,857	CN Gain	0.02492774	2.32	0
chr16:3,100,910-3,476,369	chr16:3,100,910-4,213,825	CN Gain	0.02267356	2.37	0
chr17:3,702,574-3,825,817	chr17:3,052,892-9,579,356	CN Gain	0.01648036	2.48	0
chr18:28,415,627-28,671,965	chr18:28,415,627-28,890,920	CN Gain	5.13E-04	3.64	0
chr18:49,052,924-49,392,277	chr18:48,509,665-53,200,246	CN Gain	8.98E-11	7.18	0
chr19:32,550,976-32,746,669	chr19:32,225,673-32,806,005	CN Gain	0.02720893	2.30	0
chr20:40,230,971-40,780,518	chr20:40,208,746-40,780,518	CN Gain	0.0041088	2.96	0
chr20:43,468,559-43,575,482	chr20:43,468,559-49,771,075	CN Gain	4.89E-09	6.37	0
chr20:60,767,150-61,000,000	chr20:56,358,468-61,000,000	CN Gain	4.22E-07	5.59	0
chr20:7,525,125-7,605,556	chr20:3,024,722-7,605,556	CN Gain	0.02338029	2.36	0
chr21:24,569,743-24,698,749	chr21:24,569,743-24,698,749	CN Gain	9.96E-07	5.35	0
chr21:43,460,055-43,535,921	chr21:43,460,055-43,747,598	CN Gain	0.00294658	3.06	0
chr23:23,552,949-23,759,722	chr23:23,552,949-23,759,722	CN Gain	7.85E-10	6.76	0
chr24:49,984,397-50,000,000	chr24:44,368,974-50,000,000	CN Gain	5.31E-05	4.40	0
chr25:53,312,633-54,000,000	chr25:53,312,633-54,000,000	CN Gain	0.01346224	2.56	0

Table 2.4. Differential chromosome regions with CN aberrations between primary canine oral melanoma (OM), primary canine cutaneous melanoma (CM), and canine benign melanocytoma (B).

CM v B										
Region	Cytoband	Event	Length	Freq. in <B> (%)	Freq. in <CM>(%)	Difference	Probe-level p-value	p-value	q-bound	Genes
chr3:65,296,031-65,432,693	q32	CN Loss	136662	0.00	60.00	-60.00	2.97E-05	0.00564653	0.19585384	0
chr3:91,078,961-91,201,866	q35.2	CN Loss	122905	0.00	60.00	-60.00	7.97E-07	0.00564653	0.19585384	1
chr6:56,621,808-57,009,959	q23.3	CN Loss	388151	0.00	60.00	-60.00	8.88E-16	0.00564653	0.19585384	1
chr6:57,985,210-61,768,589	q23.3	CN Loss	3783379	0.00	60.00	-60.00	0	0.00564653	0.19585384	31
chr6:63,509,729-70,150,848	q24.1 - q24.3	CN Loss	6641119	0.00	60.00	-60.00	0	0.00564653	0.19585384	36
chr6:71,434,654-71,483,100	q25.1	CN Loss	48446	0.00	60.00	-60.00	0.001409013	0.00564653	0.19585384	2
chr6:71,931,091-73,247,675	q25.1	CN Loss	1316584	0.00	60.00	-60.00	0	0.00564653	0.19585384	12
chr6:73,811,433-73,959,664	q25.1	CN Loss	148231	0.00	60.00	-60.00	2.26E-10	0.00564653	0.19585384	3
chr7:80,902,509-81,139,225	q26	CN Gain	236716	0.00	60.00	-60.00	1.11E-16	0.00564653	0.61567496	3
chr7:81,327,702-81,535,195	q26	CN Gain	207493	0.00	60.00	-60.00	3.44E-15	0.00564653	0.61567496	2
chr8:76,326,077-76,353,946	q33.3	CN Loss	27869	13.88	80.00	-68.89	0.178096977	0.01726649	0.28225994	1
chr9:20,973,038-21,556,711	q14	CN Gain	583673	66.42	0.00	61.11	0.054758534	0.03726708	0.61567496	8
chr12:29,013,503-29,538,529	q21.2	CN Gain	525026	0.00	60.00	-60.00	0	0.00564653	0.61567496	1
chr14:5,234,860-5,273,352	q11.2	CN Gain	38492	0.00	60.00	-60.00	0.001170344	0.00564653	0.61567496	0
chr14:5,608,750-5,833,997	q21	CN Gain	225247	0.00	60.00	-60.00	1.11E-16	0.00564653	0.61567496	6
chr14:56,723,556-59,852,681	q22 - q23	CN Gain	3129125	0.00	60.00	-60.00	0	0.00564653	0.61567496	14
chr14:61,787,770-62,563,454	q23	CN Gain	775684	0.00	60.00	-60.00	0	0.00564653	0.61567496	6
chr17:59,708,757-59,737,412	q23	CN Gain	28655	0.00	60.00	-60.00	0.056738221	0.00564653	0.61567496	1
chr18:15,091,843-15,315,133	q12	CN Loss	223290	0.00	60.00	-60.00	3.10E-09	0.00564653	0.19585384	2
chr18:16,137,042-19,268,908	q12 - q21	CN Loss	3131866	0.00	60.00	-60.00	0	0.00564653	0.19585384	18
chr18:20,168,647-21,429,875	q21	CN Loss	1261228	0.00	60.00	-60.00	0	0.00564653	0.19585384	14
chr18:21,439,849-27,874,576	q21 - q22.1	CN Loss	6434727	0.82	61.20	-74.44	0	0.01726649	0.28225994	11
chr18:30,423,853-31,166,586	q22.2	CN Loss	742733	0.00	60.00	-60.00	0	0.00564653	0.19585384	0
chr18:31,519,265-33,079,982	q22.3	CN Loss	1560717	0.00	60.00	-60.00	0	0.00564653	0.19585384	2
chr18:36,976,108-37,486,136	q23	CN Loss	510028	0.00	60.00	-60.00	0	0.00564653	0.19585384	6
chr18:38,039,895-38,145,764	q23	CN Loss	105869	0.00	60.00	-60.00	1.01E-04	0.00564653	0.19585384	1
chr18:38,868,924-39,420,478	q23	CN Loss	551554	0.00	60.00	-60.00	0	0.00564653	0.19585384	4
chr18:44,055,769-44,242,185	q24	CN Loss	186416	0.00	60.00	-60.00	7.42E-12	0.00564653	0.19585384	14
chr18:45,873,209-46,030,785	q24	CN Loss	157576	0.00	60.00	-60.00	1.22E-15	0.00564653	0.19585384	3
chr18:49,368,197-49,383,331	q25.1	CN Loss	15134	0.00	60.00	-60.00	0.023046553	0.00564653	0.19585384	0
chr18:53,200,246-53,990,114	q25.1	CN Loss	789868	0.00	60.00	-60.00	0	0.00564653	0.19585384	25
chr18:58,595,017-58,606,617	q25.3	CN Loss	11600	0.00	60.00	-60.00	0.131668016	0.00564653	0.19585384	1
chr20:8,799,960-8,893,836	q11	CN Gain	93876	0.00	60.00	-60.00	1.42E-06	0.00564653	0.61567496	1
chr20:9,631,235-9,846,893	q11	CN Gain	215658	0.00	60.00	-60.00	1.96E-09	0.00564653	0.61567496	2
chr20:10,131,212-10,241,822	q11	CN Gain	110610	0.00	60.00	-60.00	5.25E-05	0.00564653	0.61567496	2
chr20:10,929,869-11,055,355	q11	CN Gain	125486	9.29	80.00	-74.44	1.62E-05	0.00775655	0.61567496	2
chr20:22,738,829-22,957,667	q13	CN Gain	218838	0.00	60.00	-60.00	1.12E-06	0.00564653	0.61567496	0
chr20:34,924,975-35,532,615	q15.1	CN Gain	607640	0.00	60.00	-60.00	0	0.00564653	0.61567496	11
chr20:39,131,105-39,615,802	q15.3	CN Gain	484697	0.00	60.00	-60.00	0	0.00564653	0.61567496	5
chr20:40,938,157-41,127,958	q15.3	CN Gain	189801	0.00	60.00	-60.00	1.50E-06	0.00564653	0.61567496	4
chr20:41,727,887-41,772,352	q15.3	CN Gain	44465	0.00	60.00	-60.00	0.016561244	0.00564653	0.61567496	2
chr20:42,838,556-43,439,311	q15.3	CN Gain	600755	0.00	60.00	-60.00	0	0.00564653	0.61567496	24
chr20:44,749,523-44,798,551	q15.3	CN Gain	49028	7.62	80.00	-74.44	0.00152604	0.01726649	0.61567496	1
chr20:44,950,054-45,273,167	q15.3	CN Gain	323113	16.67	80.00	-63.33	3.45E-11	0.01726649	0.61567496	15
chr20:47,033,081-47,166,271	q15.3	CN Gain	133190	16.67	80.00	-63.33	2.31E-05	0.01726649	0.61567496	4
chr20:48,629,806-49,134,219	q15.3	CN Gain	504413	16.67	80.00	-63.33	2.22E-16	0.01726649	0.61567496	12
chr20:49,406,077-49,583,266	q15.3	CN Gain	177189	16.67	80.00	-63.33	6.25E-06	0.01726649	0.61567496	11
chr20:50,826,543-51,074,680	q16	CN Gain	248137	16.67	80.00	-63.33	2.43E-12	0.01726649	0.61567496	6
chr20:51,626,077-51,881,639	q16	CN Gain	255562	16.67	80.00	-63.33	6.14E-09	0.01726649	0.61567496	5
chr20:52,449,099-52,462,326	q16	CN Gain	13227	16.67	80.00	-63.33	0.932161496	0.01726649	0.61567496	1
chr20:53,980,807-54,024,061	q16	CN Gain	43254	16.67	80.00	-63.33	0.0174353	0.01726649	0.61567496	2
chr20:54,160,798-54,593,373	q16 - q17	CN Gain	432575	0.00	60.00	-60.00	4.03E-13	0.00564653	0.61567496	27
chr20:56,462,668-56,555,627	q17	CN Gain	92959	22.22	100.00	-77.78	3.28E-04	0.00374454	0.61567496	6
chr22:3,056,579-3,707,698	q11.1	CN Loss	651119	0.00	60.00	-60.00	0	0.00564653	0.19585384	7
chr22:3,865,032-4,908,525	q11.1 - q11.2	CN Loss	1043493	0.00	60.00	-60.00	0	0.00564653	0.19585384	5
chr22:5,325,133-5,981,205	q11.2	CN Loss	656072	0.00	60.00	-60.00	0	0.00564653	0.19585384	7
chr22:6,406,853-7,556,541	q11.2	CN Loss	1149688	0.00	60.00	-60.00	0	0.00564653	0.19585384	8
chr22:7,906,394-12,107,407	q11.2	CN Loss	4201013	0.00	60.00	-60.00	0	0.00564653	0.19585384	31
chr22:12,618,901-18,986,118	q11.2 - q12.3	CN Loss	6367217	0.00	60.00	-60.00	0	0.00564653	0.19585384	7
chr22:19,370,270-19,470,842	q12.3	CN Loss	100572	0.00	60.00	-60.00	1.25E-05	0.00564653	0.19585384	2
chr22:39,700,274-58,811,660	q22 - q24	CN Loss	19111386	0.00	60.00	-60.00	0	0.00564653	0.19585384	56
chr22:59,940,933-63,256,620	q24	CN Loss	3315687	0.00	60.00	-60.00	0	0.00564653	0.19585384	18
chr22:63,472,754-64,369,703	q24	CN Loss	896949	0.30	61.32	-80.00	0	0.00564653	0.19585384	21
chr23:23,552,949-23,718,671	q21.1	CN Loss	165722	16.67	80.00	-63.33	1.28E-09	0.01726649	0.28225994	0

Table 2.4 continued

CM vs OM										
Region	**Cytoband**	**Event**	**Length**	**Freq. in <CM> (%)**	**Freq. in <OM>(%)**	**Difference**	**Probe-level p-value**	**p-value**	**q-bound**	**Genes**
chr18:21,439,849-21,824,376	q21	CN Loss	384527	80.00	16.55	61.82	0.003130909	0.01002001	1	1
chr18:58,785,242-58,847,127	q25.3	CN Loss	61885	60.00	0.00	60.00	2.67E-04	5.43E-04	1	1
chr20:10,929,869-11,021,062	q11	CN Gain	91193	80.00	16.13	61.82	6.69E-04	0.01002001	1	1
chr20:39,692,824-39,761,640	q15.3	CN Gain	68816	80.00	15.33	64.09	2.66E-05	0.00681845	1	2
chr20:40,295,833-40,353,458	q15.3	CN Gain	57625	80.00	18.18	61.82	0.002092106	0.01002001	1	5
chr20:40,444,954-40,780,518	q15.3	CN Gain	335564	80.00	17.87	61.82	5.57E-13	0.01002001	1	16
chr20:43,439,311-43,456,298	q15.3	CN Gain	16987	80.00	15.91	64.09	0.100734406	0.00681845	1	1
chr20:44,812,069-44,993,595	q15.3	CN Gain	181526	80.00	16.03	61.82	1.43E-06	0.01002001	1	5
chr20:45,084,782-45,097,744	q15.3	CN Gain	12962	80.00	18.18	61.82	0.908941381	0.01002001	1	1
chr20:47,033,081-47,224,687	q15.3	CN Gain	191606	80.00	18.18	61.82	2.10E-08	0.01002001	1	8
chr20:47,289,293-47,424,027	q15.3	CN Gain	134734	80.00	15.66	61.82	1.58E-05	0.01002001	1	3
chr20:47,733,306-47,878,953	q15.3	CN Gain	145647	80.00	16.81	61.82	1.30E-05	0.01002001	1	9
chr20:48,049,703-48,520,235	q15.3	CN Gain	470532	80.00	17.74	61.82	1.11E-16	0.01002001	1	29
chr20:48,534,617-48,936,628	q15.3	CN Gain	402011	80.00	17.09	61.82	3.71E-13	0.01002001	1	9
chr20:49,276,174-49,343,247	q15.3	CN Gain	67073	80.00	18.18	61.82	5.50E-07	0.01002001	1	6
chr20:49,853,240-50,112,676	q16	CN Gain	259436	80.00	14.33	61.82	1.20E-11	0.01002001	1	11
chr20:51,430,498-51,436,664	q16	CN Gain	6166	80.00	18.18	61.82	0.086233645	0.01002001	1	2
chr20:51,626,077-51,671,841	q16	CN Gain	45764	80.00	18.18	61.82	0.03731252	0.01002001	1	4
chr20:52,401,235-52,462,326	q16	CN Gain	61091	80.00	18.18	61.82	0.001991597	0.01002001	1	8
chr20:52,824,996-52,996,836	q16	CN Gain	171840	80.00	16.82	61.82	1.40E-10	0.01002001	1	14
chr20:53,009,988-53,113,442	q16	CN Gain	103454	80.00	18.18	61.82	0.007205929	0.01002001	1	4
chr20:55,265,830-55,300,554	q17	CN Gain	34724	80.00	16.49	61.82	0.057392932	0.01002001	1	2
chr20:55,466,763-55,484,948	q17	CN Gain	18185	80.00	18.18	61.82	0.101138384	0.01002001	1	1
chr20:56,362,306-57,041,431	q17	CN Gain	679125	82.74	16.13	61.82	0	0.01002001	1	25
chr30:19,102,383-19,660,901	q14.1	CN Gain	558518	0.00	61.36	-61.36	0	0.01380996	1	7
chr30:19,876,904-19,996,814	q14.1	CN Gain	119910	0.00	61.36	-61.36	1.08E-08	0.01380996	1	1
OM vs B										
Region	**Cytoband**	**Event**	**Length**	**Freq. in <OM> (%)**	**Freq. in <B>(%)**	**Difference**	**Probe-level p-value**	**p-value**	**q-bound**	**Genes**
chr10:19,910,771-20,010,497	q21	CN Loss	99726	51.52	0.00	50.00	0.29318487	7.81E-05	0.02340687	7
chr10:20,891,421-21,034,598	q21	CN Loss	143177	50.00	0.00	50.00	0.372570691	7.81E-05	0.02340687	0
chr18:49,147,788-49,270,987	q25.1	CN Loss	123199	52.53	0.00	50.00	0.052293285	7.81E-05	0.02340687	4
chr18:49,052,924-49,406,866	q25.1	CN Gain	353942	13.41	68.39	-60.86	7.92E-06	1.81E-04	0.04305597	9
chr18:49,517,445-49,534,276	q25.1	CN Gain	16831	9.09	61.11	-52.02	0.36558262	4.92E-05	0.02399501	1
chr27:5,904,167-6,011,259	q11	CN Gain	107092	18.18	72.22	-54.04	0.0579823	8.92E-05	0.03165218	3
chr27:9,965,501-10,052,495	q12	CN Gain	86994	17.39	72.22	-56.31	0.006099988	8.92E-05	0.03165218	4
chr30:8,498,046-9,636,740	q12	CN Loss	1138694	52.20	0.00	50.00	1.20E-05	7.81E-05	0.02340687	4
chr30:10,079,573-10,124,393	q13	CN Loss	44820	50.00	0.00	50.00	0.336880661	7.81E-05	0.02340687	1
chr30:10,193,135-10,720,246	q13	CN Loss	527111	52.44	0.00	50.00	0.001310898	7.81E-05	0.02340687	14
chr30:11,975,124-12,063,650	q13	CN Loss	88526	50.00	0.00	50.00	0.630135892	7.81E-05	0.02340687	2
chr30:12,380,210-12,488,823	q13	CN Loss	108613	51.08	0.00	50.00	0.109361198	7.81E-05	0.02340687	2
chr30:12,726,759-13,250,634	q13	CN Loss	523875	51.24	0.00	50.00	0.001379687	7.81E-05	0.02340687	11
chr30:18,445,429-18,848,546	q14.1	CN Gain	403117	54.10	0.00	50.00	0	7.81E-05	0.02950096	4
chr30:19,085,315-19,792,342	q14.1	CN Gain	707027	60.48	5.56	51.26	0	1.58E-04	0.0384405	9
chr30:19,812,516-21,427,202	q14.1	CN Gain	1614686	56.16	2.74	50.00	0	1.58E-04	0.0384405	20
chr30:21,471,751-21,486,205	q14.1	CN Gain	14454	50.00	0.00	50.00	0.182422439	7.81E-05	0.02950096	0
chr30:21,556,538-21,606,960	q14.1 - q14.2	CN Gain	50422	50.00	0.00	50.00	0.031808124	7.81E-05	0.02950096	0

Table 2.5. Proposed genes involved in canine oral melanoma pathogenesis.

CFA 30 Gain	Cell Function
SLC27A2	Lipid biosynthesis and fatty acid degradation.
HDC	Converts L-histidine to histamine, associated with HDC include mast cell neoplasm.
GABPB1	Transcription factor.
USP8	Required for the cell to enter the S phase of the cell cycle. Also functions as a positive regulator in the Hedgehog signaling pathway in development and downstream signaling of activated FGFR.
TRPM7	Kinase activity is essential for the ion channel function.
SPPL2A	Member of the GXGD family of aspartic proteases.
CFA 30 Loss	
SPRED1	Tyrosine kinase substrate that inhibits growth-factor-mediated activation of MAP kinase through C-KIT receptor signaling pathway.
RASGRP1	Diacylglycerol (DAG)-regulated nucleotide exchange factor specifically activating RAS through the exchange of bound GDP for GTP, which activates the Erk/MAP kinase cascade.
FAM98B	Component of the tRNA-splicing ligase complex
CFA 3 loss	
FGFR3	Tyrosine-protein kinase that plays an essential role in the regulation of cell proliferation, differentiation and apoptosis
TACC3	Motor spindle protein that may play a role in stabilization of the mitotic spindle. This protein may also play a role in growth a differentiation of certain cancer cells.
TMEM129	Multi-pass membrane protein (Potential)
SLBP	Stabilizes mature histone mRNA and could be involved in cell-cycle regulation of histone gene expression.
FAM53A	May play an important role in neural development.

Table 2.6. Aberrations with at least 60% penetrance for three subtypes of canine melanocytic lesions, oral melanoma (OM), cutaneous melanoma (CM), and melanocytoma (B), after recoding as human (HSA).

OM n=44							
Region chr:bp start-bp end	Length in bp	Cytoband	Event	Genes	Frequency %	Q-Bound	% of CNV
chr4:70,508,745-70,648,668	139923	q13.3	CN Gain	2	52.27	0	0.00
chr9:139,959,550-140,076,719	117169	q34.3	CN Loss	10	52.27	0	2.42
chr11:1,794,537-2,127,344	332807	p15.5	CN Loss	11	56.82	0	1.33
chr12:69,140,376-69,310,630	170254	q15	CN Gain	4	50.00	0	0.56
chr15:38,701,609-38,952,741	251132	q14	CN Loss	2	56.82	0	0.00
chr15:40,071,513-40,108,709	37196	q14 - q15.1	CN Loss	2	50.00	0	0.00
chr15:40,677,763-40,752,657	74894	q15.1	CN Loss	4	54.55	0	100.00
chr15:43,269,351-43,435,842	166491	q15.2	CN Loss	2	50.00	0	0.00
chr15:49,739,758-49,752,772	13014	q21.2	CN Gain	3	56.82	0	0.00
chr15:49,880,023-49,947,711	67688	q21.2	CN Gain	3	56.82	0	0.00
chr15:50,413,935-51,086,810	672875	q21.2	CN Gain	14	56.82	0	0.00
chr15:51,419,334-51,553,648	134314	q21.2	CN Gain	8	56.82	0	0.00
chr15:51,680,450-51,843,291	162841	q21.2	CN Gain	2	54.55	0	0.00
chr15:52,127,372-52,146,078	18706	q21.2	CN Gain	1	56.82	0	0.00
chr15:52,619,742-52,673,926	54184	q21.2	CN Gain	1	54.55	0	0.00
chr15:52,819,229-52,865,102	45873	q21.2	CN Gain	2	52.27	0	0.00
chr16:72,782,701-72,793,246	10545	q22.2	CN Loss	1	50.00	0	0.00
chr22:49,365,468-50,206,932	841464	q13.32 - q1	CN Loss	4	54.55	0.016	2.90
CM n=5							
Region chr:bp start-bp end	Length in bp	Cytoband	Event	Genes	Frequency %	Q-Bound	% of CNV
chr1:104,846,149-106,466,025	1619876	p21.1	CN Loss	1	80.00	1	8.36
chr3:10,330,119-10,478,665	148546	p25.3	CN Gain	5	80.00	1	0.00
chr3:23,033,528-23,227,218	193690	p24.3	CN Loss	0	80.00	1	0.00
chr3:46,895,009-47,059,073	164064	p21.31	CN Gain	6	80.00	1	0.00
chr3:48,138,725-48,550,356	411631	p21.31	CN Gain	15	80.00	1	0.00
chr3:48,668,514-48,719,793	51279	p21.31	CN Gain	4	80.00	1	0.00
chr3:49,646,565-50,156,399	509834	p21.31	CN Gain	19	80.00	1	3.16
chr3:51,722,814-52,597,921	875107	p21.2 - p21	CN Gain	42	80.00	1	0.00
chr3:53,166,746-53,305,143	138397	p21.1	CN Gain	2	80.00	1	0.00
chr7:78,150,647-78,549,045	398398	q21.11	CN Loss	1	80.00	1	0.00
chr16:72,450,875-72,793,246	342371	q22.2	CN Loss	3	80.00	1	0.00
chr17:4,602,476-4,749,428	146952	p13.2	CN Gain	12	80.00	1	0.00
chr19:6,723,282-6,941,309	218027	p13.3 - p13	CN Gain	5	100.00	1	36.31
chr19:7,915,050-11,316,157	3401107	p13.2	CN Gain	122	80.00	1	4.62
chr19:12,913,005-14,816,413	1903408	p13.2 - p13	CN Gain	62	80.00	1	2.32
chr19:15,152,417-20,370,056	5217639	p13.12 - p1	CN Gain	221	80.00	1	6.50
BM n=18							
Region chr:bp start-bp end	Length in bp	Cytoband	Event	Genes	Frequency %	Q-Bound	% of CNV
chr1:0-924,995	924995	p36.33	CN Gain	38	64.29	0	98.86
chr1:12,246,974-12,500,843	253869	p36.22	CN Gain	3	71.43	0	0.00
chr1:155,927,443-156,237,440	309997	q22	CN Gain	14	64.29	0	0.34
chr2:43,382,146-43,452,004	69858	p21	CN Gain	1	64.29	0	0.00
chr9:137,181,234-137,370,987	189753	q34.2	CN Gain	2	64.29	0	0.00
chr11:1,776,852-2,256,415	479563	p15.5	CN Gain	21	64.29	0	0.92
chr11:63,966,032-64,056,915	90883	q13.1	CN Gain	12	64.29	0	0.00
chr12:52,391,144-52,523,021	131877	q13.13	CN Gain	4	71.43	0	0.52
chr16:67,963,523-68,031,710	68187	q22.1	CN Gain	7	64.29	0	0.00
chr16:72,468,995-72,730,668	261673	q22.2	CN Gain	2	64.29	0	0.00
chr16:88,794,946-88,939,297	144351	q24.3	CN Gain	8	64.29	0	41.99
chr19:7,687,841-8,002,645	314804	p13.2	CN Gain	23	71.43	0	0.00

Table 2.7. Orthologous copy number aberrations, gain (G) or loss (L), between canine (CFA) melanocytic lesions, malignant melanoma (Mel) and benign melanocytoma (Ben) and two human (HSA) melanoma subtypes, mucosal melanoma (mucosal) and acral melanoma (acral).

Genes	Region in HSA	G/L in Mucosal	G/L in Acral	Region in CFA	G/L in Mel	G/L in Ben
CDK4	12q14 (12 - 57.74Mb)	G	G	15 - 53Mb	L	N
CDKN2A	9p21 (9 - 21.96Mb)	L	L	11 - 44.06Mb	L	N
PTEN	10q32.3 (10 - 87.86Mb)	L	L	26 - 40.0Mb	L	L
MYC	8q24.21 (8 - 127.73Mb)	G	G	13 - 27.28Mb	G	N
KIT	4q12 (4 - 75.57Mb)	G	N	13 - 49.50Mb	G	N
TP53	17p13.1 (17 - 7.66Mb)	N	N	5 - 35.0Mb	L/G	L
CCND1	11q13 (11 - 69.65Mb)	G	G	18 - 51.1Mb	L	N
RB-1	13q14.2 (13 - 48.48Mb)	N	N	22 - 6.0Mb	L	N
CDKN1A	6p21.2 (6 - 36.68Mb)	G	G	12 - 8.6Mb	L	N
B-RAF	7q34 (7 - 140.92Mb)	G	G	16 - 11.49Mb	L	N

Table 2.8. Targeted regions for FISH analysis with the corresponding BAC clones and CanFam2 genome locations chosen from the Chori-82 (CH-82) canine genome library.

Target region	key locus	CH-82 clone	start	stop	overlap
26:44253176-44256016Mb	*PTEN*	314G09	40729598	40911630	67612
		512G14	40844018	41078623	
		047M14	41052124	41230433	26499
				TOTAL	**500835**
5:35557006-35560756Mb	*TP53*	199E04	35331852	35520376	69967
		221P11	35450409	35651123	
		185K03	35592600	35820597	58523
				TOTAL	**488745**
13:50040750-50122138Mb	c-*KIT*	039J17	49827508	50021682	30319
		524B22	49991363	50201827	
		043D09	50186090	50371023	15737
				TOTAL	**543515**
15:54244626-54245248Mb	*CDK4*	403E04	53922786	54130237	55791
		227A01	54074446	54251670	
		017B02	54223578	54387481	28092
				TOTAL	**464695**
13:28,238,008-28,242,545Mb	c-*MYC*	136F15	27885453	28104973	19691
		335M01	28085282	28265714	
		209M01	28207431	28382509	58283
				TOTAL	**497056**
11:44253176-44256016Mb	*CDKN2A*	043A07	44061103	44283223	26922
		325C12	44256301	44428212	
		166H01	44393313	44561750	34899
				TOTAL	**500647**
12:8,751,893-8,755,004Mb	*CDKN1A*	060J11	8648955	8871237	52367
		465H20	8818870	9013484	
				TOTAL	**364529**
22:6,007,254-6,093,096Mb	*RB-1*	479C11	5765800	5982802	15774
		021N23	5967028	6133019	
		522K16	6084801	6248558	48218
				TOTAL	**482758**
16:11,187,222-11,275,928Mb	*BRAF*	257E03	11163065	11374118	86857
		515N08	11287261	11464323	
				TOTAL	**301258**
18:51,527,953-51,535,734Mb	*CCND1*	024F02	51293932	51503911	25056
		088I24	51478855	51688507	
		278J02	51651758	51813747	36749
				TOTAL	**519815**

CHAPTER III

Comparative Cytogenomic and Pathway Analysis of Canine Oral Melanomas: Proposal of a Novel Pathway into the Tumorigenesis of Mucosal Melanomas

3.1 Abstract

Canine oral melanoma is a highly aggressive disease affecting 2% of all dogs. Few studies investigating the underlying mechanism responsible for the development of the disease have been performed. While classical cancer pathways, such as the CDKN2A and MAPK pathway, have been shown to have some involvement in oral melanoma development, these changes cannot explain the entirety of biological observations. Based on previous copy number aberrations and suggested patterns of structural rearrangements, more in-depth cytogenetic analysis was performed. Gene expression analysis was also performed to identify new genes involved in the tumorigenesis of canine oral melanoma. Detailed karyotyping was performed on canine oral melanoma cell line (n=6) using SLP and whole chromosome FISH analysis. This revealed numerous structural rearrangements, none of which were recurrent within the population. Whole transcriptome gene expression profiling (GEP) was carried out on the same canine oral melanoma cell lines and primary oral melanoma samples (n=7). From these data, 13 genes were identified to evaluate by RT-qPCR in an additional cohort of primary oral melanomas (n=17) and benign melanocytomas (n=14). Gene expression showed dysregulation in 12 of 13 genes, many of which were part of the DNA damage pathway and mitotic spindle assembly complex, including *TP53*, *PLK1*, and *TTK*. From this, we conclude that in addition to canonical cancer pathway changes, canine oral melanomas contain gene dysregulation in the mitotic spindle assembly complex,

which may explains the complex karyotypes, comprising numerical and structural aberrations observed by cytogenetic analyses.

3.2 Introduction

Malignant melanoma is the most common tumor of the oral cavity in dogs, with over 90% of these tumors being malignant (Spangler and Kass 2006; Bergman 2007). Canine oral melanoma readily invades into normal tissue and bone and has a high metastatic propensity (Ramos-Vara *et al.* 2000; Koenig *et al.* 2002). These tumors are usually aggressive and respond poorly to standard treatments (Bergman 2007). Oral melanoma has been well established as the most malignant of the melanocytic tumors found in the dog; however, the reason for this has not yet been elucidated. The dysregulation of many proteins has also been indicated in the pathogenesis of canine melanoma. The role of many well-known tumor suppressors (*TP53, RB-1, CDKN1A, CDKN2A*, and *PTEN*) has been previously examined in canine oral melanoma, using both primary lesions and cell lines (Ritt, Wojcieszyn, and Modiano 1998; Koenig *et al.* 2002; Bianco *et al.* 2003). Gene expression analysis by end point RT-PCR and immunohistochemistry revealed a loss of expression within the cell cycle regulation pathway, primarily *CDKN2A* (Koenig *et al.* 2002). However, dysregulation of the cell cycle pathway alone cannot explain the aggressive nature of these tumors.

Studies into genetic alterations within subtypes of human melanomas established that cutaneous and mucosal melanomas develop with differing mutation loads (Curtin *et al.* 2005; Furney *et al.* 2013). Investigation into the molecular dysregulation of human oral mucosal melanomas showed no involvement of the classical markers of cutaneous melanoma (Hsieh *et al.* 2013). The CDKN2A cell cycle regulation pathway was investigated for its potential in leading to tumorigenic effects in human mucosal melanomas as well. Although the members of this pathway were shown to be dysregulated in canine mucosal melanoma (Koenig *et al.*

2002), they were not significantly dysregulated in humans (Hsieh *et al.* 2013). The MAPK cascade, an important proliferation pathway in cutaneous melanomas, has not been shown to be dysregulated in either species (Richter 2005; Murakami *et al.* 2011; Hsieh *et al.* 2013). Recently, others have suggested the dog is a good model for comparative analysis of mucosal melanomas, a fairly rare tumor in humans. Our comparative cytogenetic study of human and canine mucosal melanomas showed that oral melanomas in both species present with similar DNA copy number changes (Chapter II). Studies have yet to fully elucidate the underlying mechanism of development and progression of mucosal melanomas in either species.

Based on the high level of cytogenetic changes and the characteristic patterns of chromosome instability, we reported in canine oral melanomas (Chapter II), we hypothesizes that canine oral melanoma cell lines would recapitulate the primary cytogenetic data and that detailed karyotype analysis will show structural rearrangements involving in CFA chromosomes 10, 26, and 30. Furthermore, due to the lack of involvement of the classical cutaneous melanoma pathways and the variable dysregulation of the CDKN2A cell cycle pathway previously reported in other canine melanoma cohorts, we hypothesized that our cohort will show similar patterns, and that gene expression analysis would highlight a yet-to-be identified oncogenic pathway involved in the tumorigenesis of canine mucosal melanomas. The purpose of this study was to investigate the molecular alterations found in canine oral melanoma through karyotype, gene expression, and sequence mutation analysis.

3.3 Materials and Methods

This study was done using a representative population of previously established melanoma cell lines (n=6), fresh frozen primary oral melanomas (n=10), archival primary oral melanomas (n=14), and archival primary benign lesions (n=14). Individuals within the primary tumor cohort were of varied breed, sex, and age, as previously described (Chapter II, Table 2.1; OM5-18, OM 33, OM35, OM37-44, B1-3, B5-6, B8-15, and B17). Cell lines were used for karyotype and FISH analyses, and to isolate RNA for gene expression arrays; fresh primary tumors (OM 38-44) were used to isolate RNA for gene expression arrays; additional primary tumors (OM5-18, OM 33, OM35, OM37, B1-3, B5-6, B8-15, and B17) were used for RT-qPCR gene expression analysis.

3.3.1 Cell Lines

The cell lines used were established from primary tumors of dogs with oral melanomas (n=5) and a lung metastasis of an oral melanoma (n=1) (Table 3.1), and have been described previously (Koenig *et al.* 2001; Bianco *et al.* 2003). Frozen cells were acquired in 90% Fetal Bovine Serum (FBS) and 10% DMSO, then reestablished in closed system incubation.

3.3.2 Cell Culture

Cells were cultured in Dulbecco's Modified Eagle Medium (Mediatech Inc., Manassas, VA, USA) supplemented with 10% v/v heat-inactivated FBS (Mediatech Inc., Manassas, VA, USA) and 100ug/ml Primocin Antibiotic (InvivoGen, San Diego, CA, USA)

in a humidified atmosphere containing 5% CO_2 at 37°C. Cells were grown in T75 flasks with 0.2μM filtered lids until they reached 95% confluence, then were harvested for metaphase cellular spreads, DNA extraction, and RNA extraction. All cell lines were grown as a monolayer and were maintained by passage for no greater than eight passages after reestablishment. It was noted that all cells lines showed little contact inhibition and after reaching confluence. Cells would tend to grow on top of each other in striating patterns, often forming small mounds of numerous small, highly attached cells in the apex of cellular clusters.

3.3.3 DNA Extraction

DNA from cell lines was extracted using a DNeasy© kit (according to manufacturer's recommendations, Qiagen, Germantown, MD, USA). All DNA was assessed for quality and quantity by spectrophotometry using a NanoDrop1000 (Thermo Fisher Scientific, Wilmington, DE, USA). Genomic DNA integrity, assessed by agarose gel electrophoresis, showed little to no degradation.

3.3.4 Comparative Genomic Hybridization

Oligo array-CGH (oa-CGH) was performed by co-hybridization of tumor (test) DNA and a common reference DNA sample, where the latter comprised an equimolar pool of genomic DNA samples from multiple healthy individuals of various breeds. DNA extracted from FFPE samples was slightly degraded, as expected, but this was shown not to have an adverse effect on data quality. DNA was labeled using a SureTag Labeling Kit (Agilent

Technologies, Santa Clara, CA) with all test samples labeled with Cyanine-3-dCTP and the common reference sample labeled with Cyanine-5-dCTP. Fluorchrome incorporation and final probe concentrations were determined using routine spectrophotometric parameters with readings taken from a Nanodrop1000. Fluorescently labeled test and reference samples were co-hybridized to Canine SurePrint G3 180,000 feature CGH arrays (Agilent, AMADID 025522) for 40 hours at 65°C and 20 rpm, as described previously (Angstadt *et al.* 2011). Arrays were scanned at 3µm using a high-resolution microarray scanner (Agilent, Model G2505C) and data extracted using Feature Extraction (v10.9) software. Scan data were assessed for quality by the Quality Metrics report in Agilent's Feature extraction software (v10.5) (Agilent Technologies, Santa Clara, CA, USA) and aligned to the genome position indicated for the canine genome build CanFam2 (http://genome.ucsc.edu/cgi-bin/hgGateway?db=canFam2).

Copy number data were analyzed with NEXUS Copy Number v7.0 software (Biodiscovery Inc., CA, USA). The Log_2 data for each probe provided from Feature Extraction were centered using diploid regions. NEXUS generated copy number aberrations using a FASST2 segmentation algorithm with a significance threshold of 5.05^{-6}. Aberrations were defined as a minimum of three consecutive probes with log2 tumor: reference value of 0.2 to 1.13 (gain), >1.14 (high gain), -0.23 to -1.1 (loss), < -1.1 (homozygous loss). Recurrent copy number aberrations within each subtype were determined within NEXUS using a stringent involvement threshold of 60%. Significance of these regions was then determined in NEXUS using the GISTIC algorithm with a G-score cut off of G >1.0 and a significance of Q <0.05. Copy number aberration (CNA) frequency comparisons among

sample groups were performed in NEXUS using Fisher's exact test with differential threshold of >60% and significance $p < 0.05$. Significance of each probe between the two groups was calculated in NEXUS using a Mann-Whitney Test for median comparison.

3.3.5 Flouresence in situ Hybridization (FISH) of Cell Lines

Metaphase chromosome preparations and interphase nuclei were produced directly from cell lines using conventional techniques of ethidium bromide treatment to elongate chromosomes, colcemid arrest, hypotonic treatment, and 3:1 methanol-glacial acetic acid fixation (Breen, Bullerdiek, and Langford 1999). Multicolor single locus probe (SLP) fluorescence *in situ* hybridization (FISH) analysis was done on metaphase spreads as described previously (Breen *et al.* 2004) to evaluate the distribution of selected copy number changes identified by genome-wide oaCGH. Bacterial artificial chromosomes (BACs) that contained the coding sequence for the genes of interest were selected based on their genome position indicated for the canine genome build CanFam2 in the UCSC canine genome browser (http://genome.ucsc.edu). A summary of the BAC clones has been previously described (Chapter Two, Table 2.8). Metaphase preparations from clinically healthy canine primary lymphocytes were used to confirm that all 10 BAC pools showed the expected copy number (n=2) for autosomal loci.

Multicolor FISH analysis was performed to further investigate chromosome instability. Single chromosomes were analyzed using BAC probes located at ~10Mb intervals along the lengths of CFA chromosome 10 and 30, as previously described (Thomas *et al.* 2005). Whole chromosomes were analyzed whole chromosome paint probes for CFA

10, 26, and 30. All images were captured using the SmartCapture 3 program (Digital Scientific Ltd, Cambridge, UK) for a minimum of 30 cells.

3.3.6 mRNA Extraction

Total RNA was extracted from frozen tissues and cell lines using the RNeasy Plus Kit (according to manufacturer's recommendations, Qiagen, Germantown, MD, USA) and assessed for relative quality and quantity by standard spectrophotometry using a NanoDrop1000 (Thermo Fisher Scientific, Wilmington, DE, USA). Total mRNA was extracted from FFPE samples using the E.Z.N.A.® FFPE RNA Kit (according to manufacturer's recommendations, Omega Bio-Tek, Norcross, GA, USA). RNA integrity was assessed for all RNA samples using the BioAnalyzer 2100 and RNA 6000 Nano Kit (according to manufacturer's recommendations, Agilent, Santa Clara, CA, USA). Only RNA samples with a RIN of > 7.0 were included in the cohort for gene expression analysis via gene expression profiling (GEP) array.

3.3.7 Gene Expression Arrays

Transcriptional assessment was performed for six cell lines, seven fresh frozen samples (OM38-44), and four normal controls. Total-RNA was labeled using the Agilent One-Color Low Input Labeling Kit (according to manufacture's recommendation, Agilent Technologies, Santa Clara, CA, USA). Fluorochrome incorporation and final probe concentrations were determined using routine spectrophotometric parameters using a Nanodrop1000. Fluorescently labeled samples were hybridized to Canine 44,000 feature

GEP arrays (Agilent, AMADID 021193) for 16 hours at 65°C and 20 rpm. Arrays were scanned at 3μm, using a high-resolution microarray scanner (Agilent, Model G2505C). The raw signal intensity for each probe was provided from Feature Extraction software (Agilent Technologies, Santa Clara, CA, USA).

Gene expression data were analyzed with Nexus Gene Expression v2.0 software (Biodiscovery Inc., Hawthorne, CA, USA). Normalization of data was performed using a Quantile Normalization procedure. Data were then filtered to remove probe sets with limited variation (standard deviation < 2.0) across all arrays. Differential expression of genes was determined by comparing average signal intensity of each probe within normal samples to signal intensity of each tumor sample. Clustering of differentially expressed probes was performed using unsupervised hierarchical clustering analysis across all samples.

3.3.8 RT-qPCR

From both GEP analysis and canonical cancer pathways, 13 genes were selected based on the level of dysregulation, biological function, and availability of approved targeted drugs. Selected genes were then evaluated with RT-qPCR for fold changes in additional primary melanomas (n=17) and benign melanocytomas (n=14). Total RNA was converted to cDNA using the VILO SuperScript Reverse Transcriptase (according to manufacturer's recommendation, Invitrogen, Life Technologies Corporation, Carlsbad, CA, USA). Location and sequence of each gene were selected based on their genome position indicated for the canine genome build CanFam2 in the UCSC canine genome browser

(http://genome.ucsc.edu). Primers were then selected with the aid of PrimerQuest software (Integrated DNA Technologies) and primer sequences are listed in Table 3.2.

RT-qPCR was performed using SYBR green chemistry with a KAPA SYBR FAST qPCR Kit (according to manufacturer's recommendation, Kapa Biosystems, Wilmington, MA, USA), using the AB OneStep Plus (Applied Biosystems, Life Technologies Corporation, Carlsbad, CA, USA). Annealing temperatures were optimized for each specific primer set via a temperature gradient of plus or minus 10°C to calculated melting temperature. Cycling conditions were performed as per manufacturer's recommendations for the KAPA SYBR FAST qPCR Kit, with a melt curve performed for each RT-qPCR reaction. A reference gene for $\Delta\Delta CT$ calculations was chosen based on the smallest standard deviation across all samples. Relative levels of individual gene expression were then calculated using $\Delta\Delta CT$, where normalization was calculated as the difference in threshold PCR cycle (Ct) value of target gene and the corresponding control (*RPS5*) in each reaction. These values were compared with average Ct value from non-neoplastic oral mucosa from normal canines (n=4).

Normal variation within individuals was determined by calculating the average variation in Ct values between the four normal individuals across all target genes. For tumor samples, a fold change threshold of > 3 or < 0.3 was considered outside normal range and therefore dysregulated. Percent of melanoma and melanocytoma cases differing from normal was statistically evaluated using a two-tailed Fisher's exact test. Mitotic index was correlated against gene expression changes using non-parametric Spearman's Rank Sum analysis to identified genes that are associated with proliferation, one of the best indicators of

tumor aggression. Difference in fold change between benign melanocytomas and malignant melanomas was assessed using a non-parametric one-tailed Mann-Whitney U Test.

3.3.9 Targeted Sanger Sequencing

Sanger sequencing was performed on PCR amplicons generated from cDNA. Briefly, cDNA was produced from total RNA as described above. Location and sequence of each gene were selected based on their genome position indicated for the canine genome build CanFam2 in the UCSC canine genome browser (http://genome.ucsc.edu). Primers were then selected with the aid of PrimerQuest software (Integrated DNA Technologies). Amplicons were created using a high fidelity polymerase, KAPA HiFi HotStart ReadyMix (according to manufacturer's recommendations, Kapa Biosystems, Wilmington, MA, USA), with annealing temperatures optimized for the specific primer set. Cycling conditions were performed as per manufacturer's recommendations for the KAPA HiFi HotStart ReadyMix. Amplicons were then assessed for purity using gel electrophoresis and purified to remove non-annealed primers and unamplified cDNA using a GeneJet PCR Clean Up Kit (according to manufacture's recommendations, Thermo Fisher Scientific In, Waltham, MA, USA). Primer sequences are listed in Table 3.3.

3.4 Results

3.4.1 Detection of CNA by oaCGH in Cell Lines

Individuals represented within the cell line cohort presented with highly complex oaCGH profiles (Figure 3.1). Highly recurrent CNAs (>60% penetrance across the cohort)

were assessed in detail (Table 3.4) and given significance level based on the GISTIC algorithm (Table 3.5). The most frequent aberrations comprised of large segmental changes with few local amplifications or delections. The most statistically significant DNA copy number gains were located at dog chromosome CFA 10: 13,401,327-15,552,957 (q= 16.27E-07), CFA 26: 30,235,074-30,241,704 (q= 9.67E-05), and CFA 30: 19,196,241-19,743,852 (q= 6.79E-07). The most statistically significant losses were located at CFA 11: 44,241,313-44,299,261 (q= 4.46-06), CFA 26: 40,924,095-40,940,186 (q= 4.89E-05), and CFA X: 74,942,593-75,297,878 (q= 5.09E-05).

Several regions, most notably on CFA 10, CFA 26, and CFA 30, had oaCGH profiles suggestive of structural changes. These changes were denoted by a copy number gain followed immediately by a loss, and all were found to be statistically significant (Table 3.5). The suggested chromosome break point region on CFA 30, evident in 66% of tumors analyzed, spans 5Mb of sequence located between 14Mb and 19Mb. In all cases where the characteristic prolife was detected, the log2 values on either side of the breakage region of CFA30 indicated a heterozygous loss followed by an immediate gain with a copy number of $\geq$4.

3.4.2 Differential CNA Aberrations between Cell Lines and Primary Oral Melanoma Tumors

Overall, the cell lines and primary tumors presented with similar genome-wide copy number profiles (Figure 3.1). Statistically different copy number aberrations between populations were assessed in detail (Table 3.6). One notable gene-specific loss only observed in cell lines and not present in the majority of primary tumors was the homozygous

loss of CFA 11: 44,241,313-44,299,261. This gene region specific for *CDKN2A,* was present in 86% (n=5 of 6) of cell lines, but only 25% (n=10 of 44) of primary tumors (p= 1.02E-07). The largest continuous genomic region with significant difference between the two populations was a gain of CFA 13. Within both populations, CFA 13 was gained in semi-contiguous blocks. A large proximal region of CFA 13 gained in 83% (n=5/6) of cell lines and only 22% of primary melanomas (n=10/44) and a large distal region of CFA 13 gained in 100% of cell lines and approximately of 30% of primary melanomas (n=13/44).

3.4.3 Detection of CNA by SLP-FISH of Metaphase Cell Lines

SLP-FISH validated overall copy number changes for specific genes identified by oaCGH (Figure 3.2). The most frequent aberrations were a gain of *C-MYC* (n=5/6), a gain of *C-KIT* (n=6/6), and a loss of *RB-1* (n=3/6). The *PTEN* region was shown to have variable CN, demonstrating cases with all three CN status categories CN loss, CN gain, and CN neutral (n=2, 2, 2 respectively). A large degree of intra-case copy number variability was also observed in the cells assessed. The most notable variation in CN between cells within the same case was for *C-MYC* and *C-KIT*, which showed a range of loss, neutral, and gains in 83% of cases (n=5/6).

3.4.4 Detection of Chromosome Rearrangements by FISH on Metaphase Cell Lines

SLP-FISH data demonstrated frequent structural changes (Figure 3.3). The most recurrent chromosome rearrangement was the separation of *C-MYC* and *C-KIT* SLPs, indicating a breakage of chromosome CFA 13 (n=3). SLP-FISH also revealed a fusion of

chromosomes CFA 15 and 26 (CL5) and a fusion of chromosomes CFA 18 and 26 (CL1), but neither fusion was recurrent. Oligo-aCGH sigmoidal copy number pattern profiles and SLP-FISH suggested breakage/fusion events occurring between chromosomes CFA 10, 26, and 30. When chromosomes were further analyzed, FISH validated copy number aberrations suggested by oaGCH and revealed numerous additional fusion and rearrangement events (Figure 3.4). Fusions between CFA 10, 26, and 30 were confirmed; however, the type of fusion event was not recurrent between cases. Double minuet chromosomes were present on multiple metaphase spreads in numerous cases (n=3).

3.4.5 Gene Expression Analysis

Whole-transcriptome gene expression profiling (GEP) revealed a high level of gene expression changes (Figure 3.5). Genes with the highest level of expression changes were inspected for biological relevance. These included *PLK1, PLK2, TTK, B-Myb, HAS2, BRCA1, Kif4A, IL8, ACVRL1, NEK2, TSCOT, AURKB, CCNA2, CCNB2,* and *CCNB3*. RT-qPCR analysis of selected genes confirmed direction of gene expression change as was identified by GEP (Figure 3.6). RT-qPCR analysis of thirteen selected genes, based on identification by GEP or involvement in classic cancer pathways, found numerous gene expression changes in the cohort of additional primary cases. Genes with the greatest fold changes were *PLK1* and *TTK (MPS1)*, both overexpressed with an average fold change of 83.63 and 912.12, respectively. For both of these genes, 100% of malignant samples were overexpressed ($p= 0.0000421$). Of the additional 11 genes analyzed, nine showed significantly different expression from normal (*RB-1* $p= 0.00147$, *HAS2* $p= 0.0002105$,

BRAF p= 0.002947, *c-MYC* p= 0.0006315, *MYB* p= 0.00884, *c-KIT* p= 0.0208, *TP53* p= 0.02084, *FOXP1* p= 0.02084, *NME2* p= 0.0301). Within the cohort of benign lesions, five genes showed significantly dysregulated gene expression (*c-KIT* p= 0.000326, *MYB* p= 0.0228, *BRAF* p= 0.000326, *TTK* p= 0.000326, *ACVRL1* p=0.000326). All genes but one were down-regulated (*MYB*).

When gene expression was compared between benign and malignant samples, all but two, *PTEN* and *MYB*, showed significantly higher expression in malignant samples (*TTK* p= 0.000319, *PLK1* p= 2.162E-05, *RB-1* p= 0.000115, *HAS2* p= 0.00169, *BRAF* p= 4.05E-06, *c-MYC* p= 0.000853, *c-KIT* p= 0.00235, *TP53* p= 0.000170, *FOXP1* p= 0.000292, *NME2* p= 0.000383, *ACVRL1* p= 5.962E-05). Four genes were shown to positively correlate with mitotic index of the malignant samples (*TTK* p= 0.002308, *PLK1* p= 0.0592, *c-MYC* p= 0.0487, *TP53* p= 0.00496).

3.4.6 Targeted Sanger Sequencing

Results showed no sequence mutations. Mutations were not found in *BRAF* at the V600 codon or at any location in *TP53*, confirming previously published findings within our data set.

3.5 Discussion

Cell cycle and mitotic control are key to proper cellular function. Aberrations within the mechanisms of regulation of the cell cycle can lead to altered proliferation and decreased mutation monitoring. Aberrations at the mRNA level in such pathways, including the

CDKN2A and p53 checkpoints, have been shown in both human and canine mucosal melanomas (Koenig *et al.* 2002; Swick and Maize 2012). However, alterations to the CDK2NA pathway, shown to vary among cases (Hsieh *et al.* 2013), cannot alone explain tumorigenesis of oral malignant melanoma (OMM) or the complex chromosome rearrangements observed suggesting a high level of chromosome instability. Whole genome- and exome-sequencing of human mucosal melanomas also showed a significant number of chromosomal aberrations (Furney *et al.* 2013). Alterations to only the canonical molecular melanoma pathways, such as MAPK and CDK2NA, cannot lead to chromosome alteration and propagation within mucosal melanoma cells. However, large-scale chromosomal aberrations have been linked to several mitotic check point and chromosome separation regulation pathways (Hoi Tang and Poon 2011).

3.5.1 Detection of Structural Aberrations

We first validated the presence of numerous structural aberrations within our cohort of canine oral melanoma cell lines. In contrast to oaCGH, metaphase FISH analysis is key in identifying cytogenetic instability in the form of structural aberrations, not just copy number imbalances. Genome reorganization was suggested through oaCGH profiling due to the presence of sigmoidal patterns on CFA 10, 26, and 30, and semi-continuous gains of CFA 13. Oligo-aCGH indicated a trisomy of CFA 13 with an additional region of amplification (n=4) of CFA 13 at ~20-40Mb. FISH analysis revealed that CL3 had one grossly normal CFA 13 and then two aberrant copies with fragments located on separate chromosomes (Figure 3.2 (C)). FISH analysis also detected structural aberrations that oaCGH did not

suggest. Oligo-aCGH analysis of CL5 showed a focal region of amplification on CFA 30 at ~17-19Mb. FISH BAC tiling of CFA 30 demonstrated that CL5 had two grossly normal copies of CFA 30 and validated the targeted amplification of ~19Mb of CFA 30, however it revealed the aberrant locus was located on a large, unknown derivative chromosome. Another intriguing finding of FISH analysis of CL5 (undetectable by oaCGH) was that in 30% of cells, the two grossly normal copies of CFA 30 were fused at the centromere (Figure 3.4 (E)). Such structural aberrations would be undetectable via oaCGH, as the copy number is balanced, but the arrangement of the loci is altered.

A semi-continuous amplification of CFA 13, indicative of a chromosome breakage as seen in CL3, was suggested by oaCGH profiling of both melanoma cell lines and primary tumors. All six cell lines, showed a copy number gain of the distal half of CFA 13, while only five cases showed a gain of the proximal half. CL2, the one cell line without a gain of the proximal half of CFA 13, showed a dramatic oaCGH pattern of chromosome instability on CFA 13 from 30-48Mb. Breakage between the two continuous regions occurred at ~46Mb (Table 3.6), close to where the orthologous regions of human (HSA) 8 and 4 join at CFA 13: 41Mb. Similar findings were seen in the primary tumors; 22% had a gain of the proximal half of CFA 13, and 30% had a gain of the distal portion. This suggests regions of fragile chromatin where large syntenic blocks of the genome join (e.g. evolutionarily conserved break points). Fragility in chromosome packaging increases the possibility of breakage events at these locations. Normally, these breakage events would result in apoptotic cell death; however, when paired with gene expression changes that permit cells with damaged genomes to proliferate, cells with altered karyotypes propagate within the

tumor. This, taken with the gene expression changes in the mitotic spindle assembly checkpoint pathways, may explain the frequency of semi-continuous amplifications in oral melanomas.

The presence of intra-tumor copy number variability was suggestive of a lack of molecular clonality within canine oral melanoma tumor cells. Recent studies have also shown high levels of cytogenetic heterogeneity within malignant and metastatic melanomas in human patients (Anaka *et al.* 2013). A loss of genetic stability along with alteration to DNA damage checkpoints, can lead to the development and proliferation of multiple clones. The presence of variable cellular clones can add to tumor aggression, as persistence of multiple clones within a tumor population can make targeted treatments ineffective. Research has also linked the degree of chromosomal instability and karyotypic abnormality with treatment failure (Hu *et al*. 2013; Roschke and Rozenblum 2013; Bakhoum and Swanton 2014). Many theories exist on how multi-clonal tumors arise (Teixeira and Heim 2011); however, all cells with altered karyotypes must maintain cellular viability for the altered karyotypes to proliferate within the tumor population.

3.5.2 Identification of Key Genes Dysregulated in Mucosal Melanomas

Numerous genes were identified by gene expression profiling (GEP) as being dysregulated within the cohort of six canine melanoma cell lines and seven primary tumors. Thirteen genes, selected based on involvement in classical melanoma pathways (n=7) or identification from GEP (n=6), were validated in 17 additional primary oral melanomas via RT-qPCR. Three genes were found either to not recapitulate GEP changes in a significant

percentage of additional primary cases (*ACVRL1*) or were observed to be single genes altered within their pathway (*FOXP1, MYB)*. *HAS2* was significantly overexpressed in malignant samples (p= 0.00021). While, 50% of benign cases showed overexpression of *HAS2* the frequency was not enough to be significant in terms of the entire population. The level of overexpression in the malignant populations was significantly higher when compared to benign samples (p= 0.0442). This suggests the involvement of *HAS2* in the development or propagation of melanocytic tumors. These data are in concordance with the observation that melanocytic tumors tend to be highly fibrous solid tumors that express large amounts of hyaluronan (Hanna *et al.* 2013).

Of genes selected based on their involvement in classical melanoma and cancer pathways, c-*KIT*, c-*MYC, BRAF,* and *RB-1* were dysregulated in the cohort of additional primary melanomas. While these genes are essential in several steps in melanoma tumorigenesis, the presence of significant genetic instability and complex chromosome alterations suggests dysregulation of the mitotic checkpoints, which classic melanoma mutations have not been implicated in. Therefore, additional dysregulated genes were interrogated for their involvement in mitotic regulation pathways. These pathways, such as the mitotic spindle assembly, may add to the tumorigenesis of canine oral melanomas.

Several of the genes identified as dysregulated though GEP and validated by RT-qPCR are involved in the spindle assembly and mitotic DNA damage checkpoints. Of the four genes that positivity correlated with cellular proliferation, three, *TP53*, *PLK1*, and *TTK,* are part of the DNA damage/mitotic spindle assembly pathway, and one, *c-MYC*, is a transcription factor that regulate cellular mitosis. *TP53* was investigated as a mechanism of

mitotic dysregulation due to the common loss of *TP53* expression or its mutation in numerous cancers and its regulatory role in the mitotic checkpoint pathway (Hoi Tang and Poon 2011). However, *TP53* was neither down regulated nor mutated in canine oral melanoma, suggesting dysregulation of this pathway is facilitated through a mechanism(s) other than alteration of *TP53*.

Within the mitotic spindle assembly pathway, there are numerous kinases identified as having altered expression by GEP, including *PLK1*, and *TTK* (also known as *MPS1)*. These kinases function in centrosome regulation, maturation, and the mitotic response to DNA-damage (Hoi Tang and Poon 2011). *PLK1* and *TTK* showed the highest level of dysregulation within the malignant melanomas. PLK1 is critical for centrosome maturation and separation and plays a key role in centrosome functions and the assembly of bipolar spindles. Essential to the G2/M transition of mitotic cell cycle, PLK1 phosphorylates numerous downstream proteins, such as cyclin-B1 (*CCNB1*) during prophase (Toyoshima-Morimoto *et al.* 2001; Hoi Tang and Poon 2011). It also functions in the regulatory circuit that promotes the activation of CDK1 by phosphorylating the positive regulator CDC25C and inhibiting the negative regulators TOPORS, WEE1, and MYT1 (van de Weerdt and Medema 2006).

PLK1 expression has been shown to be increased in tumors with a poor prognosis, suggesting a role in malignant transformation (Hoi Tang and Poon 2011). In the canonical pathway, PLK1 is inactivated by WEE1 after DNA-damage. However, overexpression of PLK1 can allow for the inhibition of normal p53 function and localization of cdc25 to the nucleus, ultimately leading to the ability to bypass mitotic inhibition from DNA damage (Hoi

Tang and Poon 2011). PLK1 then acts as a negative regulator of p53 by phosphorylation of TOPORS, inhibiting the SUMOylation of p53 and simultaneously enhancing the ubiquitination and subsequent degradation of p53 (an Vugt, Bras, and Medema 2004). In our cohort of mucosal melanomas, *PLK1* was significantly overexpressed, allowing *PLK1* to inactivate p53 at the protein level; thus further elucidating why cells with DNA damage are propagated in the presence of normal *TP53* expression and sequence. This overexpression of *PLK1* and subsequent inhibition of p53 would ultimately lead to the complex chromosomal rearrangements observed in our canine melanoma cell lines.

PLK1 also has previously been investigated as a potential therapeutic target for its role in melanoma (Jalili *et al.* 2011). This study reported an overexpression of PLK1 in primary and metastatic melanomas. Inhibition of PLK1 led to induction of apoptosis, independent of p53 function. This finding further supports the theory that *PLK1* overexpression is responsible for the proliferation of cells with DNA damage in the presence of normal *TP53*. Jalili and colleagues also found that concurrent inhibition of the MAPK signaling cascade and PLK1 had an additive effect on reduced cell viability. Within our cohort of mucosal melanomas, *PLK1* overexpression correlated with cellular proliferation. Our study also observed an overexpression of the *c-MYC* transcription factor, which is a downstream effector of MAPK activation. Our data are consistent with previous findings that show overexpression of *PLK1,* mediated through activation of the MAPK pathway, can inhibit apoptosis of DNA-damaged cells. This would lead to a cellular phenotype in which a genetically instable cell with a highly altered karyotype would be able to bypass the normal DNA damage checkpoints and continue to proliferate.

The major checkpoint in mitosis is the spindle assembly checkpoint that ensures accurate chromosome segregation by delaying anaphase until all chromosomes are properly attached to the mitotic spindle (Aarts, Linardopoulos, and Turner 2013). TTK (or MPS1) is a dual specificity protein kinase with the ability to phosphorylate tyrosine, serine, and threonine. Associated with cell proliferation, this protein is essential for chromosome alignment at the centromere during mitosis and enhancing Aurora Kinase B (AURKB) activity (van der Waal *et al.* 2012). TTK has been found to be a critical mitotic checkpoint protein for accurate segregation of chromosomes during mitosis. In addition to its role in the spindle-assembly checkpoint a portion of the TTK protein localizes to centrosomes and helps facilitates centrosome duplication (Fisk, Mattison, and Winey 2003).

Tumorigenesis can also occur when *TTK* is overexpressed (Yuan *et al.* 2006; Hoi Tang and Poon 2011), as was observed in our cohort of canine melanomas. Tumor development primarily occurs when the TTK protein fails to degrade and produces excess centrosomes, resulting in aberrant mitotic spindles (Liu and Winey 2012). Cells with this alteration tolerate aneuploidy, which normal, genetically stable cells cannot. This may be an additional mechanism by which canine oral melanoma cells continue to proliferate in the presence of significant aneuploidy, as observed in our cell lines. Another study investigating the role of TTK in tumor cells with high levels of aneuploidy found that the reduction of TTK protein levels in cultured human breast cancer cells led to induction of apoptosis and decreased ability of cells to grow as xenografts in nude mice (Daniel *et al.* 2011). Breast cancer cells that survived reduced levels of TTK also had relatively less aneuploidy, suggesting the overexpression of TTK is crucial for the propagation of aneuploid cells. The

study performed by Daniel and colleagues, along with several others (Colombo *et al.* 2010; Tardif *et al.* 2011), found that inhibition of TTK led to increased aberrant mitoses and eventual cellular crisis and death. This suggests that overexpression of *TTK* allowing the bypass of the mitotic checkpoint and regulation of spindle assembly may be required for aberrant cells to proliferate and maintain an altered karyotype. The role of *TTK* overexpression in overcoming apoptosis in the face of chromosomal dysregulation may explain why mucosal melanoma cells, shown to carry significant chromosome aberrations in both canines and humans, survive.

Oligo-aCGH analysis of primary oral canine melanomas and whole-genome sequencing of primary human mucosal melanomas, suggest patterns of structural aberrations in primary tumors. Our data show both intra- and inter-tumor copy number heterogeneity is found in canine oral melanomas. Furthermore, high levels of structural chromosome aberrations were observed within canine oral melanoma cell lines. When detailed gene expression analysis was performed, alterations within the mitotic and spindle assembly checkpoint pathways were found in both primary tumors and cell lines. Therefore, we propose the involvement of the mitotic and spindle assembly checkpoint pathways in the development and/or propagation of mucosal melanomas (Figure 3.7).

It is difficult to determine the ultimate cause of abnormal karyotypes in mucosal melanomas. The dysregulation of the mitotic regulation and spindle assembly could be an underlying cause, as high expression levels of Cyclin B1 (*CCNB1),* a key member of the mitotic regulatory mechanism that can also contribute to the chromosomal instability and the aggressive nature of certain cancers, have been observed in tumor cells before the

development of aneuploidy (Suzuki *et al.* 2007). However, genomic instability can occur through other means, such as telomere crisis. Regardless of the initial mechanism(s) of dysregulation, cells with disruption to the mitotic checkpoint are able to proliferate, even with DNA damage and an altered karyotype, within the cell population. Inhibitions of such checkpoints force the cell through mitosis without repairing the damage.

The dysregulation of the mitotic DNA damage pathway and the spindle assembly complex has considerable clinical implications. The lack of tumor clonality results in phenotypically different cells with variable response to traditional treatments within a single tumor. Intra-tumor heterogeneity emphasizes the need for further investigation into more effective and diverse treatment options, such as chemotherapeutics. Several members of these pathways including PLK1 and TTK have been identified as therapeutic targets, which has resulted in the development of chemotherapeutic inhibitors. We suspect that further investigation into this pathway will reveal key tumorigenic mechanisms and possible therapeutic targets for treatment of mucosal melanomas, in both dogs and humans.

Acknowledgements

I would like to acknowledge Dr. Jamie Modiano and Dr. R. Curtis Bird for providing access to their established melanoma cell lines.

REFERENCES

Aarts, M., Linardopoulos, S. and Turner, N. C. (2013). "Tumour selective targeting of cell cycle kinases for cancer treatment." Curr Opin Pharmacol **13**(4): 529-535.

an Vugt, M. A., Bras, A. and Medema, R. H. (2004). "Polo-like kinase-1 controls recovery from a G2 DNA damage-induced arrest in mammalian cells." Mol. Cell **15**: 799-811.

Anaka, M., Hudson, C., Lo, P.*, et al.* (2013). "Intratumoral genetic heterogeneity in metastatic melanoma is accompanied by variation in malignant behaviors." BMC Med Genomics **6**(40).

Angstadt, A. Y., Motsinger-Reif, A., Thomas, R.*, et al.* (2011). "Characterization of canine osteosarcoma by array comparative genomic hybridization and RT-qPCR: Signatures of genomic imbalance in canine osteosarcoma parallel the human counterpart." Genes, Chromosomes and Cancer **50**(11): 859-874.

Bakhoum, S. F. and Swanton, C. (2014). "Chromosomal instability, aneuploidy, and cancer." Molecular and Cellular Oncology **4**: 161.

Bergman, P. (2007). "Canine Oral Melanoma." Clinical Techniques in Small Animal Practice **22**(2): 55-60.

Bianco, S. R., Sun, J., Fosmire, S. P.*, et al.* (2003). "Enhancing antimelanoma immune responses through apoptosis." Cancer Gene Therapy **10**(9): 726-736.

Breen, M., Bullerdiek, J. and Langford, C. F. (1999). "The DAPI banded karyotype of the domestic dog (Canis familiaris) generated using chromosome-specific paint probes." Chromosome Research **7**(7): 575.

Breen, M., Hitte, C., Lorentzen, T. D.*, et al.* (2004). "An intergrated 4249 marker FISH/RH map of the canine genome." BMC Genomics **5**(1): 65.

Colombo, R., Caldarelli, M., Mennecozzi, M.*, et al.* (2010). "Targeting the mitotic checkpoint for cancer therapy with NMS-P715, an inhibitor of MPS1 kinase." Cancer Res **70**: 10255-10264.

Curtin, J. A., Fridlyand, J., Kageshita, T.*, et al.* (2005). "Distinct Sets of Genetic Alterations in Melanoma " New England Journal of Medicine **353**(20): 2135-2147.

Daniel, J., Coulter, J., Woo, J. H.*, et al.* (2011). "High levels of the Mps1 checkpoint protein are protective of aneuploidy in breast cancer cells." Proc Natl Acad Sci U S A **108**(13): 5384-5389.

Fisk, H. A., Mattison, C. P. and Winey, M. (2003). "Human Mps1 protein kinase is required for centrosome duplication and normal mitotic progression." Proc Natl Acad Sci U S A **100**(14875-14880).

Furney, S. J., Turajlic, S., Stamp, G.*, et al.* (2013). "Genome sequencing of mucosal melanomas reveals that they are driven by distinct mechanisms from cutaneous melanoma." J Pathol **230**(3): 261-269.

Hoi Tang, M. and Poon, R. (2011). "How protein kinases co-ordinate mitosis in animal cells." Biochem J **435**: 17-31.

Hsieh, R., Nico, M., Coutinho-Camillo, C.*, et al.* (2013). "The CDKN2A and MAP Kinase Pathways: Molecular Roads to Primary Oral Mucosal Melanoma." Am J Dermatopathol **35**(2): 167-175.

Hu, Y., Ru, N., Xiao, H.*, et al.* (2013). "Tumor-specific chromosome mis-segregation controls cancer plasticity by maintaining tumor heterogeneity." PloS one **8**(11): e80898.

Jalili, A., Moser, A., Pashenkov, M.*, et al.* (2011). "Polo-like kinase 1 is a potential therapeutic target in human melanoma." J Invest Dermatol **131**(9): 1886-1895.

Koenig, A., Wojcieszyn, J., Weeks, B. R.*, et al.* (2001). "Expression of S100a, Vimentin, NSE, and Melan A/MART-1 in Seven Canine Melanoma Cell Lines and Twenty-nine Retrospective Cases of Canine Melanoma." Veterinary Pathology **38**(4): 427-435.

Koenig, A., Bianco, S. R., Fosmire, S.*, et al.* (2002). "Expression and Significance of p53, Rb, p21/waf-1, p16/ink-4a, and PTEN Tumor Suppressors in Canine Melanoma." Veterinary Pathology **39**(4): 458-472.

Liu, X. and Winey, M. (2012). "The MPS1 Family of Protein Kinases." Annual Review of Biochemistry **81**: 561-585.

Murakami, A., Mori, T., Sakai, H.*, et al.* (2011). "Analysis of KIT expression and KIT exon 11 mutations in canine oral malignant melanomas." Veterinary and Comparative Oncology **9**(3): 219-224.

Ramos-Vara, J. A., Beissenherz, M. E., Miller, M. A.*, et al.* (2000). "Retrospective Study of 338 Canine Oral Melanomas with Clinical, Histologic, and Immunohistochemical Review of 129 Cases." Veterinary Pathology **37**(6): 597-608.

Richter, A. (2005). "RAS Gene Hot-Spot Mutations in Canine Neoplasias." Journal of Heredity **96**(7): 764-765.

Ritt, M. G., Wojcieszyn, J. and Modiano, J. F. (1998). "Functional Loss of p21/Waf-1 in a Case of Benign Canine Multicentric Melanoma." Veterinary Pathology **35**(2): 94-101.

Roschke, A. V. and Rozenblum, E. (2013). "Multi-layered cancer chromosomal instability phenotype." Frontiers in oncology **3**.

Spangler, W. L. and Kass, P. H. (2006). "The Histologic and Epidemiologic Bases for Prognostic Considerations in Canine Melanocytic Neoplasia." Veterinary Pathology **43**(2): 136-149.

Suzuki, T., Urano, T., Miki, Y.*, et al.* (2007). "Nuclear cyclin B1 in human breast carcinoma as a potent prognostic factor." Cancer Sci **98**(5): 644–651.

Swick, J. M. and Maize, J. C. (2012). "Molecular biology of melanoma." Journal of the American Academy of Dermatology **67**(5): 1049-1054.

Tardif, K., Rogers, A., Cassiano, J.*, et al.* (2011). "Characterization of the cellular and antitumor effects of MPI-0479605, a small-molecule inhibitor of the mitotic kinase Mps1." Mol Cancer Ther **10**: 2267-2275.

Teixeira, M. R. and Heim, S. (2011). "Cytogenetic analysis of tumor clonality." Adv Cancer Res **112**: 127-149.

Thomas, R., Scott, A., Langford, C. F.*, et al.* (2005). "Construction of a 2-Mb resolution BAC microarray for CGH analysis of canine tumors." Genome Research **15**: 1831-1837.

Toyoshima-Morimoto, F., Taniguchi, E., Shinya, N.*, et al.* (2001). "Polo-like kinase 1 phosphorylates cyclin B1 and targets it to the nucleus during prophase." Nature **410**: 215-220.

van de Weerdt, B. C. M. and Medema, R. H. (2006). "Polo-Like Kinases: A Team in Control of the Division." Cell Cycle **5**(8): 853-864.

van der Waal, M., Saurin, A., Vromans, M.*, et al.* (2012). "Mps1 promotes rapid centromere accumulation of Aurora B." EMBO Rep **13**(9): 847-854.

Yuan, B., Xu, Y., Woo, J.*, et al.* (2006). "Increased expression of mitotic checkpoint genes in breast cancer cells with chromosomal instability." Clin Cancer Res **12**(2): 405-410.

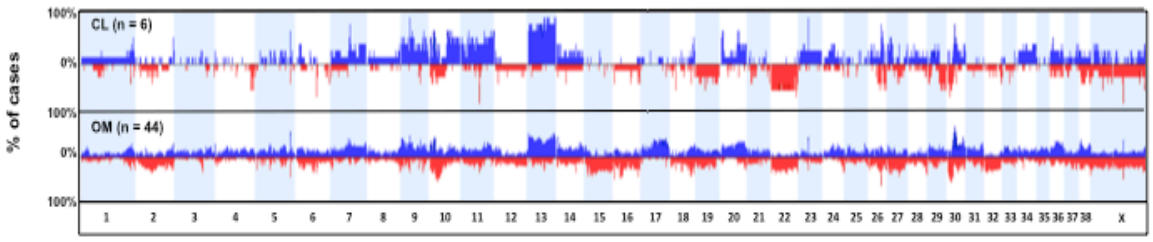

Figure 3.1 Oligo-aCGH profiles of canine oral melanoma cell lines (CL) (n=6) and primary oral melanomas (OM) (n=44). aCGH plots for each cohort are represented as a penetrance plot, which establishes the percentage of cases with a common aberration within each population. Percentages are plotted along the y-axis. Losses and gains are called in proportion to a CN of two, set at y=0. Regions of red and blue bars delineate regions of copy number loss and gain, respectively. The x-axis denotes individual chromosomes. Cytogenetic analyses of cell lines and primary tumors show numerous similar CNAs, notably on chromosomes 2, 10, 13, 26, and 30. These data indicate that cell lines grossly recapitulate the CNAs seen in primary tumors.

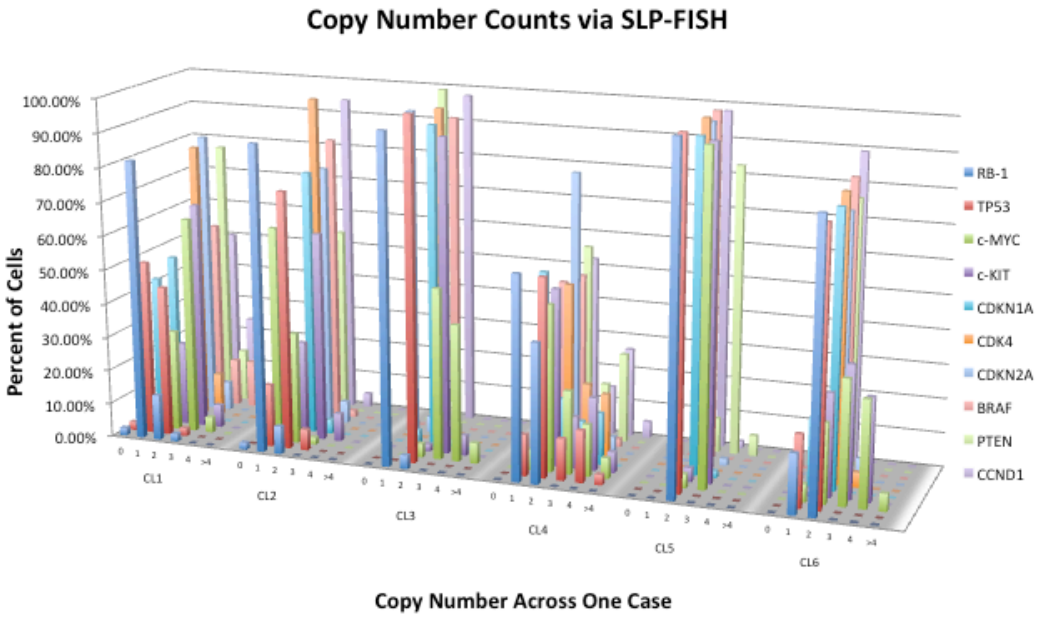

Figure 3.2 Copy number counts of canine oral melanoma cell lines (n=6) based on single-locus FISH analysis. The x-axis denotes the copy number status in 30 cells from each cell line. The y-axis indicates the percent of cells with each copy number. The z-axis denotes 10 individual genes containing BAC contigs enumerated using SLP FISH. CL3 and CL5 showed fairly homogenous CN status among all cells. CL1 and CL4 had the largest amount of CN variability between cells. Of the genes analyzed, *c-MYC* and *c-KIT* showed the largest amount of variation with CNs of 2, 3, 4, or >4.

Figure 3.3 Targeted gene single-locus FISH analysis of canine oral melanoma cell lines (n=6). (A) Ideogram of selected chromosomes and base pair location of each single-locus BAC used for FISH analysis of targeted gene loci. All FISH images were captured at 100X magnification. **(B)** Image of metaphase spread from CL 1 showing a fusion chromosome (arrowed) that contains SLP from CFA 18 and 26. CCND1 is labeled in spectrum aqua (blue) and PTEN is labeled in spectrum gold (yellow). **(C)** Image of metaphase spread from CL 3 showing a split of SLPs located on CFA 13 into two chromosomes (arrowed), indicating a breakage of one CFA 13 allele. C-KIT is labeled in spectrum gold (yellow) and C-MYC is labeled in Cy-4 (pink). **(D)** Image of metaphase spread from CL 5 showing a fusion chromosome (arrowed) that contains SLP from CFA 15 and 26. CDK4 is labeled in spectrum red (red) and PTEN is labeled in spectrum gold (yellow).

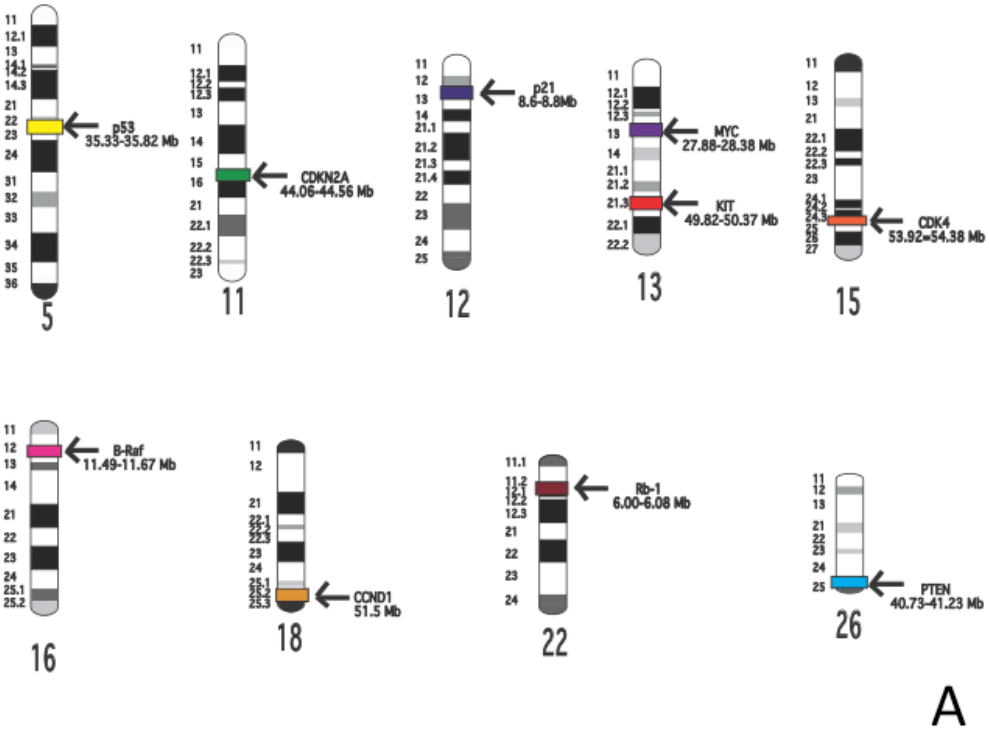
p53
35.33-35.82 Mb
5
CDKN2A
44.06-44.56 Mb
11
p21
8.6-8.8Mb
12
MYC
27.88-28.38 Mb
KIT
49.82-50.37 Mb
13
CDK4
53.92-54.38 Mb
15
B-Raf
11.49-11.67 Mb
16
CCND1
51.5 Mb
18
Rb-1
6.00-6.08 Mb
22
PTEN
40.73-41.23 Mb
26

A

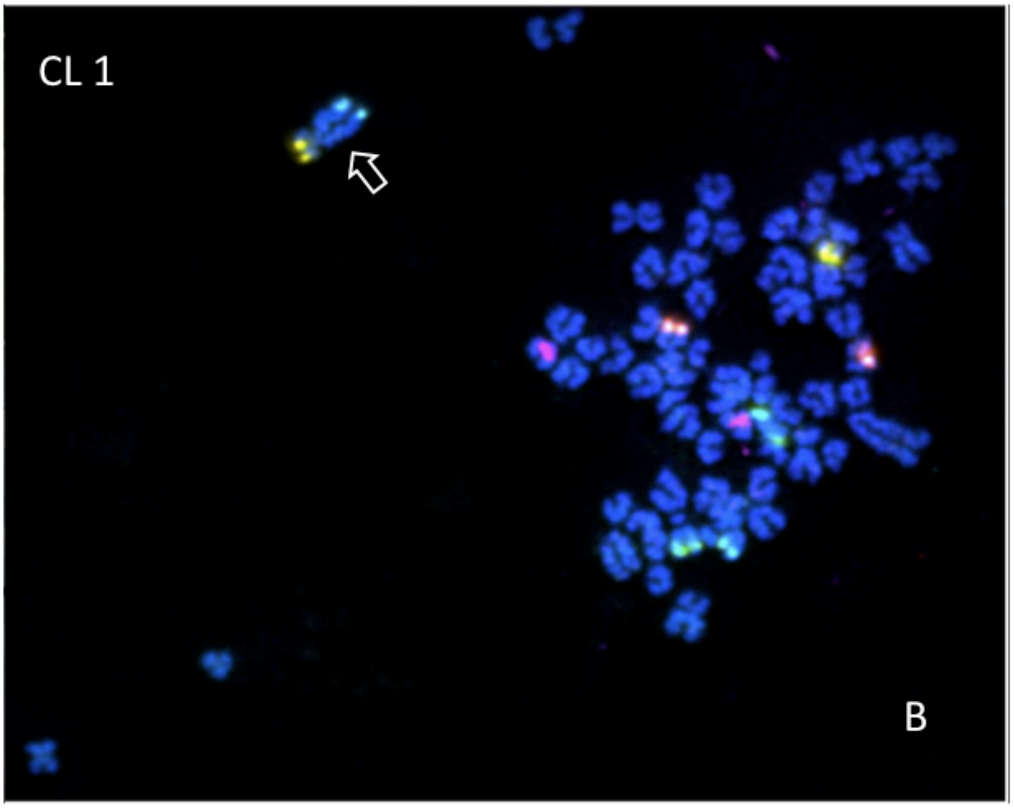
CL 1
B

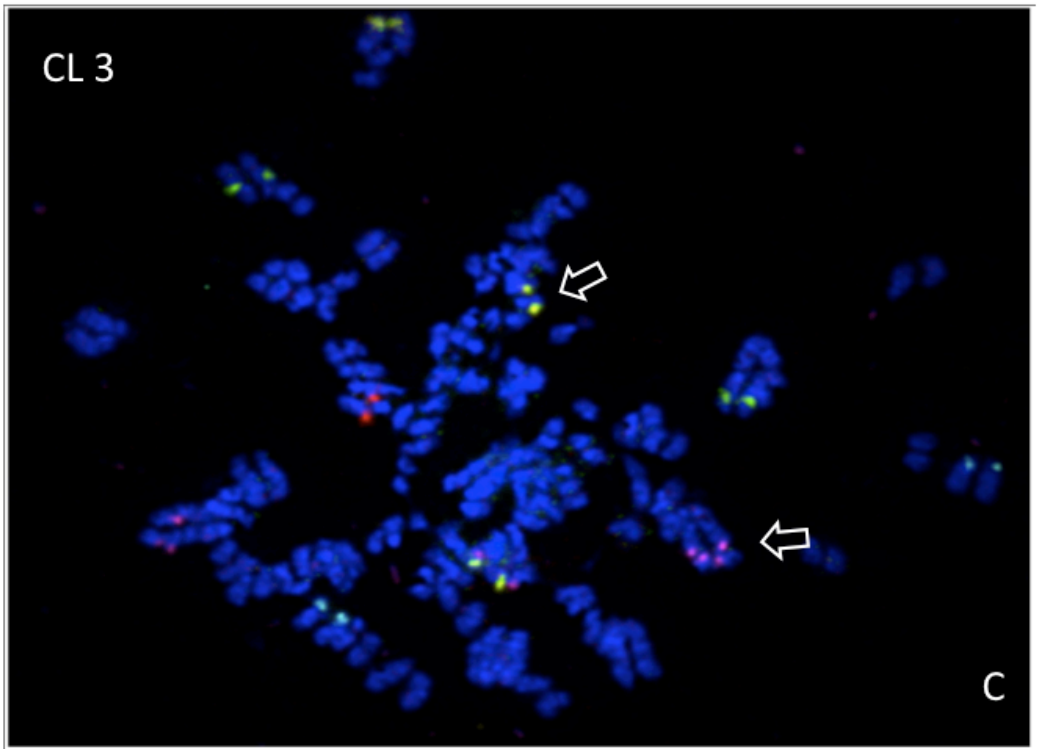
CL 3
C

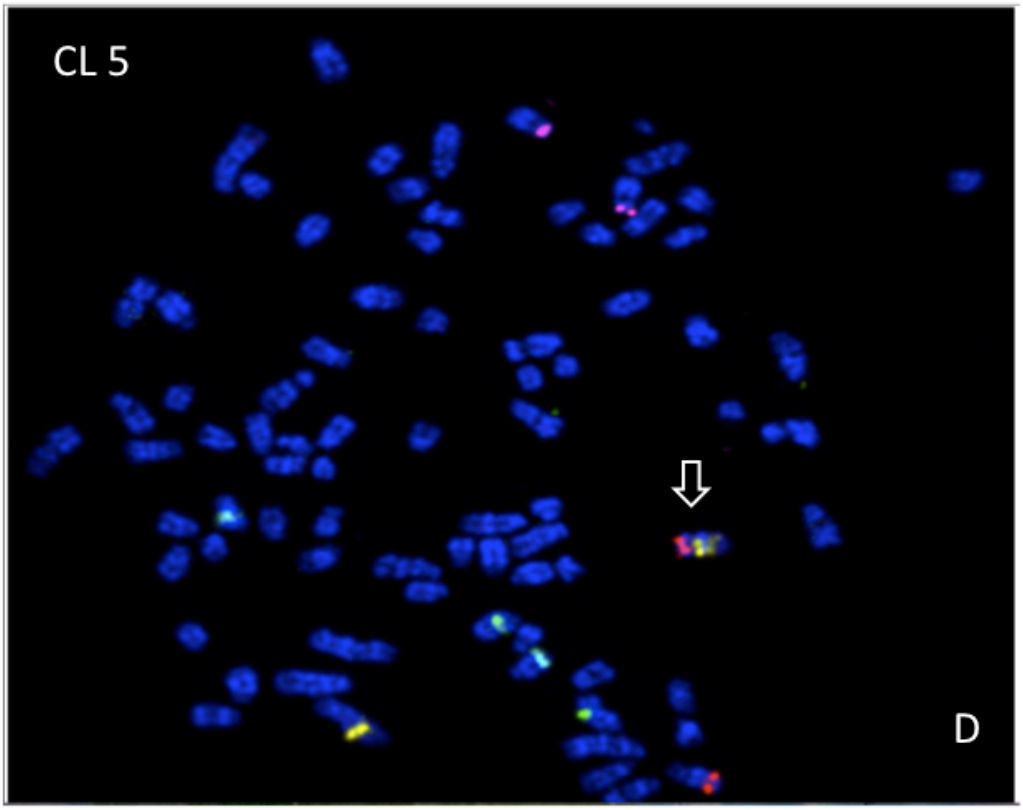
CL 5
D

Figure 3.4 Whole chromosome FISH analysis of CFA 10, 26, and 30 in canine oral melanoma cell lines (n=6). Each illustration contains four images: oaCGH profile of each cell line, FISH tiling analysis of CFA10, FISH chromosome painting analysis of CFA 10, 26, and 30, and FISH tiling analysis of CFA 30. All FISH images were captured at 100X magnification. Oligo-aCGH profiles from each individual were visualized using Agilent Genomic Workbench with CNAs called using the ADM2 algorithm. FISH tiling analysis consists of hybridizing individual BACs spaced every 10Mb along one chromosome. For FISH analysis of CFA10, only the first 5 BACs along the proximal half of the chromosome are shown. FISH chromosome painting analysis consists of hybridizing BACs along the length of an entire chromosome, all labeled in a single fluorescence channel. Here CFA 10 is represented in blue (spectrum aqua), CFA 26 is represented in pink (Cy-5), and CFA 30 is represented in yellow (spectrum gold). **(A)** CL1 showed two grossly normal copies of CFA 10 with focal amplification of a single BAC loci (~14Mb) on two separate unknown derivative chromosomes. It also showed one grossly normal copy of CFA 30 with focal amplifications of two loci (~3Mb and ~33Mb) on two separate unknown derivative chromosomes. Several translocations events were observed involving CFA 10, 26 and 30 including t(10;26), t(26;30), and t(10;30). **(B)** CL2 showed one grossly normal copy of CFA10 with numerous focal amplifications of BAC loci (~5Mb and ~14Mb) on several unknown derivative chromosome. Additionally, one derivative chromosome contained alternating tandem amplifications of the ~5Mb and ~14Mb loci (see insert). CFA 30 showed one grossly normal chromosome and a second complete chromosome fused to an unknown derivative chromosome. **(C)** CL3 showed two normal copies of CFA 10. It also showed one grossly normal copy of CFA 30 with an additional a grossly normal CFA 30 fused to an unknown derivative chromosome. CFA 26 presented with complex rearrangements with loci on several unknown derivative chromosomes. **(D)** CL4 showed one grossly normal copies of CFA 10 with a focal tandem amplifications of a single BAC loci (~14Mb) on two to three unknown derivative chromosomes (see insert). CFA 30 presented with one grossly normal copy of CFA30 with focal tandem amplifications of a single BAC loci (~23Mb) on two or three unknown derivative chromosomes (see insert). Chromosome painting revealed the focal tandem amplifications of CFA 10 and CFA 30 that were located on the same derivative chromosomes. **(E)** CL5 showed two grossly normal copies of CFA 10 with focal tandem amplification of a single BAC loci (~14Mb) on an unknown derivative chromosome. A second amplification of single BAC loci (~5Mb) was also present on an unknown derivative chromosome. Two grossly normal copy of CFA 30 were fused at the centromere (see insert), with additional focal amplifications of two BAC loci (~3Mb and ~33Mb) on two separate unknown derivative chromosomes. A large fusion chromosome of t(30;26;10) was also present (see insert). **(F)** CL6 showed two grossly normal copies of CFA 10. One grossly normal copy of CFA 30 was present with focal amplification of two single loci on separate unknown derivative chromosomes.

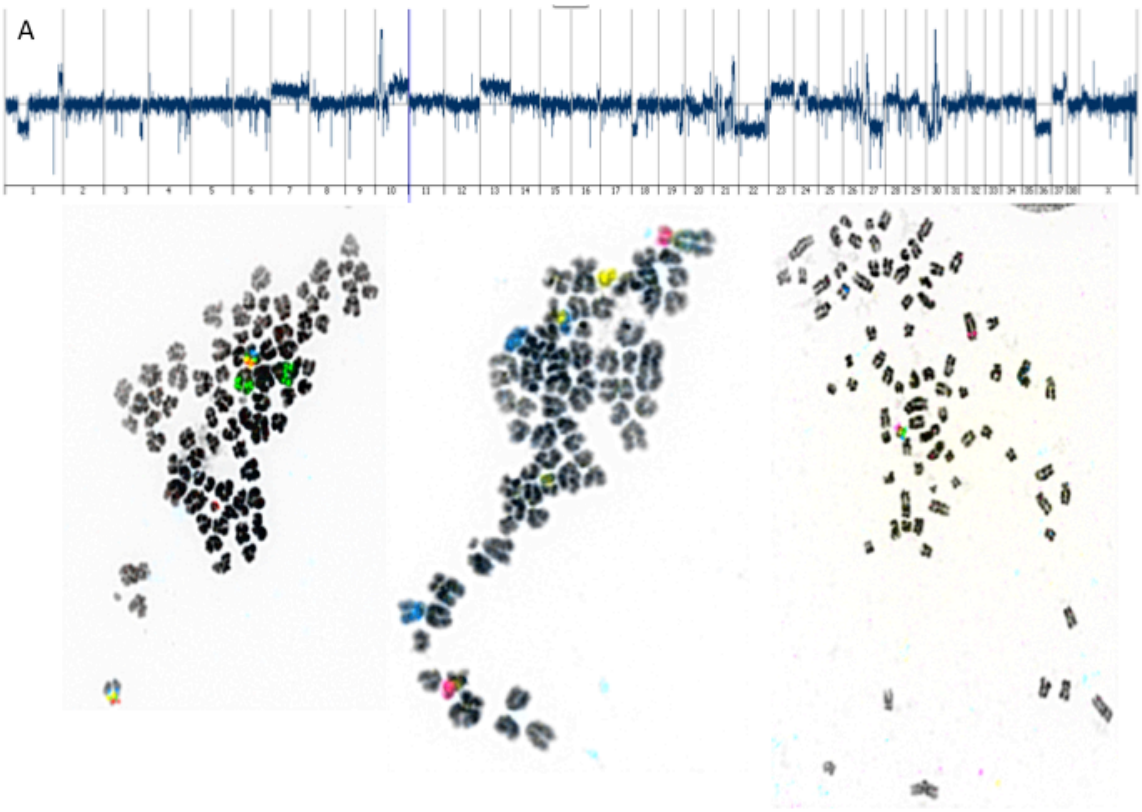

CFA 10 Tile 10,26,30 Paints CFA 30 Tile

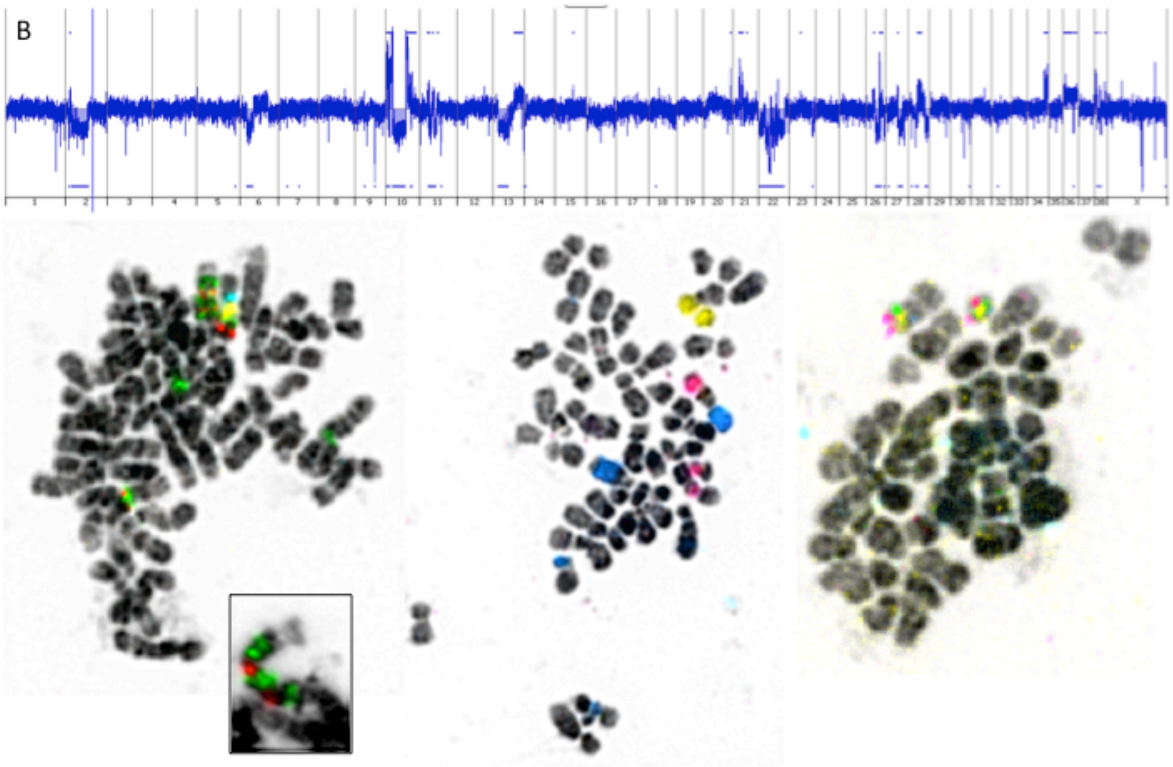

CFA 10 Tile

10,26,30 Paints

CFA 30 Tile

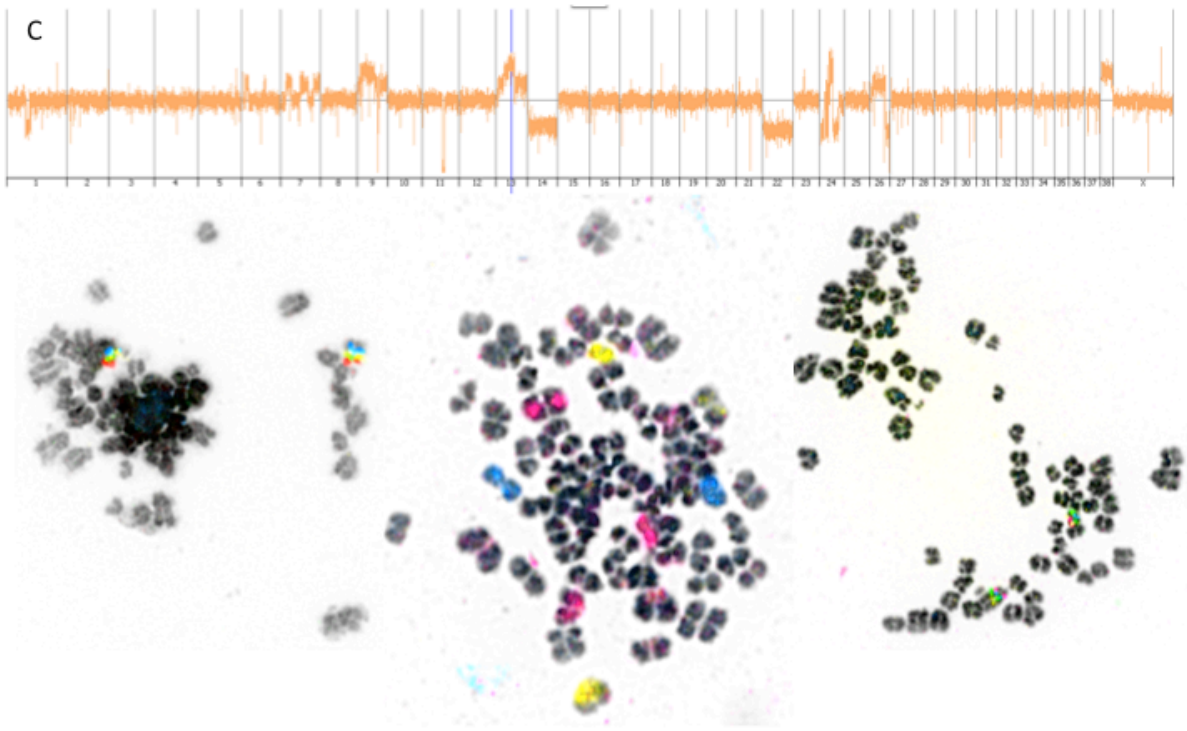

CFA 10 Tile 10,26,30 Paints CFA 30 Tile

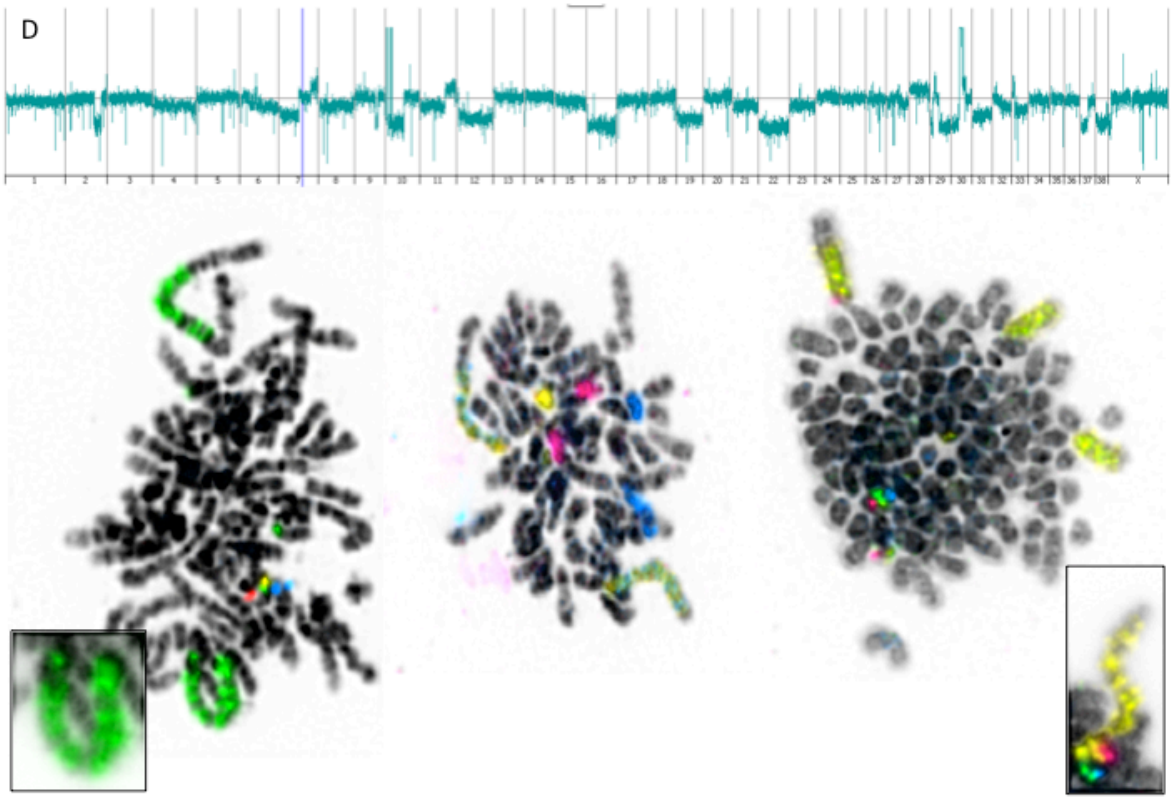

CFA 10 Tile 10,26,30 Paints CFA 30 Tile

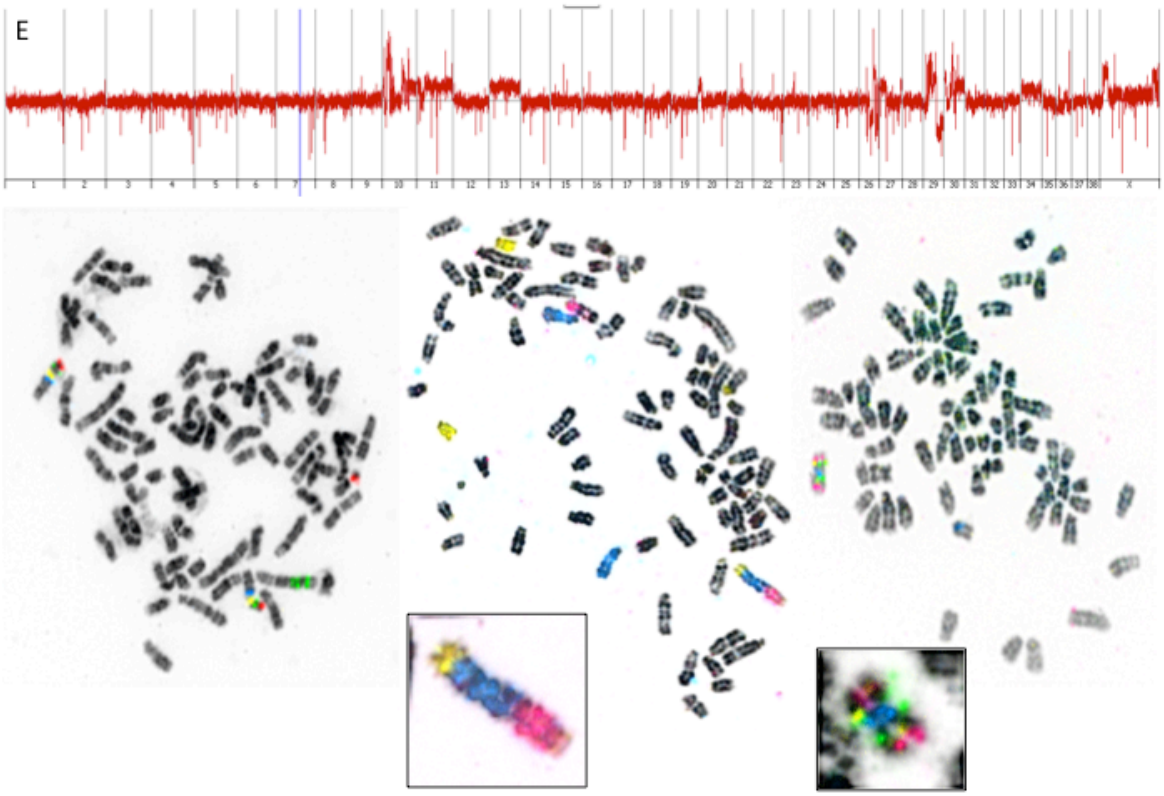

CFA 10 Tile 10,26,30 Paints CFA 30 Tile

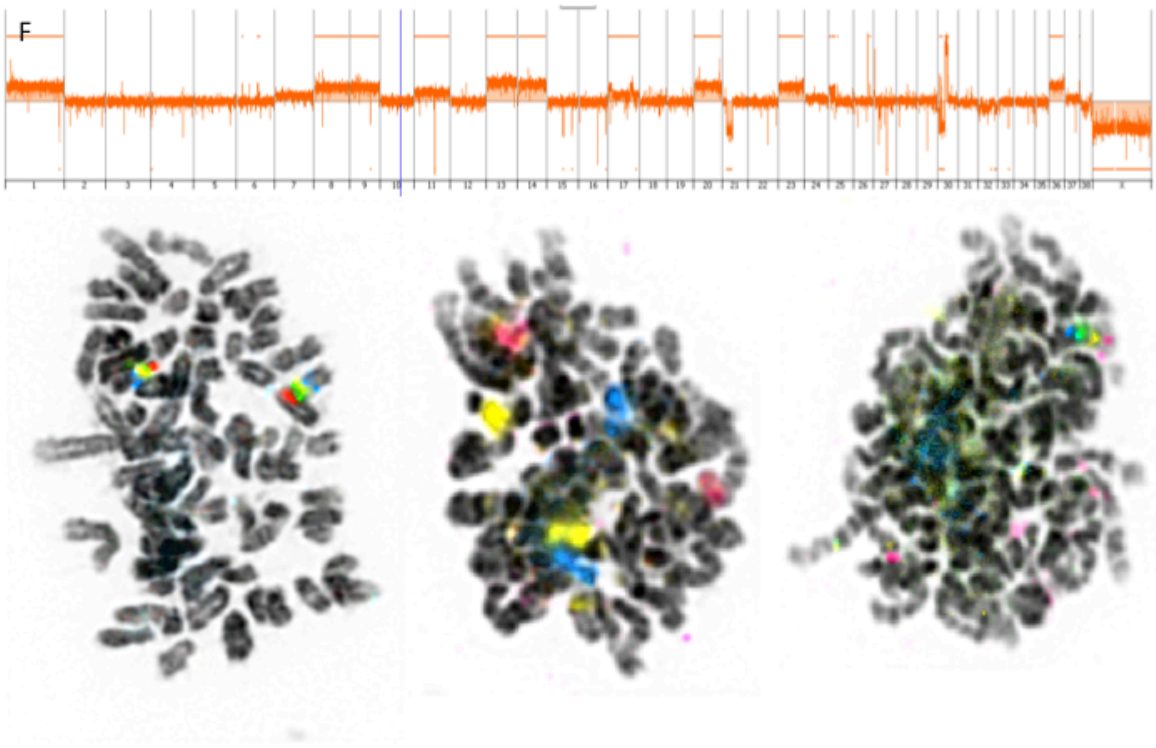

CFA 10 Tile

10,26,30 Paints

CFA 30 Tile

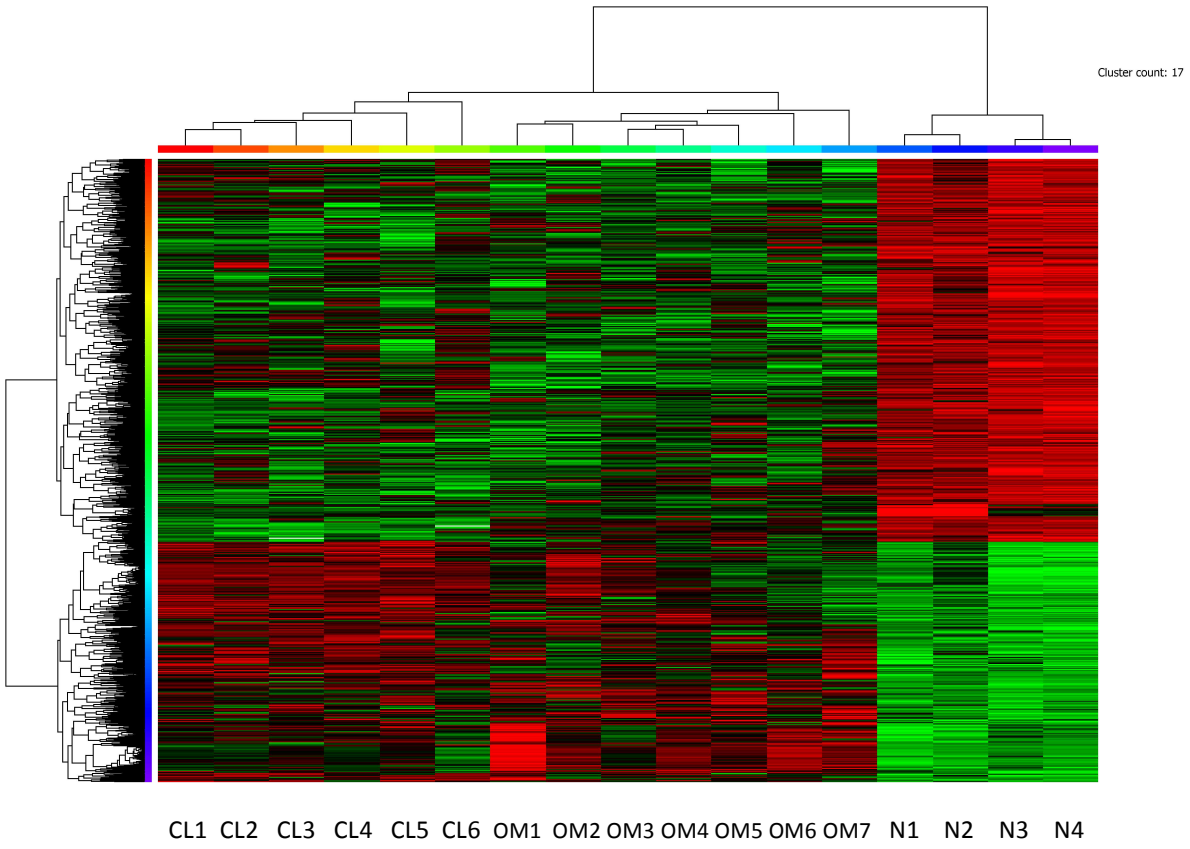

Figure 3.5 Whole genome expression profiling analysis of canine oral melanoma cell lines (n=6) and primary melanomas (n=7). Cases are plotted along the bottom x-axis. Hierarchical clustering of cell lines, primary cases, and normal samples is denoted along the top x-axis. Single genes are plotted along the y-axis. Differential expression of a single gene is denoted by color intensity with green indicating lower expression, red indicating overexpression, and black indication no expression change compared to normal non-neoplastic canine oral mucosa. Genes were then hierarchically clustered by their expression patterns. The normal cases clustered away from all melanoma samples. Within the cluster containing melanoma cases, the cell lines cluster together and primary cases cluster together. Dysregulated genes include *PLK1, TTK, B-Myb, HAS2, BRCA1, Kif4A, IL8, ACVRL1, Nek2, TSCOT, CCNA2, CCNB2, CCNB3,* and *Ki-67*.

Figure 3.6 Gene expression analyses of canine primary melanomas (n=17) and benign melanocytomas (n=14) for thirteen selected genes. RT-qPCR analysis was performed on an additional cohort of malignant melanomas and benign melanocytic lesions. Statistical analysis of gene expression between malignant and benign samples performed by a non-parametric Mann Whitney U test. Correlation of gene expression fold change to mitotic index was performed on malignant samples with a non-parametric Spearman's Rank Sum test. Percent of cases outside normal gene expression range was determined by Fisher's Exact Test. Statistical findings are indicated by symbols in the top right corner of each graphic, where *indicates, statically significant in expression between melanomas and benign lesions; § indicates a significant positive correlation of gene expression to mitotic index; ◆indicates a significant percentage of malignant cases with dysregulated gene expression; and ✚ indicates significant percentage of benign cases with dysregulated gene expression.

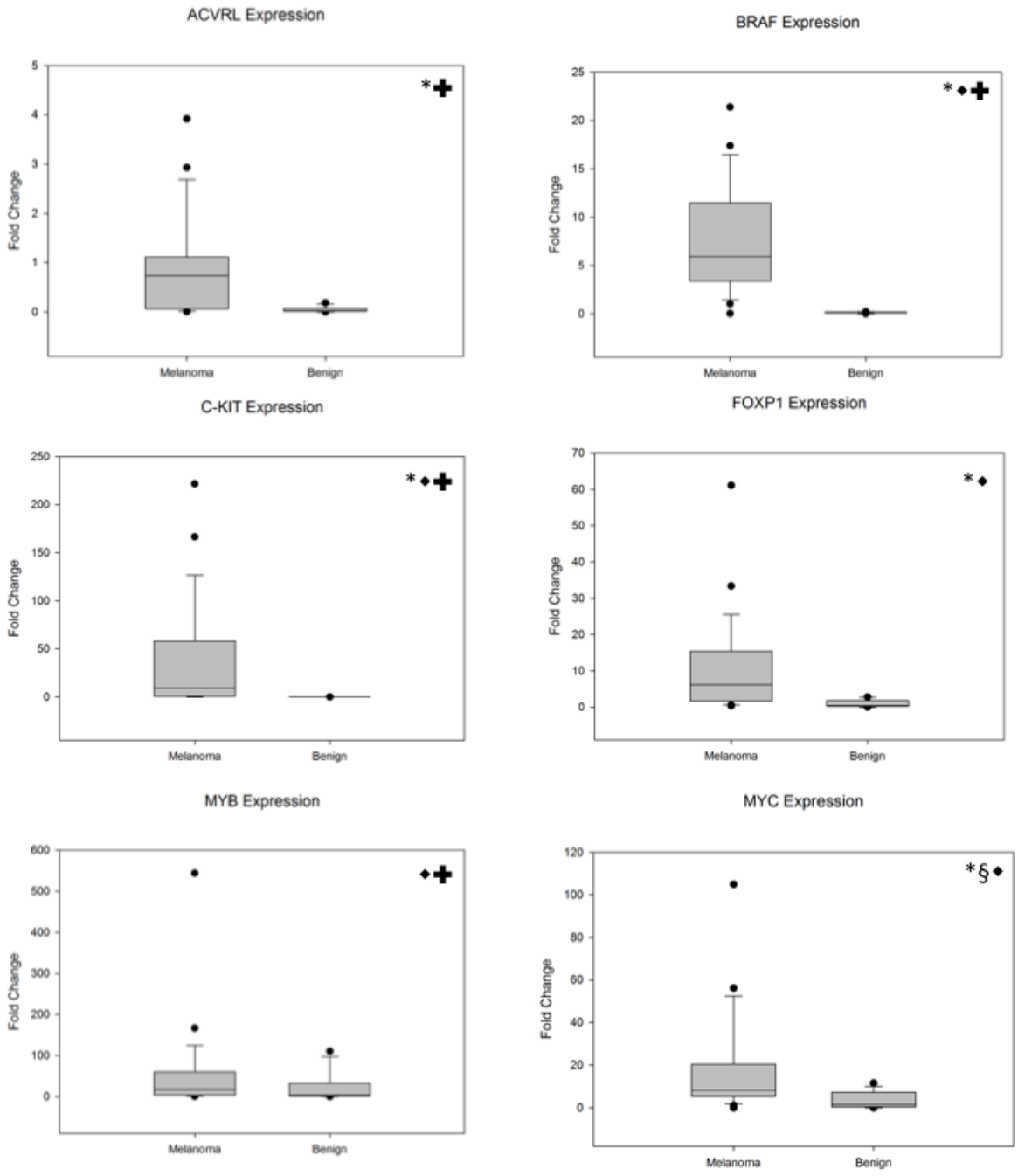
ACVRL Expression
Fold Change
Melanoma
Benign
BRAF Expression
C-KIT Expression
FOXP1 Expression
MYB Expression
MYC Expression

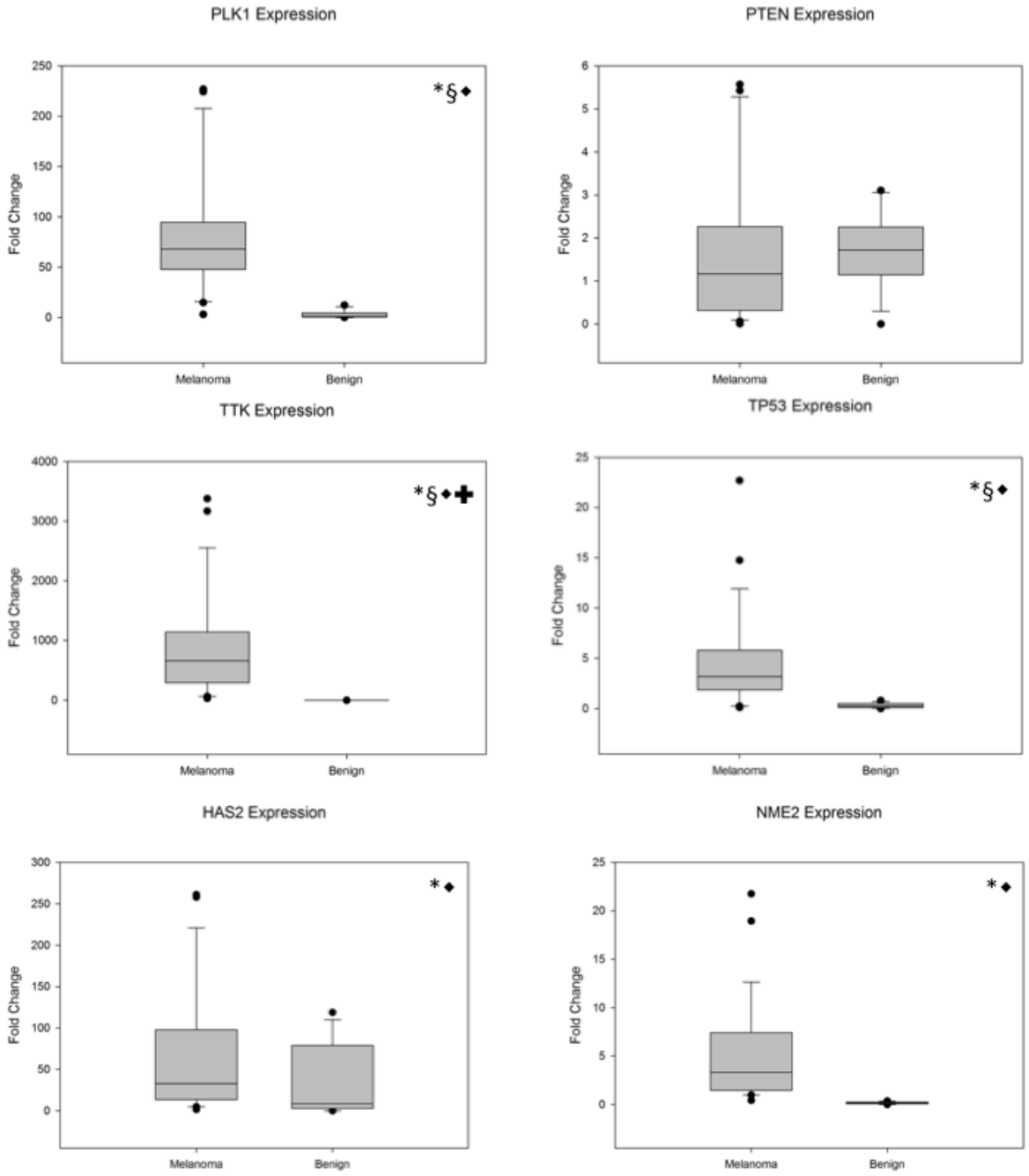
PLK1 Expression
Fold Change
250
200
150
100
50
0
*§◆
Melanoma
Benign
PTEN Expression
Fold Change
6
5
4
3
2
1
0
Melanoma
Benign
TTK Expression
Fold Change
4000
3000
2000
1000
0
*§◆✚
Melanoma
Benign
TP53 Expression
Fold Change
25
20
15
10
5
0
*§◆
Melanoma
Benign
HAS2 Expression
Fold Change
300
250
200
150
100
50
0
*◆
Melanoma
Benign
NME2 Expression
Fold Change
25
20
15
10
5
0
*◆
Melanoma
Benign

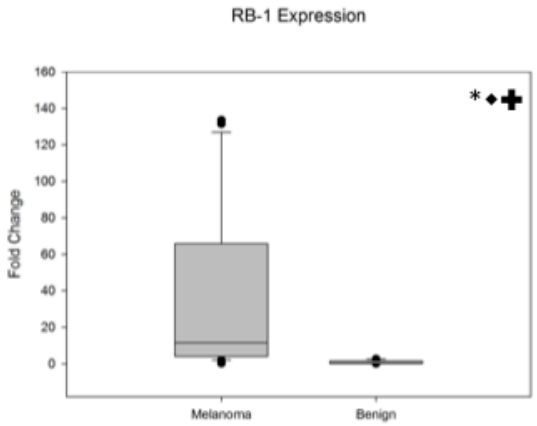
RB-1 Expression
Fold Change
160
140
120
100
80
60
40
20
0
Melanoma
Benign

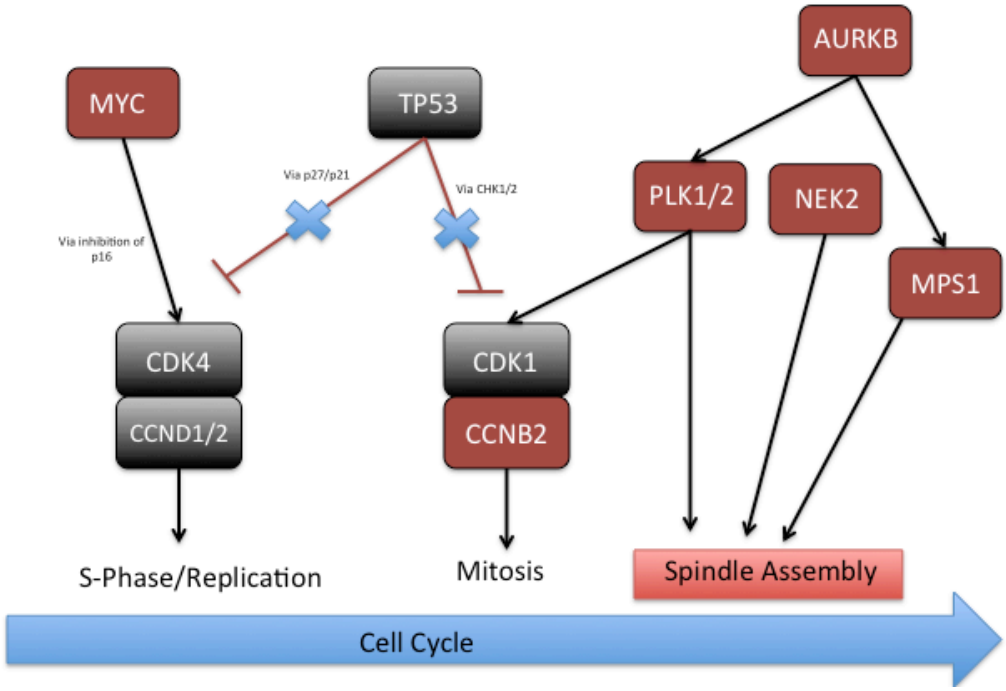

Figure 3.7 Schematic of altered spindle assembly checkpoint pathway in canine oral melanoma. Schematic of the dysregulated genes and their associated pathways involved in tumorigenesis and melanoma development. Genes labeled in red were identified to be overexpressed; genes labeled in black showed no gene expression change.

Table 3.1 Description of canine oral melanoma cell lines

Cell Line	Source	Reference
CL1	Lung Met	Koenig et al, Vet Pathol. 2001 Jul;38(4):427-35
CL2	Primary	Bianco et al, Cancer Gene Ther. 2003 Sep;10(9):726-36
CL3	Primary	Koenig et al, Vet Pathol. 2001 Jul;38(4):427-35
CL4	Primary	Koenig et al, Vet Pathol. 2001 Jul;38(4):427-35
CL5	Primary	Koenig et al, Vet Pathol. 2001 Jul;38(4):427-35
CL6	Primary	Bianco et al, Cancer Gene Ther. 2003 Sep;10(9):726-36

Table 3.2 Primer sequences for RT-qPCR of thirteen genes.

Gene	Forward	Reverse
RPS5	GGG AAA TGG AGC ACT GAT GA	GGC AGG TAC TTG GCA TAC TT
TP53	ACC ATG AAC GCT GCT CTG	TGT TTC TGT CGT CCA GGT ACT
TTK (MPS1)	TGT GGC AGA TTC CAG AGG TTT CTC	GTG CTG ATA TTG GTG GTG ACT GCT
FOXP1	TCA AGT GGC AAG ACA GCT TCT CCT	AAC CTG AAG GGC TGG TTG TTT GTC
HAS2	ATT CCT GGA TCT CCT TCC TCA GCA	CAC TAA TGC ACT GGA CAC ACC CAA
NME2	AGG GAC TGA ATG TGG TGA AGA CAG	ACG AAT GGT GCC TGG CTT AGA ATC
C-MYC	AGG AGA ATG ACA AGA GGC GAA CAC	ATC TGA TCA CGC AGG GCA AAG AAG
MYB	ACA GTG CAC CTG TTT CCT GTT TGG	TTT CTT CAG GTA GGG AGC CAG GAT
ACVRL1	AGG ACT ACA GGC CAC CCT TCT ATG A	TCT GCT GAT CAA CAC ACA CCA CCT
PTEN	CAA TCC TCA GTT TGT GGT CTG CCA	ATG AAC TTG TCT TCC CGT CGT GTG
PLK1	TCT ACA ATG ATG GTG ACA GCC TGC	TTC ATC AGG GAG TTG GGA TGG GAA
KIT	TTA CCA GGT GGC CAA GGG TAT G	GTG ATT CGA CCA TGA GTA AGG AGG
BRAF	GCC AAG TCA ATC ATC CAC AGA GAC CT	ATG GGA CCC ACT CCA TCG AGA TTT
RB-1	GGT CTT CAT GCA GAG ACT GAA A	TTG TAA GGG CTT CGA GGA ATG

Table 3.3 Sequencing primers for targeted regions evaluated in canine oral melanoma.

Gene	Forward	Reverse
BRAF	GCC AAG TCA ATC ATC CAC AGA GAC CT	ATG GGA CCC ACT CCA TCG AGA TTT
TP53 set 1	AGG AGT CGC AGT CAG AGC TCA ATA	GTA CTT GGC CCG CAA ATT TCC TTC
TP53 set 2	ACC ATG AAC GCT GCT CTG ACA GTA	GTC TGA GTC AAG CCC TTC TCT CTT

Table 3.4 Aberrations with at least 60% penetrance in canine oral melanoma cell lines (n=6).

Region	Region Length	Cytoband Location	Event	Genes	miRNAs	Frequency %
chr5:81,157,085-81,406,580	249495	q35	CN Gain	0	0	66.6666667
chr6:48,589,778-49,420,729	830951	q23.1	CN Loss	0	0	66.6666667
chr7:43,935,432-44,838,743	903311	q17	CN Gain	40	1	66.6666667
chr7:45,182,304-45,579,782	397478	q17	CN Gain	31	1	66.6666667
chr9:3,008,950-4,015,642	1006692	q11.1 - q11.2	CN Gain	48	1	66.6666667
chr9:5,846,054-6,006,856	160802	q11.2	CN Gain	10	0	66.6666667
chr9:7,499,638-7,557,894	58256	q11.2	CN Gain	4	0	66.6666667
chr9:16,568,017-16,697,850	129833	q13	CN Gain	1	0	66.6666667
chr9:20,973,038-21,556,711	583673	q14	CN Gain	8	0	66.6666667
chr9:21,568,246-21,849,710	281464	q14 - q21.1	CN Gain	11	0	66.6666667
chr9:22,358,307-22,523,259	164952	q21.1	CN Gain	9	0	66.6666667
chr9:24,037,751-24,074,035	36284	q21.2	CN Gain	4	0	66.6666667
chr9:25,565,335-25,665,672	100337	q21.3	CN Gain	3	0	66.6666667
chr9:26,120,084-26,175,919	55835	q21.3	CN Gain	5	0	66.6666667
chr9:26,991,881-27,199,655	207774	q21.3	CN Gain	4	0	66.6666667
chr9:29,229,550-29,534,218	304668	q21.3	CN Gain	8	0	66.6666667
chr9:29,699,355-29,901,928	202573	q21.3	CN Gain	8	0	66.6666667
chr9:51,763,258-52,502,238	738980	q25	CN Gain	53	1	66.6666667
chr9:52,865,266-53,052,041	186775	q25	CN Gain	9	0	66.6666667
chr9:53,793,547-53,944,034	150487	q25	CN Gain	1	0	66.6666667
chr9:57,494,161-58,018,330	524169	q26.1	CN Gain	11	0	66.6666667
chr9:58,575,617-58,916,870	341253	q26.1	CN Gain	15	1	66.6666667
chr10:11,943,170-12,169,632	226462	q13	CN Gain	1	0	66.6666667
chr10:12,966,821-13,191,394	224573	q13	CN Gain	1	0	66.6666667
chr10:13,449,360-15,234,834	1785474	q14	CN Gain	18	0	66.6666667
chr10:43,664,456-43,946,153	281697	q21	CN Gain	5	0	66.6666667
chr10:44,175,114-44,356,327	181213	q21	CN Gain	1	0	66.6666667
chr10:48,093,179-48,444,921	351742	q21	CN Gain	11	0	66.6666667
chr10:48,818,794-48,931,217	112423	q21	CN Gain	2	0	66.6666667
chr10:51,999,417-53,515,998	1516581	q21	CN Gain	15	0	66.6666667
chr11:18,636,602-18,779,997	143395	q12.3	CN Gain	2	0	66.6666667
chr11:44,144,370-44,355,744	211374	q16	CN Loss	4	0	66.6666667
chr11:55,204,045-55,275,213	71168	q21	CN Gain	7	0	66.6666667
chr11:70,554,899-70,677,121	122222	q22.2	CN Gain	5	0	66.6666667
chr11:76,547,833-76,922,651	374818	q23	CN Gain	4	0	66.6666667

Table 3.4 cont.

Region	Region Length	Cytoband Location	Event	Genes	miRNAs	Frequency %
chr13:3,033,844-4,310,612	1276768	q11	CN Gain	11	0	66.6666667
chr13:5,240,212-11,227,149	5986937	q11 - q12.1	CN Gain	35	0	66.6666667
chr13:11,234,869-66,000,000	54765131	q12.1 - q22.2	CN Gain	331	3	66.6666667
chr19:23,045,304-23,266,348	221044	q21	CN Loss	0	0	66.6666667
chr20:5,205,254-5,303,298	98044	q11	CN Gain	1	0	66.6666667
chr20:5,681,252-5,788,459	107207	q11	CN Gain	1	0	66.6666667
chr20:7,468,784-7,605,556	136772	q11	CN Gain	1	0	66.6666667
chr20:42,058,697-42,199,207	140510	q15.3	CN Gain	5	0	66.6666667
chr20:43,456,298-43,503,487	47189	q15.3	CN Gain	3	0	66.6666667
chr22:3,056,579-25,858,121	22801542	q11.1 - q12.3	CN Loss	100	3	66.6666667
chr22:27,166,005-27,240,067	74062	q12.3	CN Loss	1	0	66.6666667
chr22:27,508,525-29,318,089	1809564	q12.3 - q21	CN Loss	1	0	66.6666667
chr22:29,647,998-36,110,412	6462414	q21 - q22	CN Loss	24	0	66.6666667
chr22:37,393,336-40,629,550	3236214	q22	CN Loss	3	0	66.6666667
chr22:40,698,530-56,485,785	15787255	q22 - q24	CN Loss	53	6	66.6666667
chr22:60,136,837-60,492,853	356016	q24	CN Loss	1	0	66.6666667
chr23:23,552,949-23,759,722	206773	q21.1	CN Gain	0	0	100
chr26:30,235,074-30,306,343	71269	q24	CN Gain	2	0	66.6666667
chr26:30,450,246-30,634,182	183936	q24	CN Gain	2	0	66.6666667
chr26:32,807,362-33,695,808	888446	q24	CN Gain	27	0	66.6666667
chr30:6,948,946-7,353,963	405017	q12	CN Loss	1	0	66.6666667
chr30:18,265,504-22,459,196	4193692	q14.1 - q14.2	CN Gain	37	0	66.6666667
chr36:7,019,065-7,080,681	61616	q12	CN Gain	0	0	66.6666667
chrX:74,807,177-75,308,693	501516	q21.3	CN Loss	0	0	66.6666667

Table 3.5 Significant genome-wide DNA copy number aberrations using GISTIC in canine oral melanoma cell lines (n=6).

Region	Extended Region	Type	Q-Bound	G-Score	% of CNV Overlap
chr10:13,870,848-15,192,139	chr10:10,401,327-15,552,957	CN Gain	6.27E-07	10.439489	0
chr10:4,760,299-5,022,687	chr10:3,431,462-5,919,335	CN Gain	0.00335177	6.72610056	0
chr26:30,235,074-30,241,704	chr26:30,235,074-30,241,704	CN Gain	9.67E-05	8.25553225	0
chr30:19,196,241-19,743,852	chr30:18,265,504-22,754,532	CN Gain	6.79E-07	10.2916239	0
chr9:44,805,758-44,910,444	chr9:44,797,898-46,124,377	CN Loss	0.03529703	6.60130572	0
chr11:44,241,313-44,299,261	chr11:44,144,370-44,355,744	CN Loss	4.46E-06	14.0387858	0
chr22:19,881,874-20,109,996	chr22:3,056,579-57,967,908	CN Loss	0.00569807	7.74065723	0
chr26:40,924,095-40,940,186	chr26:40,886,045-42,000,000	CN Loss	4.89E-05	12.4663035	0
chrX:74,942,593-75,297,878	chrX:74,807,177-75,308,693	CN Loss	5.09E-05	12.220865	0

Table 3.6 Chromosome regions with differential CN aberrations between canine oral melanoma cell lines (CL) and primary canine oral melanomas (OM).

Region	Cytoband	Event	Region Length	CL %	% OM	Difference	Probe p-value	Max p-value	q-bound
chr9:20,973,038-21,029,083	q14	CN Gain	56045	100	38.6363636	61.3636364	0.232414265	0.00635258	0.696089
chr9:21,042,128-21,086,878	q14	CN Gain	44750	100	38.6363636	61.3636364	0.031444365	0.00635258	0.696089
chr11:44,241,313-44,299,261	q16	CN Loss	57948	83.3333333	22.3037739	60.6060606	1.02E-07	0.00692921	1
chr13:5,458,646-5,505,233	q11	CN Gain	46587	83.3333333	22.7272727	60.6060606	0.001758395	0.00692921	0.696089
chr13:25,027,519-25,045,996	q13	CN Gain	18477	83.3333333	22.7272727	60.6060606	0.006766649	0.00692921	0.696089
chr13:37,141,917-37,235,115	q21.1	CN Gain	93198	83.3333333	20.4545455	62.8787879	0.002504572	0.00472446	0.696089
chr13:38,601,954-38,615,905	q21.1	CN Gain	13951	83.3333333	22.7272727	60.6060606	0.126166168	0.00692921	0.696089
chr13:38,646,106-40,792,374	q21.1	CN Gain	2146268	89.9677021	17.9708367	60.6060606	0	0.00692921	0.696089
chr13:40,899,665-40,952,804	q21.1	CN Gain	53139	83.3333333	22.7272727	60.6060606	0.004758627	0.00692921	0.696089
chr13:41,245,851-41,369,635	q21.2	CN Gain	123784	83.3333333	22.7272727	60.6060606	5.06E-04	0.00692921	0.696089
chr13:45,545,184-45,930,547	q21.3	CN Gain	385363	83.3333333	22.7272727	60.6060606	3.38E-10	0.00692921	0.696089
chr13:46,831,629-48,134,810	q21.3	CN Gain	1303181	100	29.6908767	63.6363636	0	0.00469539	0.696089
chr13:48,813,041-49,937,985	q21.3	CN Gain	1124944	100	28.5988781	65.9090909	0	0.00341483	0.637531
chr13:50,486,696-51,878,689	q21.3	CN Gain	1391993	100	30.4898346	68.1818182	0	0.00243916	0.537348
chr13:62,803,526-63,397,107	q22.2	CN Gain	593581	100	27.8556339	70.4545455	4.31E-14	0.00170741	0.537348
chr13:64,220,772-64,798,997	q22.2	CN Gain	578225	100	31.0465688	65.9090909	1.08E-13	0.00341483	0.637531
chr13:65,094,165-65,152,260	q22.2	CN Gain	58095	100	30.6312936	68.1818182	9.94E-06	0.00243916	0.537348
chr13:65,497,490-65,689,697	q22.2	CN Gain	192207	100	30.3928482	68.1818182	3.92E-05	0.00243916	0.537348
chr13:65,730,802-66,000,000	q22.2	CN Gain	269198	100	36.3812983	61.3636364	4.77E-08	0.00635258	0.696089
chr26:30,235,074-30,241,704	q24	CN Gain	6630	83.3333333	13.6363636	69.6969697	1	0.00116294	0.537348
chr26:30,467,463-30,527,983	q24	CN Gain	60520	83.3333333	22.7272727	60.6060606	0.060867723	0.00692921	0.696089

CHAPTER IV

Investigation into the Mechanism of Chemotherapeutic Resistance in Canine Oral Melanomas

4.1 Abstract

Canine oral melanoma is an almost uniformly fatal disease of dogs and is typically resistant to a wide range of chemotherapeutics. While drug resistance is partially responsible for low survival rates, studies suggest that some patients do respond to and benefit from chemotherapeutics. Identifying which patients will respond to treatment is essential for both choosing an effective course of treatment and determining an accurate prognosis. In humans, it has been well established that the ATP-binding cassette transporters (ABC protein family) are responsible for one mechanism of chemotherapeutic resistance; however, the mechanism of chemotherapeutic resistance and the role of ABC proteins has yet to be elucidated in the dog. We hypothesized tumors that demonstrate resistance to chemotherapeutics doxorubicin and mitoxantrone, substrates of the ABC transporters, would highly express efflux pumps in the ABC protein family, specifically *ABCB1* and *ABCG2*.

To test our hypothesis, canine oral melanoma cell lines (n=6) were treated with doxorubicin and mitoxantrone for 72 hours, and then measured for cell viability and metabolic activity via an MTT-like colorimetric metabolic assay. Gene expression of *ABCB1* and *ABCG2*, export pumps specific for doxorubicin and mitoxantrone, respectively, was measured using RT-qPCR. Results showed a direct association between expression of cellular drug pumps *ABCB1* and *ABCG2* and resistance to chemotherapeutic agents ($p= 0.008$ and $p= 0.0029$, respectively). Expression of *ABCC1*, a multi-drug resistance efflux

pump, demonstrated no significant difference with either doxorubicin or mitoxantrone resistant cells ($p= 0.34$ and $p= 0.27$, respectively). Our results suggest these drugs are being regulated through specific drug pumps, and not through a generalized efflux pathway. These data indicate that cellular chemoresistance to doxorubicin and mitoxantrone can be predicted through monitoring expression of *ABCB1* and *ABCG2*, respectively. These findings suggest a direct clinical application in targeting effective treatments to individual patients most likely to respond, avoiding unnecessary courses of chemotherapy in patients with predicted resistance.

4.2 Introduction

Canine oral melanoma is the most common tumor of the oral cavity and is highly aggressive, with over 90% of these tumors being malignant. The average life expectancy post-diagnosis is on average 12 months (Bergman 2007). Treatments include surgical excision and radiation, but not chemotherapy, due to the frequency of chemotherapeutic resistance (Bergman 2010). Overall response rate to carboplatin for dogs with malignant melanoma was 28% (Rassnick, Ruslander, and Cotter 2001). A similar response rate of 18% was observed for treatment with cisplatin and piroxicam (Boria, Murry, and Bennett 2004). Limited responses have also been observed to melphalan, DITC, mitoxantrone, and doxorubicin (Bergman 2007). However, such drugs have shown to be effective in producing either total or partial response in other canine neoplasia.

Mitoxantrone is primarily used to treat canine lymphoma (Lucroy *et al.* 1998) and transitional cell carcinoma (Henry *et al.* 2003) and also been used in the treatment of mammary adenocarcinoma, squamous cell carcinoma, renal adenocarcinoma, fibroid sarcoma, thyroid carcinoma, and hemangiopericytoma. However, the same study showed that dogs with malignant melanomas showed limited response (n=1/12) to single-agent mitoxantrone treatment (Ogilvie *et al.* 1991). Doxorubicin is used most often in the treatment of B- and T-cell lymphoma (Price *et al.* 1991) and certain types of sarcomas (Ogilvie *et al.* 1989). Doxorubicin has been shown to provide limited benefit in the treatment of canine oral melanoma. The effectiveness of chemotherapeutic drugs in other cancers suggests a mechanism of chemotherapeutic resistance present in canine oral melanomas yet to be identified.

The ATP-binding cassette (ABC) family of proteins transports numerous molecules across the cell membrane. Members of the ABC protein family have been indicated in many disease processes and have also been identified as providing a major mechanism of resistance to chemotoxic agents (Schinkel and Jonker 2003). Forty-eight ABC transporters have been identified in humans, of which at least eight are capable of transporting cytostatic drugs and being involved in multi-drug resistances. ABC proteins can be located on either the basolateral or apical surface of polarized cells (Figure 4.1). The *ABCB1* gene encodes one of the most studied of these proteins p-glycoprotein (P-gp) also known as multi-drug resistance gene 1 (MDR1). P-gp has broad substrate specificity and has been noted for decreased drug accumulation in multidrug-resistant cells and often mediates the development of resistance to anticancer drugs, notably doxorubicin (Aller *et al.* 2009).

Breast cancer resistance protein (BCRP) is encoded by the gene *ABCG2*. Like P-gp, BCRP aids in multi-drug resistance to chemotherapeutic agents, especially mitoxantrone and camptothecin analogues (Doyle and Ross 2003). BCRP has been shown to be overexpressed in different cancer types (Ejendal and Hrycyna), and cells overexpressing BCRP are more resistant to mitoxantrone than cells with P-gp-mediated multidrug resistance (Litman *et al.* 2000). BCRP has also been investigated for its potential role in regulating stem cell differentiation. The *ABCC1* gene encodes the first member of the multi-drug resistance protein family (MRP1). MRP1 has a much wider function in mammalian cells including multispecific organic anion transporter for conjugates of steroid hormones and bile salts and for cell detoxification (Schinkel and Jonker 2003). MRP1 has also been implicated in chemoresistance of a broad range of cytotoxic drugs (Munoz *et al.* 2007). While these

proteins have been shown to be integral to the chemoresistance pathway of many cancers, their role in canine cancers has yet to be fully elucidated.

We hypothesize that tumors demonstrating resistance to the clinically relevant chemotherapeutics doxorubicin and mitoxantrone will overexpress efflux pumps in the ABC protein family, encoded by *ABCB1*, *ABCG2,* and *ABCC1.* The goal of this study was to characterize the resistance phenotype of seven canine oral melanoma cell lines, determine the expression level of *ABCB1*, *ABCG2,* and *ABCC1,* and correlate resistance phenotype to drug pump expression.

4.3 Materials and Methods

4.3.1 Cell Lines and Primary Tumors

Malignant oral melanomas comprising the tumor cohort of this study have been previously described (primary tumor samples in Chapter II and cell lines in Chapter II). Cells were cultured in Dulbecco's Modified Eagle Medium (Mediatech Inc., Manassas, VA, USA) supplemented with 10% v/v heat-inactivated FBS (Mediatech Inc., Manassas, VA, USA) and 100ug/ml Primocin Antibiotic (InvivoGen, San Diego, CA, USA) in a humidified atmosphere containing 5% CO_2 at 37°C. Cells were grown in T75 flasks with 0.2μM filtered lids until they reached 95% confluence, then harvested for RNA extraction. All cell lines were grown as a monolayer and were maintained by passage for no greater than eight passages after reestablishment.

4.3.2 Cellular Chemotherapeutic Phenotyping

Sensitivity to 96 total chemotherapeutic agents was established using Biolog Mammalian Chemotherapy Screening Plates (according to manufacturer's recommendation, Biolog Inc., Hayward, CA, USA). Briefly, cells were washed in Dulbecco's PBS (Mediatech Inc., Manassas, VA, USA) and resuspended in 50µl of Biolog IF-M1 RPMI 1640 supplemented with 1.1mL/100mL penicillin/streptomycin (Life Technologies, Grand Island, NY, USA), 0.3mM GlutaMAX (Life Technologies, Grand Island, NY, USA) and 5% v/v heat-inactivated FBS (Mediatech Inc., Manassas, VA, USA) at a density of $4X10^4$/mL. Cells were then plated into 96-well culture plates (20,000 cells per well) that contained lyophilized chemotherapeutic chemical (Biolog Panel PM-M11-PM-M14) and incubated at 37°C for 72 hours. After 72 hours, 10µl of Biolog's tetrazolium based Redox Dye Mix MA (6X) (proprietary formula, Biolog Inc.) was added to each well and plates were incubated in the OmniLog Plate Reader (Biolog Inc., Hayward, CA, USA) for 24 hours and 37°C. The measure of cellular activity was determined by the ability of cells to reduce the dye to insoluble formazan, producing a purple color. Color density was measured at 562nm. Color changes were recorded by the Omnilog system at 15-minute intervals. Images of both color density and metabolic curve outputs are shown in Figure 4.2. Sensitivity was determined if >2/4 wells showed decreased color intensity.

4.3.3 mRNA Extraction

Total RNA was extracted from cell lines using the RNeasy Plus Kit (according to manufacturer's recommendations, Qiagen, Germantown, MD, USA) and assessed for quality

and quantity by spectrophotometry. Total mRNA was extracted from FFPE samples using the E.Z.N.A.® FFPE RNA Kit (according to manufacturer's recommendations, Omega Bio-Tek Norcross, GA, USA). RNA integrity of all samples was assessed using the BioAnalyzer 2100 and RNA 6000 Nano Kit (according to manufacturer's recommendations, Agilent, Santa Clara, CA, USA).

4.3.4 Gene Expression Analysis via RT-qPCR

Total RNA was converted to cDNA using the VILO SuperScript Reverse Transcriptase (according to manufacturer's recommendation, Invitrogen, Life Technologies Corporation, Carlsbad, CA, USA). Location and sequence of each gene were selected based on their genome position indicated for the canine genome build CanFam2 in the UCSC canine genome browser (http://genome.ucsc.edu). Primers were then selected with the aid of PrimerQuest software (Integrated DNA Technologies). Primer sequences are listed in Table 4.1.

RT-qPCR was performed using SYBR green chemistry, KAPA SYBR® FAST qPCR Kit, with annealing temperatures optimized for the specific primer set (according to manufacturer's recommendation, Kapa Biosystems, Wilmington, MA, USA) using the AB OneStep Plus (Applied Biosystems, Life Technologies Corporation, Carlsbad, CA, USA). Cycling conditions were performed as per manufacturer's recommendations for the KAPA SYBR® FAST qPCR Kit. A melt curve as performed for each RT-qPCR reaction. A reference gene for $\Delta\Delta CT$ calculations was chosen based on the smallest standard deviation across all samples. Relative mRNA levels of individual gene expression were then

calculated, where Δ*CT* normalization is difference in the threshold PCR cycle (Ct) value of target gene and the corresponding control (*RPS5*) in each reaction. These values were compared with the average Ct value from non-neoplastic oral mucosa from normal canines (n=4).

Expression changes away from normal were determined by calculating the average variation in Ct between the four normal individuals across all target genes. Fold change values outside the normal range, greater than 3 or less than 0.3, were considered not normal. Difference in fold change between mitoxantrone and doxorubicin resistant and sensitive cell lines for *ABCG2*, *ABCB1*, and *ABCC1* was analyzed for statistical significance using a one-tailed non-parametric Mann-Whitney U test. For primary oral melanomas, expression of each gene was correlated to the mitotic index using a non-parametric Spearman's Rank Sum analysis.

4.3.5 Sequencing Analysis

Mutation screening of *ABCG2* was performed using targeted Sanger sequencing of total mRNA, converted to cDNA. Briefly, cDNA was produced from total RNA as described above. Location and sequence of each gene were selected based on their genome position indicated for the canine genome build CanFam2 in the UCSC canine genome browser (http://genome.ucsc.edu). Primers were then selected with the aid of PrimerQuest software (Integrated DNA Technologies). Amplicons were created using a high fidelity polymerase, KAPA HiFi HotStart ReadyMix, with annealing temperatures optimized for the specific primer set (according to manufacturer's recommendations, Kapa Biosystems, Wilmington,

MA, USA). Cycling conditions were performed as per manufacturer's recommendations for the KAPA HiFi HotStart ReadyMix. Amplicons were then assessed for purity using gel electrophoresis and purified to remove non-annealed primers and unamplified cDNA using a GeneJet PCR Clean Up Kit (according to manufacture's recommendations, Thermo Fisher Scientific In, Waltham, MA, USA). Primer sequences are listed in Table 4.2.

4.4 Results

4.4.1 Phenotyping of Cell Lines

Cell lines were determined to be either resistant or sensitive to mitoxantrone and doxorubicin (Figure 4.2). Two of six cell lines showed resistance only to doxorubicin; two cell lines showed resistance to both doxorubicin and mitoxantrone. The remaining two cell lines showed to be sensitive to both mitoxantrone and doxorubicin.

4.4.2 Gene Expression of ABCB1, ABCG2, and ABCC1

Gene expression was upregulated for both *ABCG2* and *ABCB1* (Figure 4.3). For *ABCG2,* the mean fold change with cells with mitoxantrone resistance was 4.01, where sensitive cells had a mean fold change of 0.556. The mean fold change of *ABCG2* with cells resistant to doxorubicin was 2.13, where doxorubicin sensitive cells had a mean fold change of 0.501. For *ABCB1,* the mean fold change with cells with doxorubicin resistance was 15.72, where sensitive cells had a mean fold change of 1.92. The mean fold change of *ABCB1* with cells with mitoxantrone resistance was 20.61, where sensitive cells had a mean fold change of 3.84. No gene expression change was seen for *ABCC1*. The mean fold

change for mitoxantrone resistant and sensitive cells was 2.01 and 1.66, respectively; doxorubicin resistant and sensitive cells had a mean fold change of 2.03 and 2.99, respectively.

Gene expression of all three drug pumps was also analyzed in primary oral melanomas (n=17) using RT-qPCR (Figure 4.4). *ABCB1* had a bimodal distribution; 52.9% (9/17) of primary cases had a fold change of greater than three, 35.2% (6/17) had a fold change less than 0.3, and only 11.7% (2/17) of cases were within the range of normal expression. *ABCG2* had a more normal expression with an average fold change of 3.47. Within primary cases, 47.1% (8/17) had a fold change of *ABCG2* greater than 3.0; however, the average fold change in samples with increased expression was 5.65. No cases showed a loss of expression of *ABCG2*. *ABCC1* was also mostly normally expressed, with just 17.6% (3/17) of primary cases having a fold change greater than 3.0, and 5.88% (1/17) of cases having a fold change less than 0.3. For the primary cases no gene was correlated to mitotic index; *ABCB1* (p= 0.29), *ABCG2* (p= 0.088), *ABCC1* (p= 0.056). Unfortunately, treatment or survival data was not available for these cases.

4.4.3 Association of Gene Expression to Drug Resistance Phenotype

Resistance to doxorubicin and mitoxantrone was associated with expression of specific drug pumps *ABCB1* and *ABCG2*, respectively (p= 0.0081, p= 0.0029) (Figure 4.5). Resistance to doxorubicin was not associated with *ABCG2* overexpression (p= 0.34). Association of *ABCB1* to mitoxantrone resistance was significant (p= 0.015), though weaker than *ABCB1* to doxorubicin resistance. This is most likely caused by the resistance of two

cell lines to both agents along with corresponding gene overexpression. Additionally, resistance to these drugs is not through a generalized efflux pathway mediated by *ABCC1,* as over expression was not associated to resistance to doxorubicin or mitoxantrone (p= 0.27, p= 0.32, respectively).

4.4.4 Sequencing of ABCG2

Previous studies (Honjo et al, 2001) showed wild type (WT) *ABCG2* was an effective exporter of mitoxantrone, but not doxorubicin. However, cells with an *ABCG2* activating mutation were able to exclude both mitoxantrone and doxorubicin. As our data did not see concurrent exclusion of both drugs in our cell lines, we performed sequencing analysis to confirm WT status of the gene. Wild type sequence was detected in all six cell lines (Figure 4.6).

4.5 Discussion

Chemotherapy is one of the most effective cancer treatments available. Unfortunately, due to molecular defense mechanisms, many cancer cells evade the cytotoxic effects of chemotherapeutic agents. Understanding of the mechanism of resistance can help researchers develop more effective treatments. In this study, we investigated the role of specific drug pumps as a mechanism of chemoresistance in canine oral melanoma through the use of cell lines representative of the primary disease (Chapter III, Figure 3.1). When screened with various chemotherapeutic agents, canine melanoma cell lines showed variable resistance to both doxorubicin and mitoxantrone, traditional intercalating topoisomerase II

inhibitors used for cancer treatments. One of the most studied mechanisms of chemoresistance is altered expression of drug transports, such as *ABCG2*, *ABCB1*, and *ABCC1*.

When expression of *ABCG2*, *ABCB1*, and *ABCC1* was measured by RT-qPCR, overexpression was observed within cases for both *ABCG2* and *ABCB1,* not *ABCC1.* Based on the pattern of chemoresistance and overexpression within our cell lines, we hypothesized overexpression of *ABCG2* and *ABCB1* would be associated with resistances to mitoxantrone and doxorubicin. Statistical analyses confirmed our hypothesis that resistance to doxorubicin and mitoxantrone was positively associated with expression of specific drug pumps *ABCB1* and *ABCG2,* respectively. However, these drugs can also be exported through other pumps so expression of a third, more generalized pump, *ABCC1*, was also evaluated. It was determined that resistance to these drugs was not through a generalized efflux pathway, mediated by *ABCC1*, as resistant phenotypes to either drug did not associate with *ABCC1* overexpression. All six canine oral melanoma cell lines also have wild type sequence for *ABCG2*. This suggests that in canine melanomas, mutations to *ABCG2* are not common, allowing tumors overexpressing *ABCG2* to be resistant only to mitoxantrone. Such data further supports that resistance to each therapeutic is mediated specifically through a single drug pump.

There was no correlation of mitotic index of the primary tumor to expression of any drug pump, suggesting tumor proliferation is not correlated with drug pump expression and therefore treatment resistance. This may represent two separate mechanisms of tumor aggression; those that rapidly divide and metastasize and those that are resistant to treatment.

Due to the fact that these two characteristics are not correlated to each other, it provides a rationale for screening all oral melanomas, regardless of size, and identifying those most likely to respond to chemotherapeutic treatments. In the clinical setting, this could provide options for small tumors, which are identified as resistant to chemotherapeutics, not to receive additional chemotherapeutic treatments but to be managed locally with large surgical margins and radiation therapy. Alternately, large tumors, which may not be able to be fully excised due to their size, identified as sensitive could be treated with chemotherapeutics to manage distant micrometastases in addition to radiation therapy for local tumor control. However, an important follow-up critical for validation and further clinical application is correlation of *in vivo* treatment response to gene expression.

The establishment of a pattern of chemotherapy resistance has direct benefit to clinical patients. This knowledge can lead to the development of assays that can identify patients who may respond positively to chemotherapeutics. Treatment assays could also be translated into human medicine, as others have shown the dog to be a suitable preclinical model for therapeutics (Fukumoto *et al.* 2013). Understanding the mechanism of resistance can also lead to the development of better therapeutics that are not substrates for overexpressed drug pumps. While these drugs pumps are among most studied, they are only two members of a large family of proteins. There are several other pumps that can effectively export both mitoxantrone and doxorubicin from cells. Before a functional assay could be developed, other members of the ABC family of pumps must also be evaluated and directly correlated to chemoresistance.

While mRNA expression is a fast and quantitative way to monitor gene expression, it does not validate the actual biological processes responsible for exportation. For example, CL3 was sensitive to mitoxantrone, despite the fact there was a slight overexpression of *ABCG2*. This suggests that BCRP protein in this cell line may not be expressed, properly located within the cell membrane, or fully functional. To assess the functionality of these pumps within canine melanomas cell lines, small molecule inhibitors can be utilized. Numerous small molecules have already been developed, such as GF120918, which inhibit both MDR1 and BCRP (Hyafil *et al.* 1993). GF120918, also known as Elacridar, is a potent inhibitor and has been tested *in vitro* and *in vivo* in mouse, rat, dog, and monkey (Ward and Azzarano 2004). A measure of the ability of such an inhibitor to rescue susceptibility within these lines could have a direct impact on the treatment of veterinary patients resistant to chemotherapeutics. Studies evaluating the increased bio-availability of numerous agents with concurrent administration of Elacridar have been performed and showed significantly higher levels of target drug when MDR1 and BCRP have been inhibited (Durmus *et al.* 2012; Chuan Tang *et al.* 2014).

While several studies have used MDCK (immortalized canine kidney) cells as a tool for *in vitro* models of inhibition efficacy, few directed studies had been performed into the inhibition of ABC proteins specifically in veterinary medicine (Mealey, Northrup, and Bentjen 2003; Griffin *et al.* 2005). One study observed a tyrosine kinase inhibitor (masitinib) prevented P-gp function and was able to reverse doxorubicin resistance in an *in vitro* model of canine lymphoma (Zandvliet *et al.* 2013). Use of ABC inhibitors to increase chemotherapeutic efficacy has a potential for rapid translation to a clinical setting, as

masitinib is conditionally licensed for veterinary use in the treatment of canine mast cell tumors. However, as veterinary oncology has not yet developed a commonly accepted chemotherapy regime for the treatment of canine oral melanoma, it is difficult to fully suggest the role of MDR1 and BCRP in multi-drug resistance in canine melanoma patients.

These findings also have a much broader impact to veterinary medicine beyond the treatment of oral melanoma. While there is extensive investigation into inhibition of MDR1 and BCRP human medicine, little had been performed in veterinary medicine. However, these drug pumps are expressed in numerous canine cancers and limit the activity on both generalized and targeted therapeutics. There is also no known assay to screen individuals for resistance to current chemotherapeutic agents. A simple screening assay could provide crucial information to clinicians when deciding how best to treat a particular patient. Such an assay could also be used in validation of the efficacy of new drugs that may be a substrate for these pumps, by limited trials to patients who do not overexpress them. This information could provide treatments to patients who would benefit the most, while sparing patients who would not receive any clinical benefit the cytotoxic effects of such agents.

Acknowledgements

I would like to thank Dr. Luke Borst for access to reagents, equipment, and for help with data analysis.

REFERENCES

Aller, S. G., Yu, J., Ward, A.*, et al.* (2009). "Structure of P-glycoprotein reveals a molecular basis for poly-specific drug binding." Science **323**(5922): 1718-1722.

Bergman, P. (2007). "Canine Oral Melanoma." Clinical Techniques in Small Animal Practice **22**(2): 55-60.

Bergman, P. J. (2010). "Cancer Immunotherapy." Veterinary Clinics of North America: Small Animal Practice **40**(3): 507-518.

Boria, P., Murry, D. and Bennett, P. (2004). "Evaluation of cisplatin combined with piroxicam for the treatment of oral malignant melanoma and oral squamous cell carcinoma in dogs." J Am Vet Med Assoc **224**(3): 288-294.

Chuan Tang, S., Nguyen, L., Sparidans, R.*, et al.* (2014). "Increased oral availability and brain accumulation of the ALK inhibitor crizotinib by coadministration of the P-glycoprotein (ABCB1) and breast cancer resistance protein (ABCG2) inhibitor elacridar." Int J Cancer **134**(6): 1484-1494.

Doyle, L. and Ross, D. D. (2003). "Multidrug resistance mediated by the breast cancer resistance protein BCRP (ABCG2)." Oncogene **22**(47): 7340-7358.

Durmus, S., Sparidans, R., Wagenaar, E.*, et al.* (2012). "Oral availability and brain penetration of the B-RAFV600E inhibitor vemurafenib can be enhanced by the P-GLYCOprotein (ABCB1) and breast cancer resistance protein (ABCG2) inhibitor elacridar." Mol Pharm **9**(11): 3236-3245.

Ejendal, K. and Hrycyna, C. (2002). "Multidrug Resistance and Cancer: The Role of the Human ABC Transporter ABCG2." Current Protein and Peptide Science **3**(5): 503-511.

Fukumoto, S., Hanazono, K., Fu, D.*, et al.* (2013). "A new treatment for human malignant melanoma targeting L-type amino acid transporter 1 (LAT1): a pilot study in a canine model." Biochem Biophys Res Commun **439**(1): 103-108.

Griffin, J., Fletcher, N., Clemence, R.*, et al.* (2005). "Selamectin is a potent substrate and inhibitor of human and canine P-glycoprotein." J. Vet. Pharmacol. Therap **28**(257-265).

Henry, C. J., McCaw, D. L., Turnquist, S. E.*, et al.* (2003). "Clinical Evaluation of Mitoxantrone and Piroxicam in a Canine Model of Human Invasive Urinary Bladder Carcinoma." Clin Cancer Res **9**: 906.

Hyafil, F., Vergely, C., Vignaud, P. D.*, et al.* (1993). "In vitro and in vivo reversal of multidrug resistance by GF120918, an acridonecarboxamide derivative." Cancer Res **53**(19).

Litman, T., Brangi, M., Hudson, E.*, et al.* (2000). "The multidrug-resistant phenotype associated with overexpression of the new ABC half-transporter, MXR (ABCG2)." Journal of Cell Science **113**: 2011-2021.

Lucroy, M., Phillips, B., Kraegel, S.*, et al.* (1998). "Evaluation of single-agent mitoxantrone as chemotherapy for relapsing canine lymphoma." J Vet Intern Med **12**(5): 325-329.

Mealey, K., Northrup, N. and Bentjen, S. (2003). "Increased toxicity of P-glycoprotein-substrate chemotherapeutic agents in a dog with the MDR1 deletion mutation associated with ivermectin sensitivity." Journal of the American Veterinary Medical Association **223**(10): 1453-1455.

Munoz, M., Henderson, M., Haber, M.*, et al.* (2007). "Role of the MRP1/ABCC1 multidrug transporter protein in cancer." IUBMB Life **59**(12): 752-757.

Ogilvie, G., Reynolds, H., Richardson, R.*, et al.* (1989). "Phase II evaluation of doxorubicin for treatment of various canine neoplasms." J Am Vet Med Assoc **195**(11): 1580-1583.

Ogilvie, G., Obradovich, J., Elmslie, R.*, et al.* (1991). "Efficacy of mitoxantrone against various neoplasms in dogs." J Am Vet Med Assoc **198**(9): 1618-1621.

Price, G., Page, R., Fischer, B.*, et al.* (1991). "Efficacy and toxicity of doxorubicin/ cyclophosphamide maintenance therapy in dogs with multicentric lymphosarcoma." J Vet Intern Med **5**(5): 259-262.

Rassnick, K., Ruslander, D. and Cotter, S. (2001). "Use of carboplatin for treatment of dogs with malignant melanoma: 27 cases (1989-2000)." J Am Vet Med Assoc **218**(9): 1444-1448.

Schinkel, A. H. and Jonker, J. W. (2003). "Mammalian drug efflux transporters of the ATP binding cassette (ABC) family: an overview." Advanced Drug Delivery Reviews **55**: 3-29.

Ward, K. and Azzarano, L. (2004). "Preclinical pharmacokinetic properties of the P-glycoprotein inhibitor GF120918A (HCl salt of GF120918, 9,10-dihydro-5-methoxy-9-oxo-N-[4-[2-(1,2,3,4-tetrahydro-6,7-dimethoxy-2-isoquinolinyl)ethyl]phenyl]-4-acridine-carboxamide) in the mouse, rat, dog, and monkey." Pharmacol Exp Ther **310**(2): 703-709.

Zandvliet, M., Teske, E., Chapuis, T.*, et al.* (2013). "Masitinib reverses doxorubicin resistance in canine lymphoid cells by inhibiting the function of P-glycoprotein." J Vet Pharmacol Ther **36**(6): 583-587.

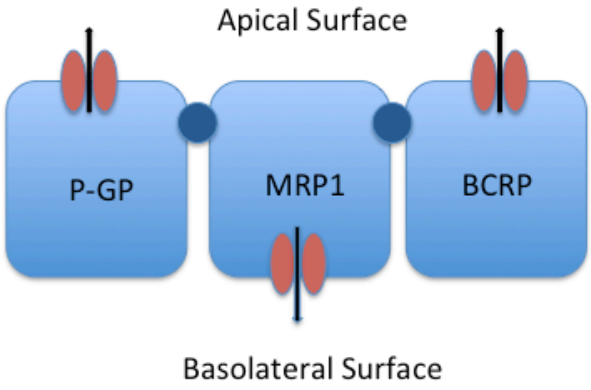

Figure 4.1. Schematic of ABC protein locations in polarized cells. P-gp, encoded by *ABCB1*, and BCRP, encoded by *ABCG2*, are both located on the apical surface of polarized cells. MRP1, encoded by *ABCC1*, is located on the basolateral surface.

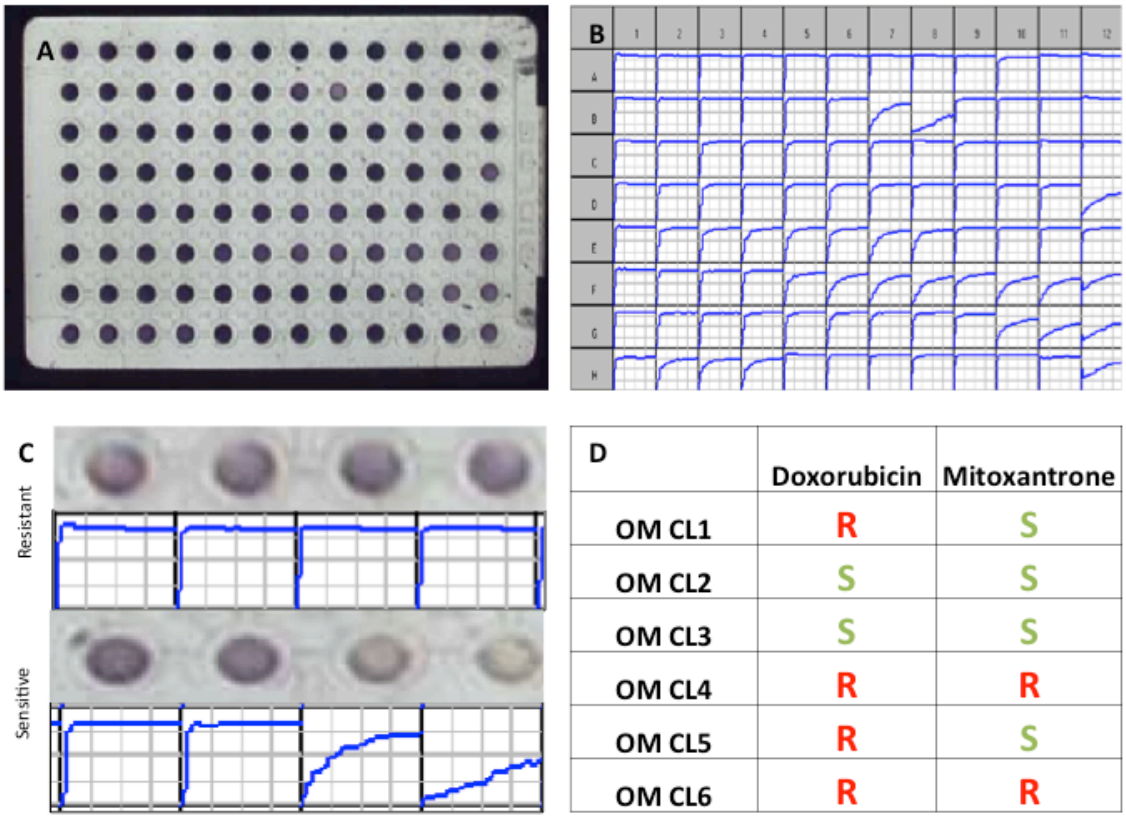

D	Doxorubicin	Mitoxantrone
OM CL1	R	S
OM CL2	S	S
OM CL3	S	S
OM CL4	R	R
OM CL5	R	S
OM CL6	R	R

Figure 4.2. Chemoresistant phenotyping of canine oral melanoma cell lines (n=6). (A) Image of 96-well chemoresistance plate with plated cells 24 hours after MTT dye was added. **(B)** Schematic of colorimetric conversion of the MTT dye over 24 hours. **(C)** Representation of chemoresistance phenotyping of canine oral melanoma cell lines. For each drug, four concentrations of drug were represented. Resistance was determined if two or more wells showed decreased color intensity. **(D)** Determination of chemoresistance phenotype for each of the six canine oral melanoma cell lines screened. Resistance to doxorubicin was found in n=4 cell lines, while resistance to mitoxantrone was found in n=2 cell lines.

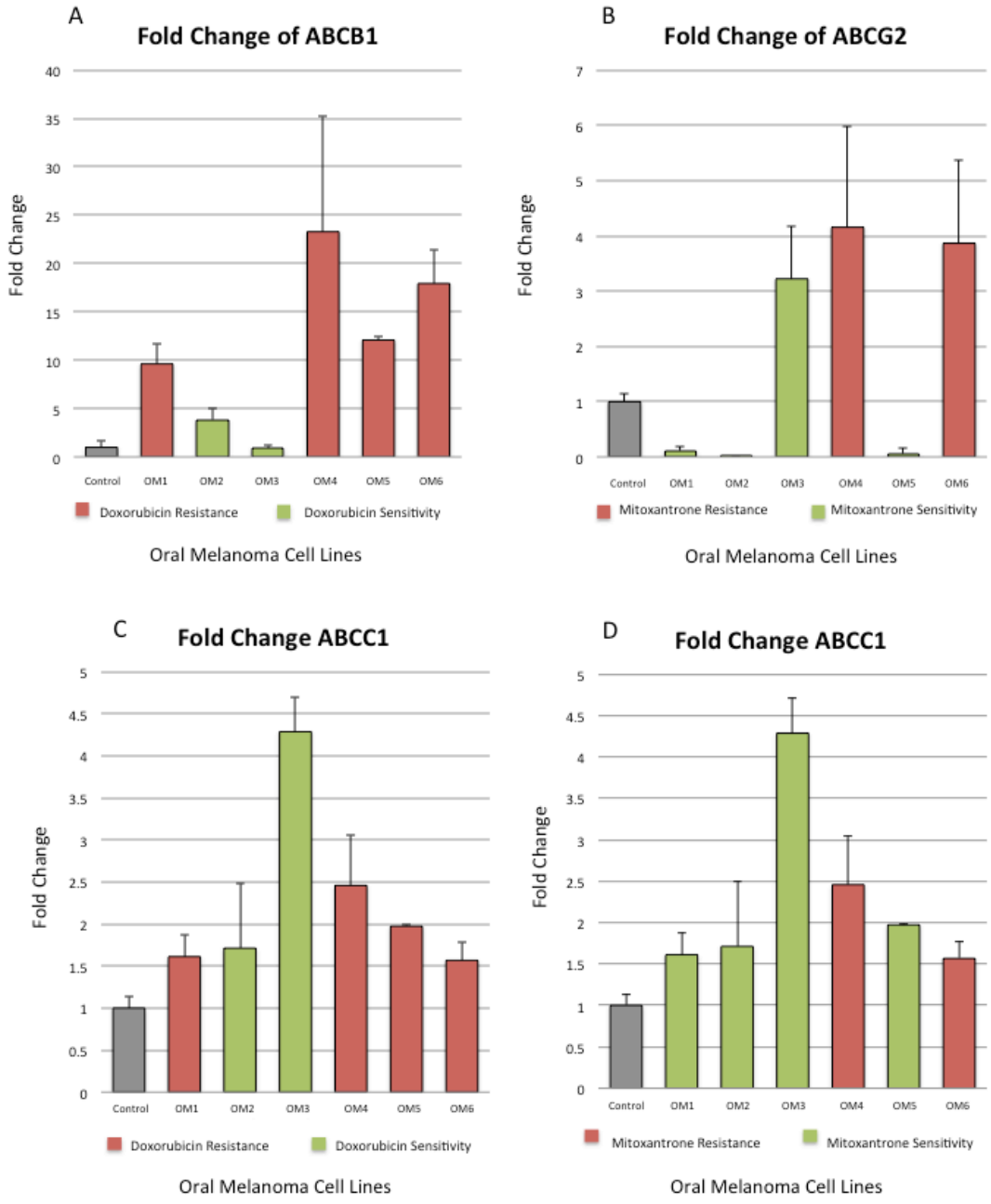

Figure 4.3. Gene expression changes of *ABC* genes in canine oral melanoma cell lines (n=6). Gene expression changes were plotted with cases on the x-axis and fold change on the y-axis. Chemoresistance phenotype was then coded in each graph with resistance colored in red and sensitivity colored in green. **(A)** Fold change of *ABCB1*, overexpression was seen in n=4. **(B)** Fold change of *ABCG2*, overexpression was seen in n=2. **(C and D)** Fold change of *ABCC1*, overexpression was seen in n=1.

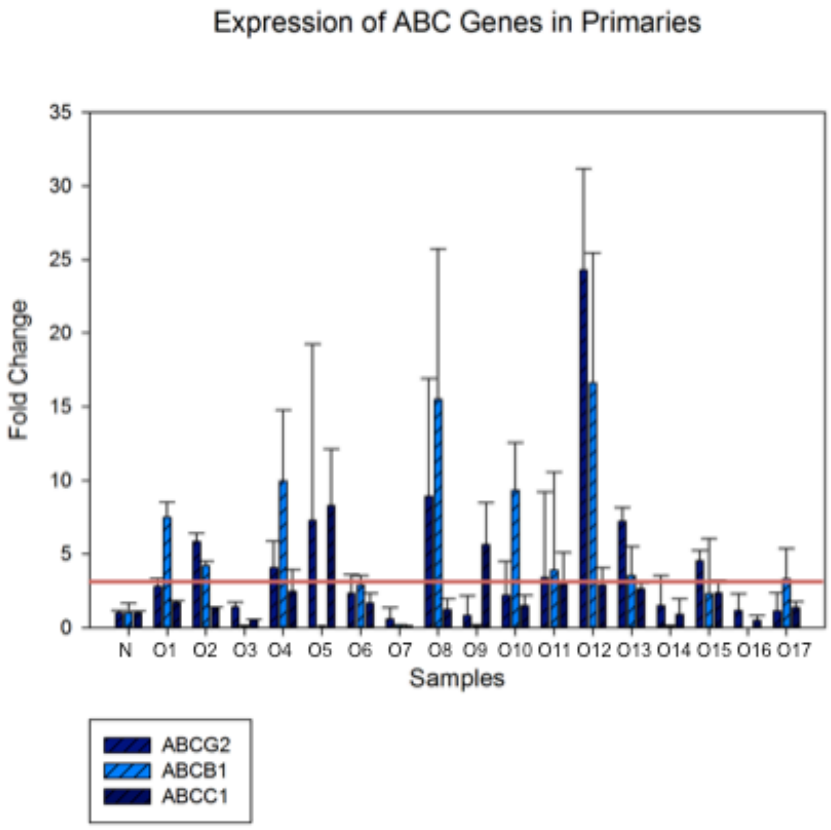

Figure 4.4. Gene expression changes of *ABC* genes in primary lesions of canine oral melanoma (n=17). Gene expression of *ABCG2*, *ABCB1*, and *ABCC1* was measured in 17 primary oral melanoma tumors (O1-17) by RT-qPCR. Expression was normalized using a ΔΔCT method using an average of four non-neoplastic oral mucosal tissues as a base line (N). Overexpression cutoff value is demarcated with a red line at y=3.0. Expression of all three genes was variable in primary tumors.

	ABCG2 Fold Change	*ABCB1* Fold Change	*ABCC1* Fold Change
Mito RvS	p=0.0029*	p=0.015*	p=0.32
Doxo RvS	p=0.34	p=0.008*	p=0.27

Figure 4.5 Correlation of chemoresistance to fold change of ABC genes. Mann-Whitney U test was performed to determine the significance of gene expression changes of *ABCG2*, *ABCB1*, and *ABCC1* between drug resistance phenotypes. Associations were found between overexpression of *ABCG2* and mitoxantrone resistance, and between overexpression of *ABCB1* and resistance to both mitoxantrone and doxorubicin and overexpression of *ABCB1*. However, there was a much stronger correlation of overexpression to doxorubicin resistance. Boxes indicated in red are those we hypothesized to be associated.

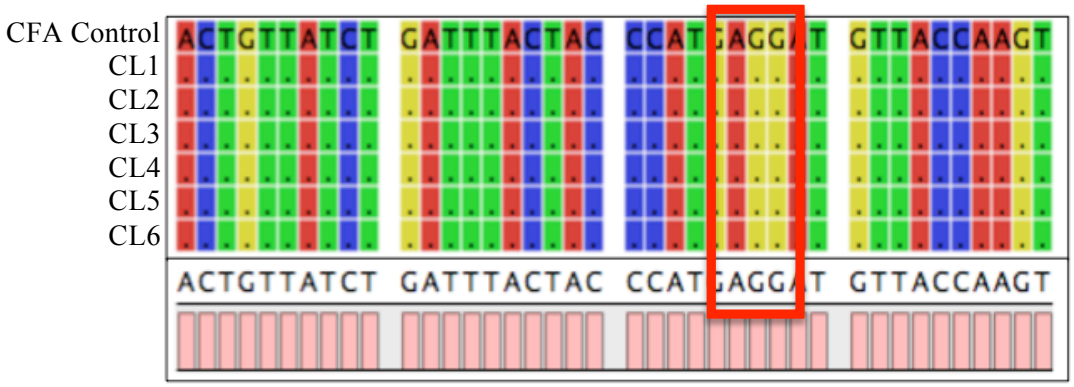

Figure 4.6. Sequence of *ABCG2* in canine oral melanoma cell lines (n=6). Canine *ABCG2* was sequenced using targeted Sanger sequencing. Wild type sequence was detected in all six cell lines at the base orthologous to the human mutation R482T. CFA control used is the dog genome reference (CanFam2).

Table 4.1 Sequence of RT-qPCR primers for ABC genes.

Gene	Forward	Reverse
ABCG2	ACC CTG CAG ACT TCT TCT TG	AAG GCT CTT CAG TCA CCT TG
ABCC1	CGG ACA GAG ATT GGT GAG AA	GAG GTA GAT GTC AGA GTC ACA G
ABCB1	GCT GTT AAG GAA GCC AAT GC	CTG TTT CTG TCC ACC ACT CA

Table 4.2 Sequencing primers for *ABCG2*.

Gene	Forward	Reverse
ABCG2	GTC ATC CTG GGA TTG GTT T	GGT AGG CAA TTG TAA GGA AG

SUMMARY AND FUTURE DIRECTIONS

Canine oral melanoma is a common and highly metastatic disease. There are limited treatment options, with a predicted survival time of only 12 months after diagnosis. Even though this disease affects nearly 50,000 dogs every year in the US, little was known about the cytogenomoics of canine oral melanomas prior to the completion of this study. Early cytogenetics studies observed irregular karyotypes, but no information has been added to the literature since that time. Similarly, little is known about the molecular changes that occur during tumorigenesis of mucosal melanomas in human patients. This is primarily due to the fact that mucosal melanoma is one of the least common subtypes of melanoma. With this type of melanoma only affecting 1,500 patients each year in the US, few efforts have been made to investigate the mechanisms underlying tumor development.

For both species, the main focus of previous studies was to establish if mucosal melanomas were similar at the molecular level to common cutaneous melanomas in humans. This is the most common type of melanoma, with 76,000 new diagnoses every year in the US, and significant research has been done to understand the causative changes that occur during tumor development and progression. While many of the genes identified are part of classic cancer pathways, few similarities have been found between cutaneous and mucosal melanomas. This is especially true in terms of activation mutations of cutaneous melanomas, such as the BRAF V600E point mutation. Along this line, a hallmark paper established differential copy number (CN) profiles between different subtypes of melanoma. This was the first time that melanomas were considered different diseases at the molecular level.

No such analysis had been performed on canine melanocytic lesions. Melanocytic lesions can arise from numerous locations in canines. Oral lesions are primarily considered to be malignant; however, histology of the mass can be ambiguous as melanomas of the oral cavity have a propensity to dedifferentiate and present with no pigmentation. Cutaneous lesions in the dog are almost always considered benign. Unlike with human cutaneous melanomas, benign melanocytomas in dogs rarely progress to a malignant phenotype. However, these two lesions were considered to be molecularly similar and to develop with the same underlying genetic changes. Analysis of the incidence of individual mutations could be key to quantifying the level of heterogeneity within melanocytic tumors and identifying those alterations with the greatest impact toward tumor development and ultimately biological behavior. Matching mutations with physical and histopathologic characteristics would also allow for development of targeted therapies and refinement of diagnostic capabilities.

To establish a baseline molecular genome-wide copy number profile of malignant oral melanomas, benign cutaneous melanocytomas, and malignant cutaneous melanomas, we performed oaCGH on a cohort of individuals. Targeted genes were also evaluated with FISH analysis. From this, we observed different genome-wide and targeted copy number changes present in canine oral and cutaneous melanocytic lesions. We found unique copy number aberrations only present in canine oral melanomas, which were not present in either cutaneous cohort or in any other tumor type previously analyzed. We also established a similarity in copy number profiles between canine cutaneous melanomas and benign

melanocytomas. This is suggestive that benign cutaneous lesions may develop into malignant melanomas, contrary to previous assumptions.

Comparison to published aCGH and targeted CN profiles of human melanomas was performed, demonstrating canine and human mucosal melanomas present with similar whole genome and targeted CN profiles. Additionally, mucosal melanomas in humans had a higher level of similarity to canine mucosal melanomas than to human cutaneous melanomas. This suggests that mucosal melanomas develop with a distinctive set of copy number alterations, possibly related to a common mechanism of disease.

We noted a suggestive pattern of chromosomal structural aberrations in our primary canine oral melanoma population via oaCGH. We then confirmed similar patterns of aberrations within an established population of canine oral melanoma cell lines. To validate chromosome aberrations, we assessed metaphase spreads from cell lines using FISH based analyses. Cell lines showed significant levels of structural chromosome aberrations; however, few were recurrent. This suggested a high level of chromosome instability, as was reported elsewhere in whole genome sequencing of human mucosal melanomas. To investigate and identify dysregulated genes involved in the mechanism of genomic instability, we performed whole transcriptome gene expression profiling (GEP) analysis on a population of canine cell lines (n=6) and primary tumors (n=7).

The GEP highlighted genes were identified from the mitotic check-point pathway, including *AURKB*, *TTK* (or MPS1), *PLK1*, and *NEK2*. This pathway has previously not been indicated in the pathogenesis of mucosal melanomas. We then selected an extended set of 13 candidate genes, comprising those highlighted by GEP analysis, supplemented with genes

involved in classical melanoma pathways. To evaluate if these gene expression changes were consistent across additional primary tumors, this set of 13 genes was analyzed by RT-qPCR to determine gene expression changes in a group of 31 canine melanocytic lesions (primary melanoma (n=17) and benign (n=14) tumors). Gene expression changes were consistent across the entire cohort of malignant tumors. The absence of involvement of classical cutaneous melanoma pathways, as previously demonstrated in other studies, was confirmed by mutational sequencing analysis in our subset of canine mucosal melanomas. Mutations were not found in *BRAF* and *TP53*, confirming the cases in our study were consistent with previous findings.

From these data, we identified an alternate pathway of tumorigenesis in mucosal melanomas. Unlike cutaneous melanomas, which rely on UV-induced point mutations to activate growth pathways and deactivated tumor suppressor genes, mucosal melanomas must rely on other mechanisms to activate and propagate tumorigenesis. We hypothesized a mechanism of tumor development initiated by mutations within cell cycle control that then lead to aberrations within the chromosome stability pathways. Chromosome instability then allows for additional structural aberrations that further alter cellular regulations and allows for uncontrolled proliferation of transformed cells. The proposed mechanism involves the abnormal cell cycle regulation, the dysregulation of mitotic division of chromosomes leading to atypical karyotypes, and the inhibition of apoptosis monitoring. By overexpression of key genes involved in mitotic progress, mucosal melanomas are able to bypass the DNA checkpoints that inhibit cellular proliferation. The ability of cells to proliferate with DNA

damage also allows for multiple minor clones to develop, leading to an increased possibility of resistance to traditional therapies.

One reason canine melanoma can be highly aggressive is that most tumors develop resistance to numerous chemotherapeutic agents. However, the mechanism(s) of resistance has/have yet to be fully elucidated. If an underlying mechanism could be identified, more effective therapeutics could be developed, as well as an assay to identify patients most likely to respond. To evaluate patterns of chemotherapeutic resistance in canine oral melanomas, six canine melanoma cell lines were screened for resistance to two common therapeutics, mitoxantrone and doxorubicin. Variable resistance was observed, which led to the investigation of the main mechanism of chemotherapeutic resistance, overexpression of efflux pumps. Three main members of the ATP-binding cassette drug pump family were evaluated for differential expression within the cell lines. Analysis of resistance compared to gene expression found a positive association of overexpression to cellular resistance.

It was observed that this association was specific to which drug pump was overexpressed in the cell lines. Mitoxantrone resistance was associated with *ABCG2* overexpression, while doxorubicin resistance was associated with overexpression of *ABCB1*. To ensure the resistance was not being mediated through an alternate mechanism, such as expression of a generalized efflux pump, expression of another ABC gene, *ABCC1*, was evaluated. Normal expression of *ABCC1* was observed in all cell lines and no association was found to either doxorubicin or mitoxantrone resistance. Previous studies showed a mutated form of *ABCG2* would be responsible for exportation of both mitoxantrone and doxorubicin. However, Sanger sequencing of the *ABCG2* genes in the six cell lines revealed

wild type *ABCG2*, suggesting a single mechanism of mitoxantrone and doxorubicin resistance. Based on these data, we propose a mechanism of chemotherapeutic resistance in canine oral melanoma using ABC drug pumps, such as *ABCG2* and *ABCB1*. Such information has direct clinical benefit that can be translated to evaluate patients most likely to respond to treatments and to develop more effective therapeutics.

While many of these conclusions have the potential for significant clinical applications, several steps must first be taken. One key follow-up to any gene expression study is the assessment of biological functionality of the changes observed. Several experimental methods evaluate gene functionality, including quantitative protein assessment, measurement of enzymatic activity, and, as previously mentioned, *in vitro* RNAi knockout or knockdown experiments. The need for functional validation spurs from the fact that an increased gene dosage may be representative of non-functional alleles or that heterozygous deletions do not directly affect the level of mRNA or protein being expressed. A dysregulation of gene function may also be caused downstream of gene expression, so normal copy number at the genetic level or mRNA at the gene expression level may inevitably show down-regulation of the protein. Validation of protein expression dysregulation would further support the involvement of a particular gene in formation of the malignant phenotype.

Another key factor needed before any clinical translation can be made is validation in a larger cohort, in terms of both additional primary cases and evaluation of more genes within identified pathways. For any assay, either copy number or gene expression, a significant number of cases must be evaluated with detailed clinical follow-up. Such clinical

follow-up allows for molecular changes to be correlated with epidemiological factors, outcome, and response to various treatments. With this information, the predictive nature of specific changes can be determined. Further investigation into additional genes within identified pathways, such as the spindle assembly complex, supports the contribution of these pathways and further elucidates the mechanism of tumorigenesis. Finally, investigation into potential drug targets identified by both CN and gene expression analysis, such as *TTK*, *PLK1* and *TRPM7*, must be tested using *in vitro* and *in vivo* methods. Testing of the effectiveness of targeted drug inhibitors not only evaluates the biological effect of inhibition on tumor cells as possible *in vivo* treatments, but act also as validation of the involvement of the genes in tumor viability.

There must also be investigation into other cellular mechanisms that may be involved in developing the observed phenotypes. There are several mechanisms, in addition to those discussed previously, which may be responsible for both genetic instability and chemotherapeutic resistance. Another mechanism that leads to genetic instability is telomeric crisis, which occurs in aging and damaged cells. Telomere crisis has also been shown to be key in the survival of DNA-damaged cell in several cancer types, but has not been investigated in canine oral melanoma. Chemoresistance to doxorubicin and mitoxantrone in canine oral melanoma may also be due to the mechanism of action of these agents and the cellular response to such action. Doxorubicin and mitoxantrone are intercalating agents, which act to inhibit topoisomerase II, causing double stranded breaks and eventually stalling mitosis. Overexpression of the genes that regulate mitotic DNA

damage repair, shown in our canine oral melanoma cases, may allow canine mucosal melanomas cells to bypass the DNA damage caused by topoisomerase II inhibition.

The onset of molecular medicine can increase knowledge into the underlying mechanism of disease and give insights into the specific changes that mark the development and progression of cancers. The applications of such knowledge are vast. Understanding early changes can increase the efficacy of diagnostic markers used in early detection screens. Discovery of mutations unique to malignant melanomas could help expedite diagnostic processes. Correlation of malignancy to alterations of key genes can be used as predictive markers for more accurate prognosis and allows for local invasiveness and metastatic propensity to be quantitatively assessed. Understanding key pathways involved can also lead to the development of therapeutics beyond merely palliative care to curative treatments. Comparative genomic studies, such as the one described here that incorporates the full range of traditional cytogenetics, gene expression changes, and correlation of dysregulation to treatment response, can aid predictive, targeted, and personalized medicine for the benefit of both man and dog.

APPENDICES

APPENDIX I

Evaluation of Expression of *TRPM7* Located Within a Region of Significant Copy Number Gain

AI.1 Abstract

The gene *TRPM7* has been indicated in the proliferation and migration of melanocytes and melanoma cells. The genome region encoding for *TRPM7* was highly amplified in canine oral melanomas. To investigate if this amplification had an effect on gene expression, RT-qPCR of the *TRPM7* gene was performed. Non-parametric correlation analysis was then performed to assess gene expression association to DNA amplification and tumor proliferation. Overexpression of *TRPM7* was observed in 73% of cases with an average fold change of 33.12. DNA copy number of *TRPM7* was not correlated with mitotic index ($p= 0.157$). However, *TRPM7* expression was correlated with both copy number and mitotic index ($p= 0.000109$ and $p= 0.0437$, respectively), suggesting that copy number can affect the overall expression of *TRPM7* in canine oral melanomas. This also suggests a role of *TRPM7* in melanoma development or propagation, as *TRPM7* has previously been shown to have two major roles in the cell: detoxifying melanin production intermediaries and aiding in cell migration. In conclusion, we suggest *TRPM7* may be a novel gene involved in canine oral melanoma and may be a target for gene inhibition therapy.

AI.2 Introduction

There is much discussion on the role of chromosomal aneuploidy in tumorigenesis and progression (Weaver and Cleveland 2009). The ability of chromosomal copy number changes to affect gene expression primarily relies on access to gene regions on which transcription can occur (Spivey *et al.* 2012). Previous investigations into correlation of copy number changes and gene expression in melanoma suggest a limited relationship, with genomic imbalances detectable by aCGH contributing to only 25% of the transcriptional changes observed (Sabatino *et al.* 2008). However, the direct relationship between alterations in gene copy number and respective gene expression remains unclear.

Members of the transient receptor potential cation channel, subfamily M (TRPM) are non-selective cation channels involved in numerous cellular processes, including control of Mg^{2+} homoeostasis, cell proliferation, and cell death (Fleig and Penner 2004). TRPM, member 7 (*TRPM7*), is a fusion protein with an ion transport domain and an enzymatically active COOH-terminal alpha-kinase, which acts as an atypical serine/threonine kinase (Drennan and Ryazanov 2004). *TRPM7* functions primarily as an ion channel that mediates calcium entry into the cell; however, it has also been observed that TRPM7 regulates cell migration, which is reliant on the activity of the regulatory kinase domain (Guilbert *et al.* 2013). *TRPM7* has recently emerged as a key player in embryonic development, global ischemia, cardiovascular disease, and cancer (Fleig and Chubanov 2014). New experimental evidence indicates that altered expression of *TRPM7* is frequently observed in cancer cells, adenocarcinomas and breast cancer, and correlates with cell proliferation and migration (Rybarczyk *et al.* 2012; Guilbert *et al.* 2013; Meng *et al.* 2013; Trapani *et al.* 2013). It has

also recently emerged as a key regulator of melanocytes and melanoma development, specifically as a detoxifier of melanin synthesis intermediates in both normal melanocytes and melanoma cells (Guo, Carlson, and Slominski 2012).

TRPM7 is found on canine chromosome CFA 30:19465566 to 19579841 (CanFam2, UCSC, http://genome.ucsc.edu). Previous studies (Chapter II) found this region of CFA 30 to be highly amplified; therefore, we hypothesized that *TRPM7*, located within this region of DNA amplification, will show a correlated level of gene amplification. The goal of this study was to evaluate the impact of DNA amplification of CFA 30: 19465566 to 19579841 on tumor proliferation and gene expression of *TRPM7*, and if gene expression had an impact on either tumor proliferation or pigmentation status.

AI.3 Materials and Methods

AI.3.1 Tumor Population and Proliferation Status

Malignant oral melanoma tumor cohorts have been previously described: primary tumor samples (Chapter II) and cell lines (Chapter III). DNA and RNA extraction have been previously described: Chapter II, section 2.3.2 and Chapter III, section 3.3.6. Proliferation status was determined by evaluation of mitotic index, which was taken by counting total mitotic figures present in 10 consecutive, non-overlapping, 40X fields. Pigmentation was calculated as a percent of tumor with visible melanin granules present.

AI.3.2 Copy Number of CFA 30: 19465566-19579841

Copy number for the genomic region of CFA 30 at basepair location 19465566 to 19579841 was determined via Agilent 4X180K oligo-CGH array as previously described (Chapter II, section 2.3.4). Log_2 ratios were extracted using Agilent Feature Extraction software and then reverse-calculated to determine the predicted copy number for the region in each case. Mitotic index was then correlated to copy number using a non-parametric Spearman's Rank Sum to assess association of amplification of this gene region with tumor proliferation.

AI.3.3 Gene Expression of TRPM7 via RT-qPCR

Total RNA was converted to cDNA using the VILO SuperScript Reverse Transcriptase according to manufacturer's recommendation (Invitrogen, Life Technologies Corporation, Carlsbad, CA, USA). Location and sequence of *TRPM7* were selected based on their genome position indicated for the canine genome build CanFam2 in the UCSC canine genome browser (http://genome.ucsc.edu). Primers were then selected using the aid of the PrimerQuest software (Integrated DNA Technologies). Primer sequences are listed in Table AI.1. RT-qPCR was performed using SYBR green chemistry (KAPA SYBR FAST qPCR Kit, Kapa Biosystems, Wilmington, MA, USA) on cDNA using the AB OneStep Plus (Applied Biosystems, Life Technologies Corporation, Carlsbad, CA, USA). Reference gene for $\Delta\Delta CT$ calculations was chosen based on the smallest standard deviation across all samples. Relative mRNA levels of individual gene expression were then calculated, where ΔCT normalization is the difference in the threshold PCR cycle (Ct) value of target gene and

the corresponding control (*RPS5*) in each reaction. These values were compared with mRNA from non-neoplastic oral mucosa from normal canines (n=4). Normal variation within individuals was determined by calculating the average variation in Ct values between the four normal individuals across all target genes. For tumor samples, a fold change threshold of > 3 or < 0.3 was considered outside normal range and therefore dysregulated.

Copy number was first correlated against gene expression changes using linear regression; however, due to the non-normal distribution of data points, a linear regression was inconclusive. Copy number was then correlated against gene expression using a non-parametric Spearman's Rank Sum analysis. Mitotic index was also correlated with gene expression using a non-parametric Spearman's Rank Sum analysis to assess if expression of this gene was associated with proliferation, one of the best indicators of tumor aggression. Percent pigmentation was also correlated with gene expression using a non-parametric Spearman's Rank Sum analysis.

AI.4 Results

AI.4.1 Copy Number of CFA 30: 16465566-16579841

Copy number within the region of CFA 30 at 19.5Mb was variable across cases. The average copy number across the cohort was 6.8, with the maximum being 28.5. When copy number of this region was correlated to mitotic index, no significant correlation was found ($p= 0.157$).

AI.4.2 Gene Expression Changes of TRPM7 in Canine Oral Melanomas

Gene expression changes were variable across the cohort. Overall, cases presented with an overexpression of *TRPM7* in 73% of cases (n=17/23). The average fold change was 33.12 with a maximum fold change of 120.41. However, the tumor with the highest fold change did not have the highest amplification of this region. Linear regression modeling (Figure AI.1) found no direct correlation of fold change to DNA amplification (R^2= 0.26). This was most likely to do the fact the data were not normally distributed. However, when a non-parametric analysis was performed via Spearman's Rank Sum, significant correlation was observed (p= 0.000109). Gene expression was then correlated with proliferation status via mitotic index, which was also significantly correlated (p= 0.0437). Gene expression was not correlated with pigmentation (p= 0.322).

AI.5 Discussion

Previous studies have shown the power of copy number aberration as a method of dysregulation of gene-loci expression (Ortiz-Estevez *et al.* 2011). Expression of *TRPM7* showed a strong positive correlation to copy number data, suggesting that copy number may have an affect on the overall expression of *TRPM7* in canine oral melanomas. However, amplification of this gene region alone may not necessarily be a causative effect on canine melanoma tumor growth, as DNA copy number gain was not correlated with tumor proliferation. One study that investigated the role of *TRMP7* expression in adenocarcinomas found overexpression had a more dramatic effect on cell migration and not cell proliferation (Rybarczyk *et al.* 2012). This is in concordance with our data that suggests that while

TRPM7 is overexpressed in aggressive melanoma cells, it is only weakly correlated with proliferation. This suggests that *TRPM7* overexpression may play a role in tumor growth; however, only partially regulated through amplification of the loci-encoding region. However, overexpression of *TRPM7* can lead to many other positive effects on melanoma tumor aggression, without effecting cell proliferation.

Studies in cultured cells implicate *TRPM7* in regulation of cell growth, spreading, and survival. In a study investigating double knockouts of *TRPM7,* it was observed that melanophores experienced cell death via necrosis (McNeill *et al.* 2007), possibly through the inability of these cells to excrete the toxic byproducts of melanin synthesis. This suggests *TRPM7* may be critical in the propagation of melanoma cells that produce large amounts of melanin pigment. The same study also saw an inhibition of melanin synthesis largely prevented melanophore cell death in cells with no *TRPM7* expression. Therefore, melanomas without *TRPM7* expression may develop amelanotic histology as a way to prevent cell death due to build up of toxins during melanin synthesis. Therefore we hypothesized that tumors with low or no pigmentation would also be lacking *TRPM7.* However, we saw no correlation of gene expression to percent pigmentation. This suggests the toxic effects of large levels of melanin production may have little effect on aggressive melanomas, or that melanomas may find another mechanism(s) of detoxification, not mediated through *TRPM7*.

There is also evidence that *TRPM7* plays a significant role in cell differentiation, proliferation, and migration especially through the MAPK signaling pathway, a cascade shown to be key in melanoma development (Guo, Carlson, and Slominski 2012). In a study

investigating the concurrent action of *TRPM7* with MAPK, silencing of *TRPM7* in breast cancer cells resulted in a significant decrease in migration and invasion capability. The same study also observed that gene silencing resulted in decreased phosphorylation levels of Src protein and members of the MAPK cascade, suggesting *TRMP7* regulates migration and invasion of tumor cells (Meng *et al.* 2013), however this has not been investigated directly in melanoma cells that show an activation of the MAPK pathway. In conclusion, we suggest *TRPM7* may have a potential role in canine oral melanoma proliferation, acting in concordance with MAPK, and as a result may be a target for gene inhibition therapy.

REFERENCES

Drennan, D. and Ryazanov, A. G. (2004). "Alpha-kinases: analysis of the family and comparison with conventional protein kinases." Progress in Biophysics and Molecular Biology **85**(1): 1-32.

Fleig, A. and Penner, R. (2004). "The TRPM ion channel subfamily: molecular, biophysical and functional features." Trends Pharmacol Sci **25**(12): 633-639.

Fleig, A. and Chubanov, V. (2014). TRPM7. Mammalian Transient Receptor Potential (TRP) Cation Channels. B. Nilius and V. Flockerzi, Springer Berlin Heidelberg. **222:** 521-546.

Guilbert, A., Gautier, M., Dhennin-Duthille, I.*, et al.* (2013). "Transient receptor potential melastatin 7 is involved in oestrogen receptor-negative metastatic breast cancer cells migration through its kinase domain." Eur J Cancer **49**(17): 3694-3707.

Guo, H., Carlson, J. A. and Slominski, A. (2012). "Role of TRPM in melanocytes and melanoma." Experimental Dermatology **21**(9): 650-654.

McNeill, M. S., Paulsen, J., Bonde, G.*, et al.* (2007). "Cell death of melanophores in zebrafish trpm7 mutant embryos depends on melanin synthesis." J Invest Dermatol **127**(8): 2020-2030.

Meng, X., Cai, C., Wu, J.*, et al.* (2013). "TRPM7 mediates breast cancer cell migration and invasion through the MAPK pathway." Cancer Letters **333**(1): 96-102.

Ortiz-Estevez, M., De Las Rivas, J., Fontanillo, C.*, et al.* (2011). "Segmentation of genomic and transcriptomic microarrays data reveals major correlation between DNA copy number aberrations and gene-loci expression." Genomics **97**(2): 86-93.

Rybarczyk, P., Gautier, M., Hague, F.*, et al.* (2012). "Transient receptor potential melastatin-related 7 channel is overexpressed in human pancreatic ductal adenocarcinomas and regulates human pancreatic cancer cell migration." Int J Cancer **131**(6): E851-861.

Sabatino, M., Zhao, Y., Voiculescu, S.*, et al.* (2008). "Conservation of genetic alterations in recurrent melanoma supports the melanoma stem cell hypothesis." Cancer Res **68**(1): 122-131.

Spivey, T. L., De Giorgi, V., Zhao, Y.*, et al.* (2012). "The stable traits of melanoma genetics: an alternate approach to target discovery." BMC Genomics **13**(1): 156.

Trapani, V., Arduini, D., Cittadini, A.*, et al.* (2013). "From magnesium to magnesium transporters in cancer: TRPM7, a novel signature in tumour development." Magnes Res **26**(4): 149-155.

Weaver, B. and Cleveland, D. (2009). "The role of aneuploidy in promoting and suppressing tumors." J. Cell Biol. **185**(6): 935-937.

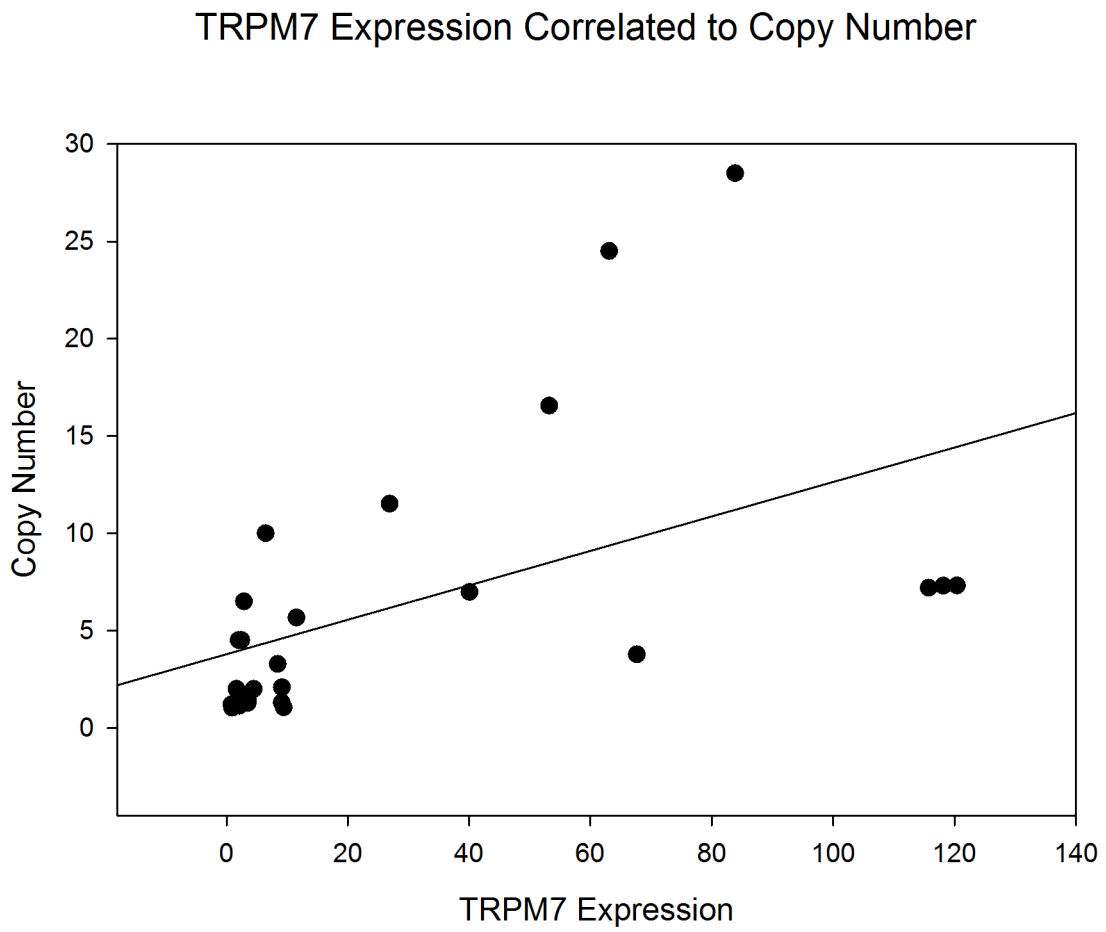

Figure AI.1 Linear correlation of copy number to gene expression of *TRPM7*. Copy number for the region containing *TRPM7* was derived from oaCGH data for primary canine oral melanomas (n=17) and canine oral melanoma cell lines (n=6). This was then correlated with RT-qPCR fold change expression of *TRPM7*. There was no linear correlation, r^2= 0.216.

Table AI.1 Primer sequences for *TRPM7* gene expression analysis.

Gene	Forward	Reverse
TRPM7	CGA AAT ACC TCT AGC AGC ACT C	CGA TAG GGC TGT GCT GTT T

APPENDIX II

Clinical and Cytogenetic Analysis of a Biologically Ambiguous Amelanotic Malignant Oral Melanoma in a Flat-Coated Retriever

AII.1 Abstract

A 10-year-old neutered Flat-Coated Retriever presented with a biologically and histologically ambiguous primary gingival neoplasm and corresponding distant metastases to the dorsal skin. Both primary neoplasm and metastases were diagnosed as amelanotic melanoma on cytology; however, histology and immunohistochemistry was inconclusive for melanoma. Cytogenetic analysis was performed to assist in tumor typing. Copy number analysis revealed oaCGH genome-wide aberration patterns similar to what has been established for canine oral malignant melanomas in both the primary and metastatic lesion. Our findings support a diagnosis of oral malignant melanoma and demonstrate the utility of molecular diagnostics for histologically ambiguous lesions in a clinical setting.

AII.2 Introduction

Melanoma is the most common tumor of the oral cavity in dogs (Bergman 2007), with over 80% of these tumors being malignant (Spangler and Kass 2006). Canine oral melanoma readily invades into normal tissue and bone and has a high metastatic propensity (Ramos-Vara *et al.* 2000; Koenig *et al.* 2002). These tumors are usually aggressive and respond poorly to standard treatments, with the average life-span post-diagnosis of a stage I tumor being only 12 months (Bergman 2007). Biological behavior of these tumors is highly variable. Diagnosis is confirmed using histopathology; however, melanoma tumor morphology can be variable and overlaps considerably with several other common tumors (Withrow, Vail, and Page 2013). Recent literature reviews highlight the difficulties surrounding the diagnosis and prognosis of melanoma (Spangler and Kass 2006; Smedley *et al.* 2011). Currently, the principal means of determining biological outcome of a melanocytic growth is by assessing a combination of physical characteristics like anatomical site, size, stage at time of diagnosis, and histological parameters, including nuclear atypia and mitotic figures among others (Bergman 2007). This leaves a great deal of variation in determination of differentiation and prognosis, leading to unreliable characteristics by which these tumors are assessed. Multiple authors (Bergman, Modiano, and Smedley) have commented on the need for alternate methods for determining deferential diagnosis of histologically ambiguous cases.

Genetic testing for novel chromosomal copy number aberrations has been used to improve the diagnostic and prognostic accuracy in human oncology (Bastian *et al.* 2003; Bauer and Bastian 2006; Bastian and Bauer 2007; Greshock *et al.* 2009; Lazar *et al.* 2009;

Vergier *et al.* 2011). Recent developments in molecular veterinary oncology have made it possible to characterize tumors based on copy number variations within genomic tumor DNA (Thomas *et al.* 2008). This allows researchers to analyze mutations across the entire genome of an individual and compare aberrations to those of a known population. In this report we apply oligo-array comparative genomic hybridization (oaCGH) to assist in the diagnosis of a primary and metastatic tumor with ambiguous morphology.

AII.3 Case History

A 10-year-old neutered Flat-Coated Retriever was presented to the University of Pennsylvania Ryan Veterinary Hospital (UPenn) for evaluation of a gingival mass. The 3cm in diameter mass was detected by the referring veterinarian on routine dental examination and was located on the right side of the hard palate (Figure AII.1). Patient history included a removal of a squamous cell carcinoma of the fifth right rear digit five months before presentation, and several subcutaneous small masses, which had persisted for six or seven months prior to initial presentation, but no history of melanoma. Thoracic radiographs were within normal limits. The gingival tumor was excised and submitted for histopathology and the tumor was diagnosed as an amelanotic melanoma. The animal was then scheduled to receive radiation treatment.

At the time of the pre-radiation examination, one-week post initial visit, it was noted the animal had a prominent right submandibular lymph node (RSMLN) and CT revealed a moderately enlarged and irregular right retropharyngeal lymph node. Ultrasound-guided aspirates were of low cellularity and cytology was consistent with a reactive lymph node,

with no malignant cells seen. However, given the size and appearance of the CT scan, a tentative diagnosis of metastatic disease was made for the right retropharyngeal lymph node. Palliative radiation of six treatments to the primary oral mass was started at UPenn.

During return visits for radiation therapy, multiple new cutaneous masses were observed. The first two cutaneous mass was identified a month after primary diagnosis, one at the right lateral thorax and one on the sternum. Both superficial cutaneous masses were firm, pale tan and 1.4cm in diameter. Five days after the third radiation treatment, a third mass was noted on the left prescapular area. This mass was also superficial cutaneous, firm, pale tan and was 0.8cm in diameter. Throughout this period the thoracic radiographs were within normal limits. Fine-needle aspirates of all cutaneous masses were performed. Cytology showed similar cell morphologies for all masses however; due, to the location of the masses, the anaplastic cellular morphology and the absence of melanin granules a definitive diagnosis could not be made. Major differentials included histiocytic disease including histiocytosic scarcoma due to the location and breed predisposition. By the fourth radiation visit, a new dermal mass was noted over his left hip measuring 0.6 cm in diameter, firm, superficial, and mildly inflamed. It was again noted the right mandibular lymph node (RMLN) was enlarged (1.3cm) and firm. Additional aspirates of all masses and the RMLN were taken and showed malignant, highly dedifferentiated neoplasia. One week later, a new firm 0.4cm mass at the left inguinal area was noted. A punch biopsy was taken of the dermal mass at this left hip. At the final radiation treatment, no new masses had presented and thoracic radiographs were unchanged from initial radiographs.

Four months post-radiation, the primary tumor and lymph node metastases were well-controlled with the radiation therapy; however, the subcutaneous metastases were progressing slowly with the largest 1cm in diameter. Further radiation treatments were declined. Radiation therapy was discontinued. A month later, chest rads revealed multiple nodules and additional ulcerated dermal masses were identified over the next three months when re-growth of the gingival mass was noted. Nine months after initial diagnosis, the decision was made to euthanize. Post-mortem necropsy was performed and tissue sections of six lesions were taken for histological and molecular analysis.

AII. 4 Materials and Methods

AII.4.1 Tissue Collection

En bloc resections and punch biopsies of tumor tissue were performed at UPenn. Tissues were stored on ice and submitted to NCSU Breen Lab for further evaluation. At NCSU, tissues were divided into three equal sections for histology, nucleic acid removal, and cell culture. Specimens for histology were fixed in neutral buffered formalin for 24 hours then blocked in paraffin. Sections for nucleic acid removal were snap frozen in liquid nitrogen.

AII.4.2 Immunohistochemistry

Histology and pathological assessment of all tumor sections was performed at NCSU College of Veterinary Medicine Anatomic Pathology Laboratory.

AII.4.3 Cell Culture

Tissue sections for cell culture were subjected to enzymatic disaggregation using collagenase IV (Invitrogen, Life Technologies Inc., Grand Island, NY, USA) at a final concentration of 1X in Hank's Balanced Salt Solution (HBSS) (Mediatech Inc., Manassas, VA, USA) at 37°C overnight. Cells were cultured in Dulbecco's Modified Eagle Medium (Mediatech Inc., Manassas, VA, USA) supplemented with 10% v/v heat-inactivated FBS (Mediatech Inc., Manassas, VA, USA) and 100ug/ml Primocin Antibiotic (InvivoGen, San Diego, CA, USA) in a humidified atmosphere containing 5% CO_2 at 37°C. Cells were grown in T75 flasks with 0.2µM filtered lids until they reached 95% confluence, then harvested for metaphase cellular spreads and DNA extraction. All cell lines were grown as a monolayer and were maintained by passage for no greater than eight passages after reestablishment.

AII.4.4 Genomic DNA Extraction

Genomic DNA was extracted from frozen tissues using the DNeasy Kit (according to manufacturer's recommendations, Qiagen, Germantown, MD, USA) and assessed for quality and quantity by spectrophotometry. Genomic DNA integrity was assessed by agarose gel electrophoresis and showed little to no degradation.

For DNA extraction from FFPE samples, areas of tissue enriched for tumor were identified and indicated on a representative Hematoxylin and Eosin (H&E)-stained 5µm slides by a veterinary pathologist (LB). Three adjacent 25µm sections were obtained from each FFPE specimen and tumor regions were macro-dissected away from any normal tissue.

Genomic DNA was extracted from the remainder of the 25μm sections using a QIAamp DNA FFPE Tissue Kit (according to manufacturer's recommendations, Qiagen, Germantown, MD, USA) and assessed for quality and quantity by spectrophotometry. Genomic DNA integrity was assessed by agarose gel electrophoresis. All FFPE derived samples had DNA exhibiting some degree of degradation, but the majority of the DNA was >10kb.

AII.4.5 Fluorescence in situ Hybridization

Metaphase chromosome preparations and interphase nuclei were produced directly from cultured cells using conventional techniques of ethidium bromide treatment to elongate chromosomes, colcemid arrest, hypotonic treatment, and 3:1 methanol-glacial acetic acid fixation (Breen, Bullerdiek, and Langford 1999). Multicolor single locus probe (SLP) fluorescence *in situ* hybridization (FISH) analysis was done on metaphase spreads as described previously (Breen *et al.* 2004) to evaluate the distribution of selected copy number changes identified by genome-wide oaCGH. Bacterial artificial chromosomes (BACs) that contained the coding sequence for the genes of interest were selected based on their genome position indicated for the canine genome build CanFam2 in the UCSC canine genome browser (http://genome.ucsc.edu). Metaphase preparations from clinically healthy canine primary lymphocytes were used to confirm that all 10 BAC pools showed the expected copy number (n=2) for autosomal loci.

AII.4.6 DNA Array Comparative Genomic Hybridization

Oligo-aCGH was performed by cohybridization of tumor (test) DNA and a common reference DNA sample comprising of an equimolar pool of high molecular weight (HMW) DNA from multiple healthy individuals of various breeds. DNA was labeled using an Agilent SureTag Labeling Kit (Agilent Technologies, Santa Clara, CA) with all tumor (test) samples labeled with Cyanine-3-dCTP and the common reference sample labeled with Cyanine-5-dCTP. Fluorochrome incorporation and final probe concentrations were determined using routine spectrophotometric parameters with reading taken from a Nanodrop1000. Fluorescently labeled test and reference samples were co-hybridized to Canine G3 SurePrint 180,000 feature CGH arrays (Agilent, AMADID 025522) for 40 hours at 65°C and 20 rpm, as described previously (Angstadt *et al.* 2011). Arrays were scanned at 3μm, using a high-resolution microarray scanner (Agilent, Model G2505C).

Copy number data were analyzed with NEXUS Copy Number v6.0 software (Biodiscovery Inc., CA, USA). The raw copy number data for each probe provided from Feature Extraction were centered using diploid regions. NEXUS generated copy number aberrations using a FASST2 Segmentation method with a significance threshold of 5.05^{-6}. Aberrations were defined as a minimum of three consecutive probes with log2 tumor: reference value of 0.2 to 1.13 (gain), >1.14 (high gain), -0.23 to -1.1 (loss), < -1.1 (homozygous loss). Recurrent copy number aberrations were determined within NEXUS using an involvement threshold of 60%. Significance of these regions was then determined in NEXUS using the GISTIC algorithm with a G-score cut off of G>1.0 and a significance of Q<0.05. CNA frequency comparisons amongst sample groups were performed in NEXUS

using Fisher's exact test with differential threshold of >50% and significance $p<0.05$. Significance of each probe between the two groups was calculated in NEXUS using a Mann-Whitney U Test for median comparison.

AII.5 Results

AII.5.1 Histologic and Immunohistochemical Findings of Primary Tumor

Histologically, the initial tumor biopsy showed the submucosa to be infiltrated by a dense cellular neoplasm of polygonal cells with a fine fibrovacscular stroma. Pigment-laden macrophages were observed in the superficial stroma. The neoplastic tissue had moderate anisocytosis and anisokaryosis. However, no vascular or lymphatic invasion was observed. Neoplastic cells presented with moderately pale amphophilic cytoplasm with round to oval nuclei. Nuclei had prominent atypia with finely stippled chromatin and one to two nucleoli. Proliferating cells were associated with or embedded in the overlying mucosal epithelium (junctional activity). Thirty-eight mitotic figures were found in 10 consecutive, non-overlapping, 40X fields. The diagnosis was determined as amelanotic malignant oral melanoma.

After tissue was submitted to NCSU, secondary histopathological analysis (Figure AII.2a) showed the submitted tumor section had almost identical tissue morphologies; however, this sectioned showed fewer mitotic figures, 15 in 10 consecutive, non-overlapping, 40X fields, and two areas were suspicious for intravascular invasion. This was suggestive of heterogeneity within the tumor substructure. Due to a lack of sufficient differentiation,

pathology could not confirm a final diagnosis, but it was suggested as either a carcinoma or neuroendocrine tumor.

Neoplastic cells did not label with Melan-A. Negative results do not rule out melanoma as amelanotic melanomas do not always stain with Melan-A (Figure AII.2b). S-100 stain was then applied to the same section. There was moderate staining of all neoplastic cells exhibiting cytoplasmic reactivity. However, S-100 has a low specificity and other spindle cell neoplasms have also been reported as positive for S-100 (Figure AII.2c). Finally, a PNL-2 stain, melanoma specific marker, was applied to the tissue section. The neoplastic cells did not label with PNL-2 (Figure AII.2d).

AII.5.2 Histologic Findings of Metastatic Tumor from Left Hip

Cytology of fine-needle aspirates from the left hip mass showed neoplastic cells in sheets and cohesive aggregates. The majority of neoplastic cells were round with few showing fusiform shape and with all showing marked anisocytosis, anisokaryosis, binucleation, micronuclei, coarsely stippled chromatin, many nucleoli, anisonucleoliosis, and moderate basophilic to blue-grey cytoplasm. Frequent mitotic figures were observed.

H&E analysis of the dermal metastatic tumor (Figure AII.2e) revealed the dermis contained an unencapsulated, poorly demarcated neoplasm arranged in anastomosing islands, trabeculae, cords, and rare packets separated by a thin fibrovascular stroma. Neoplastic cells were oval to polygonal, had indistinct cell borders, moderate amounts of pale, eosinophilic foamy cytoplasm, round to oval nuclei with finely-stippled chromatin and one to two nucleoli. There was moderate anisocytosis and marked anisokaryosis. Thirty-five mitotic

figures were observed in 10 consecutive, non-overlapping, 40X fields. In the center of the tissue, there was an area of necrosis and small amounts of hemorrhage. There were few hair follicles observed on the periphery of the tissue; however, neoplastic cells were not observed within the follicular epithelium.

For this tissue section, epithelium/epidermis was not included in the biopsy sample, which hinders interpretation of histologic findings, as certain tumors, such as melanoma, will exhibit junctional activity. Histological findings were similar to the primary neoplastic tissue, with more pleomorphism and a higher mitotic rate observed in the metastatic tissue. The diagnosis was a malignant neoplasia, but due to the advanced dedifferentiation of the tissue, no further definitive diagnosis could be made. However, taken with the previous diagnosis, it was concluded that this could be a metastasis from an amelanotic malignant melanoma. S-100 stain was then applied to the same section. There was moderate staining of all neoplastic cells exhibiting cytoplasmic reactivity (Figure AII.2f). Finally, a PNL-2 stain, melanoma specific marker, was applied to the tissue section. The neoplastic cells did not label with PNL-2 (Figure AII.2g).

AII.5.3 Histologic Findings of Distant Metastatic Tumors

Similar histologic findings are present in oral mass (Figure AII.2h), lung (Figure AII.2j), and haired skin tissues (Figure AII.2k-m) and are reported together. Normal parenchyma is expanded and replaced by a poorly demarcated, unencapsulated, moderately cellular neoplasm arranged in sheets to anastomosing islands and trabeculae and supported by a scant fibrous stroma. Neoplastic cells are oval to polygonal with indistinct cell borders,

and a moderate amount of finely vacuolated amphophilic cytoplasm. Nuclei are oval with a moderate amount of finely stippled to vesiculated chromatin and an indistinct to 1 nucleolus. Anisocytosis and anisokaryosis are moderate and there are 32 mitotic figures in 10 consecutive, non-overlapping, 40X fields. Scattered individual cells are rounded, with hypereosinophilic cytoplasm and pyknotic nuclei. Multifocally, the pericardium (Figure AII.2n) is expanded by small clusters and anastamosing trabeculae of hypertrophied mesothelial cells with variably sized aggregates of lymphocytes with admixed areas of hemorrhage and hemosiderin-laden macrophages.

CD18 staining of the local recurrence from the primary oral mass was diagnostically negative (Figure AII.2i) as over 95% of neoplastic cells failed to positively label. Scattered cells at the periphery of the neoplasm display strong, granular, cytoplasmic labeling with CD18, suggesting a high level of inflammation at the periphery of the tumor.

AII.5.4 Molecular Findings

Our molecular analysis of both the primary tumor and the metastatic lesions are supportive of a diagnosis of amelanotic malignant oral melanoma. The genetic profile determined from the primary and all metastatic tumors closely resembles that of previously characterized canine oral melanomas (Chapter II).

AII.5.4.1 oaCGH Data

Whole-genome oligo-array comparative genomic hybridization (oaCGH) further supported a diagnosis of amelanotic oral melanoma. The oaCGH prolife of the primary and

all metastatic lesions (Figure AII.3) presented with characteristic genetic markers found only in malignant oral melanoma, a gain of CFA 17 and a sigmoidal pattern of CFA 10 and 30 (Chapter II). The only principal difference to copy number aberrations of the established population of canine oral melanomas was a loss of CFA 13. The left hip metastatic lesion showed some copy number differences to those present in the primary tumor, the largest of which was a gain of CFA 33 from 9.2-17.8Mb. Oligo-aCGH profiles of the later metastatic lesions showed remarkable similarity to both the primary tumor and the metastatic lesion from the left hip (Figure AII.3). When aberrations present in the population of all metastatic lesions were compared to those in the primary tumor, no significant differences were found.

AII.5.4.2 FISH Data

Analysis of cultured cells from the primary tumor showed atypical nuclear morphology in both shape and chromatin consistency. The copy number status for individual genes showed high levels of variability (Figure AII.4), suggestive of tissue heterogeneity. However, the overall trend of targeted-gene copy number aberrations was suggestive of oral malignant melanoma.

AII.6 Case Outcome and Discussion

In this study we have demonstrated the ability of molecular analysis to aid in the diagnosis of histologically ambiguous neoplasia. The initial diagnosis of amelanotic melanoma was questioned by the biological presentation, the lack of histologic differentiation, and the location of metastatic lesions. Further immunohistochemistry

analysis was unable to confirm differential diagnosis, as clinical marker staining was unremarkable (Figure AII.2a-g). At this point, due to the prevalence in Flat-Coated Retrievers, a possibility of histyocitic scarcoma was discussed. This diagnosis would also fit the biological spread of the disease to the cutaneous epithelium, an unusual occurrence in oral melanomas. However, CD18 immunostaining was negative as seen in Figure 1i. Molecular analysis, however, was able to show similar genome-wide copy number profiles to that of canine oral melanoma (Chapter II). Similarly, these tumors did not present with genetic aberrations similar to other canine tumors (Angstadt *et al.* 2011; Hedan *et al.* 2011; Thomas *et al.* 2011; Frantz *et al.* 2013; Seiser *et al.* 2013). With this detailed genetic analysis, we were able to confirm the initial diagnosis of oral melanoma (Figure AII.5).

Detailed copy number analysis of the primary tumor and the corresponding metastatic lesion can reveal aberrations that are advantageous to the advancement of this disease. Regions of differences between the primary tumor and the first dermal metastatic lesion were few. When the most significant region of difference (CFA 33: 9.2-17.8Mb) present in the metastatic lesions was analyzed for gene involvement, it was found that s100a10, an isoform of the s100a protein, was found within this region of high amplification. S100a10, the specific isoform found in this region, induces the dimerization of ANXA2/p36 and may function as a regulator of protein phosphorylation. However, there is much debate on the role of s100a10 gene in melanogenesis (Leclerc, Heizmann, and Vetter 2009; Petersson *et al.* 2009).

Another finding was that although the various metastatic lesions had very different histologic phenotypes, they all had essentially identical genetic profiles. This suggests clonal

origin of disseminating cells. The variation in phenotype of the metastatic lesions may arise from the dedifferentiated status of the primary tumor and the cellular changes that accompany metastasis. When circulating metastatic cells embed in a distant tissue, neighboring somatic cells then regulate changes in gene expression. The presence of non-uniform morphologies of the different metastatic lesions, with identical genetic background, suggests the importance of the tissue microenvironment to tumor differentiation and phenotypic appearance. This could have a large impact on diagnosis as genetically similar tumors arising from various locations may present with distinct histological profiles. In summary, we have shown that genetic analysis can aid in diagnosis of tumors that present with histologically ambiguous characteristics.

It is apparent that, in the advent of affordable biotechnological tools, molecular based medicine will take a forefront in patient care in terms of both diagnosis and treatment. It is clear from this individual that traditional methodologies may lack the ability to assess non-traditional tumors. Currently, few methods allow for differential diagnosis and prognosis to be made for tumors that present with ambiguous histology. Such ambiguous tumors represent situations where accurate information is needed, as they tend to be highly aggressive and act biologically irregular. As we have shown here, genetic-based assays can give fast and accurate diagnoses where traditional immunohistochemical methods fail. Molecular diagnostics give clinicians a way to assess biologically irregular tumors, conserving the time of pathologists and ultimately benefiting patient care.

Acknowledgements

I would like to thank Dr. Luke Borst (LB) with histology and pathology and Alice Harvey, Medical Illustrator, for help with the compilation of AII.5.

REFERENCES

Angstadt, A. Y., Motsinger-Reif, A., Thomas, R.*, et al.* (2011). "Characterization of canine osteosarcoma by array comparative genomic hybridization and RT-qPCR: Signatures of genomic imbalance in canine osteosarcoma parallel the human counterpart." Genes, Chromosomes and Cancer **50**(11): 859-874.

Bastian, B. C., Olshen, A. B., LeBoit, P. E.*, et al.* (2003). "Classifying Melanocytic Tumors Based on DNA Copy Number Changes." The American Journal of Pathology **163**(5): 1765-1770.

Bastian, B. C. and Bauer, J. A. (2007). "DNA copy number changes in the diagnosis of melanocytic tumors." Pathologe **28**(6): 464-473.

Bauer, J. and Bastian, B. C. (2006). "Distinguishing melanocytic nevi from melanoma by DNA copy number changes: comparative genomic hybridization as a research and diagnostic tool." Dermatologic Therapy **19**: 40-49.

Bergman, P. (2007). "Canine Oral Melanoma." Clinical Techniques in Small Animal Practice **22**(2): 55-60.

Breen, M., Bullerdiek, J. and Langford, C. F. (1999). "The DAPI banded karyotype of the domestic dog (Canis familiaris) generated using chromosome-specific paint probes." Chromosome Research **7**(7): 575.

Breen, M., Hitte, C., Lorentzen, T. D.*, et al.* (2004). "An intergrated 4249 marker FISH/RH map of the canine genome." BMC Genomics **5**(1): 65.

Frantz, A. M., Sarver, A. L., Ito, D.*, et al.* (2013). "Molecular profiling reveals prognostically significant subtypes of canine lymphoma." Vet Pathol **50**(4): 693-703.

Greshock, J., Nathanson, K., Medina, A.*, et al.* (2009). "Distinct patterns of DNA copy number alterations associate withBRAFmutations in melanomas and melanoma-derived cell lines." Genes, Chromosomes and Cancer **48**(5): 419-428.

Hedan, B., Thomas, R., Motsinger-Reif, A.*, et al.* (2011). "Molecular cytogenetic characterization of canine histiocytic sarcoma: A spontaneous model for human histiocytic cancer identifies deletion of tumor suppressor genes and highlights influence of genetic background on tumor behavior." BMC Cancer **11**: 201.

Koenig, A., Bianco, S. R., Fosmire, S.*, et al.* (2002). "Expression and Significance of p53, Rb, p21/waf-1, p16/ink-4a, and PTEN Tumor Suppressors in Canine Melanoma." Veterinary Pathology **39**(4): 458-472.

Lazar, V., Ecsedi, S., Szollosi, A. G.*, et al.* (2009). "Characterization of candidate gene copy number alterations in the 11q13 region along with BRAF and NRAS mutations in human melanoma." Mod Pathol **22**(10): 1367-1378.

Leclerc, E., Heizmann, C. W. and Vetter, S. W. (2009). "RAGE and S100 protein transcription levels are highly variable in human melanoma tumors and cells." Gen. Physiol. Biophys **28**: F65–F75.

Petersson, S., Shubbar, E., Enerbäck, L.*, et al.* (2009). "Expression patterns of S100 proteins in melanocytes and melanocytic lesions." Melanoma Research **19**(4): 215-225.

Ramos-Vara, J. A., Beissenherz, M. E., Miller, M. A.*, et al.* (2000). "Retrospective Study of 338 Canine Oral Melanomas with Clinical, Histologic, and Immunohistochemical Review of 129 Cases." Veterinary Pathology **37**(6): 597-608.

Seiser, E. L., Thomas, R., Richards, K. L.*, et al.* (2013). "Reading between the lines: molecular characterization of five widely used canine lymphoid tumour cell lines." Vet Comp Oncol **11**(1): 30-50.

Smedley, R. C., Spangler, W. L., Esplin, D. G.*, et al.* (2011). "Prognostic Markers for Canine Melanocytic Neoplasms: A Comparative Review of the Literature and Goals for Future Investigation." Veterinary Pathology **48**(1): 54-72.

Spangler, W. L. and Kass, P. H. (2006). "The Histologic and Epidemiologic Bases for Prognostic Considerations in Canine Melanocytic Neoplasia." Veterinary Pathology **43**(2): 136-149.

Thomas, R., Duke, S. E., Karlsson, E. K.*, et al.* (2008). "A genome assembly-integrated dog 1 Mb BAC microarray: a cytogenetic resource for canine cancer studies and comparative genomic analysis." Cytogenetic and Genome Research **122**(2): 110-121.

Thomas, R., Seiser, E. L., Motsinger-Reif, A.*, et al.* (2011). "Refining tumor-associated aneuploidy through 'genomic recoding' of recurrent DNA copy number aberrations in 150 canine non-Hodgkin lymphomas. ." Leukemia and Lymphoma **52**(7): 1321-1335.

Vergier, B., Prochazkova-Carlotti, M., De la Fouchardiere, A.*, et al.* (2011). "Flourescence *in situ* hybridization, a diagnositc aid in ambiguous melanocytic tumors: European study of 113 cases." Modern Pathology **24**: 613-623.

Withrow, S. J., D. M. Vail, and R. Page (2013). Small Animal Clinial Oncology, Elsevier.

Figure AII.1 Image of an amelanotic mass from a 10 year-old Flat-Coated Retriever located on the right dorsal hard palate. A 10 year-old neutered Flat-Coated Retriever presented with 3cm in diameter gingival mass located on the right side of the hard palate (arrowed) detected by the referring veterinarian on routine dental examination.

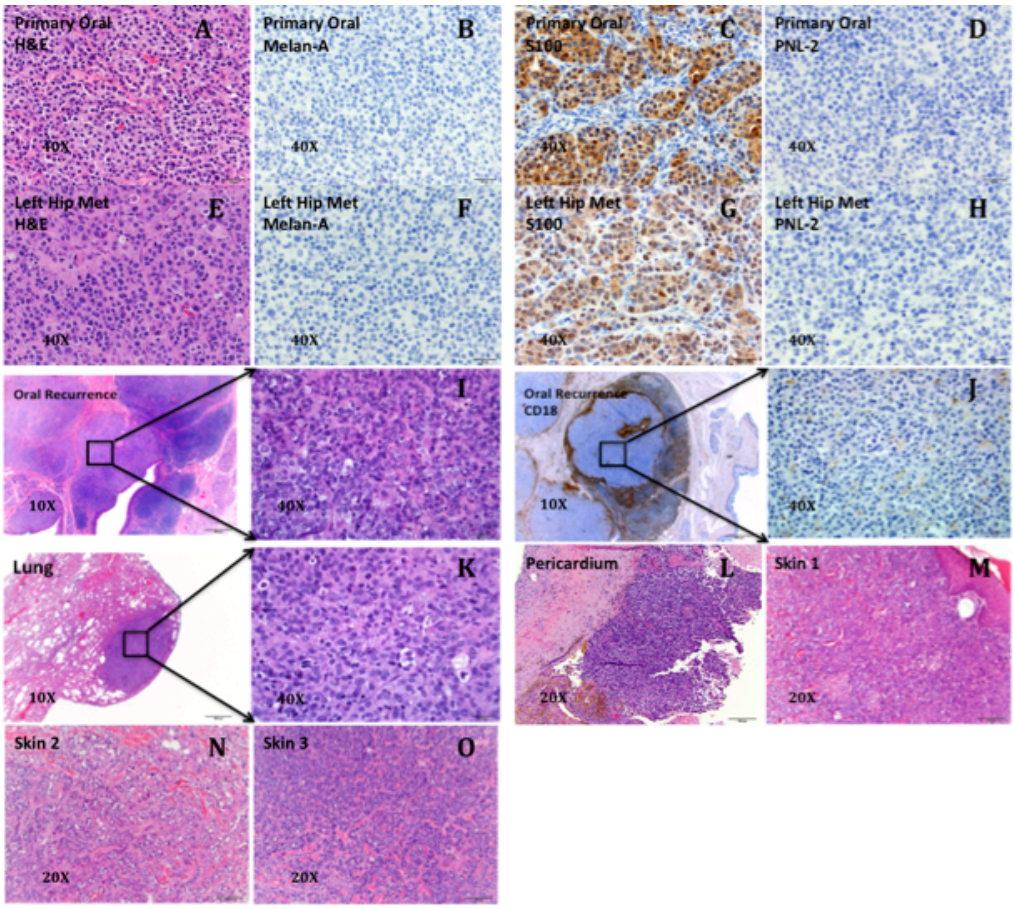

Figure AII.2 Histological images of eight tumors from a Flat-Coated Retriever. (A) Section displaying amelanotyic neoplastic cells from primary oral mass. H&E. Bar, 20 µm. **(B)** Section displaying a Melan-A IHC stain on primary oral mass. Melan-A. Bar, 20 µm. **(C)** Section displaying an s100 IHC stain on primary oral mass. S100. Bar, 20 µm. **(D)** Section displaying a PNL-2 IHC stain on primary oral mass. PNL-2. Bar, 20 µm. **(E)** Section displaying amelanotyic neoplastic cells from metastatic left hip subcutaneous mass. H&E. Bar, 20 µm. **(F)** Section displaying a Melan-A ICH stain from metastatic left hip subcutaneous mass. Melan-A. Bar, 20 µm. **(G)** Section displaying a s100 IHC stain from metastatic left hip subcutaneous mass. s100. Bar, 20 µm. **(H)** Section displaying a PNL-2 IHC stain from metastatic left hip subcutaneous mass. PNL-2. Bar, 20 µm. **(I)** Section displaying amelanotyic neoplastic cells from recurrent mass from the oral cavity. H&E. Bar, 20 µm. **(J)** Section displaying CD18 IHC stain from recurrent mass from the oral cavity. CD18. Bar, 20 µm. **(K)** Section displaying amelanotyic neoplastic cells from metastatic lung mass. H&E. Bar, 20 µm. **(L)** Section displaying amelanotyic neoplastic cells from metastatic pericardial mass. H&E. Bar, 20 µm. **(M-O)** Section displaying amelanotyic neoplastic cells from metastatic skin masses. H&E. Bar, 20 µm.

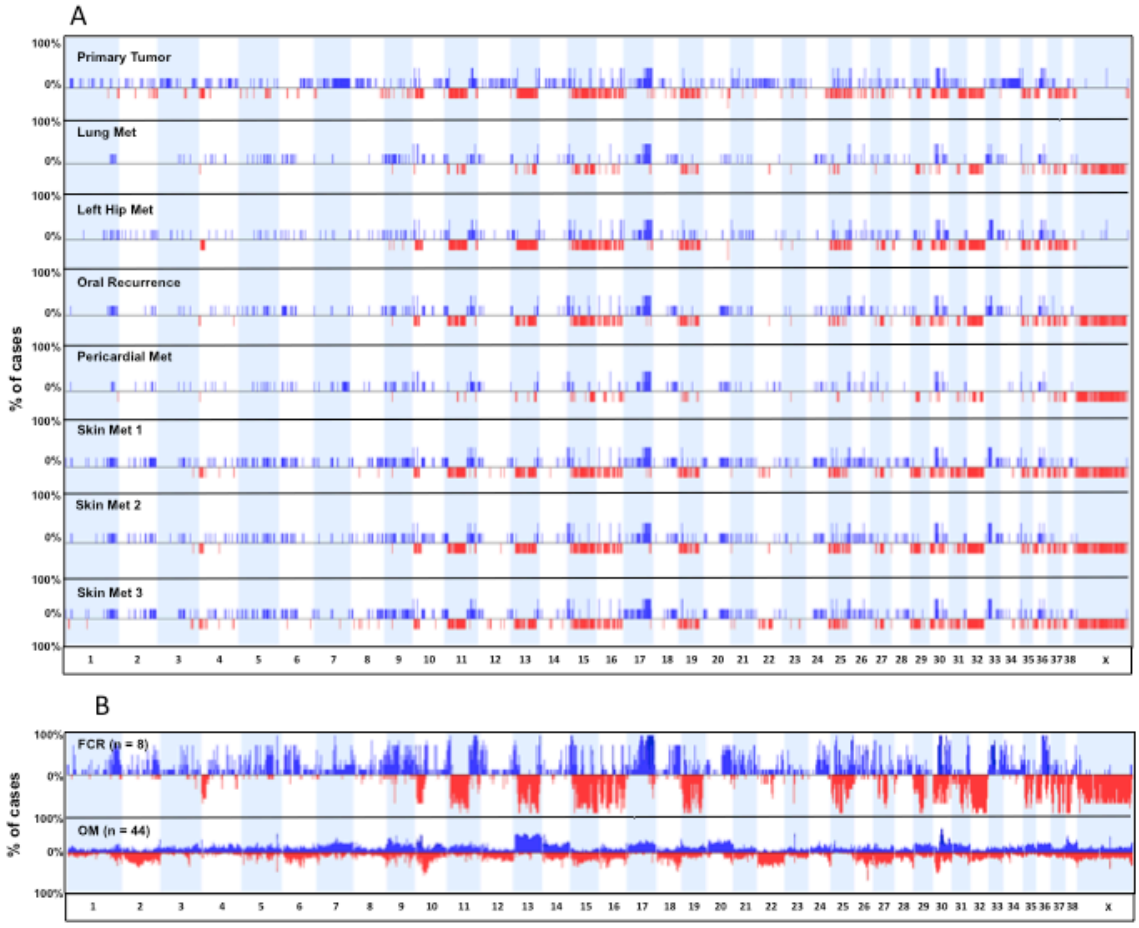

Figure AII.3 (A) Oligo-aCGH profiles of eight tumors from a Flat-Coated Retriever (FCR) and (B) combined oaCGH profile of the eight tumors compared to established oaCGH profile of canine oral melanoma (OM). Oligo-aCGH plots for each cohort are represented as a penetrance plot, which establishes the percentage of cases with a common aberration within each population plotted along the y-axis. Losses and gains are called in proportion to a CN of two set at y=0. Regions of red delineate a copy number loss, where regions of blue show a gain. Each chromosome is plotted along the x-axis. **(A)** Cytogenetic analysis showed similar copy number aberrations present in all masses removed from the animal. **(B)** Comparison of masses from the FCR showed similarity to the established copy number profiles of primary canine oral melanomas. The only notable difference was a loss of CFA 13 within the FCR lesions, which is found to have copy number gain in 50% of primary oral melanomas.

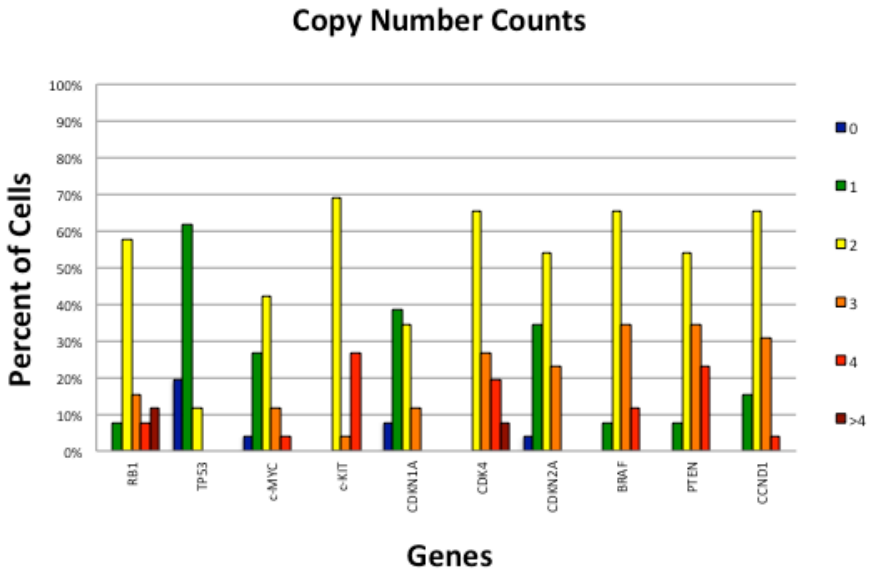

Figure AII.4 Copy number counts of 10 targeted genes in a Flat-Coated Retriever with oral melanoma. FISH analysis of ten targeted genes was performed on cultured cells from the primary oral mass. Genes are plotted along the x-axis with percent of cells showing a particular copy number status plotted along the y-axis. Bars indicate percent of cells counted with a particular copy number. All genes showed intra-tumor heterogeneity in terms of copy number status. Most genes showed 50% normal copy number with a both copy number loss and gain present. *TP53* was the only gene that showed copy number imbalance in greater than 50% of cells.

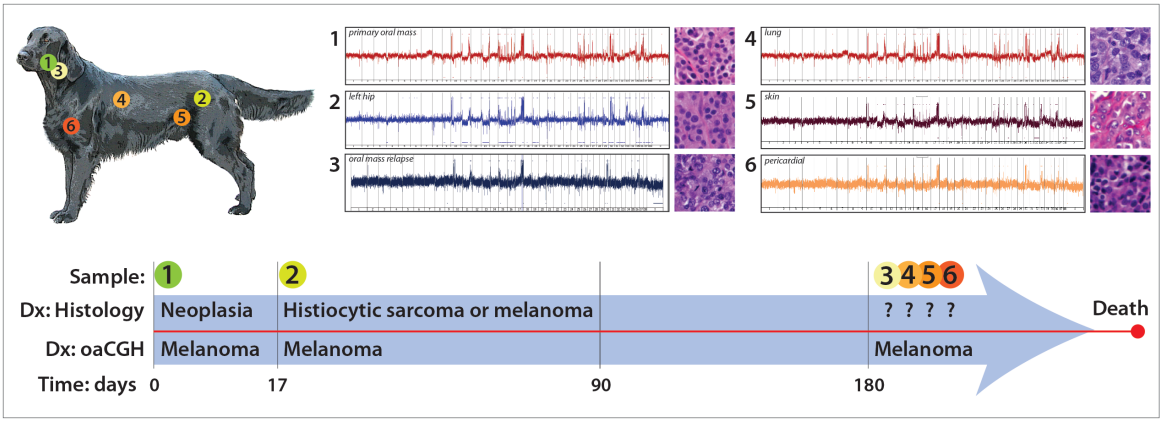

Figure AII.5 Summary of tumor development, histologic, and molecular data from a Flat-Coated Retriever with an ambiguous neoplastic lesion. Illustration of the location, histology, oaCGH cytogenetic profile, and diagnosis of each tumor sampled. These were then plotted along a timeline with the time from diagnosis to death presented in days.